Reconstructing Lateglacial and Early Holocene Landscape Evolution Using a Combination of Numerical and Relative Dating Methods – Examples from Eastern Switzerland and Eastern France

---

Dissertation
zur
Erlangung der naturwissenschaftlichen Doktorwürde
(Dr. sc. nat.)

vorgelegt der

Mathematisch-naturwissenschaftlichen Fakultät

der

Universität Zürich

von

Ralph Böhlert

von

Adliswil ZH

Promotionskomitee
Prof. Dr. Wilfried Haeberli (Vorsitz)
PD Dr. Markus Egli (Leitung der Dissertation)
Prof. Dr. Max Maisch
Dr. Dagmar Brandová

Zürich, 2010

Summary

Understanding past climatic conditions is crucial for modelling approaches pointing to the future and to answer questions about interregional and –hemispherical synchronicity of climatic events and their impacts. Glacial and periglacial landforms as terrestrial archives contain spatial and temporal information about the forming processes behind them. To unravel the wider palaeoclimatic context and to estimate process rates, dating these landforms is necessary. With the development and improvement of numerical dating methods, an increasingly large field of (glacial-)geomorphological questions can be addressed.

As a result of the highly unstable climate during the Lateglacial (c. 19-11.5 ka) and the early Holocene, a variety of climate-related landforms developed in mountain areas of the Alps. The main goal of this work was, on one hand, to improve the absolute chronology in this time window by dating geomorphologic situations not yet or only sparsely dealt with in other studies using multi-proxy approaches. On the other hand, a methodological aim was to cross-check the applied methods in order to estimate uncertainties and to calibrate relative dating techniques. Three main parts can be distinguished:

(1) An integral temporal assessment of the main geomorphic features and consequently landscape evolution was the primary aim in the wider area of the Albulapass (including Val Mulix) and the neighbouring Val Burdun (eastern Swiss Alps). Both numerical (surface exposure dating using ^{10}Be) and relative dating techniques (weathering rinds, Schmidt-hammer r-values, soil chemistry and mineralogy) were used and combined wherever possible. At high elevation sites near the Last Glacial Maximum (LGM) trimline, exposure ages varied from 11 ka to 13.5 ka. This suggests long-lasting local ice after the breakdown of the LGM ice domes or, alternatively, a reglaciation during the Younger Dryas. In Val Mulix we measured one of the first acceptable ages for Daun-stadial moraines with 14.7 ± 1.8 ka, supporting the assumed pre-Bølling chronological position. ^{10}Be-ages of boulders from a relict rock glacier give a meaningful picture of mean annual deformation rates and the main activity phase that lasted from the Lateglacial until the early Holocene. Exposure ages from glacially polished rock barriers near the Little Ice Age (LIA) moraines (ranging from 8.9 ± 0.7 ka to 11.7 ± 0.8 ka) give direct evidence of a fast ice-retreat towards the end of the Younger Dryas, with subsequent length-variations that did not exceed the 1850 extension (Little Ice Age maximum). Ages from a rock avalanche in Val Burdun, surrounded by Lateglacial moraines, point to a single event that happened around 8.9 ka, shortly after the ice-retreat.

While weathering rind thicknesses turned out to be an appropriate tool to support the reconstruction of Lateglacial landscape evolution, Schmidt-Hammer r-values were only applicable with a less-detailed time resolution. The r-values enabled a temporal distinction only within the Holocene (represented by a LIA moraine and active rock glaciers) but not within the Lateglacial. Particularly on the relict rock glacier in Val Mulix, soil formation seemed to be influenced by the existence of pre-weathered material as shown by soil chemical and (clay-)mineralogical investigations. Integrative analyses treating the soils as a whole – namely mass balance calculations and inventories of meteoric ^{10}Be – provided more consistent results than approaches that refer to single horizons. For the measurement of meteoric ^{10}Be in soils, the determination of the annual ^{10}Be-deposition rate is crucial. Similarly, the calculation of surface exposure ages is strongly dependent on the overlying snow coverage. An appropriate choice of corresponding values is in both cases of central importance but difficult to achieve.

(2) In the same region, one of the first attempts to date materials in active rock glaciers using luminescence techniques was made. Despite samples with problematic material-inherent characteristics, reasonable (minimum-)ages in the range of 3-8 ka could be achieved. This goes well along with ages derived by other relative and semi-quantitative approaches. A decisive determination as to whether the ages obtained must be interpreted as minimum or maximum ages was not possible on the database available.

(3) At Aiguille du Midi in the Mt. Blanc area (eastern France), exposure ages and spectral properties of rock surfaces in the steep S-face were compared. Besides a remarkably old age of almost 40 ka, a well-pronounced relation of exposure ages and the surface redness as a measure for the time-dependent weathering state could be detected. This could be a first step towards rock fall dating derivable from spectral signatures and consequently towards a remote sensing monitoring of rock fall activities in larger, high Alpine or Arctic areas. Putting observed rock falls influenced by permafrost degradation into long-term perspective might be considered as a potential application of this approach.

Zusammenfassung

Das Verständnis paläoklimatologischer Bedingungen ist von zentraler Bedeutung für zukunftsgerichtete Modellansätze und um Fragen bezüglich interregionaler und –hemisphärischer Synchronität von Klimaereignissen und deren Auswirkungen auf natürliche Systeme der Erdoberfläche zu beantworten. Glaziale und periglaziale Landschaftsformen als terrestrische Archive enthalten räumliche wie auch zeitliche Informationen über die Prozesse, welche sie entstehen liessen. Um den paläoklimatologischen Kontext auszuleuchten und um Prozessraten abschätzen zu können, ist die Datierung dieser Landschaftsformen unumgänglich. Mit der Etablierung und Weiterentwicklung numerischer Datierungsmethoden ist es möglich geworden, ein zunehmend breiteres Spektrum (glazial-)geomorphologischer Fragestellungen anzugehen.

Als Folge eines ausgesprochen instabilen Klimaverlaufes während des Spätglazials (ca. 19-11.5 ka) und des anschliessenden frühen Holozäns entstand eine Vielzahl klimagekoppelter Landschaftsformen in den Gebirgsregionen der Alpen. Hauptziel dieser Arbeit ist einerseits eine Verbesserung der absoluten Chronologie in diesem Zeitraum. Hierzu wurden geomorphologische Situationen, welche in bisherigen geochronologischen Studien keine oder kaum Beachtung fanden, mit Multi-Proxy-Ansätzen datiert. Ein weiterer, methodischer Aspekt sind Kreuzvergleiche relativer und numerischer Datierungstechniken, um Unsicherheiten und Fehlerbandbreiten besser abschätzen zu können und relative Ansätze zu kalibrieren. Die vorliegende Studie ist in drei Teile gegliedert:

(1) Im Albulagebiet (welches auch das Val Mulix miteinbezieht) und im benachbarten Val Burdun (östliche Schweizer Alpen) war eine integrale zeitliche Zuordnung der vorherrschenden geomorphologischen Formen das Hauptziel. Sowohl numerische (Expositionsaltersdatierung mit ^{10}Be) als auch relative Datierungstechniken (Verwitterungsrinden, Schmidt-hammer r-Werte, Bodenchemie und –mineralogie) kamen, wo immer möglich und sinnvoll, zu einem kombinierten Einsatz. Expositionsalter von hohen Lagen nahe der hocheiszeitlichen Schliffgrenze (LGM = Last Glacial Maximum) variierten von ca. 11 ka bis 13.5 ka. Dies weist auf eine lange anhaltende Vereisung nach dem Zusammenbruch der hochglazialen Eisdome oder auf eine erneute lokale Vergletscherung während der Jüngeren Dryas hin. Im Val Mulix konnte dem Daun-Stadial erstmals ein sinnvolles Alter zugewiesen werden (14.7 ± 1.8 ka). Dies bestätigt die vermutete chronologische Position im prä-Bølling. ^{10}Be-Alter von einem relikten Blockgletscher zeichnen ein sinnvolles Bild von mittleren jährlichen Deformationsraten im dm-Bereich und einer Hauptaktivitätsphase vom ausgehenden Spätglazial bis ins frühe Holozän. Glazial überschliffene Felsriegel im hinteren Talbereich nahe der Ausdehnung von 1850 ergaben Alter von 8.9 ± 0.7 ka bis 11.7 ± 0.8 ka, was als

direkter Beweis eines schnellen Eisrückganges gegen Ende der Jüngeren Dryas und darauf folgender nur kleinräumiger Gletscherschwankungen gewertet werden darf. Expositionsalter von einem Felssturz im Val Burdun, der von spätglazialen Moränen eingerahmt wird, sprechen für ein Einzelereignis, welches sich um 8.9 ka kurz nach Eisrückzug ereignet haben dürfte.

Während die Messung von Verwitterungsrindenmächtigkeiten sich als taugliches Instrument zur Rekonstruktion der spätglazialen Landschaftsentwicklung erwiesen hat, scheint das Auflösungsvermögen des Schmidt-Hammers in diesem zeitlichen Abschnitt an die Grenzen zu stossen. Wohl ergab sich unter Einbezug von Landschaftsformen, welche dem Holozän zugeordnet werden können (aktive Blockgletscher, Moräne der Kleinen Eiszeit), ein sinnvolles Bild, innerhalb des Spätglazials jedoch war keine Unterscheidung mehr möglich. Speziell auf dem relikten Blockgletscher im Val Mulix scheint die Bodenentwicklung von vorverwittertem Material beeinflusst, wie mit bodenchemischen und (ton-)mineralogischen Analysen gezeigt werden konnte. Integrative Analysen, welche das Bodenprofil als Ganzes betrachten – namentlich Massenbilanzberechnungen und das Inventar von meteorischem ^{10}Be – ergaben konsistentere Resultate als Ansätze, die sich auf einzelne Horizonte beziehen. Für die Altersberechnung basierend auf meteorischem ^{10}Be in Böden ist die jährliche ^{10}Be-Depositionsrate von grundlegender Bedeutung. In ähnlicher Weise reagieren Oberflächenexpositionsalter sehr sensibel auf unterschiedliche Mächtigkeiten der gewählten Schneebedeckung. Die möglichst genaue Bestimmung dieser Grössen ist gleichermassen wichtig wie schwierig.

(2) In der gleichen Region wurde einer der ersten Versuche unternommen, aktive Blockgletscher mittels optischer Lumineszenz zu datieren. Trotz Probenmaterial mit problematischen Lumineszenzeigenschaften konnten sinnvolle Alter im Bereich von 3-8 ka gemessen werden. Diese Werte sind gut mit Ergebnissen anderer relativer und semi-quantitativer Ansätze in Einklang zu bringen. Ob die festgestellten Alterswerte als Minimal- oder Maximalalter zu werten sind, ist aufgrund der verfügbaren Datenbasis nicht eindeutig zu entscheiden.

(3) In der steilen Süd-Wand der Aiguille du Midi im Mt. Blanc Gebiet (F) wurden Expositionsalter und spektrale Eigenschaften von Felsoberflächen miteinander verglichen. Neben einem bemerkenswert hohen Alter von fast 40 ka, konnte eine klare Relation zwischen Expositionsalter und dem verwitterungsbedingten Rötungsgrad der Felsoberflächen festgestellt werden. Dies könnte ein erster Schritt zur Herleitung von Steinschlaggeschichten aufgrund spektraler Signaturen bedeuten. Damit könnten in jüngster Zeit beobachtete und aller Wahrscheinlichkeit nach mit Permafrostdegradation zusammenhängende Stein-/Felsstürze in einen erweiterten zeitlichen Rahmen gestellt werden.

Contents

List of Figures

List of Tables

List of Abbreviations

AdS	Atlas der Schweiz
Bø/All	Bølling/Allerød
ELA	Equilibrium Line Altitude
HADES	Hydrologischer Atlas der Schweiz
ka	a = annum = 1 year; 1 ka = 1000 years
LGM	Last Glacial Maximum
LIA	Little Ice Age
OM	Organic matter
SED	Surface Exposure Dating
SOM	Soil organic matter
YD	Younger Dryas

About this work

This Ph.D. thesis is based on five papers and completed with additional unpublished data.

Böhlert, R., Gruber, S., Egli, M., Maisch, M., Brandová, D., Haeberli, W. 2008. *Comparison of exposure ages and spectral properties of rock surfaces in steep, high alpine rock walls of Aiguille du Midi, France*. In: Proceedings of the 9th International Conference on Permafrost, University of Alaska, Fairbanks: 143-148.

Böhlert, R., Egli, M., Maisch, M. 2008. *Untersuchungen zur spätglazialen und frühholozänen Landschaftsentwicklung im Albulagebiet (Graubünden, Schweiz)*. In: Rothenbühler, C. (Ed.), Klimaveränderungen auf der Spur, Studien des Europäischen Tourismus Instituts, 5, Academia Engiadina, pp. 4-17.

Böhlert, R., Egli, M., Maisch, M., Brandová, D., Ivy-Ochs, S., Kubik, P.W., Haeberli, W. 2010a. *Application of a combination of dating techniques to reconstruct the Lateglacial and early Holocene landscape history of the Albula region (eastern Switzerland)*. Geomorphology, submitted.

Böhlert, R., Compeer, M., Egli, M., Brandová, D., Maisch, M., Kubik, P.W., Haeberli, W. 2010b. *Dating of Lateglacial and Holocene rock glacier activity in a high Alpine region using a combined relative-numerical dating approach*. The Open Geography Journal, submitted.

Egli, M., Brandová, D., Böhlert, R., Favilli, F., Kubik, P.W. 2010. *^{10}Be inventories in Alpine soils and their potential for dating land surfaces*. Geomorphology, in press.

Acknowledgements

This study was supported by the Swiss National Science Foundation grant number 20-109565/1 and the "Stiftung für wissenschaftliche Forschung an der Universität Zürich".

I am especially indebted to the following people and would like to thank them very much:

- PD Dr. Markus Egli for his incredible helpfulness, even in busy times. His patience and constant scientific support were essential for me to stay on the path.
- Prof. Dr. Max Maisch for his tireless help. Max showed me how to deal critically and honestly with scientific questions and that detours sometimes are necessary to reach the goal. The legendary Lateglacial excursions are something I won't forget.
- Dr. Dagmar Brandová for mixing acids and cappuccino. Her tremendous efforts with preparing ^{10}Be-samples were of central importance for this work.
- PD Dr. Susan Ivy-Ochs for kindly sharing her expertise and experience in exposure dating issues.
- Prof. Dr. Wilfried Haeberli for his interest and for sometimes convincing me of the relevance of my own things.

Without the support of the following people this work would not have been possible. I would like to express my appreciation to:

- Dr. Michael Plötze (ETH Zurich, Institute for Geotechnical Engineering) and his lab crew for their support during the XRD and AUTOQUAN measurements.
- Daniele Giaccai (Istituto Sperimentale per lo Studio e la Difesa del Suolo, ISSDS, Firenze, Italy) for using the laboratory and helping me during additional XRD measurements.
- Dr. Matthias Krbetschek (TU Freiberg, Germany) for his interest and readiness to support me during slightly awkward fieldwork. Thanks also to Christine.
- Margreth Fuchs did a great job by preparing and measuring all the luminescence samples.
- Bruno Kägi and Ivan Woodhatch for their help in, and many discussions beyond, the lab.

Many thanks also go to:

- The GIUZ-crowd and especially my office mates. Lucky are those who can work with you!
- Stephan Heer, Reto Waldmeier and my father for fun days in field.
- Christian Keller for sharing his flat in the beautiful Engadine with me.

My dear parents and friends, thanks for your support and encouragement in difficult moments.

Liebe Anna, danke dass du mich während dieser Zeit begleitet hast.

Chapter 1

Introduction

1.1 Relevance and positioning of the study in the scientific field of palaeoenvironmental and palaeoclimate research

1.1.1 Overview

At least since the fourth report of the Intergovernmental Panel on Climate Change (IPCC, 2007) global climate change is generally accepted to already be in progress and that action towards adaptation and mitigation on a global scale is urgently needed. Scenarios showing possible development paths of climate-relevant parameters like greenhouse gas concentrations, air temperature or precipitation patterns are mainly based on increasingly complex and interconnected modelling approaches. Their reliability in predicting the future is tested by the ability to represent past conditions as accurately as possible (UNEP, 2009). This strategy sometimes is summarised as "the past is the key for the future", referring to the uniformitarianism popularised by Charles Lyell and his *Principles of Geology* (1830-1833), essentially stating that the acting modern natural laws and processes are the same as in the past, or more succinctly: "the present is the key to the past".

Starting point of any direct measurement series relevant in this context of climate change – in the best case – dates back to the 19th century. Therefore, in order to set modern climate-related observations into a long-term perspective, alternative proxy-parameters recorded and stored in various natural archives are needed to reconstruct palaeoclimate and landscape evolution. In mountain areas, highly climate sensitive glacial and periglacial processes are the main agents modulating earth's surface, leaving accumulative and erosive traces. Beyond that, these regions are of special interest because within short horizontal distances they host climatic regimes similar to those of widely separated latitudinal belts (Beniston *et al.*, 1997; Beniston,

2005). The resulting sensitivity to climate changes in combination with preserved landforms bearing witness to ancient climatic conditions constitute mountain areas key regions for observing, reconstructing and finally predicting (the impacts of) climate changes and associated processes leading to characteristic landforms.

The deciphering of such geo-archives requires a temporal assignment. Without dating, we just know that a process creating some kind of landform once took place. Maybe a relative chronology can be established, for instance based on morphostratigraphy, as is the case with moraines. But we will fail when the process happened on a numerical timescale, nor will we be able to treat questions about synchronicity on different spatial scales. Furthermore, the connection to already known climatic events cannot be drawn. For these reasons, the development and refined application of dating techniques is of central importance for landscape evolution and palaeoclimatology studies in general. As each dating technique has its own strengths and weaknesses in respect to resolution, applicability and expense, very often a combination of several suitable dating methods is advisable in order to reach a maximum of both reliability and efficiency.

Over the last decades, newly developed dating methods and the improvement of existing techniques opened a broad field of potential applications and enabled the treatment of an increasing number of scientific questions covering a large temporal range. Landscape evolution studies in general and glacial history in particular experienced substantial progress, mainly due to the advent of numerical dating methods such as surface exposure dating and luminescence. This study focuses on filling remaining gaps in the knowledge about Lateglacial and early Holocene landscape development in mountain areas. A second, methodological part concentrates on the comparison of different dating techniques.

1.1.2 Goals of the study

Three goals for this study can be formulated (all the methods, landforms and processes named here are described in detail in the Chapters 3 and 4):

(1) A contribution to landscape evolution history in three neighbouring areas in eastern Switzerland. In each area we placed the main emphasis on a different landform (see below, Chapter 1.2). Focus is on the Lateglacial and early Holocene time period. This time window following the Last Glacial Maximum (LGM, around 21 ka, Ivy-Ochs *et al*., 2004, see Chapter 3.1) was characterised by a highly unstable climate causing several re-advances of glaciers in

the mountain valleys. The overall trend of ice retreat after the last glacial cycle (the Würmian) was thereby interrupted and complex interactions with periglacial processes such as rock glacier development and soil formation during warmer phases took place.

(2) A combined application of numerical (absolute) and relative dating methods, including surface exposure dating, luminescence dating, radiocarbon dating, the measurement of Schmidt-hammer rebound values and weathering rind thicknesses as well as soil chemical and mineralogical analyses. Wherever possible and meaningful, several techniques were used on one and the same carefully selected landform. Results from other authors were incorporated as far as available. Cross-checking methods allows us to estimate uncertainties and, under ideal circumstances, provides the possibility to calibrate relative methods using results from numerical methods.

(3) A correlation of spectral properties of rock surfaces with their exposure age in the steep rock walls of the south face of Aiguille du Midi in France. The aim was to provide the first step towards a procedure enabling a rough estimation of rock fall history in a homogeneous lithology based on differences of the surface colour, representing the primarily time-dependent degree of weathering. Although the subject area is geographically separated, this study also includes the main aim of this work – a methodological combination - in a landscape historical context.

Points (1) and (2) are not treated separately. However, they constitute two different aspects of discussing landscape evolution. The methodological part (2) is both self-purpose and a means to providing guidance for the interpretation of landform ages derived from different dating methods. Whereas the innovative component of (1) and (2) is the combined application of standardised methods to a set of interconnected landforms (Chapters 1.2.1 and 1.2.2), (3) is a completely new approach (see Chapter 1.2.3).

1.2 Short-description of scientific questions addressed in the different investigation areas

1.2.1 Landscape evolution in the Albula area and in Val Burdun

The Albula area on the western and the Val Burdun on the opposed eastern side of the Upper Engadine (Fig. 2.1) both show a very interesting geomorphological setting with a variety of

partly morphostratigraphically connected glacial and periglacial landforms. These include moraines and glacially polished bedrock at both sites, a relict rock glacier in Val Mulix as part of the Albula area and a rock avalanche deposit in Val Burdun (see chapter 2 for detailed information).

Since the initial work of Penck and Brückner (1901/1909), identification and spatial parallelisation of glacigenic traces in the Alps and the alpine foreland has been based upon morphology, stratigraphy and the estimation of equilibrium line depression values. Later on, basal radiocarbon ages from peat bogs in front of moraines provided first minimum deposition ages. In the last approx. 15-20 years, considerable progress has been made in the assignment of glacial deposits to Lateglacial and early Holocene stadials, to a great extent thanks to the establishment and increasingly improved application of dating techniques using in-situ produced cosmogenic nuclides in rock surfaces (summary for the European Alps in Ivy-Ochs *et al.*, 2008, 2009a). Due to their good preservation and blocky appearance, mostly moraines deposited towards the end of the Lateglacial (during the Younger Dryas) have been dated. For both older (early to mid-Lateglacial) and younger (early Holocene) deposits and erosional features, the database is still sparse.

Another relevant field of interest is the timing of large mass movements (rock avalanches, landslides). With the improvement of dating techniques, the traditional perception of large-scale slope failures as a direct consequence of (Lateglacial) ice retreat has become obsolete. A number of studies report on events that happened in the Holocene, partly with a time lag of several thousand years with respect to the end of the Würmian ice age (e.g. Dapples *et al.*, 2003; Prager *et al.*, 2008). The modern conception to describe the vulnerability of a rock slope to fail comprises *causes* that change the state of a system (the disposition) over time, and *triggers*, factors that lead to the actual start of the movement (e.g. Erismann and Abele, 2001). A mass movement will only occur when all dispositions together with a trigger exceed factors stabilising the rock wall. The disposition model (Bollinger *et al.*, 2000) complements the paraglacial model (Ballantyne, 2002), which is described in more detail in Chapter 3.2.3.

Knowing the date of an event as precisely as possible allows for placing it in a palaeoclimatologic context and thus for estimating potential causes. This in turn may serve to draw parallels with the modern situation with permafrost degradation and increasingly accelerated deglaciation (Kohler and Maselli, 2009), each creating preconditions for dislocation processes potentially hazardous in populated areas.

According to the landforms present, we concentrated on the following focal points:

Greater area of Albulapass (subdivided in Albula area and Val Mulix)

- Providing the first reliable age of a pre-Bølling moraine, namely from the Daun stadial
- Improving the database of exposure ages at high altitudes by dating polished bedrock sites with the aim of highlighting the early Lateglacial breakdown of the pleniglacial ice masses
- Dating a relict rock glacier with cosmogenic nuclides
- Providing direct evidence for the generally accepted but barely proved small glacier length variations during the Holocene by dating a polished rock barrier close to the Little Ice Age (LIA) moraines deposited around 1850
- Applying a set of relative dating techniques with the goal to either cross-check with numerical ages and to examine whether an expansion of the temporal range of application beyond the Holocene is possible with an acceptable resolution
- Inclusion of already available datasets from the region in order to complement the picture

Val Burdun

- Dating of a rock avalanche and of Lateglacial moraines
- Providing direct evidence for the generally accepted but rarely proved small glacier length variations during the Holocene by dating a polished rock barrier close to the Little Ice Age (LIA) moraines deposited around 1850
- Applying a set of relative dating techniques with the goal to either cross-check with numerical ages and to examine whether an expansion of the temporal range of application beyond the Holocene is possible with an acceptable resolution

1.2.2 An attempt to date active rock glaciers using luminescence methods

Rock glaciers are perennially frozen and ice-rich debris on non-glacierised mountain slopes that creep steadily under the influence of gravity (Haeberli *et al*., 2006). Active rock glaciers (i.e., they contain ice and deform) are assumed to have formed and evolved during the Holocene and can thus be seen as transport systems bearing palaeoclimatic information (Frauenfelder *et al*., 2005). Relict forms on lower altitudes have lost their ice content and do not creep anymore. As they initially must have formed under permafrost conditions, they have a considerable potential for constraining former climatic conditions (Ballantyne *et al*., 2009). Thus, dating of such landforms is relevant.

We tried to date three active rock glaciers in the Piz Julier area and in the Val Tschitta (see Fig. 2.1 and 2.6) using optically stimulated luminescence (OSL with quartz, IRSL with feldspars). Some preliminary results from a neighbouring rock glacier already exist (Haeberli *et al*., 2003). However, this is one of the first attempts and certainly has a rather explorative character. Besides a substantiation of already measured and derived rock glacier age estimations using other methods, a main goal shall be an extensive discussion of involved processes potentially acting on the flow path of a single grain and thus influencing measured luminescence ages.

1.2.3 Colour of rock surfaces as age indicators? – A pilot study at Aiguille du Midi (F)

Permafrost thaw is an important process, which affects the stability of steep bedrock slopes in many alpine areas (cf. Haeberli *et al*. 1997, Gruber & Haeberli 2007). Slope failures like rock falls, landslides and debris flows that are assumed to be triggered or at least conditioned by changes in the permafrost distribution are known from numerous locations in high mountains and especially in the Alps (e.g. Noetzli *et al*. 2003, Schiermeier 2003, Gruber *et al*. 2004b). These processes cover magnitudes from small rock falls (Steinschlag) to huge rock slides (Bergsturz). In comparison with debris-covered slopes, steep rock faces react quickly to climate change (Chapter 3). This rapid reaction, together with the effect of destabilisation, make rock fall due to permafrost degradation a likely and well perceivable impact of climate change in the present and also in the near future (Gruber et al. 2004b).

While recent advances in permafrost modelling have enabled the derivation of permafrost maps for steep bedrock (Gruber et al. 2004a), information about long-term rock fall activity is required to put recent observations and changes in temperature into a long-term perspective. Aim of this pilot study is thus to investigate the potential of combined imaging spectrometry and exposure dating to derive approximate surface ages in steep bedrock walls of homogeneous lithology. Exposure ages from polished bedrock (indicating deglaciation at higher altitudes) or from areas that were not glaciated during Last Glacial Maximum are sparse so far.

Remote sensing techniques with multispectral and hyperspectral sensors are widely used to investigate different aspects of mountain areas. Kääb *et al*. (2005) provide an overview of air- and spaceborn remote sensing methods, which are applicable for glacier and permafrost hazard assessment and disaster management. Other approaches discuss methodologies for mapping glacio-geological features such as trim lines or terminal moraines in order to reconstruct glacier changes and related past climate (e.g. Huh *et al*. 2006). Spectral field measurements and airborn

hyperspectral data have enabled an approach to date and map other geomorphic features such as arid and semi-arid alluvial fans (Crouvi *et al*. 2006). The development of a rock coating significantly influences the overall reflectance of the surface. The redness of rock material or soil is directly related to the age. In oxidising environments and with increasing weathering time, colour hues become redder and chromas become brighter (rubification). This fact is, among others, used in the calculation of the profile development index, which gives a direct indication of soil age (e.g. Harden, 1982; Goodman *et al*., 2001).

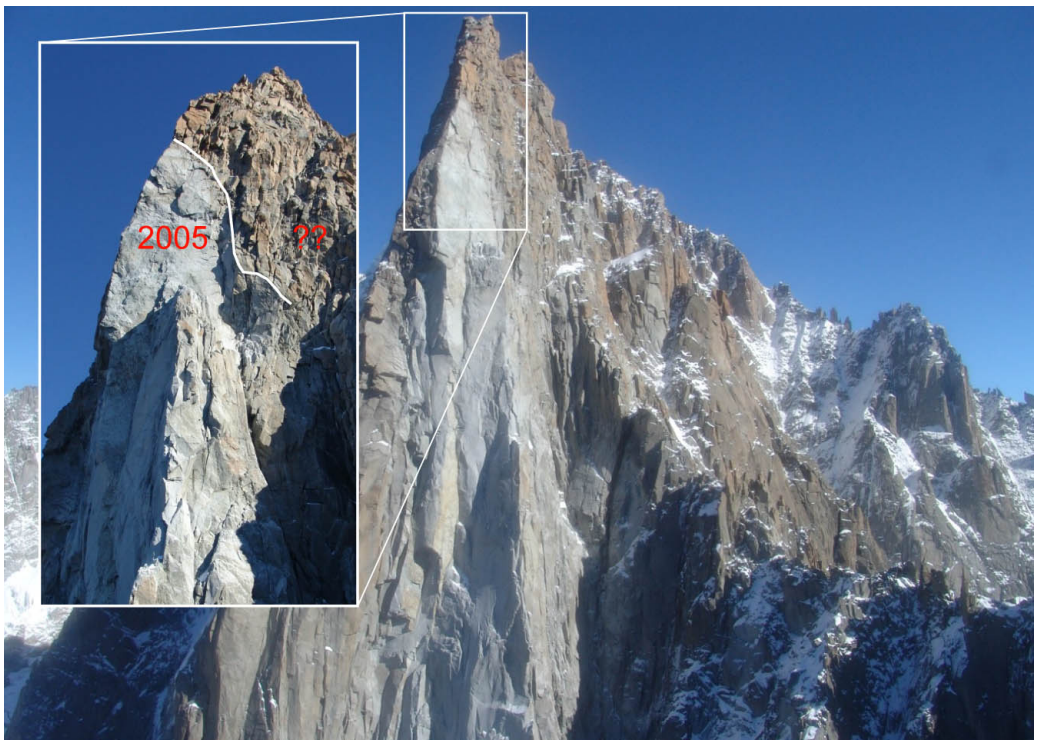

Fig. 1.1 The Drus in the French Alps near the investigation site. The rock fall at Pilier Bonatti occurred in 2005 with an approx. volume of 250000 m^3 (indicated by the white area). The blow-up shows the grey, freshly exposed rock nicely against the older, reddish surface with an unknown exposure age (Fotos: S. Gruber).

The geometric and radiometric correction of hyperspectral imagery over steep terrain is challenging but generally possible (cf. Gruber *et al*. 2003). The spatial data fields of estimated age resulting from this method would permit deriving the area and relative frequency of surfaces that belong to a certain age class and that are uninterrupted by older surfaces over a certain distance. This information is related to the frequency of rock fall events during a certain period and is a useful long-term background for assessing whether presently observable large rock fall shows an unusual abundance as suggested by the relevance of permafrost for slope stability.

Our hypothesis is that the surface ages in this high alpine region can be directly related to the redness of the rocks. The redder a rock surface is, the higher the age that should be measured.

Chapter 2

Description of investigation areas and sampling sites

As this study deals with different landforms that are spatially and genetically interconnected, it makes sense to describe the investigated areas in all the relevant details. On one hand, this chapter provides a macroscale insight into the geographical characteristics and the geological properties in general. On the other hand, detailed information about the geomorphological setting on a more local scale and the localisation and description of the sampling sites is provided. For the Aiguille du Midi study area, both parts are combined in Chapter 2.5. Place names and tournaments are given as they can be found in the official topographical map (Swisstopo LK25). In case of eastern Switzerland these are partly Romansh expressions like "Val" (valley) or "Piz" (Mountain). For the Aiguille du Midi site, the corresponding French names are used. Some of them are translated or shortly explained when they occur for the first time in the following chapters.

2.1 Investigation areas in eastern Switzerland – Overview

There are two main investigation areas: (1) the greater area of the Albulapass together with two tributary valleys of the nearby Upper Engadine in eastern Switzerland, the Val Burdun and the Piz Julier region and (2) the Aiguille du Midi which is part of the high Alpine area of the Mont Blanc massif near Chamonix in eastern France. Fig. 2.1 provides an overview. In the following, the greater area of the Albulapass will be subdivided into the Val Mulix and the Albula area. More detailed overviews of each area are given in the Figures 2.5 and 2.6 (greater area of Albulapass) as well as in Figures 2.7 and 2.8 (Val Burdun).

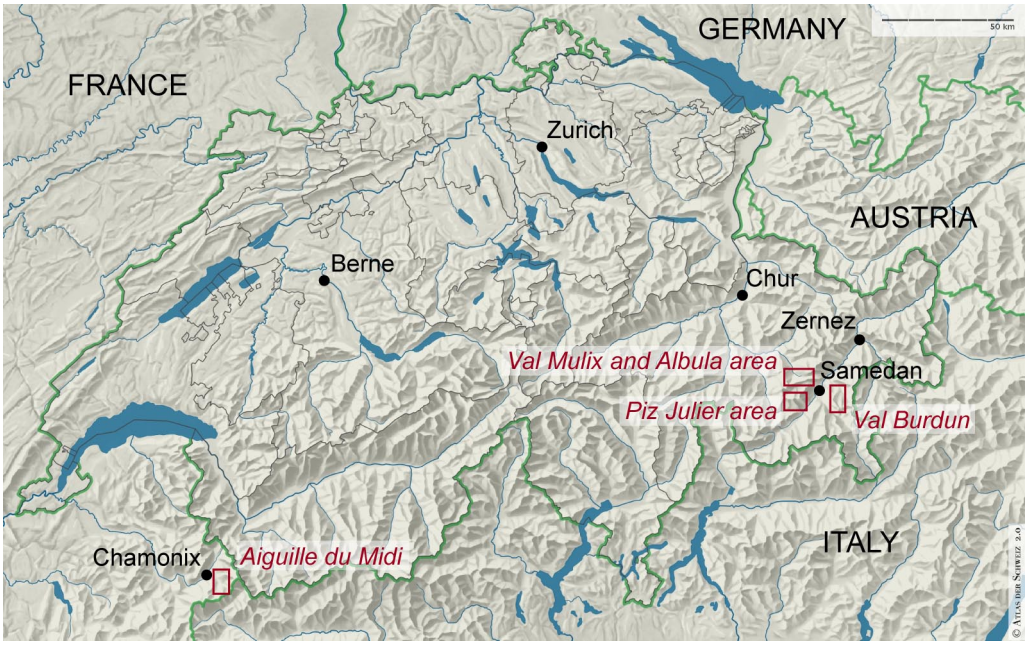

Fig. 2.1 Map of Switzerland and surrounding countries with the investigation areas in eastern France and eastern Switzerland given in red (source: Atlas der Schweiz (AdS), 2004).

2.1.1 Climate

The Upper Engadine is a typical inneralpine dry valley and the investigation areas receive comparably small amounts of precipitation. Characteristic mean annual precipitation values (MAAP, 1971-1990, AdS) in the greater area of Albulapass range from 900-1000 mm/year, whereas the Piz Julier area is a bit more humid with 1100 mm/year, very similar to the Val Burdun (reference values: northern foreland: 1250 mm/year, northern border of the Alps: 2000 mm/year, MeteoSchweiz, 2010). Compared to average precipitation amounts measured at individual weather stations (MeteoSchweiz, 2010) near the investigation areas, the values given here seem rather low. Mean annual air temperatures (MAAT, values from 1961-1990, AdS, Schwarb *et al.*, 2000) are low with slightly more than 0°C in St. Moritz, which is in the main valley of the Upper Engadine at about 1800 m. MAAT values in the investigation areas are between -1 and -4°C, mainly depending on the altitude of the sampling spots.

Although mountain peaks often reach altitudes of 3000 m and more, the three investigation areas are only marginally glacierised. Little glaciers can be found on the east side of Piz Julier and on the north side of Piz Laviner at the end of Val Mulix (Maisch *et al.*, 2000). The latter one is completely debris covered. However, the cold and dry climate provides favourable conditions for permafrost and rock glacier development and numerous exemplars of all activity stages are present in the investigation areas. Some of them – the most prominent

example is the rock glacier Murtèl (just outside the investigation area of this study) – are subject to intensive research work, which is commented on in more detail in Chapters 2.4 and 3.2.2.

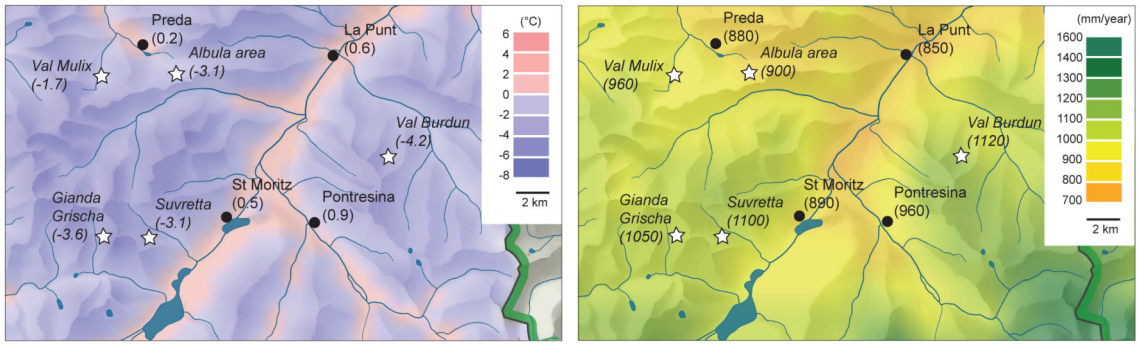

Fig. 2.2 MAAT (1961-1990) and MAAP (1971-1990) in the investigation areas as indicated by stars (in about 2000 m a.s.l.). In each case a corresponding temperature and precipitation value, respectively, is given. Gianda Grischa together with Suvretta represent the Piz Julier area (based on maps derived from AdS, 2004). Compared to station values (MeteoSchweiz, 2010), the amounts of precipitation shown here are somewhat lower, especially in the greater area of Albulapass northwest of the Engadine.

2.1.2 Geology

The European Alps record the closure of ocean basins located in the Mediterranean region during convergence of the African and European plates (Schmid *et al.*, 2004 and references therein). Major palaeogeographical domains and tectonic units of the Alps referring to the palaeogeographical situation in the Late Cretaceous are:

(1) the Dauphinois-Helveticum north of the Alpine Tethys;

(2) the Penninicum made up of slivers detached from (a) subducted European lithosphere, (b) the Valais ocean, (c) the Briançonnais ribbon continent of the Western Alps and (d) the Piedmont-Liguria ocean;

(3) the Southern Alps and

(4) the Austroalpine nappe system, (3) and (4) being south of the Alpine Tethys (Schmid *et al.*, 2004; Pfiffner, 2009).

All investigation areas are within the Austroalpine nappes, which are the uppermost units of the nappe stack making up the Alps. Palaeotectonically speaking, these units consist of African material (e.g. Pfiffner, 2009). The Autroalpine nappes overlie the Penninic units. This is very clearly expressed by tectonical windows such as the Engadine window in the Lower Engadine, where (north-penninic) Bündnerschiefer and ophiolites are surrounded and overthrusted by rock material of the Austroalpine Silvretta nappe (Schmid *et al.*, 2004; Spicher, 1980).

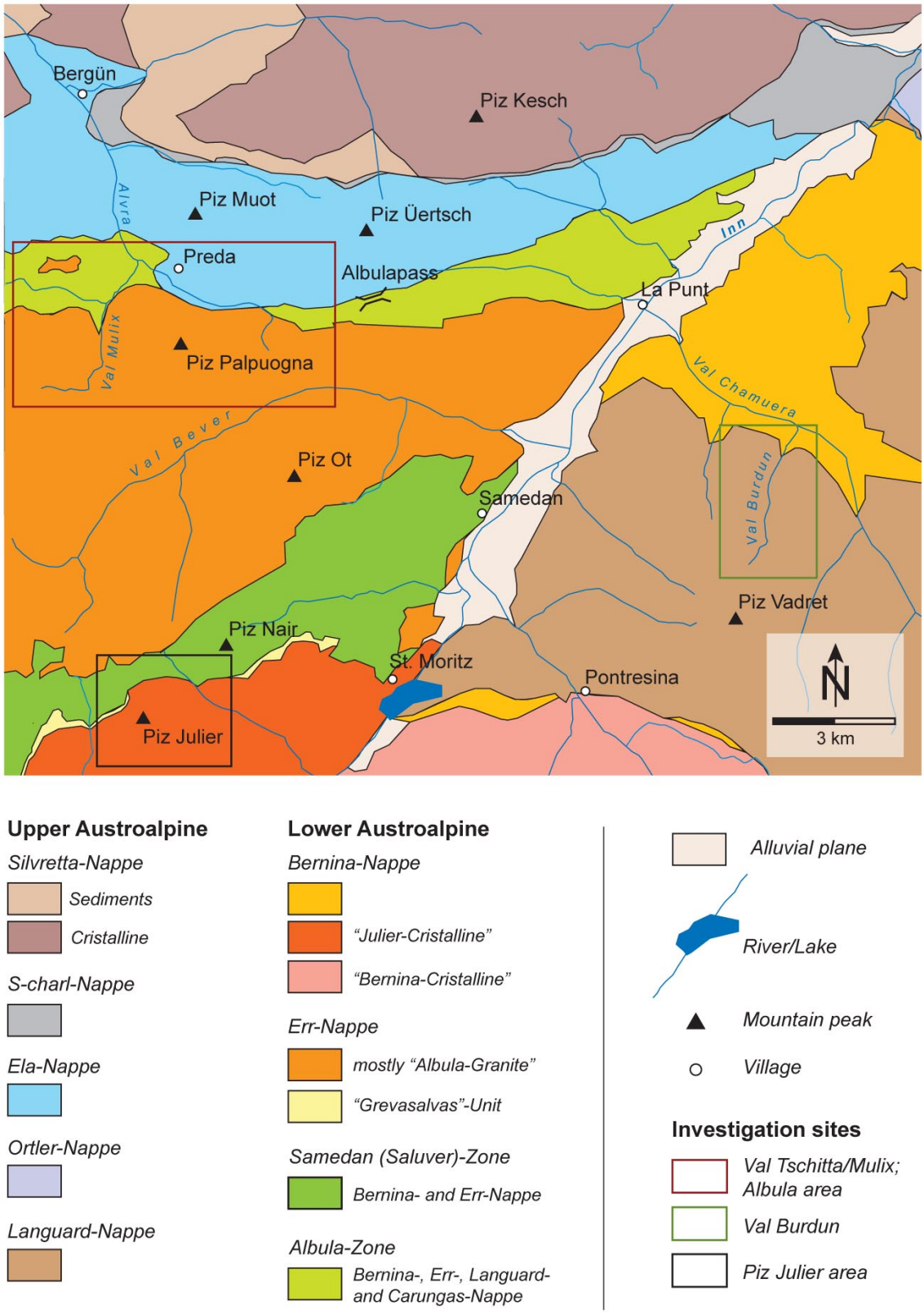

Fig. 2.3 Tectonic map of the investigation areas. The greater Albulapass area and the Piz Julier area are both part of the Lower Austroalpine and consist of Albula-granite and the very similar Julier-granite, respectively. Val Burdun is situated in the crystalline part of the Silvretta nappe, which belongs to the Upper Austroalpine (redrawn and simplified from Bearth, Heierli and Roesli, 1987).

As shown in Fig. 2.3, the greater Albula area and the Piz Julier area are situated in the Err nappe and in the Bernina nappe, respectively. Both belong to the Lower Austroalpine. The Err-Julier-group was already studied and described thoroughly by Cornelius (1929, 1935, 1950). The Val Mulix and the Albula area are strongly dominated by Palaeozoic granites and granodiorites, summarised as "Albula-Granite". The Albula-Granite provides the source material for all samples taken in this area. Mesozoic sedimentary rocks are sparse (Bearth *et al.*, 1987) and their influence to parent material chemistry is negligible. North to the Err nappe the mixed Albula zone follows, leading to the transition from the Lower of the Upper Austroalpine, namely to the sedimentary Ela nappe. Prominent mountains in the Ela nappe sloping down to the spacious high plane of the Albulapass are the Piz Üertsch (dolomite) and the Piz Blaisun (schist). The southern margin of the Albula zone is overrun by active rock glaciers (Maisch, 1981; Compeer, 2009) and Lateglacial moraine systems assigned to the Egesen stadial (Maisch, 1981), both originating from the north slope of the ridge stretching from the Dschimels (twins) in the west to the Crasta Mora (black ridge) in the east. The mixed zone itself consists of various sedimentary rocks and is described in detail by Heierli (1955).

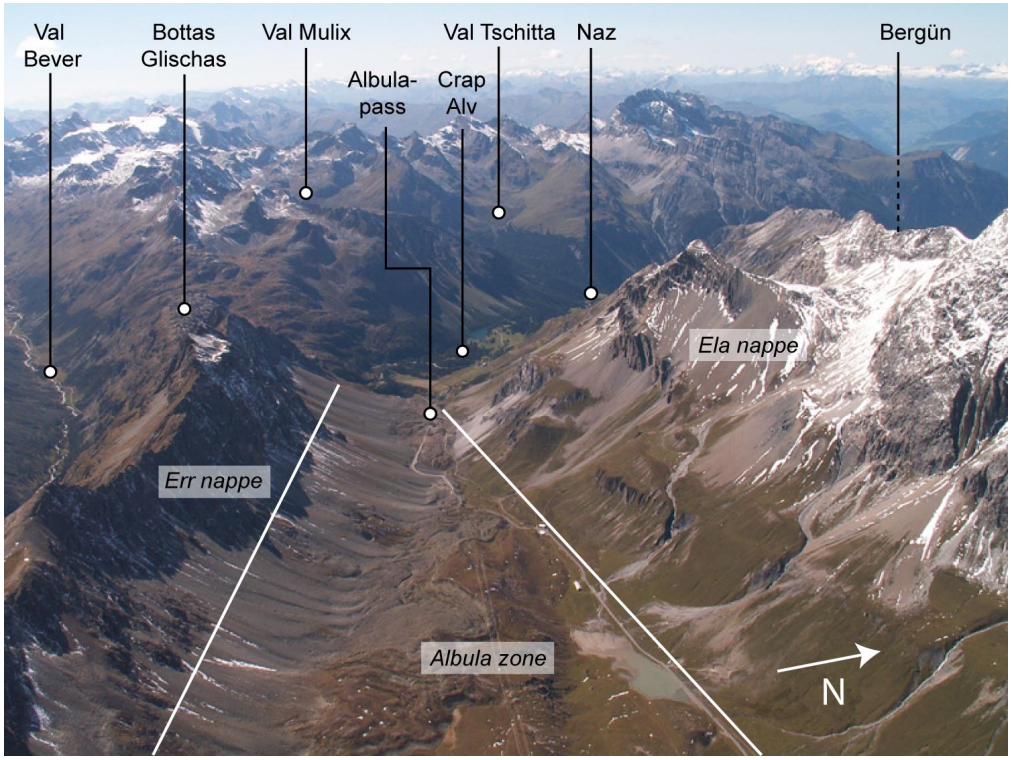

Fig. 2.4 View from east to west over the high plane of the Albulapass. Important locations are highlighted with white dots (see also Fig. 2.6) and the main tectonical units are given in italics. Fault lines are approximated with white lines. Moraine sequences and rock glaciers coming from the left side are clearly visible (Foto: C. Rothenbühler).

In the Julier area the "Julier-Granite" is the main constituent, showing a composition comparable to that of the Albula-Granite, though the grain size is slightly smaller. Both rock glaciers investigated here are composed of Julier-Granite. A characteristic property of both granites is their greenish colour that originates from plagioclase components, making erratics of this rock type reliable tools to reconstruct ancient glacier flow paths.

The Val Burdun lies within the crystalline part of the Upper Austroalpine Languard nappe. At the junction with the Val Chamuera, parts of the Bernina nappe (Lower Austroalpine) are touched. The analysed moraine and rock avalanche deposits, however, are consistently of the same quartz- and biotite-rich mineralogical composition and originate from the NE-slope of the Crasta Burdun and the NW-slope of the ridge between pt. 2918 and pt. 2870 (Fig. 2.7). The rock type can be described as an early-Palaeocene granite with a weak metamorphic overprint (Peters, 2005). Whereas the quartz and feldspar components have a massy to slightly porphyric texture, biotite minerals show a preferential orientation, providing non-optimal conditions for Schmidt-hammer and weathering rind thickness measurements.

2.1.3 Vegetation

The calcaerous south facing slopes of the Val Tschitta (Fig. 2.3, 2.6) are covered almost entirely with *Pinus cembra*. Towards the Val Mulix with siliceous parent material, *Larix decidua* becomes more important. Above the timberline dwarf-shrubs, mostly Ericaceae, and alpine grassland are characteristic.

At the roche moutonnée Crap Alv *Pinus mugo* is typical, together with dwarf-shrubs, especially *Juniperus communis* var. *saxatilis*. At Crap Alv Laiets alpine grassland and dwarf-shrubs dominate; the timberline is some 150 m below this site. Vegetation is almost absent at Bottas Glischas. Only areas between roche moutonnées with fine-grained sediment are covered with alpine grass.

In the Val Burdun *Larix decidua* can be found on the lower part of the lower moraine. All other sampling spots show a coverage with dwarf-shrubs and grass (moraines) or no vegetation at all (rock avalanche).

2.2 Val Mulix and Albula area

2.2.1 Previous studies

A number of studies have already been performed in and around the investigated region. Jäckli (1957) mentioned the rock glaciers ("Blockströme") around Piz Salteras and Piz Üertsch and discussed possible processes participating in their genesis. He defined the creeping forms between the active rock glaciers and Egesen moraines (Maisch, 1981) south of the Albulapass as "Blockgirlanden". This situation is very morphologically reminiscent of the "Larstig Flur" as described by Heuberger (1966) in the Austrian Alps. Today these form assemblages most probably would be described as initial stages of rock glaciers (protalus ramparts).

Geomorphological mapping was carried out by Maisch (1981) based on moraine morphology, their morphostratigraphic position and ELA depression values relative to the 1850 glacier extent. Palynological analyses and ^{14}C-datings of the lowermost organic layer in a peat bog just beside the roche moutonnée at Crap Alv were also made (by C. Burga in M. Maisch, 1981). This work serves as a basis for the present study. Assignment of moraines in our study area to a given stadial (such as Egesen and Daun) in Fig. 2.6 are derived from these findings and should therefore be understood as a working hypothesis. A scheme of the Lateglacial stadials can be found in Chapter 3.1.2 Suter (1981) mapped the neighbouring area to the south (Val Bever), including the Piz Julier area.

Ivy-Ochs *et al*. (1996) dated the Egesen moraine complex and a relict rock glacier at the nearby situated Julierpass using the cosmogenic isotopes ^{10}Be, ^{26}Al and ^{36}Cl. The reconstructed LGM ice surface geometry based on glaciomorphic mapping shows that the area was situated near the "Engadine ice dome" culminating in the Upper Engadine. Trimline and other erosional features indicate that during the LGM the Albulapass formed a transfluence with ice flowing from the Engadine into the Rhine river system (Florineth, 1998; Florineth and Schlüchter, 2000). Laustela (2003) and Laustela *et al*. (2003) applied weathering rind thickness measurements to date the active granitic rock glaciers in the NE-slopes of Piz Salteras and Piz Bleis Marscha as well as around the Piz Julier. This data was partly used by Frauenfelder *et al*. (2005) to combine it with other relative (Schmidt-hammer) and semi-quantitative dating methods (photogrammetric streamline interpolations). Chapter 2.4 describes the investigations of the rock glaciers in more detail with respect to the luminescence datings carried out in this study. Compeer (2009) provided a complementary work with Schmidt-hammer and weathering rind thickness measurements on the rock glaciers north of the ridge Crasta Mora – Bottas

Glischas and soil physical/chemical investigations on the Egesen moraine Crap Alv. Kneisel *et al*. (2000) and Kneisel and Schwindt (2008) report on a peculiarity in the Val Bever: they found a sporadic permafrost occurrence below the timberline by means of geophysical soundings.

2.2.2 Geomorphological setting and description of the sampled sites

In Val Mulix, numerous landforms from the Lateglacial and the early Holocene time period can be found (Fig. 2.5, 2.6), indicating a high glacial and periglacial activity during this time period. The hamlet Naz is situated in between of several moraine fragments that together clearly represent a terminal glacier position. With an ELA depression value of 345 m they are attributable to the Daun stadial, based on the classification of Maisch (1981). Other Daun moraines are located on the southern slope of Val Tschitta and at the former confluence point of Val Tschitta and the Val Mulix glacier. A boulder on this latter moraine was sampled for exposure dating (VM7) and soils (S1). This moraine is strongly vegetated (dwarf-shrubs and pines) and shows well-developed soil formation. Boulders are almost completely absent here.

The well preserved moraines in the Val Tschitta and the Val Mulix, believed to be Egesen equivalents, show ELA depression values of ~220 and ~230m, respectively. Generally, the moraines in this area are well preserved. The Egesen I terminal moraine is sharp-crested; however, block sizes are small (diameters of approx. ≤ 80 cm) and no boulder acceptable for exposure dating could be found. The lateral moraines (upper and lower Egesen I) are less blocky and soil development stages are more advanced. Boulders on top of the moraine crests are rather sparse. The huge upper Egesen I moraine slopes down several hundred meters (from 2300 m a.s.l. to 2100 m a.s.l.) to the valley bottom of Val Mulix. The lower Egesen I moraine is less pronounced but still clearly identifiable as a distinct moraine. On its lower part, this moraine is strongly subjected to slope creeping processes. This is not the case for the part where it was sampled for exposure dating and soil analyses (S3).

A very blocky moraine about 1 km further upvalley in Val Mulix with an ELA depression of 125 m can be classified as Egesen II or as Bocktentälli substadial, according to the local nomenclature in this area (Maisch, 1981). The moraine is sharp-crested and consists of coarse blocks. As this moraine was deposited in a flat area, post depositional processes leading to moraine degradation can be ruled out with a high certainty. Samples for exposure dating were taken on the upper (VM1) and the lower Egesen I moraine (VM4), and on the Egesen II moraine two suitable boulders were found (VM6, VM11) (Fig. 2.5 D, E; 2.6).

Fig. 2.5 Geomorphologic setting and sampling sites in the Albula area (A-C) and the Val Mulix (D-F). (A) View from the roche moutonnée Crap Alv upwards to Crap Alv Laiets and the transfluence Bottas Glischas; (B) shows the situation seen from Bottas Glischas (the picture was taken approx. at the location of Alb9 in C); The transfluence situation Bottas Glischas with the LGM ice flow direction, indicated by the bold arrow; (D) Summarising overview of the orographic right side of the Val Mulix, seen from Sur la Crappa; (E) The same situation again, this time from the middle part of the Val Tschitta. In the foreground the Daun moraine is marked; (F) The rock barrier Sur la Crappa and the area of the LIA glaciation.

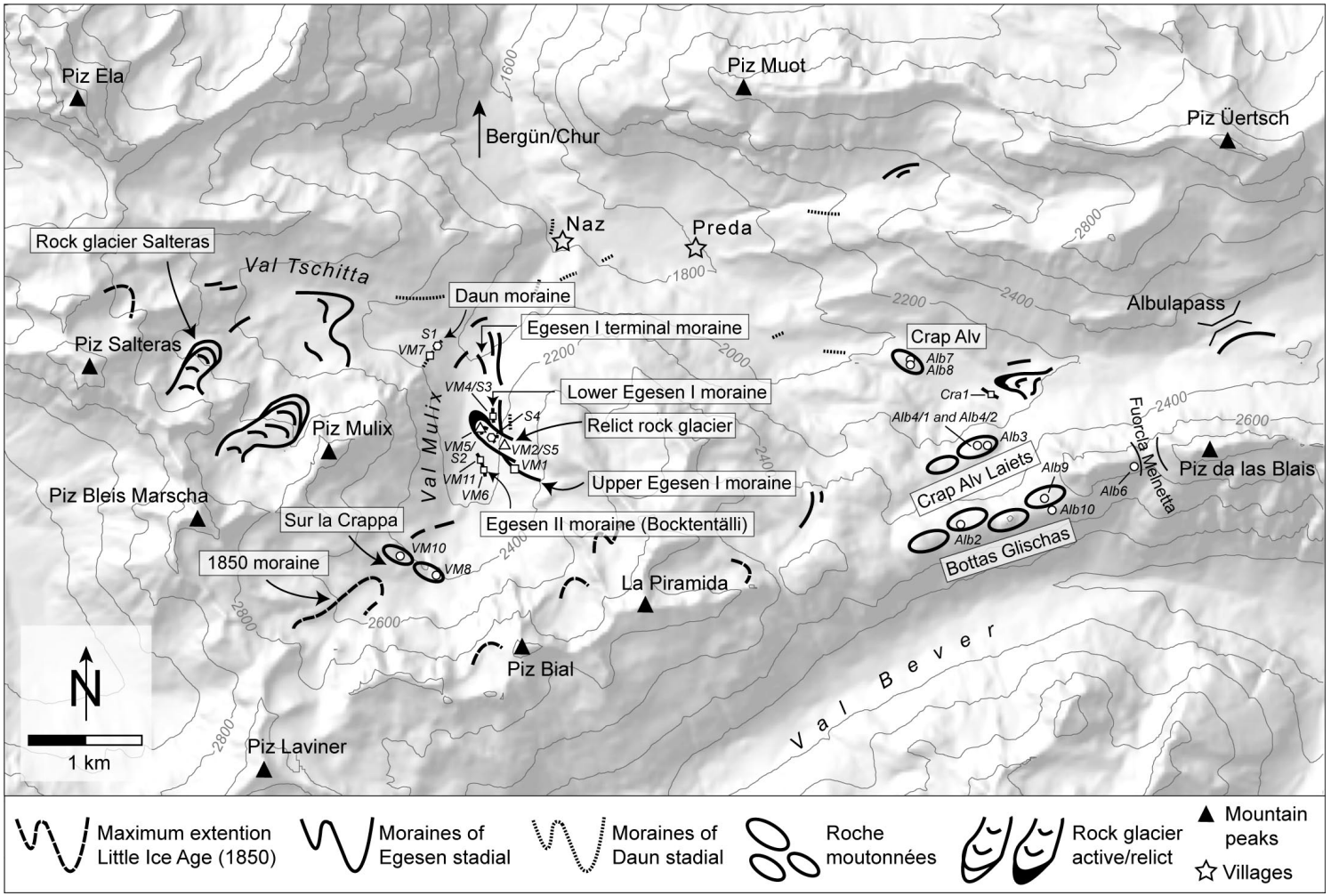

Fig. 2.6 Map of the Val Mulix and the Albula region. Names of sampling sites are given in white frames and, in the case of moraines, rely on findings of the gemorphologic map by Maisch (1981). Sampling codes from ^{10}Be-samples (VM, Alb) and soil profiles (S) are included in order to ease readability (background derived from DHM25, swisstopo).

Weathering rinds were measured on the upper Egesen I and on the Egesen II moraine. Schmidt-hammer rebound values were recorded additionally on the Egesen I terminal moraine and on the 1850 moraine.

Very remarkable from a morphostratigraphic point of view is the morphological situation on the orographically right side of the Val Mulix (see Fig. 2.5 D, E). Here, clearly after the retreat of the main ice body, a debris mass, obviously dammed behind the lateral moraine, began to move downhill – most probably under permafrost conditions – thereby creating a breach into the Egesen I moraine. This nice morphologic discontinuity makes it clear that the rock glacier must be younger than the Egesen I stage. Maisch (1981) suggests the main activity phase occurred simultaneously to the Egesen II advance. The rock glacier tongue indicates the highest possible position of the 2°C isotherm at that time, some 400 m lower than today (Haeberli, 1982). At least at an initial stage, the source material could have been provided mainly by an above deposited and deformed Daun moraine and the Egesen I moraine itself. Later on, an additional debris supply from the headwall must be assumed, otherwise the formation of an almost 700 m long rock glacier does not seem possible. According to the terminology of Frauenfelder (2005), this rock glacier can be characterized as a mixed 'moraine-derived' and 'talus-derived' form. Schmidt-hammer and weathering rind measurements were carried out in the uppermost, the middle and in the lowermost part near the front of the rock glacier. At the same localities, material for soil analyses was removed (S5, S4 and S2). Samples for exposure dating were taken in the uppermost (VM2) and the lowermost part (VM5) (Fig. 2.5 D, E; 2.6).

In the basin of Val Mulix, a barrier of glacially polished bedrock (Sur la Crappa) divides the valley into two distinct elevation levels: one at 2400 m a.s.l. and one at 2200 m a.s.l.. Here Schmidt-hammer and exposure dating (VM8, VM10) were applied (Fig. 2.5 F; 2.6).

The area near Albulapass is characterised by three distinct elevation levels of polished bedrock, namely at Bottas Glischas, Crap Alv Laiets and Crap Alv in approx. 2600, 2300 and 2000 m a.s.l., respectively (Fig. 2.5 A, B, C; 2.6). Bottas Glischas is a well-pronounced transfluence saddle near the trimline (Fig. 2.5 C). Traces of glacial erosion and plucking processes show clearly the LGM ice flow direction from the Val Bever to the north. We chose this site as it is particularly suitable for highlighting the timing of the LGM ice dome breakdown and the following separation into a more topography dominated ice flow system.

Results of Maisch (1981) show that the roche moutonnée at Crap Alv (Fig. 2.5 A, B) was most probably ice-free already during the Allerød interstadial or at least towards its end. Accordingly, the roche moutonée can be positioned within the former tongue area of the Daun glaciation. In order to assure this hypothesis, a boulder for surface exposure dating was sampled on a pre-located moraine deposited by a slope glacier, most probably during the Egesen stadial (sample Cra1) (Maisch, 1981). Both Schmidt-hammer measurements and exposure dating using ^{10}Be were applied on all three elevation levels (sample code Alb, see Fig. 2.6 and Table 2.1). Considering the potential influence of aspect on the early Lateglacial ice melt-down, sample Alb10 was taken on the south slope of Bottas Glischas some hundred meters below the highest transfluence point. An additional sample (Alb6) for surface exposure dating was taken at the nearby Fuorcla Melnetta (Fig. 2.5 C, 2.6).

Table 2.1 Summarising overview of applied methods in the Albula area and the Val Mulix, together with sample codes and information on sampling and measuring localities. SED = surface exposure dating.

Method	Sample Code	AMS Code	Localities	Altitude (m a.s.l.)
SED using ^{10}Be	VM 1	Mulix I ZB5787	Upper Egesen I moraine	2320
SED using ^{10}Be	VM 2	Mulix II ZB5578	Relict rockglacier, lobe in the uppermost part	2280
SED using ^{10}Be	VM 4	Mulix IV ZB5579	Lower Egesen I moraine	2150
SED using ^{10}Be	VM 5	Mulix V ZB5580	Relict rockglacier, lobe near terminus	2080
SED using ^{10}Be	VM 6	Mulix VI ZB5581	Egesen II moraine (Bocktentälli)	2145
SED using ^{10}Be	VM 7	Mulix VII ZB5788	Daun moraine	2120
SED using ^{10}Be	VM 8	Mulix VIII ZB7156	Sur la Crappa, polished bedrock	2423
SED using ^{10}Be	VM 10	Mulix X ZB6321	Sur la Crappa, polished bedrock	2460
SED using ^{10}Be	VM 11	Mulix XI ZB7157	Egesen II moraine (Bocktentälli)	2145
SED using ^{10}Be	Alb2	Alb II ZB5944	Bottas Glischas, polished bedrock	2570
SED using ^{10}Be	Alb 3	Alb III ZB5945	Crap Alv Laiets, polished bedrock	2325
SED using ^{10}Be	Alb 4/1	Alb IV/I ZB5946	Crap Alv Laiets, polished bedrock	2320
SED using ^{10}Be	Alb 4/2	Alb IV/II ZB5948	Crap Alv Laiets, polished bedrock	2320
SED using ^{10}Be	Alb 6	Alb VI ZB7158	Fuorcla Melnetta	2680
SED using ^{10}Be	Alb 7	Alb VII ZB5949	Crap Alv, polished bedrock	2060
SED using ^{10}Be	Alb 8	Alb VIII ZB5950	Crap Alv, polished bedrock	2070

Method	Sample Code	AMS Code	Localities	Altitude (m a.s.l.)
SED using ^{10}Be	Alb 9	Alb IX ZB7159	Bottas Glischas, polished bedrock Highest point	2607
SED using ^{10}Be	Alb 10	Alb X ZB7160	Bottas Glischas, polished bedrock Uppermost S-slope	2585
SED using ^{10}Be	Cra1	Crap Alv ZB7223	Crap Alv moraine (Compeer, 2009)	2055
Schmidt-hammer	—	—	All polished bedrock sites; Relict rockglacier at all three elevation levels; Upper Egesen I moraine; Egesen II moraine (Bocktentälli); Egesen I terminal moraine; 1850 moraine	—
Weathering rinds	—	—	Relict rockglacier at all three elevation sites; Upper Egesen I moraine; Egesen II moraine (Bocktentälli)	—
Soil analyses	S1 and S3	—	Daun moraine and lower Egesen I moraine, respectively	2100 2150
Soil analyses	S2, S4-S5	—	Lobes in the lower, middle and upper part of the relict rockglacier	2060 2130 2280

2.3 Val Burdun

The Val Burdun is a very remote area, difficult to access. A spatial partitioning of the valley can be done as follows: a relatively steep part starts from 1940 m at the valley entry up to approx. 2280 m, where the valley length profile changes into a flat middle part with an extension of c. 1.5 km, reaching up to 2500 m. Southwards a steep rock barrier characterised by polished bedrock follows, leading at 2700 m again into a flatter region with several small lakes and finally steepening towards a nameless 3169 m high mountain peak, some 250 m SSE to Il Corn (Fig. 2.7). This setting is very similar to the situation in Val Mulix. Looking from the region around 2500 m SE-wards the slope is getting continuously steeper – shortly interrupted by a terrace-like space between 2560 m and 2640 m – ending in vertical rock walls that lead to the ridge between pt. 2918 m and pt. 2870 m. This niche is the starting zone of a coarse-grained debris mass, covering the valley bottom of the Val Burdun over a length of approx. 1.8 km. This deposit is certainly the most eye-catching geomorphic feature in this area. Following the classification scheme of Hungr *et al*. (2001), it should most likely be described as a rock avalanche. The rock fragments it consists of reach heights of >3 metres. The volume can be estimated at 600,000 to 800,000 m^3, based on a mean thickness assumed to be 2 to 3 metres and an approximate area of 270,000 m^2. Unlike in the upper steep part, the boulders in the flat part

of Val Burdun are mostly separated and not stacked anymore. Striking is the fact that this rock avalanche is framed very nicely by Lateglacial moraines (Fig. 2.7; 2.8 B). Structure and position of the rock avalanche within the gently sloping valley surrounded by moraines led Beer (2005) to the assumption that it was originally deposited on and afterwards transported by the still active glacier towards the end of the Younger Dryas. Analysing this assumption and evaluating connected potential trigger factors of the rock avalanche are subgoals of this study. Therefore samples for surface exposure dating were taken in the upper (VB4), the middle (VB9) and the lower part (VB10) of the rock avalanche to exclude a potential age gradient from the top to the frontal zone of this particular debris accumulation. All sampled boulders were flat-topped and at least 1.5 m high, more likely exceeding 2 m.

Also Schmidt-hammer and weathering rind thickness measurements were carried out in all three parts of the rock avalanche. In order to embed this event into a broader context of landscape evolution, additional ^{10}Be samples were also analysed from the rock barrier (bedrock, VB1) and from the upper moraines (VB5, VB6) and the lower moraine (VB7, VB12) (see below). All sampling sites are shown in Fig. 2.7 and summarised in Table 2.2.

Beer (2005), who designed the geomorphological map of this area, did not calculate ELA depression values for the evident glacier stages. Moraine names suggesting a supra-regional classification are therefore not used here. Moraines of at least three glacial sub-stages can be differentiated on the orographic right side of the rock glacier. The youngest moraine starts near the terrace already mentioned, which is occupied by an active rock glacier and, following to the north, by a protalus rampart. Especially in the upper part, this moraine is strongly influenced by creep phenomena, making it unsuitable for surface exposure dating. Besides solifluction lobes not necessarily connected to permafrost above the morainic ridge, ground moraine material and the lateral moraine itself seem to have crept downslope, creating large-scale creeping phenomena (Fig. 2.7; 2.8, C).

These creep phenomena most likely formed soon after glacier retreat but still under permafrost conditions, possibly when ice cores were preserved, allowing the moraine material to deform plastically under the influence of gravity. Following the moraine downvalley, it becomes more distinct and a boulder large enough for surface exposure dating was found (VB6).

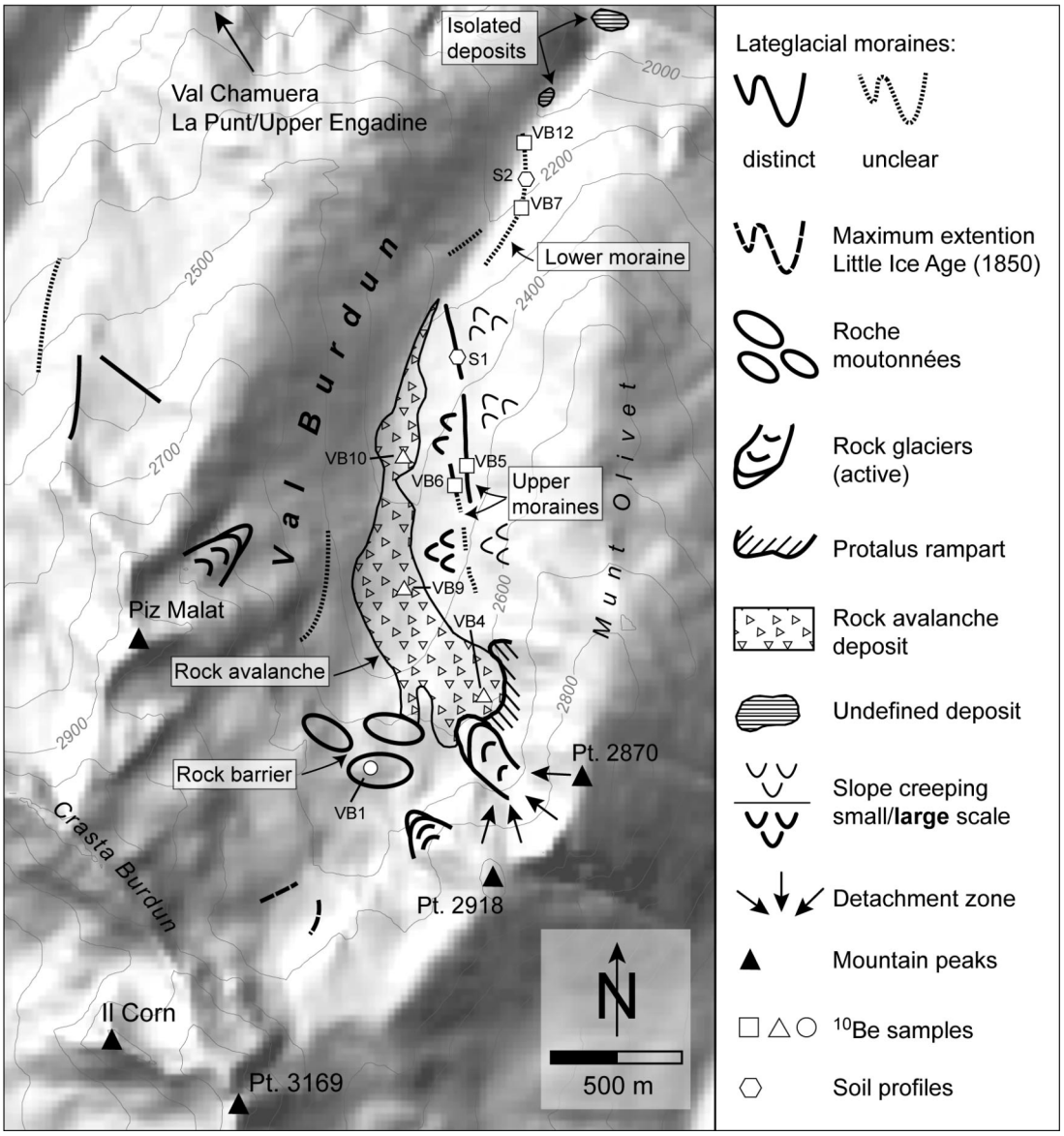

Fig. 2.7 Overview map of geomorphic features and sampling spots in the Val Burdun. Geomorphology is slightly modified after Beer (2005). VB codes refer to SED-samples, S codes to soil profiles. Locality names are given in white frames (background derived from DHM25, swisstopo).

Here, a second moraine becomes visible on a slightly higher level. This higher moraine descends to its end position near 2300 m, coinciding with the transition to the steeper part of the valley. Another boulder was sampled at this position (VB5), and, approx. 100 m lower after a short interruption of the moraine ridge, a soil profile was dug (S1). Both boulders (VB5, VB6) were found right on the top of the moraine ridge; however, they were rather small (heights of ≤ 1 m). To keep things simple, in the following these two moraines are summarised and referred to as the "upper moraines", divided in a higher (with VB5 and S1) and a lower level (with VB6,

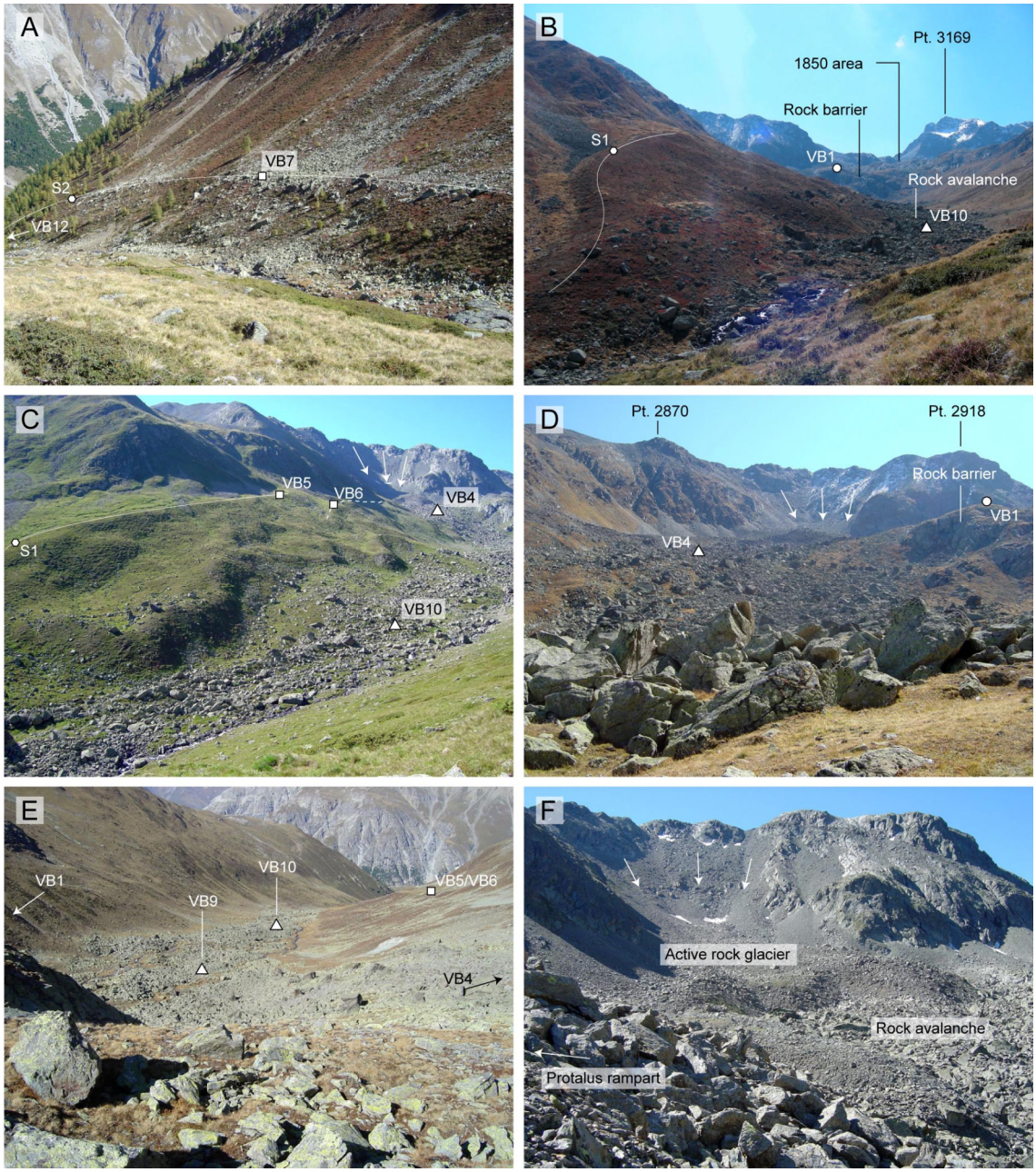

Fig. 2.8 Overview of geomorphologic setting and sampling sites in the Val Burdun. (A) The lower moraine in the steeper part of the Val Burdun; (B) View towards the valley cirque with the upper moraine (higher level), the lower part of the rock avalanche deposit and the rock barrier; (C) View from the orographic left valley side. Both solifluction lobes above the moraine (white line) and large scale creeping phenomena below the moraine are clearly visible. The lower level of the upper moraine with the site VB6 is less pronounced and represented by a dashed line. The detachment zone of the rock avalanche is indicated with arrows; (D) Middle and upper part of the rock avalanche with starting zone; (E) View down the Val Burdun from the rock barrier towards the Val Chamuera; (F) Area near the starting zone with the active rock glacier occupying the niche and overrunning the uppermost part of the rock avalanche.

see Fig. 2.7; 2.8 C). Both moraines are not very blocky and are completely covered with dwarf shrubs and alpine grass.

Leaving the flat part of Val Burdun, still on the orographic right side, another moraine-like deposit is identifiable, reaching from about 2250 m down to near 2100 m (Fig. 2.8, A). This "lower moraine" is very blocky but shows no well-developed ridge on its whole length and describes in its upper part no characteristic curve, as one would expect at this position near the terminus. As backfilled debris material coming from the above slope and nearby slope-creeping processes suggest, this part of the moraine has most likely experienced a certain en bloc-dislocation. In this flattened section, rock material clearly geologically different than the one from the cirque of the Val Burdun is mixed in, obviously originating from the NW-slope of Munt Olivet (Fig. 2.7) and overrun discordantly by the glacier.

The lower part of the lower moraine, however, shows a more typical morphology and contains some huge blocks arranged in a row. Overall, taking the points discussed above into account, this linear deposit clearly has to be classified as a moraine, despite the imperfect moraine morphology (Fig. 2.7 A). To avoid the influence of the creeping process and to minimise the effect of instability, two large boulders (height ≥2 m) were sampled in the lower part of the moraine (VB7 and VB12). Near the upper sample, another soil profile was analysed (S2).

The morainic remnants on the orographic left side are even less clearly developed and were not taken into account. To be named are also two separated blocky and spatially confined deposits at 2080 m and at 1940 m, where the Val Burdun discharges into the Val Chamuera (Fig. 2.7). The lower accumulation is surrounded by autochthonous calcareous material. The crystalline erratics therefore most probably have their origin in the Val Burdun (Beer, 2005) and might be interpreted as single rock fall events transported and deposited subsequently by the Val Burdun glacier. On the upper deposit, both weathering rinds and Schmidt-hammer rebound values were measured.

Table 2.2 Summarising overview of applied methods in Val Burdun, together with sample codes and information on sampling and measuring localities.

Method	Sample Code	AMS Code	Localities	Altitude (m a.s.l.)
SED using ^{10}Be	VB 1	ZB7162	Rock barrier, polished bedrock	2670

Method	Sample Code	AMS Code	Localities	Altitude (m a.s.l.)
SED using ^{10}Be	VB 4	ZB7163	Rock avalanche, upper part	2595
SED using ^{10}Be	VB 5	ZB7164	Upper moraines, higher level	2462
SED using ^{10}Be	VB 6	ZB7165	Upper moraines, lower level	2454
SED using ^{10}Be	VB 7	ZB6322	Lower moraine, upper part	2210
SED using ^{10}Be	VB 9	ZB7167	Rock avalanche, middle part	2442
SED using ^{10}Be	VB 10	ZB7168	Rock avalanche, lower part	2387
SED using ^{10}Be	VB 12	ZB7190	Lower moraine, lower part	2125
Schmidt-hammer	—	—	Rock barrier; rock avalanche in the upper, middle and lower part; lower moraine; deposit at 1900 m	—
Weathering rinds	—	—	Rock avalanche in upper, middle and lower part; lower moraine; deposit at 1900 m	—
Soil analyses	S1	—	Upper moraines, higher level	2346
Soil analyses	S2	—	Lower moraine	2192

2.4 Rock glacier locations – Piz Julier area and Val Tschitta

This chapter describes the three active rock glaciers sampled for luminescence dating. For each rock glacier, information about general characteristics like morphology (using the terminology of Frauenfelder and Kääb, 2000) as well as documented and derived glacierisations in the Lateglacial and the Holocene is given. The inclusion of already conducted (dating-) studies – mainly based on findings already summarised in Frauenfelder *et al*. (2005) – allows us to embed and set into perspective the here-measured luminescence ages. Already available age estimations based on streamline interpolations and relative dating measurements were the main reason for the choice of the Gianda Grischa and the Suvretta rock glacier. A comparably simple geometry in combination with a data set from relative dating approaches spoke for the Salteras rock glacier as an additional site. Furthermore, the sampling sites on each rock glacier are shown. The sampling procedure itself is discussed in the methods chapter (Chapter 4).

2.4.1 Suvretta

The Suvretta rock glacier is characterised by a more than 1 km long, comparably thin monomorphic body creeping out of the cirque below the Piz Albana, closest in vicinity to Piz

Julier (Fig. 2.9). It covers an altitudinal range of about 500 m, with a starting zone at around 2800 m and a front position at 2300 m, where the rock glacier is undercut by the mountain stream coming down the Suvretta valley (Vonder Mühll, 1993). Thicknesses of the permafrost body ranging from almost 100 m in the upper part to around 20 m near the front were determined with geoelectric techniques. Active layer thickness normally doesn't exceed 2 m (Vonder Mühll, 1993). The length profile can be described as S-shaped: The slightly dipping root zone changes at 2600 m to a steep zone of extending flow in the middle part, flattening again towards the valley bottom with a zone of compressing flow in the tongue area. The area around the rock glacier was most probably not influenced by extensive ice during the end of the Lateglacial and the Holocene (Suter, 1981; Ohlendorf, 1998). The corresponding sheet from the Siegfried map (sheet St. Moritz, 1875) gives no hint that the cirque was occupied by ice masses during the LIA. However, the presence of (perennial) ice or snow patches cannot be ruled out in any case.

Using photogrammetric techniques (cf. Kääb *et al.*, 1997, 1998) horizontal surface displacement rates of up to 2 ma^{-1} and a derived surface age of approx. 3 ka was determined (Frauenfelder *et al.*, 2005; Kääb and Frauenfelder, 2001). Reconstructed streamlines represent the trajectories of individual particles on the surface. Considering that the overall advance rate of the rock glacier can be much smaller, the calculated ages have to be interpreted as minimum ages. The real age can be 2-5 times higher (Kääb, 2005). Both Schmidt-hammer rebound values (Castelli, 2000) and weathering rind thicknesses (Laustela, 2003; Laustela *et al.*, 2003) show a clear trend following the length profile and, in combination with the estimated ages from photogrammetry, make a calibration possible. The oldest parts near the tongue yielded weathering rind thicknesses between 2.5 and 3 mm and r-values ranging around 35, respectively. This equals a rind growth rate of approx. 1 mm per ka (Frauenfelder *et al.*, 2005).

2.4.2 Gianda Grischa

The double-tongued Gianda Grischa rock glacier (Fig. 2.9) on the western slopes of Piz Julier is, from a geometrical point of view, the most complex one. Multiple generations of lobes with different activity stages are distinguishable. Several situations show younger active parts overrunning older inactive or even relict parts (Fig. 2.10). This is especially pronounced at the orographic left tongue. In order to reduce complexity, we chose the right tongue for sampling (Fig. 2.10). The southern margin of the middle part of the rock glacier is steeply sloping down towards SW, in Fig. 2.10 identifiable as a bright area clearly contrasting the more gently sloping surface of the rock glacier.

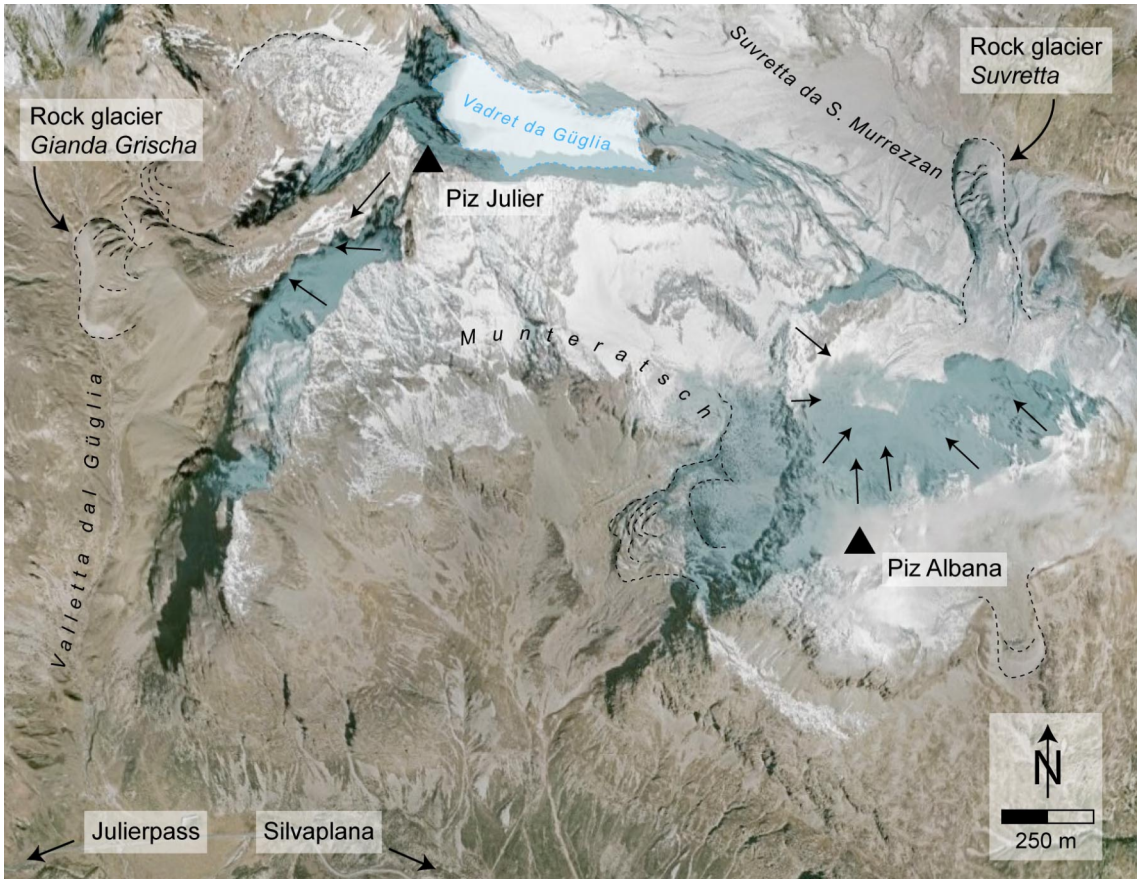

Fig. 2.9 Localisation of the rock glaciers Suvretta and Gianda Grischa. Outlines and prominent ridges in compressing zones are indicated with black dashed lines. Additional rock glaciers to the ones discussed are highlighted as well (in the west and the east of Piz Albana). In the NE-face of Piz Julier the still existing glacier ("Vadret") is marked. The arrows show the position of the debris providing headwalls. Based on a Google Earth scene.

To the north of this active polymorphic rock glacier an inactive exemplar can be separated. The flat niche where it is located was occupied by a small glacier during the LIA, unlike the cirque of the active rock glacier that was ice-free at this time (Siegfried map, sheet St. Moritz, 1875; Coaz, 1850). According to Suter (1981), a glacerisation in the Younger Dryas must be assumed as indicated by well-pronounced Egesen-equivalent moraines near Julierpass. Two-dimensional electrical resistivity tomography (ERT) surveys showed unusual high active layer thicknesses up to 4 to 5 m. Typical values in this region are 3 to 3.5 m on rock glaciers and 4 to 5 m in rock walls. Photogrammetry yields lower surface displacement rates compared to the rock glacier Suvretta, with an average velocity of 0.4 to 0.5 ma^{-1} and maximum values around 0.8 ma^{-1}. The minimum estimated surface age is 4 to 5 ka (Frauenfelder *et al.*, 2005). Schmidt-hammer measurements show no clear trend.

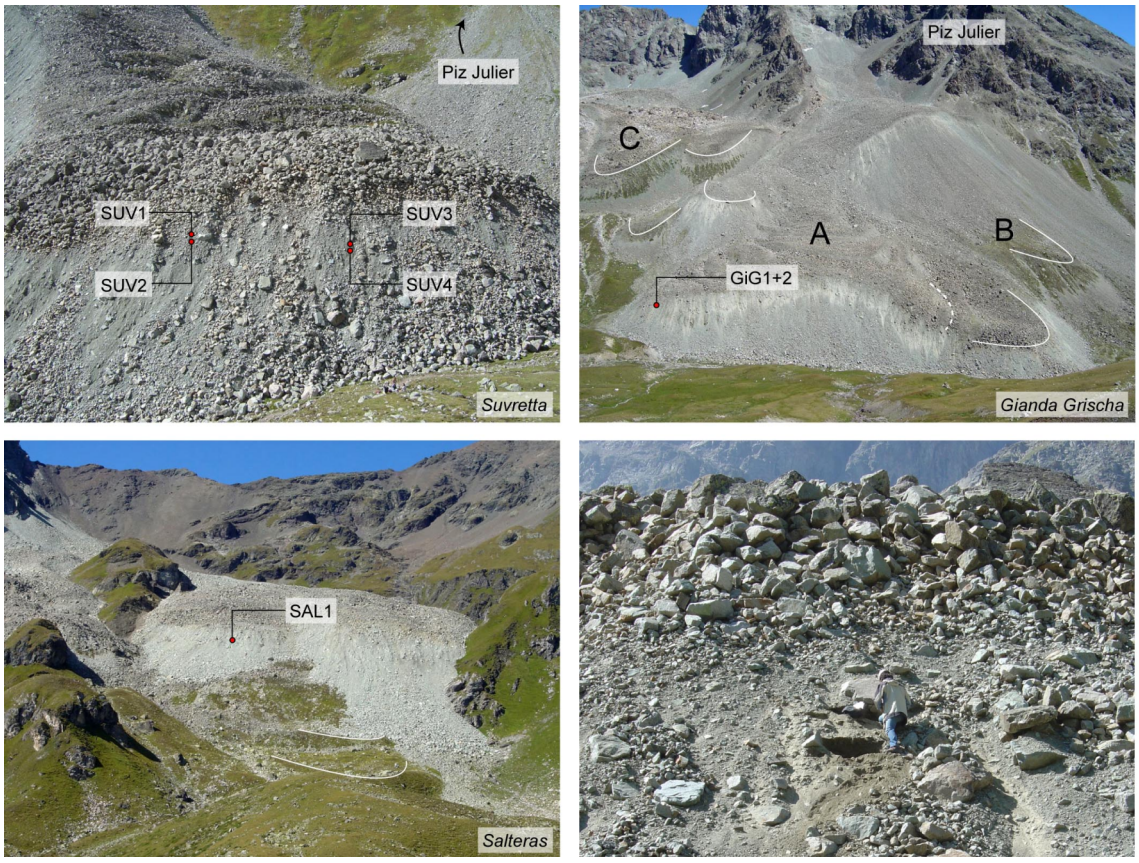

Fig. 2.10 The rock glaciers sampled for luminescence dating are shown. Sampling locations are represented by red dots. Samples are ideally taken between the coarse blocks on the surface and the eroded and accumulated material at the lower part of the slope. This zone at the rock glacier Gianda Grischa is especially clearly visible as a white band. Digging right below big boulders provides a better slope stability and increases the possible penetration depth (lower right, rock glacier Suvretta). Neighbouring and associated (potentially) inactive and relict creeping forms are indicated by white lines. The dashed line on the rock glacier Gianda Grischa approximates the zone where an older part is overrun by a more active lobus. At this site, three main parts can be distinguished: (A) active rock glacier, (B) older, possibly relict part, (C) inactive rock glacier (based on Frauenfelder *et al.*, 2008b).

This may be a result of boulders being rearranged under the influence of gravity in the steep part of the rock glacier, causing a reset of the "clock" (Frauenfelder *et al.*, 2005). Weathering rinds, however, show a meaningful development with increasing thicknesses towards the front, at least on the orographic left side (Laustela, 2003). Maximum values (median, mode) are in the range of 1.5 to 2 mm. This trend is not as clear on the orographic right side, but the measured values are in the same range, indicating a comparable age structure on both sides. Related to the age estimation, rind growth rates are about half as high as in the case of the rock glacier Suvretta, although made up of the same source material (Frauenfelder *et al.*, 2005).

2.4.3 Salteras

Rock glacier Salteras, originating from the NE-oriented cirque to the east of Piz Salteras, shows a rather simple geometry without zones of pronounced compressing or extending flow. The long profile is slightly convex with an increasing slope angle towards the tongue, which is about to creep over a steep grassy slope. The front is thereby divided into two individual lobes. In front of the talus apron, several vegetation covered lobe-shaped forms are visible (Fig. 2.10). These might be interpreted as remnants (ridges in a compressing zone or front?) of a collapsed relict form, indicating that the rock glacier Salteras has experienced several activity phases. Lacking lichen coverage and weakly consolidated coarse blocks covering the surface suggest an active stage of the rock glacier.

Neither Schmidt-hammer r-values nor modal values of weathering rind thicknesses – both measured in the middle and the lower part of the rock glacier (Laustela, 2003) – show a clear trend representing an increasing exposure time to weathering processes towards the front. R-values remain on a high level, ranging between 45 and 50. This is supported by only very thin and often completely absent weathering rinds. Using the median, there is a trend indeed; still, the values are very small (< 1 mm). This picture of surprisingly fresh and unweathered surface material might be explained by the influence of glacier ice. Although the Siegfried map (sheet Savognin, 1887) shows no ice in this position, moraines found in the upper part support the conclusion that at least the upper parts of the rock glacier have been covered by surface ice during the LIA (Maisch, 1981).

2.5 Aiguille du Midi (Chamonix, France)

Aiguille du Midi is a 3842 m high mountain peak close to the village Chamonix in the western Alps. The summit is easily accessible by cable car and therefore provides an excellent study site in a high Alpine and strongly glacierised environment where reaching a high mountain peak with heavy equipment normally means a multi-day trip. Research activities on the Aiguille du Midi have mainly focussed on investigating permafrost conditions in high Alpine steep rock slopes and related instabilities. Deline *et al.* (2009) give a comprehensive overview of past and ongoing studies.

Geologically, this area is part of the Mont-Blanc massif (Spicher, 1980) and is made up of the so-called “Mont-Blanc Granite” with an age of roughly 300 Ma (von Raumer & Bussy,

2004; Bussy *et al*., 2000). This granite type is of a quartz-rich quality and thus suitable for surface exposure dating with ^{10}Be. However, the single crystals show diameters up to several centimeters, resulting in a coarse-grained surface dominated by individual crystal faces. The application of the Schmidt-hammer technique therefore does not make sense, as the precondition of isotropy is not given.

During the LGM, the uppermost part of the Aiguille du Midi S-face, where the samples were taken, was most probably not glaciated. Paleoglaciological reconstructions based on trimline mapping by Coutterand & Buoncristiani (2006) and Kelly *et al*. (2004a) showed that Aiguille du Midi was, during this time, a Nunatak bounded in the east by the Mer de Glace, in the north by the Glacier de l'Arve and in the west by the Glacier des Bossons. Apart from local glaciations in the less steep parts of the wall, the influence of glacial ice masses on exposure ages at the sampled localities can be excluded.

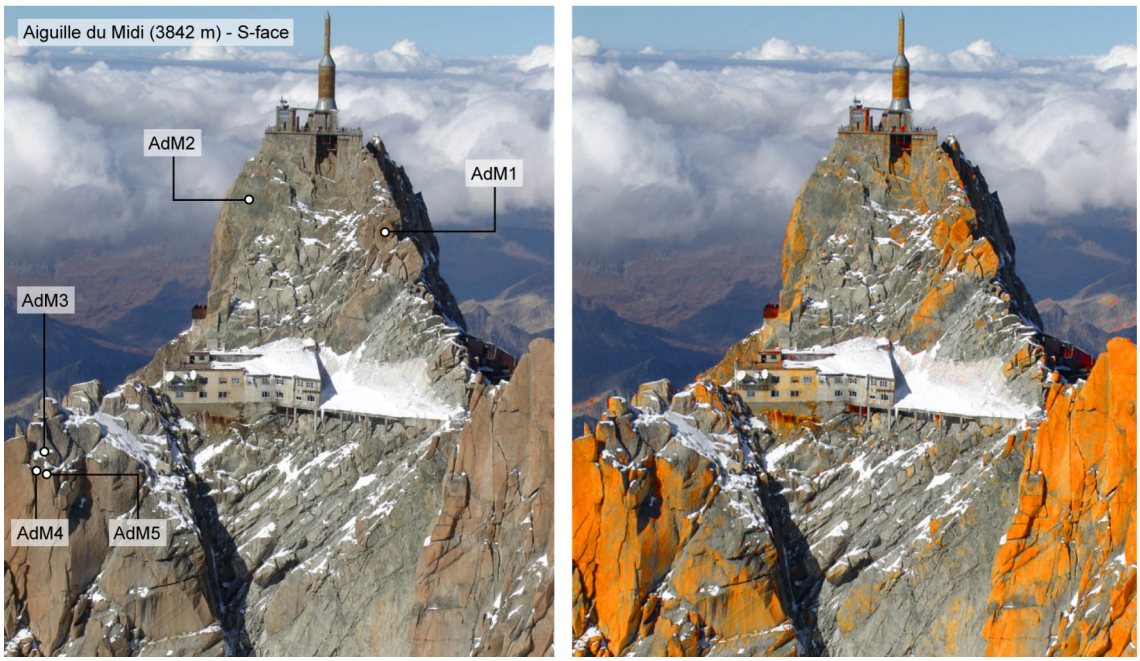

Fig. 2.11 S-face of Aiguille du Midi with sampling spots. On the right side is the same picture again but with an artificially increased red saturation in order to accentuate the differences in colour (Foto: S. Gruber).

We chose our sampling sites based on visually identifiable differences in colour on photographs taken from a helicopter (Fig. 2.11). The hypothesis was that intensively red coloured parts in the rock wall were exposed to weathering over a longer time period than fresh, grey ones and consequently should have a higher age. This assumption is based on field observations at the adjacent Drus (Fig. 1.1), where, besides several smaller events, a huge rock

fall occurred in 2005. The grey coloured area that came to light clearly contrasts to the surrounding, more or less reddish and obviously older parts of the wall. Detailed information on this event is given in Ravanel (2006) and Ravanel and Deline (2008).

Sample “AdM1” was taken at a conspicuously red spot, whereas “AdM2” was gathered from a grey part of the wall, where no red colouring was seen (Fig. 2.11). “AdM4” and “AdM5” can be placed somewhere in between with respect to colour. Thereby, sample “AdM5” presented a more intensive coloration than “AdM4”. All these sampling places had a slope ≥ 79°. The slope at “AdM3” was, however, only 49°. This sample was the only one that was partly covered by lichen, probably due to an increased water availability resulting from melting snow. For this reason, spectral analysis was not applicable and “AdM3” was not taken into account for further interpretation. We concluded that the rock surfaces should have the following order of age: AdM1 > AdM5 >AdM4 > AdM2.

Chapter 3

Scientific background

The first objective of this chapter is (a) to describe the temporal framework of this study. Besides a pure temporal positioning, an embedding of this work in the numerous studies carried out in this scientific field is provided, always with a special focus on dating issues and the Swiss Alps. Another goal is (b) to describe the landforms and main processes that are involved. Of course, each one of these points is by far complex enough to deserve its own thorough discussion. As this is not the whole purpose here, the aim is just to give the information needed to answer the questions relevant to this work: How do these landforms evolve? What are the interactions among them? Where is the connection of landforms to past climate conditions? And, essentially the main question behind all this: Why should we date them?

3.1 The temporal and glacial historical framework: the European Alps from the Last Glacial Maximum (LGM) to the early Holocene

As the title implies, the main focus of this chapter is to highlight the terminal phase of the last (Würmian) glacial cycle and the subsequent transition to the Holocene. However, in order to enable an embedding of this period and also to provide the necessary glaciological background, some basic information about the time before LGM is also given here. The following remarks concentrate on important Lateglacial events and their associated climatic evolution with a geographical emphasis on the Linth-Rhine glacier system and the area surrounding the investigation sites. For comprehensive up-to-date overviews and additional references see Ivy-Ochs *et al.* (2006a, 2007, 2008, 2009a).

During the Quaternary (the last 2.588 million years; International Stratigraphic Chart, 2009) the Earth experienced numerous glacial cycles with glacier extents by far exceeding the modern ones. Based on morphostratigraphical and lithostratigraphical evidences – in the case of older glaciations mainly river terraces – Penck and Brückner (1901, 1909) proposed the classical fourfold system for the glaciations of the Alps: The two oldest glacial cycles, *Günz* and *Mindel*, are defined by older (higher) and younger (lower) Deckenschotter, respectively (often summarized as Deckenschotter-glaciations). They are followed by *Riss* (Hochterrasse) and, separated by the Eemian interglacial, the last glaciation termed *Würm* (Niederterrasse) (Fiebig and Preusser, 2008). Although partly still in use in its original form, with the availability of new and improved dating techniques this system is constantly being expanded and refined. The current glacial record includes at least 15 major glacier advances beyond the border of the Alps and events such as the Most Extensive Glaciation (MEG, traditionally assigned to the Riss-glaciation) turned out to be multiple-phased (summary e.g. in Schlüchter, 2004). Several dating attempts have been made, mainly using cosmogenic nuclides and luminescence methods. As a rough overview reference is made to: Häuselmann *et al.* (2007, burial ages of Deckenschotter using ^{26}Al and ^{10}Be); Graf (1993, Deckenschotter in northern Switzerland); Bolliger *et al.* (1996, mammals indicating Pliocene age of higher Deckenschotter); Graf *et al.*, (2007, cosmogenic dating of pre-LGM boulders in the Jura mountains); and Preusser *et al.* (2003, focusing on the Middle Würmian with ^{230}Th/U and luminescence at the Gossau site). Van Husen (2004) provides a compilation for Quaternary glaciations in the Eastern Alps.

3.1.1 The LGM

LGM ice extent is reconstructed by a combination of mapping erosional features in high mountain areas indicating the former ice flow direction and upper limit of the ice surface (e.g. Penck and Brückner, 1901/1909; Florineth, 1998; Florineth and Schlüchter, 1998; Kelly *et al.*, 2004a, Couterrand and Buoncristiani, 2006) and by accumulative traces such as moraines and (glacio-) fluvial deposits in the lowlands (e.g. Penck and Brückner, 1901/1909; Keller and Krayss, 1993, 2005). The LGM maps by Jäckli (1970) and by Swisstopo (2009) for Switzerland and by Van Husen (1987) for Austria are very useful and provide an overall impression of the glacier extent at that time. The main characteristics in inner-alpine areas are ice flow paths originating from ice domes and connecting now separated drainage systems, as is also the case in the main investigation area of this study (Fig. 3.1). In the lower parts glaciers passed the borders of the Alps and formed distinct piedmont lobes, especially pronounced in the northern foreland. The beginning of the last advance into the foreland was around 30 ka (Keller and Krayss, 2005; van Husen, 1997).

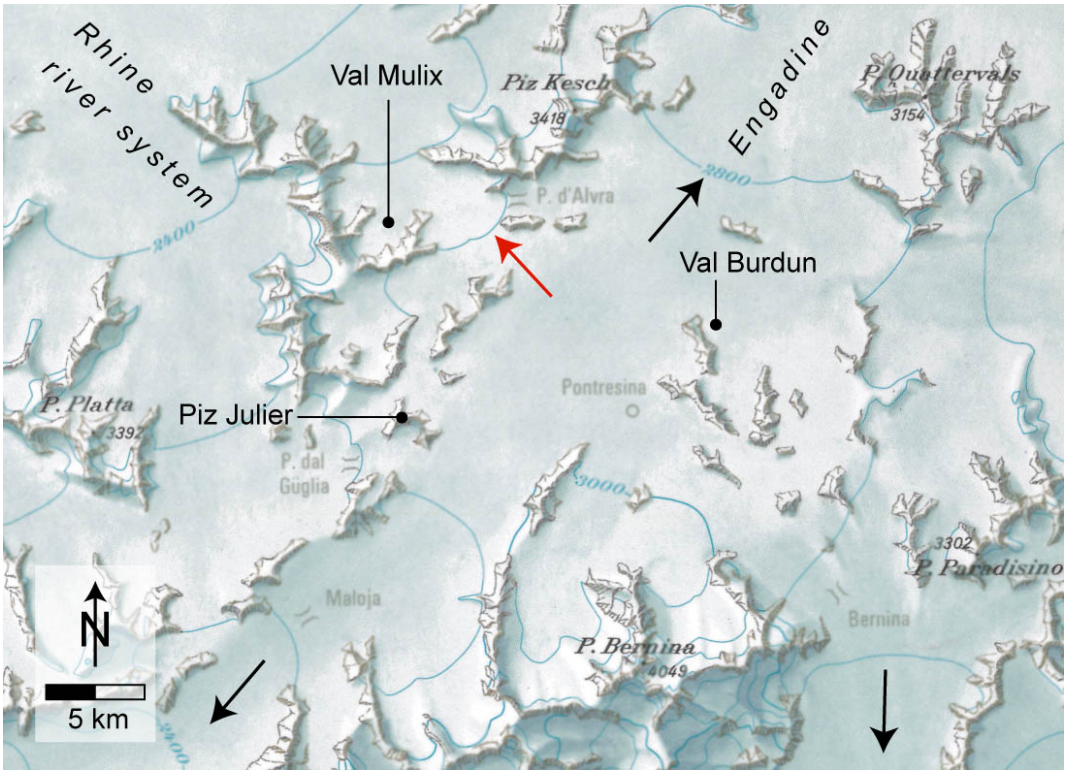

Fig. 3.1 Reconstruction of ice surface geometry during the LGM in the investigation area (Jäckli, 1970). Flow directions as indicated by arrows emphasize a local culmination of the ice surface (ice dome) in the area of Pontresina. The transfluence at the Albulapass (P. d'Alvra) and the nearby Bottas Glischas (right at the head of the red arrow) into the Rhine river system is clearly shown.

At the maximum extension the Linth/Rhine glacier terminated near Killwangen to the north of Zurich between 32.9 and 24.0 ka ago (Schlüchter and Röthlisberger, 1995). The climate at this time must have been continental with very low precipitation and mean annual temperature values, as derived from reconstructed low basal shear stresses and connected low mass turnovers and mass balance gradients of the piedmont glaciers (Haeberli and Penz, 1985). The reconstructed low deformation rates also suggest a more humid climate during the period of glacier advance. Only in this way a is progression of the ice front fast enough to travel distances of 100-150 km within the given time window possible. Equilibrium lines during the Würm maximum were below 1000 m a.s.l. (Keller and Krayss, 1993), corresponding to ELA depression values of approx. 1200 m (Keller and Krayss, 2005). Exposure ages from the terminal moraine of the Rhône glacier indicate that breakdown of the piedmont glacier system occurred between 21.1 and 19.1 ka (Ivy-Ochs *et al.*, 2004). On a global scale, compiled ^{10}Be-data speak for a near-synchronous start of glacier retreat in both hemispheres, which is consistent with the onset of temperature and atmospheric CO_2 increases in Antarctic ice cores (Schaefer *et al.*, 2006). The following glacier recession into the outlet channels was interrupted by several re-advances of

phases of temporary stabilisation, creating the so-called ice marginal complexes (Keller and Krayss, 2005). The deglaciation in the foreland is assumed to have been completed by 17.5 to 18 ka (Wessels, 1998), based on lithostratigraphy and the termination of meltwater influence around 17.1-17.9 ka, a date obtained from a sediment core taken in Lake Zürich (Lister, 1988).

3.1.2 Early Lateglacial ice decay and stadials assigned to the Oldest Dryas

The term "Alpine Lateglacial" was introduced by Penck and Brückner (1909/1909) and refers to the European Alps. Onset is, by definition, the pull-back from the innermost Würmian moraines, roughly 18-19 ka ago, based on the findings mentioned in the last chapter (Fig. 3.2). Lowering of the ice surface in the central Alps led to a more topography-dominated, dendritic glacier system.

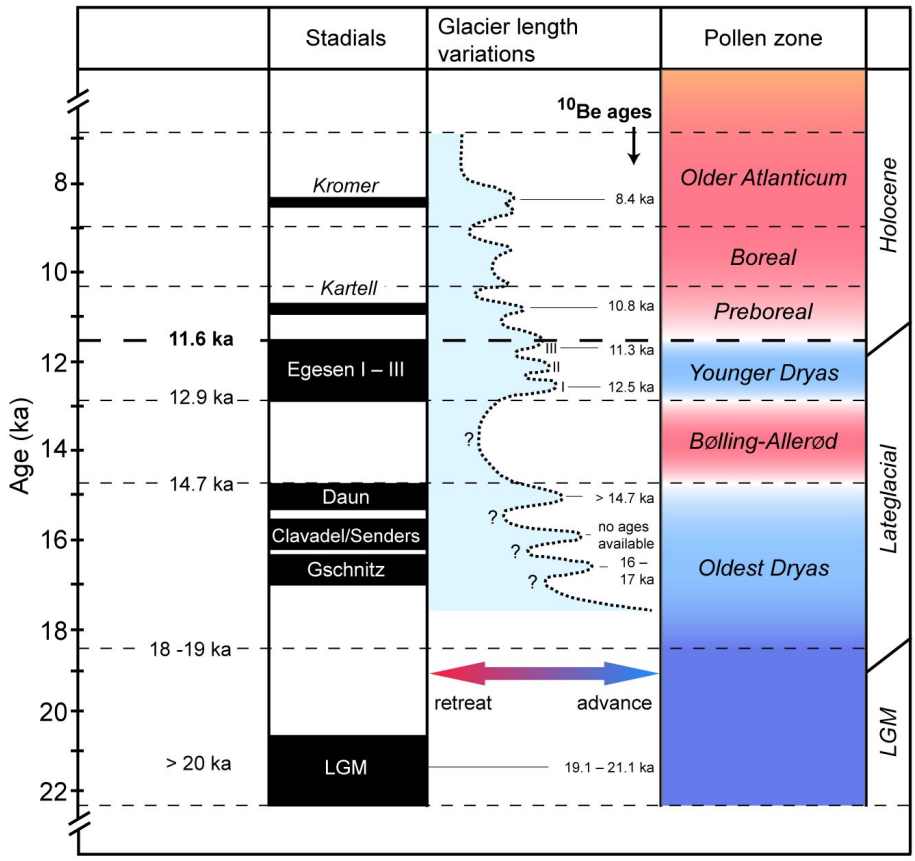

Fig. 3.2 Scheme of glacier fluctuations during the Lateglacial and early Holocene time period and temporal assignment of identified stadials as derived from surface exposure dating. References for ^{10}Be ages shown here: LGM: Ivy-Ochs *et al.*, 2004; Gschnitz: Ivy-Ochs *et al.*, 2006b; Daun: this study; Egesen: Ivy-Ochs *et al.*, 1996 (Julier Pass); Kartell: Ivy-Ochs *et al.*, 2006a; Kromer: Kerschner *et al.*, 2006 (figure modified from Maisch *et al.*, 2000).

The general downwasting was interrupted by repeated and increasingly smaller glacier readvances (stadials), accompanied by the deposition of moraines in the mountain valleys and

cirques. Although a commonly accepted rough structure of these stadials is set, the exact temporal assignment is still debated and was repeatedly adjusted in the past. The "pioneers' point of view" in this respect including description of the type localities can be looked up for instance in Heuberger (1966), Mayr and Heuberger (1968), Patzelt (1975), Kerschner and Berktold (1982) or Maisch (1981, 1987). Here, the current knowledge is briefly outlined (see also Fig. 3.3). A tabular overview with a comprehensive reference summary is provided by Ivy-Ochs *et al.* (2006b).

This first Lateglacial phase left only a few glacial traces pointing to stillstands or minor oscillations of the glaciers occupying the main valleys, including the *Bühl* and *Steinach* phase of Penck and Brückner (1901/1909; see also Mayr and Heuberger, 1968; van Husen, 1997, 2004). In contrast, there is sedimentological evidence for the activity of smaller glaciers, as a result of both short-lasting climatic oscillations and of mechanical reasons (Reitner, 2007).

The glacial deposits of the *Gschnitz* stadial are the first (lowest) that are well-developed and the blocky and sharply shaped moraines of this stadial are in many cases easily identifiable. The ELA was depressed by around 650-750 metres with respect to 1850. During this time, glaciers from tributary valleys very often still reached the main valleys, forming a dendritic glacier network. The end position of the main glacier in the Engadine was near Zernez (Fig. 2.1) (Maisch, 1981). Palaeoclimatical interpretation of the situation at the type locality in Austria suggest that precipitation was reduced to one third and summer temperatures were 10°C lower compared to modern-day values (Kerschner *et al.*, 1999). ^{10}Be ages obtained at the same locality showed that this moraine stabilised no later than 15.4 ± 1.4 ka ago (Ivy-Ochs *et al.*, 2006b). However, moraine morphology indicating an initially unstable phase and the potentially long response time of the glacier suggest a moraine deposition somewhat earlier. Ivy-Ochs *et al.* (2008) suggest the Gschnitz stadial to have occurred around 17-17.5 ka after a distinct warming phase.

Upvalley, the morphostratigraphically following stadial is the *Clavadel* (Maisch, 1981), which is probably comparable to the *Senders* stadial in the Eastern Alps (Kerschner, 1986). ELA depression values are in the range of 400-500 metres. In the Engadine the glacier reached Cinuos-chel, some 16 km NE of Samedan (Fig. 2.1). Although moraines are prominent, no ^{10}Be ages are available for this stadial so far, as boulders are mostly absent. ^{14}C ages from peat bogs show that it occurred before the Bølling warm phase. A minimum age is given by the basal ra-

diocarbon age of a peat bog at Maloja (Fig. 3.1) (Studer, 2005), indicating that the ice stream network in the Upper Engadine broke down before 15.7-16.5 ka.

The *Daun* stadial (reaching Samedan in the Upper Engadine, Fig. 2.1) was characterised by valley glaciers with ELA depression values from 250 to 400 metres. Daun moraines are the lowermost ones in the investigation area. Their age is presumably pre-Bølling (> 14.5 ka), based on palynological analyses in the anorganic base layer of a peat bog in the investigation area (Crap Alv; Burga in Maisch, 1981) and a pre-Egesen ^{10}Be minimum age from a moraine at the nearby Julierpass (Ivy-Ochs *et al*, 2006a). One of the main aims of this study is to substantiate this rather weak database.

Sedimentological analysis from the Upper Engadine lakes show that during the following Lateglacial interstadial (Bølling-Allerød) glaciers likely advanced beyond the LIA extent (Ohlendorf, 1998) for several times, as a result of a number of climatic oscillations. The resultant glacial record was overridden and eroded by the subsequent glacier advances as a reaction of the Younger Dryas cooling event.

3.1.3 Younger Dryas and early Holocene

The Younger Dryas is the last major cold phase before the Holocene. Its beginning is characterised by an abrupt drop in temperature. High resolution pollen and cladoceran stratigraphy from Gerzensee (Switzerland) suggest a mean summer temperature depression of 2 to 4 °C at the beginning of the Younger Dryas (Lotter *et al*., 2000) compared to Allerød summer temperatures. The Allerød-Younger Dryas transition lasted some 200 to 300 years, taking place c. 12.8-12.5 ka. The preferred explanation for the Younger Dryas cooling is a weakening or shutdown of the North Atlantic meridional overturning circulation as a result of a major release of meltwater into the North Atlantic (Brauer *et al*., 2008 and references therein). However, highest meltwater peaks occurred several hundred years before and after the Younger Dryas, raising the question of the water source – a question not answered satisfactorily so far. Based on analysis of annually layered sediments of the German Maar Lake, Brauer *et al*. (2008) suggest an abrupt change in the North Atlantic westerlies towards a stronger and more zonal jet as an additional contributing factor. In many respects comparable oxygen isotope records from Gerzensee and Greenland ice cores speak for an extra-regional, probably hemispheric synchronicity of this event (Schwander *et al*., 2000).

The well-preserved moraines deposited by glaciers re-advancing during this time represent the stadial known in the supraregional Lateglacial scheme of the Alps as *Egesen* (Fig. 3.2, 3.3). Very blocky and often multiple-phased (typically 2 to 3, sometimes up to 4 moraines) moraine sequences with ELA depression values of 180 to 250 metres are typical, in special cases values of > 400 m occur, especially in the western and northern fringe of the Alps. Because of their general abundance and the availability of boulders suitable for surface exposure dating, a number of relevant dating-studies have been made and the temporal assignment has been well constrained in the meantime.

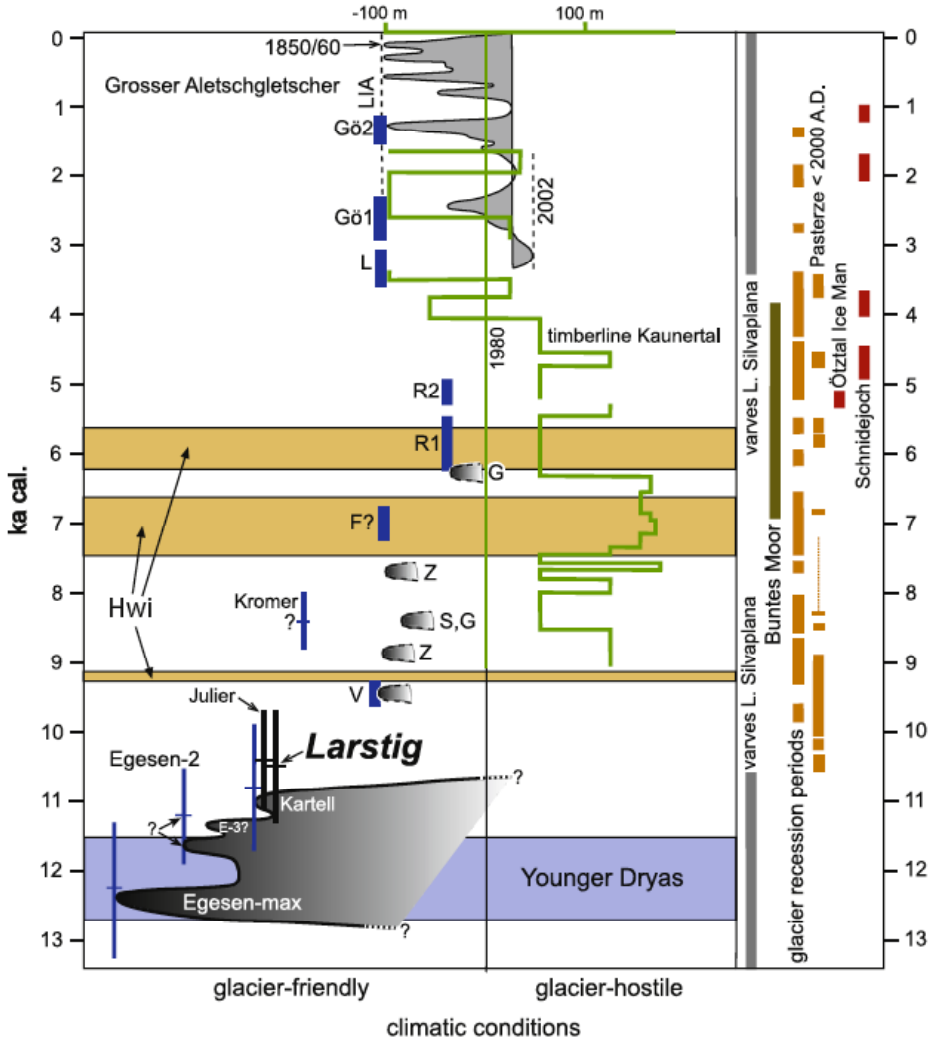

Fig. 3.3 Glacier variations (grey) and climate evolution derived from different proxies in the latest Pleistocene and the Holocene. Black bars (Julier, Larstig) indicate ^{10}Be rock glacier stabilisation ages. Long blue bars are related Younger Dryas and early Holocene glacier variations. Short blue bars = cold oscillations: V Venediger, F Frosnitz, R Rotmoos, L Löbben, Gö Göschenen. G Gepatschferner (Kaunertal), Z Zettalunitzkees, S Simonykees (from Ivy-Ochs *et al.*, 2009a, based on various authors).

The outer Egesen moraine at Julierpass very close to the investigations site yielded a stabilisation age of 12.3 ka, with that of the inner moraine (likely Egesen II "Bocktentälli") 11.3 ka (Ivy-Ochs *et al.*, 1996, 2006a). Ages in this range were obtained from boulders sampled on Younger Dryas moraines in several regions of the Alps (see Ivy-Ochs *et al.*, 2008, 2009a for a summary) as well as in other parts of the world, for instance Scotland (Golledge *et al.*, 2007) and the Carpathians (Reuther *et al.*, 2007).

Due to increasingly ice-free headwalls in the cirques and abundant glacial sediment uncovered by retreating glaciers, favourable conditions for permafrost creeping processes appeared towards the end of the Younger Dryas. As a result, rock glaciers could form. Under modern climatic conditions these forms are relictified and thus have the potential to be palaeoclimate proxies. Frauenfelder *et al.* (2001) estimated Younger Dryas mean annual air temperatures at rock glacier tongues to be c. 3 to 4°C lower than today, based on a modelling approach considering 32 relict rock glaciers in and near the investigation area. Permafrost distribution was lowered by 500 to 600 metres, considerably more than ELA depression values for the same time. Younger Dryas glaciers may have been of a polythermal type, mostly surrounded by permafrost and in a rather dry climate with up to 30-40% precipitation reductions compared to modern values (Frauenfelder et al., 2001 and references therein). Exposure ages obtained from boulders on relict rock glaciers in Switzerland and Austria (Julier and Larstig, respectively, see Fig. 3.3) suggest a stabilisation in the Preboreal, around 10.5 ka ago (Ivy-Ochs *et al.*, 2006a, 2009a).

At some places, especially well-defined in the Eastern Alps, blocky moraines lying between Egesen-equivalent moraines and LIA moraines can be identified. They mainly show ELA depression values around 120 m and are called *Kartell*, dated with cosmogenic isotopes to 10.8 ka (Ivy-Ochs *et al.*, 2006a). A parallelisation with the Preboreal oscillations seems reasonable. In the Silvretta mountains in eastern Austria, another moraine generation with an ELA depression of c. 80 m could be distinguished. This *Kromer stadial* was dated to 8.4 ka and is supposed to be the response of some smaller cirque glaciers to the 8.2-ka event as detected in Greenland ice cores (Kerschner *et al.*, 2006). However, for the Kromer stadial in particular there is no widespread evidence and to prove the autonomy of the Kartell stadial with respect to the Egesen, more dating would certainly be necessary.

With the continuously improved measurement accuracy in cosmic nuclide dating, it is now also possible to date mid- and late-Holocene deposits, even those resulting from high-

frequency glacier fluctuations. Recent studies thereby point out the highly individualistic behaviour of glaciers (e.g. Shakesby *et al.*, 2008; Schaefer *et al.*, 2009). Recent overviews of Holocene and historical glacier and climate variations are given for instance by Wanner *et al.* (2008), Solomina *et al.* (2008) and Zumbühl *et al.* (2008).

3.2 Landforms and processes

3.2.1 Glaciers, their reaction to climatic changes and accumulative and erosional traces

Principles

In places that winter accumulation in the form of snow doesn't melt over most summers, glacier ice can form as a result of a gradual densification and different processes of snow metamorphosis. Ice in the glaciological sense is present as soon as interconnecting air passages are closed off (Paterson, 1994). Ice is a plastically deformable medium and creeps under the influence of gravity (Glen, 1955). Besides internal deformation, basal sliding (Lliboutry, 1971) and deformation of sedimentary glacier beds (e.g. Boulton and Jones, 1979; Humphrey *et al.*, 1993), there are components contributing to the total deformation rate measured at the glacier surface. "Cold" glaciers below the pressure melting point creep almost exclusively by internal deformation, and basal sliding is strongly reduced or negligible, associated with a very low erosional power. This has implications for the interpretation of exposure ages achieved from polished bedrock exposed by retreating cold glaciers, as described later. Assuming a constant climate, a glacier creeps downvalley until accumulation excess in the upper part and ablation excess in the lower part level out, i.e. until the net balance over the entire glacier is zero. At the equilibrium line, annual accumulation is exactly balanced by ablation. ELAs vary annually, which means the definition of the ELA does not imply that the glacier as a whole is in equilibrium (Benn and Lehmkuhl, 2000). The climate that prevails at the equilibrium line is just sufficient to maintain the existence of a glacier (Ohmura *et al.*, 1992). The long-term climatic variability, therefore, can be inferred from the shift of reconstructed equilibrium line altitudes (ELA) (e.g. Zemp, 2007 and references therein). ELAs of former glaciers provide a powerful tool to quantify palaeoclimate where other evidence is lacking (Benn and Lehmkuhl, 2000).

Reaction of glaciers to changes in climate

The reaction of a glacier to a step change from one steady state climate to another is essentially two-staged (Johannesson *et al.*, 1989; Haeberli and Hoelzle, 1995): (1) a direct, undelayed reaction of the specific mass balance (total mass change by glacier area) and related changes to the

mass balance gradient and hypsography and (2) a delayed adaptation of glacier length to the new conditions, starting after a certain reaction time and having ended after the response time, both being unique to each glacier. As shown in Fig. 3.4., both steps are modified by local topography. Response times are slope dependent (Haeberli and Hoelzle, 1995) and proportional to the maximum thickness and the ablation at the terminus of the glacier. They vary in the range of decades to slightly less than a century for modern Alpine glaciers (Zemp, 2006).

The geologic record delineating the extent of former glaciers is normally the starting point in palaeoglaciological studies. Considering known physical laws of the flow behaviour of ice and taking analogies with modern glaciers into account, important properties of former glaciers can be derived based on their outlines by inversing the above described climate-glacier relationship (Haeberli and Penz, 1985).

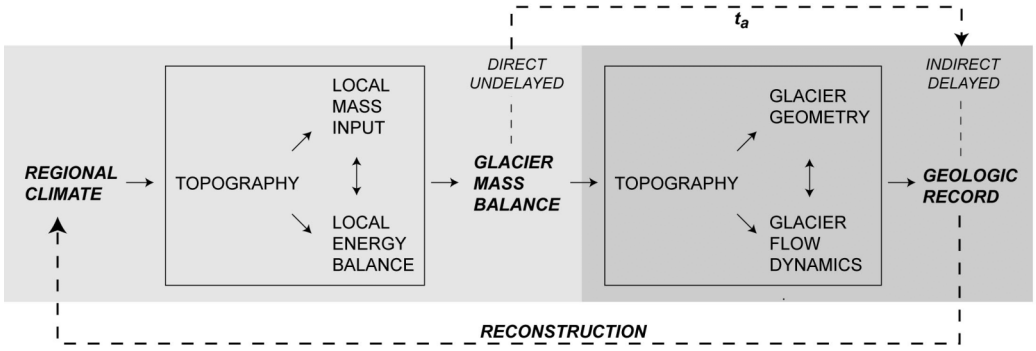

Fig. 3.4 Changes in climate have a direct impact on glacier mass balance, the adaptation of glacier length and connected geologic record (e.g. moraines) is indirect and delayed (t_a = response time). Topography influences both steps by setting framework conditions for local mass input, for interacting local surface energy balance, and for glacier geometry and coupled flow dynamics. For palaeoglaciological purposes, this climate-glacier relationship is reversed in order to derive basic information about former ice bodies (modified from Furbish and Andrews, 1984).

To correlate moraines in mountain regions and to make statements about past climate conditions, former ELA_0-values must be reconstructed in order to calculate ELA depression values. The steady state equilibrium line altitude ELA_0 is a theoretical but important concept for palaeglaciological reconstructions. ELA_0-values from LIA-glaciers normally serve as local reference levels because the maximum extent of 1850 can be easily and reliably determined throughout the Alps (Gross *et al*., 1977). Most commonly applied are area-based indices, namely the accumulation area ratio (AAR). Gross *et al*. (1977) suggested a steady-state accumulation area ratio (AAR_0) of 0.67 to approximate the ELA_0 of former glaciers in the Alps. Although in numerous studies used (e.g. Maisch, 1981, 1987; Maisch *et al*., 2000; Suter, 1981; Kerschner and Berktold, 1982), this method is not free of weaknesses. Furbish and Andrews

(1984) claim that the AAR-method implicitly relies upon similarity of glacier shape and regimen over a given geographic area and thus de facto neglect the influence of hypsography. Calculated values of modern glaciers show that steady-state AARs may lie in a range of approx. 0.4-0.8 (WGMS, 2007). However, given a "normal" hypsographic distribution, reliable results allowing for interregional comparisons can be achieved for mountain- and valley-glaciers with AAR = 0.67 (Maisch, 1992). Of special importance are glacier length profiles without pronounced irregularities in glacier bed topography like scarps and cascades. Additionally, glacier size must not fall below a threshold where accumulation and ablation are dominated by single topographical influences.

For the description of the climatic conditions at the ELA, principally two families of methods are used: (a) analytic approaches examining the processes of accumulation and ablation based on the energy balance principle (e.g. Kuhn, 1981; Klok and Oerlemanns, 2003), and (b) statistical relationships between parameters representing glacier accumulation and ablation and thus influencing the ELA (e.g. Khodakov, 1975; Ohmura, 1992). A comprehensive overview of modelling approaches is provided by Zemp (2006). The second group of models does not provide deep insights into physical glacier behaviour; however, as they need few and comparably easily derivable input data, they are more suitable for calculations that refer to the past and on wider areas (Kerschner, 2002; Zemp *et al*., 2007). For instance, Kerschner and Ivy-Ochs (2008) used statistical models and summer temperature changes from biological proxies to derive precipitation patterns during the Lateglacial time period, based on different glacial stages in the Eastern Alps.

Glacial traces relevant for dating issues

Glaciers have a great potential to model landscapes, and the resulting accumulative and erosive landforms and form-associations are numerous. Whether the accumulative or the erosional component over the whole glacier prevails is determined by the relation of debris production in the headwalls and debris evacuation by the glaciers meltwater stream (Haeberli, 1986; Zemp *et al*., 2005). In this study, *moraines* and *glacially polished bedrock* (roche moutonnées, transfluences) were dated. The following remarks, therefore, are restricted to these two classical types of glacial landforms (based on Benn and Evans, 1998 and references therein, unless differently indicated).

Focus here is on *ice-marginal moraines* that result from glacier advances or standstills. They are formed by the deposition of sediment around the edge of active glacier snouts, or by

glacially induced stresses. Ice-marginal moraines may be subdivided into frontal and lateral parts. The according deposits are termed *end moraine* or *terminal moraine* and *lateral moraine*, respectively. Moraines that form by re-advancing glaciers during an overall glacier recession are termed *recessional moraines*. *Confluence moraines* develop where two glaciers from neighbouring valleys meet and unify. Source material for ice-marginal moraines is mainly provided by supraglacially or englacially transported rock material that melts out and falls down the glacier margin. Alternatively, ground material can be pushed in front of an advancing glacier. The corresponding accumulation is called *push moraine* (Huggett, 2003).

Exposure ages yielded from moraines are normally assumed to represent the time since moraine stabilisation (Gosse, 2005). A major part of the chronology of Lateglacial and early Holocene glacier fluctuations in the Alps is based on moraine-dating (overviews in Ivy-Ochs *et al*., 2006a, 2008, 2009a). Taking the above-described glacier-climate relations and considerable scatter in SED datasets from moraines into account (Putkonen and Swanson, 2003), the age interpretation in certain cases is not straightforward and the link between landform and the climate-related forming processes is complex (Hallet and Putkonen, 1994). Several possible uncertainties may play a role. On one hand, moraines are not necessarily the result of one single event, but may reflect the sum of transient depositional events within a small spatial scale (Furbish and Andrews, 1984). On a larger scale, especially lateral moraines can be re-occupied by a following re-advance and rock material of several advances may be present (Zreda and Phillips, 1995). On the other hand, there is always the probability of the incorporation of rock material that did not undergo enough glacial erosion to "set the clock to zero". Either reworked material or boulders originating from rock falls/avalanches onto the glacier surface theoretically can contain inherited nuclides, resulting in too old ages of moraine boulders.

The opposite case is possible as well. Post-depositional circumstances have an important influence on nuclide build-up (see also Reuther *et al*., 2006). Freshly exposed moraines are geometrically not in equilibrium and show a high erosional activity after ice retreat ("paraglacial adjustment", see Chapter 3.2.3). Boulders eroding out or being upheaved under periglacial conditions were initially protected against cosmic ray flux by overlaying sediment. Periglacial creep processes and moraine degradation resulting from thawing ice cores may alter the boulder position and thus the orientation of the sampled surface over time.

Roche moutonnées are asymmetric erosional bedrock forms at scales ranging from less than 1 m to several hundred of metres across. Roche moutonnées frequently have a characteris-

tic length profile with a polished glacier upstream side often showing striae and friction cracks and a steep lee side, making them useful indicators of the former ice flow direction. Normal stresses are higher than average on the stoss side of humps, making abrasion processes driven by particles held in melting basal ice more effective. In contrast, normal pressures on the lee side are lower than average and rock material is removed by re-freezing and quarrying (plucking). Cavities and refreezing of water that was melted under pressure very effectively promote crack propagation and fracture in the bedrock on the lee side. Low-pressure cavities as an important element of the forming process are most likely expected in areas with a low average ice overburden and in areas where subglacial water pressures undergo large fluctuations. Roche moutonnées, therefore, presumably tend to develop below thin, temperate ice.

Fig. 3.5 Left: well-pronounced roche moutonnée situated at the transfluence Bottas Glischas. Former ice flow was from right to left as indicated by the clearly visible plucking zone to the left. Right: The blocky Egesen II (Bocktentälli) moraine in the Val Mulix. Moraine morphology described by freshness, shape and boulder size is besides ELA depression values and morphostratigraphy an important criterion for the assignment of moraines to Lateglacial stadials, if no numerical dating is available.

A sufficient erosional power of the glacier to remove considerable amounts of cosmogenic isotopes is a necessary precondition for determining the time that has elapsed since the glacier disappeared using cosmogenic nuclides. This precondition is fulfilled in case of temperate glaciers with a high sliding component. Even short periods of sliding are in some cases sufficient to produce polished landforms (Harbor *et al.*, 2006). Landscapes under cold ice may be preserved through multiple glacial cycles with only marginal erosion. This leads to complex exposure-burial histories, making multi-isotope approaches and/or the inclusion of other climate proxy records necessary for a meaningful age interpretation and its implications on landscape history (e.g. Stroeven *et al.*, 2002; Fabel *et al.*, 2002; Li *et al.*, 2008). Isotope build-up in surfaces of roche moutonnées and polished bedrock sites in general can be influenced by a thin

sediment layer remaining for a certain time after glacier recession. However, these landforms would not have formed in the case of too thick a basal sediment layer. Still visible small-scale glacial polish in turn is accepted as evidence of negligible erosion since ice retreat (Nishiizumi *et al*., 1989; Gosse and Phillips, 2001). Dating glacially polished features at (transfluence-) passes at higher-elevation sites potentially provides information about the early-Lateglacial breakdown of the ice domes being present in the high Alps during the LGM (Florineth and Schlüchter, 1998, 2000; Kelly *et al*., 2006; Cossart *et al*., 2010). Investigations in the Grimsel-pass-area in Switzerland show surprisingly low ^{10}Be and ^{26}Al ages in the range of 10.8 ka to 13.0 ka (Ivy-Ochs, 1996; Kelly *et al*., 2006). Furthermore, the youngest ages were measured at the highest altitudes, which is the opposite of what one would expect, assuming a scenario of glacier surface lowering during deglaciation. A continued activity of small cirque glaciers until the early Holocene might be a possible explanation (Florineth and Schlüchter, 1998; Ivy-Ochs *et al*., 2006). In this study, the aspect of deglaciation at high altitudes is pursued by focusing on well-pronounced morphological situations, i.e. on polished bedrock sites in palaeoglaciologically relevant positions. Furthermore, both in Val Mulix and Val Burdun, polished rock barriers in the vicinity of the LIA glacier extent were dated to set additional temporal pinpoints for the final Lateglacial glacier recession (see Chapter 1).

3.2.2 Rock glaciers

Definition and characteristics

According to Barsch (1996) three main aspects should be addressed to define rock glaciers: process, material and form. The following definition takes all of them into account (Barsch, 1996): "Active rock glaciers are lobate or tongue-shaped bodies of perennially frozen unconsolidated material supersaturated with interstitial ice and ice lenses that move downslope or downvalley by creep as a consequence of the deformation of ice contained in them and which are, thus, features of cohesive flow". Other definitions exist, attaching a higher importance to one or another of the three concerns named. Fundamental commonality is that rock glaciers are creeping permafrost phenomena in non-glacierised slopes, which means they are defined by the thermal state of their material, which is at the same time the central criterion to separate them from dead glacier ice and debris-covered glaciers (Haeberli *et al*., 2006; Harris *et al*., 2009). Permafrost is defined here as ground material with ≤ 0°C during ≥ 2 years (Permafrost Subcommittee NRC Canada, 1988). This definition is not bound to the presence of ice. Rock glaciers can be classified based on their activity-status: *active rock glaciers* contain ice and deform at rates of decimeters to meters per year, i.e., one to two orders of magnitude slower than glaciers; *inactive rock glaciers* still contain ice, but their movement is very low or zero and parts of

the rock glacier can show vegetation coverage; *relict (often termed as fossil) rock glaciers* have no ice content anymore and show a collapsed appearance, normally combined with an area-wide vegetation coverage.

All rock glaciers studied in this work formed in crystalline areas and can be described as "bouldery rock glaciers" with mean boulder diameters of ≥ 15-20 cm, following the classification scheme of Matsuoka *et al*. (2005) and Ikeda and Matsuoka (2006). Prerequisites for a rock glacier to develop (Fig. 3.6) can be summarised with, (a) material supply and a topographical setting permitting the accumulation of a talus ("talus-derived" rock glaciers), (b) a slope angle steep enough for the creep process, and (c) a hydrological and temperature regime that enables the build-up and persistence of an ice content (Frauenfelder, 2005).

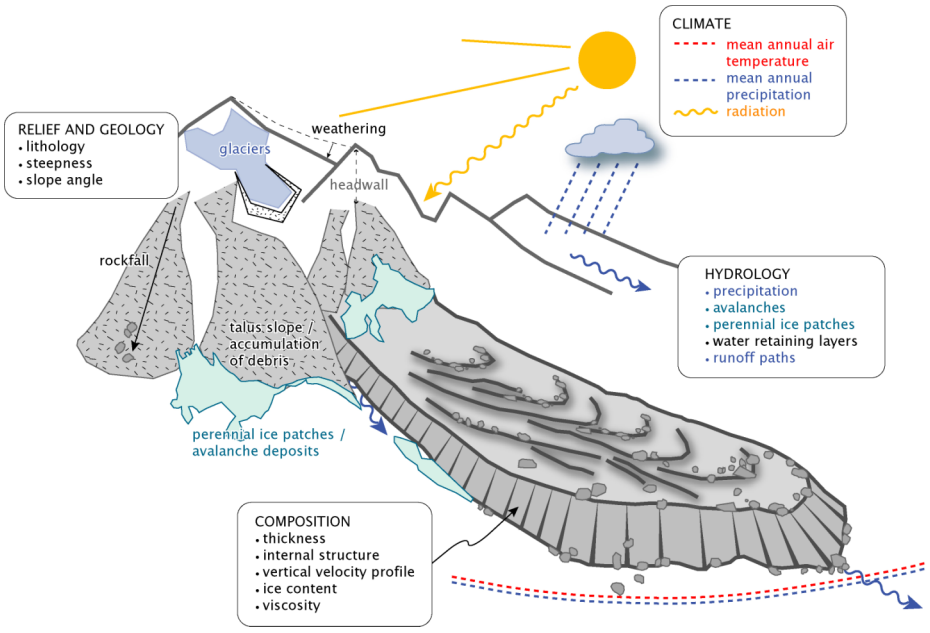

Fig. 3.6 Sketch of important boundary conditions for initiation, growth and inactivation/relictification of talus-derived rock glaciers. Illustration from Frauenfelder *et al*. (2008a).

Origins of input material and ice are numerous and various complex interactions with glaciers are imaginable (Haeberli *et al*., 2006), sometimes making a clear identification of the landform difficult. For instance, the source material can alternatively be provided by ice-cored moraines ("moraine-derived" rock glaciers) or – especially in case of "pebbly rock glaciers" (Matsuoka *et al*., 2005) in areas with sedimentary rocks – by debris flows and solifluction. Inactivation and subsequent relictification are initiated either by excessive temperatures (climatic inactivity) or slope angles below the threshold or reduced/stopped debris supply, alternatively (dynamic inactivity).

Characteristic active layer thicknesses range from a few centimetres to a few meters (Humlum, 1997). Whereas in the fine-grained and often ice supersaturated material of the lower parts energy fluxes are mainly conduction-controlled, the uppermost part, normally consisting of increasingly blocky material, represents a highly heterogeneous layer that is strongly influenced by the thickness and temporal distribution of the snow cover (Haeberli *et al*., 2006). As a consequence of the rock glacier's own characteristic microclimate, they show a considerably slow reaction (thermal inertia) to air temperature changes (Frauenfelder, 2005). However, differences in flow velocities as a direct reaction to temperature increase were measured (e.g. Roer *et al*., 2005, 2008; Kääb *et al*., 2006; Delaloye *et al*., 2008). Thermal characteristics of the active layer and coupling mechanisms to the atmosphere play a key role in understanding the age, climatic sensitivity and palaeoclimatic significance of rock glaciers (Humlum, 1996; Haeberli *et al*., 2006).

Active rock glaciers occupy a well-defined climatic niche above the lower boundary of (discontinuous) permafrost, approximated by the -1 to -2°C mean annual air temperature isotherm and below the ELA of glaciers (Haeberli, 1985). Favourable conditions for rock glacier formation can be found in cold and rather dry regions, but also or especially at sites where the input of talus is high in relation to the accumulation of snow (Humlum, 1998). The factors separating glaciers and rock glaciers, therefore, are not exclusively the result of regional climatic differences but are rather of a topoclimatic nature. Still, temperatures in the permafrost body often are close to the melting point, making rock glaciers highly sensitive to temperature variations. Outside the High Arctic, many rock glacier end positions are close to the limits of local permafrost occurrence (Haeberli *et al*., 2006). This makes relict forms reliable tools for reconstructing past permafrost conditions (e.g. Frauenfelder *et al*., 2000, 2001; Aoyama, 2005; Ballantyne *et al*., 2009). Furthermore, considering the typically low deformation rate, the debris accumulated in rock glaciers reflects past frost weathering and rock fall activity over time scales of centuries to millennia. For the decipherment of rock glaciers as (palaeo-)climatic geoindicators, dating them is required (Haeberli *et al*., 2003).

Dating rock glaciers

To date rock glaciers, an application of both relative and numerical dating techniques proved to be the most promising strategy. These include photogrammetry, radiocarbon dating, weathering rind thicknesses, Schmidt-hammer rebound values, lichenometry, luminescence and surface exposure dating. This combined approach was described in detail by Haeberli *et al*. (2003). In this study, differing subsets of the above methodological configuration were used, whenever possi-

ble together with already available complementary data. Whereas relative methods – especially Schmidt-hammer and weathering rind measurements – are routinely used (for references see the correspondent sections in Chapter 3 and Chapter 1), results from exposure dating on rock glaciers are scarce (e.g. Ivy-Ochs *et al*., 1996, 2006a, 2009a; Hippolyte *et al*., 2009; Ballantyne *et al*., 2009) and luminescence ages virtually inexistent (preliminary results from the rock glacier Murtèl yielding ages in the range of 4-8 ka are reported in Haeberli *et al*., 2003). Datings from organic impurities underline the concept of active rock glaciers as Holocene features (Haeberli *et al*., 1999; Konrad *et al*., 1999)

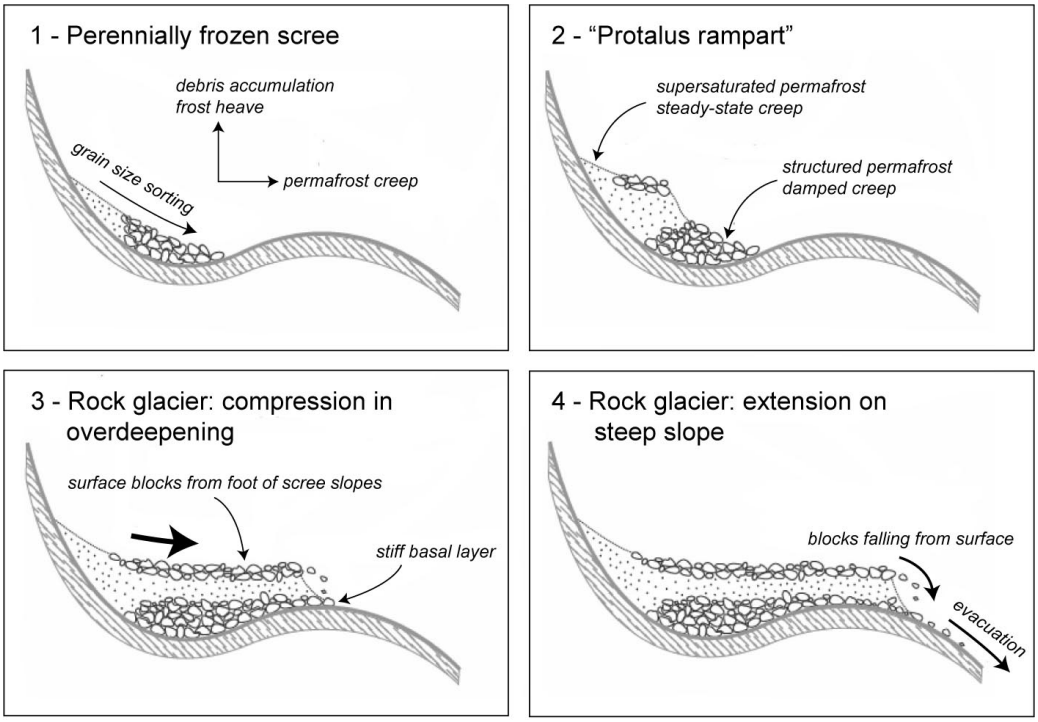

Fig. 3.7 Idealised sequence of rock glacier development (after Haeberli *et al*., 1998a).

A model of rock glacier development helps to illustrate the concepts behind dating rock glaciers (Fig. 3.7). A main element is that boulders initially deposited on the surface may fall down the oversteepened front and are subsequently overridden by the creeping supersaturated fine material ("caterpillar effect"). This results in an age inversion: at the surface, the age of the blocky material increases towards the front; for the overridden base-layer, the opposite is true (Haeberli, 1985). For exposure ages obtained from boulders at the surface near the front of active rock glaciers, this means that they must be interpreted as minimum ages, as the oldest material representing the true age of the rock glacier is inaccessible underneath the rock glacier body. This must also be taken into account with derived ages from Schmidt-hammer and weathering rind measurements. Luminescence ages from fine material taken at the front are inter-

preted as true travel times of buried particles that have participated in the long-term creep process of the perennially frozen talus (Haeberli *et al*., 2003). Crucial precondition is a sufficient bleaching of the material before being incorporated into the rock glacier. Factors that must be considered for a valuable interpretation of luminescence ages are discussed in Chapter 6 (Discussion).

3.2.3 Rock wall stability and mass movements

With the rock wall at Aiguille du Midi and the rock avalanche in the Val Burdun, there are two sites in this study that not only ask for a pure temporal assignment of the involved events, but also pose questions about the factors making the events possible to happen. Therefore, a quick overview of general characteristics and important processes influencing the stability of steep rock slopes (≥ 35°-37°, depending on author; Fischer, 2009) in high-alpine environments is given here.

General characteristics and involved processes

"High-alpine environments" in this context refer to rock walls that are (a) glacierised or (b) situated in the vicinity of and influenced by glacial environments, i.e. in the periglacial zone in its strictest sense (Huggett, 2003). These zones are often associated with permafrost conditions. Both hanging glaciers and extensive ice coverage in steep slopes are indicators for the presence of permafrost (Haeberli *et al*., 1997; Lüthi and Funk, 1997).

Besides topography, the geologic setting defining the hydrological properties; and thus the susceptibility to weathering processes (e.g. Matsuoka and Murton, 2008), are the most important factors determining the vulnerability of rock slopes to destabilise (Dorren, 2003). Possible reasons for slope failure are manifold and in most cases cannot be explained with one single factor, but rather by a combination of interacting processes (Fischer, 2009). Making a clear distinction between material-supplying processes (promoters or conditioning processes) and triggers that cause the actual start of the movement is often impossible (Dorren, 2003), especially for prehistoric events (Fischer, 2009; Matthews *et al*., 1997). Seismic or volcanic activity certainly can be accepted as triggers. Water input as a result of heavy rainfall or melting of snow causes high water pressures in joint systems and can thus act as a trigger as well (e.g. Gruner, 2006), but also promotes other processes that contribute to the weakening of the rock material. Two of them, namely changes in permafrost conditions and effects subsequent to deglaciation are strongly climate-dependent and likely play a role in the studied sites herein. They are, therefore, described in some detail.

The influence of permafrost thaw on the stability of steep rock walls

Various mass movement processes in high-alpine areas covering magnitudes from small rock-falls up to landslides are assumed to be influenced by changes of permafrost conditions (Haeberli *et al*., 1997; for references see e.g. Gude and Barsch, 2005 or Gruber and Haeberli, 2007). Magnitude and time scales are linked. *Active layer formation* as an immediate and shallow reaction to the actual weather normally provides small grain sizes. The high number of events that occurred during summer 2003 gave an impression of the effects of *active layer thickening* as a result of an exceptionally hot summer or rising temperatures over several years (Gruber *et al*., 2004a). *Deep permafrost degradation* (warming at depth) supporting big events may be delayed by decades, centuries or even millennia (Gruber and Haeberli, 2007).

Fig. 3.8 Ice in the starting zone of a rock fall occurred in summer 2003 at Matterhorn provides a hint that thawing permafrost might have contributed to the weakening of the rock material (left). At lower altitudes within the area that was ice-covered during the last glacial cycle, paraglacial adjustment may lead to mass movements in glacially steepened rock walls (right, Mont Rouge de Peuterey).

Although in numerous cases the correlation between rock fall initiation and changes in the permafrost conditions is weak (Gude and Barsch, 2005), the observation of massive ice in the starting zone of many recent rock fall events (e.g. Deline, 2001; Noetzli *et al*., 2003) indicates an influence of the climate-induced degradation of permafrost on the stability of steep rock slopes. Furthermore, measurements of permafrost degradation and physical concepts that link warming and destabilisation exist and underline the assumed effect of permafrost (Gruber and Haeberli, 2007). Permafrost in steep bedrock is affected by temperature changes very effectively for several reasons: (1) the complex topography in mountainous areas allows for a faster warming from different sides than is the case for flat surfaces (Noetzli and Gruber, 2009), (2) bedrock usually contains less ice than other permafrost, supporting heat penetration by heat con-

conduction (latent heat is limited) and (3) increasingly steep slopes have a snow coverage with decreasing thickness or no snow at all, resulting in the absence of the insulating effect of snow and thus in a more direct coupling of atmosphere and rock surface (Gruber and Haeberli, 2007). Near the surface, joints and fractures play a vital role as they enable advective heat transport by percolating water, inducing temperature changes in a very fast way.

Effects of deglaciation on rock slope stability

An initial effect is the exposition of *steepened rock slopes* resulting from glacial erosion. The reaction of glacially steepened rock slopes is strongly dependent on lithology and structure. Especially the joint density as well as the orientation and inclination of discontinuities and planes of weakness relative to that of the newly exposed rock face are characteristics defining slope stability after ice retreat (Augustinus, 1995a). Increased self-weight shear stresses acting within the rock promote rock slope failure along pre-existing joint sets or other planes of weakness during or after ice recession (Augustinus, 1995b; Ballantyne, 2002).

A second effect is termed as *debuttressing*, meaning the relaxation of internal stresses after deglaciation and the associated propagation of internal joint networks resulting in a time-dependent rock slope weakening (Augustinus, 1995a; Ballantyne, 2002; Cossart *et al*., 2008 and references therein). Similar to the effects caused by permafrost thawing in rock walls, also glacial unloading (as sometimes used synonymously with debuttressing) is hard to identify either as an isolated conditioning process or as a failure trigger itself, which is especially true in tectonically active mountain ranges (Cossart *et al*., 2008).

Both mechanisms are important elements of the "paraglacial" concept. Introduced by Ryder (1970) and conceptualised by Church and Ryder (1972), this term has a dimension regarding both processes and time. Firstly, it describes non-glacial processes that are directly conditioned by glaciations, peculiarly proglacial processes and those occurring around and within the margins of a former glacier. At the beginning restricted to certain processes, Ballantyne (2002) proposed a concept of a paraglacial geomorphology with the unifying element of *glacially conditioned sediment availability*. Secondly, there is the temporal meaning: a period is described as paraglacial when paraglacial processes occur. It is a transitional time window starting after a glacial period when glacial debris is abundant and ending when the relatively rapid adjustment to non-glacial conditions is finished (Fig. 3.9 A). During this period, a wide range of enhanced processes including slope failures, debris flows and fluvial reworking of sediment is active with decreasing intensity, until a geological «norm» is reached (Ballantyne, 2002; Mercier, 2008).

With focus on debuttressing-induced large-scale slope failures, Cruden and Hu (1993) have proposed a rapidly decreasing number of events with time after deglaciation, expressible by a negative exponential exhaustion model (Fig. 3.9 B). Slope instabilities caused by tectonic stresses and seismic events in turn are not related to the time elapsed since ice recession (Cossart *et al*., 2008). In order to confine triggers coming into question in general and to estimate the possible contribution of paraglacial processes, dating mass movements is indispensable. Deposits with an accurately known age can also serve for deriving production rates of cosmogenic nuclides (e.g. Kubik and Ivy-Ochs, 2004).

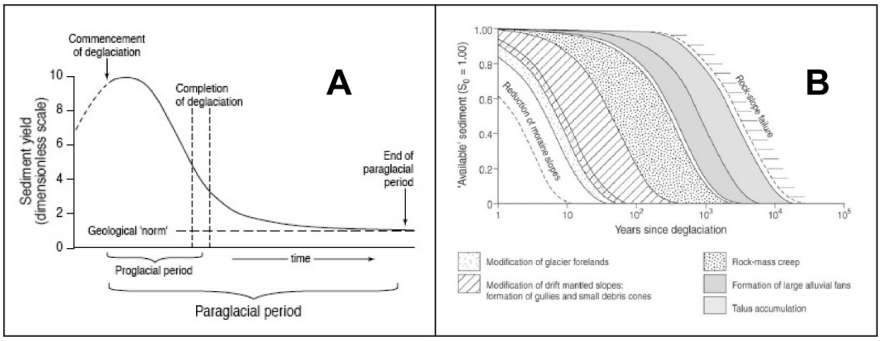

Fig. 3.9 Schematic representation of the paraglacial concept (A) and families of exhaustion-curve envelopes, describing the state of (primary) paraglacial landscape adjustment at any time after deglaciation (B) (from Ballantyne, 2002).

Dating mass movements

Recently, an increasing number of studies explicitly or implicitly refer to the paraglacial concept. Determining temporal and spatial coincidences of deglaciation and rock slope failure events requires adequate dating of the deposits and related glacial remnants, as far as possible. Lang *et al*. (1999) discuss different methods for assessing the temporal occurrence of mass movements. In the European Alps, many of the large-scale landslides occurred during the marked transition to warmer, wetter conditions during the Holocene, complicating the identification of possible causes. Most prominent examples dated using ^{10}Be (partly combined with ^{14}C) are the Köfels landslide in Austria (9.8 ka; Ivy-Ochs *et al*., 1998), the Flims landslide, (8.9 ka; Ivy-Ochs *et al*., 2009b) and the Kandertal landslide (9.6 ka; Tinner *et al*., 2005), both situated in Switzerland. A combined approach including ^{10}Be datings of rock slope failures in southeastern France, glacier extent reconstructions, and GIS techniques suggests that major rock falls and rock avalanches are associated with areas subject to the highest decompression stresses (Cossart *et al*., 2008). A rock avalanche event from the Italian Alps with a similar geomorphological setting as in the Val Burdun is discussed by Hormes *et al*. (2008). Surface exposure dating yielded an age of 7.4 ka for the rock avalanche deposit and around 11 ka for the nearby moraines that

were used to constrain the timing of the last deglaciation. Based on the time lag of roughly 4 ka, the authors concluded that slope stress release must have played a minor role. Instead, enhanced seismicity caused by regional isostatic glacial rebound coupled with tectonic stress or an upwards movement of the lower permafrost limit must be expected as important triggering processes. Deline (2009) provides an overview of interactions between rock avalanches and glaciers, focussing on Holocene events dated with the radiocarbon method as well as on modern events. In addition to possible triggering mechanisms, interactions influencing run out distances and possible effects of deposits on flow and melt behaviour of glaciers are discussed. A very recent event in western Austria – dated by historical photographic evidence and lichenometry to the late twentieth century – was studied by Matthews and Shakesby (2004). An extreme rainfall is suggested as the main triggering factor; however, paraglacial processes taking place after the melting of the Little Ice Age glaciation ("neoparaglacial") were likely important contributors to rock weakening.

3.2.4 Weathering processes and soil formation

Two main types of weathering are distinguished: *physical (mechanical) weathering* and *(biogeo-)chemical* weathering. In nature they act together, and it may be difficult to separate their effects (Birkeland, 1999). The main component of physical weathering is the repeated generation of stress, resulting in fatigue of rocks and an increased susceptibility to fracture. Involved processes include unloading, frost action, thermal stress caused by heating and cooling, swelling and shrinking due to wetting and drying, and pressures exerted by salt-crystal growth (Huggett, 2003). Biomechanical effects like pressure caused by root growth or changed albedo of rock surfaces due to lichen cover and linked thermal properties may be added. Frost weathering – acting where rocks experience a temperature fluctuation across the freezing point with moisture present – is likely the most fundamental weathering process in high mountain areas. A state-of-the-art report on this issue is provided by Matsuoka and Murton (2008).

Mechanical weathering leads to progressively smaller fragments and thus increases the surface area exposed to chemical weathering. A huge number of chemical reactions factor into chemical weathering. Oxidation and dissolution are the main reactions for weathering rind genesis (Oguchi, 2004 and references therein), although biogeochemical processes through organic and inorganic acid production seem to play an important role as well, even in glacial and periglacial environments (Etienne, 2002).

Chemical weathering processes are constitutive for soil formation. Diverse processes including depletion of original minerals, alteration and neoformation of clays and oxides/oxihydroxides, changes in major-element chemistry compared to parent material and dislocation processes lead to specific chemical and physical properties of the different soil types (Birkeland, 1999). Soils can be described as a transitional medium between, and interacting with, atmosphere, biosphere and lithosphere. In this sense, they are open systems and their characteristics cover a wide range, according to the different and varying forming factors their development depends on (Birkeland *et al*., 2003; Dixon and Thorn, 2005). Traditionally, soils are understood as a function of several state factors (Jenny, 1941, 1980): parent material, climate, topography, biological activity and time. By choosing sampling sites minimising the effect of soil forming factor other than time, the influence of time on soil formation can be studied (chronosequence). Soils can thus be used as archives of changing weathering conditions. Sampled on moraines and other glacial and periglacial deposits, soils can either be helpful relative age indicators to estimate the age of the landform or, provided that independent dating is available, to derive rates of different time-dependent processes (Egli *et al*., 2001, 2003; Munroe, 2008; Schaller *et al*., 2009).

In this thesis, a number of soil forming processes and derived weathering indices from soils developed on Lateglacial moraines and rock glacier lobes were applied. Here, the principles behind them are briefly introduced, and laboratory procedures and mathematical background information can be found in Chapter 4.

Mass balance calculation

Differences in the chemical composition of fresh source rock and soil material can be used to derive weathering properties. In most cases, chemical and biophysical weathering is not isovolumetric and an elementary volume may dilate or collapse during soil evolution. Considering these enrichment/depletion factors ("strain") - determined using concentration profiles of immobile elements such as Ti or Zr - element specific gains and losses and, in the case of known landform ages, long-term weathering rates can be calculated. See also April *et al*. (1986) and Eggenberger (1995), for theoretical and mathematical background Chadwick *et al*. (1990) and Egli and Fitze (2000).

Clay mineral formation

Clays are minerals that occur as grains that are less than 2 μm in their largest dimension. The overwhelming part is made up of hydrated alumino-silicates with a layered structure. The large

ratio of surface area to volume and their chemical structure makes them highly reactive and they are important contributors to cation exchange capacity and influence plastic properties of soils due to the ability of some clays to shrink and swell (vermiculite, smectite) (Moore and Reynolds, 1997). Clays are mostly secondary products that crystallise in the aqueous environment at the Earth's surface from constituent ions released by dissolving primary minerals such as feldspars (Schulze, 2005). During soil formation, mineralogical characteristics of clays are modified. Although clay formation can be influenced by vegetation (Zanelli *et al*., 2007) and topographical characteristics (Egli *et al*., 2007), the presence and amount of specific clay minerals is directly coupled to the weathering stage and thus the age of the soil. For instance, investigations on moraine sequences in Switzerland showed that smectite is the end product of mica alteration (Righi *et al*., 1999; Egli *et al*., 2001). Alternative formation paths starting with chlorite or inherited smectite, respectively, were found as well (Egli *et al*., 2001). Significant losses of chlorite and mica and corresponding clay mineral transformations are especially pronounced within the first 3,000 years of soil formation (Egli *et al*., 2003).

Podsolisation process

The soils investigated in this study are different types of podzols, which are typical for Alpine soils developed on silicatic parent material. The weathering state of the soil is indicated by the visible differentiation of soil horizons and by chemical parameters changing during soil development. Characteristic for podzols is the downward migration of Al, Fe and OM from the eluvial (E) horizon with a re-accumulation in the spodic horizon (illuvial – Bs/Bhs). Main process causing this dislocation is chelation, that is, the removal of metal ions bound on organic acids at low pH values forming soluble organic matter-metal complexes.

Quickly adapting processes like acidification are not applicable as soil age classification methods on very old soils because they reach state of equilibrium within a few hundred years (Fitze, 1982). However, the formation of different solid phases of Al and Fe as determined by selective chemical dissolution techniques seems to take place over thousands of years. Ratios changing over time (e.g. Al_d/Fe_d increasing with time) as a result of differing weathering stability and mobility behaviour can thus be used as relative age indicators.

Inventory of meteoric ^{10}Be

Cosmogenic nuclides such as ^{10}Be not only allow superficial features to be dated (section 3.1), they are also suitable for exploring denudation and – in combination with another nuclide like ^{26}Al – burial processes and to estimate their rates (e.g. Braucher *et al*., 2009; Granger *et al*.,

2006). In soils depth profiles of both in situ-produced and meteoric ^{10}Be are used to derive exposure time and denudation rates. Braucher *et al.* (2009) and Lal and Chen (2005) provide a detailed mathematical basis for different scenarios of the first case. In this study, however, the focus is on meteoric ^{10}Be.

$Be(OH)_2$ has a very reactive nature and binds tightly to soil and sediment particles. In near-neutral conditions, adsorption to the clay fraction plays an important role (e.g. Maejima, 2004, 2005). Beryllium in acidic soils is present mainly in oxide-bonded forms (Barg *et al.*, 1997) and, in the presence of humic acid, as a humate complex. ^{10}Be shows a low mobility at $pH > 4$ (Willenbring and von Blackenburg, 2009). At $pH < 4.1$, Al^{3+} is released and may compete with Be for exchange sites. However, only at sites with very high precipitation might dissolved Be be lost into the ground water (Willenbring and von Blanckenburg, 2009 and references therein). It can be therefore assumed that the overwhelming part of ^{10}Be is adsorbed in the fine earth fraction, also in acidic alpine soils as studied here. Thus, the inventory of ^{10}Be (atoms cm^{-2}) since the initiation of soil formation is increasing with soil age (Pavich *et al.*, 1984; Pavich and Vidic, 1993). Based on this inventory, a soil age can be calculated (see Chapter 4.5.6).

Radiocarbon dating of the stable fraction of soil organic matter (SOM)

Recent investigations show that chemical isolation and radiocarbon dating of resilient material (i.e. the fraction of soil organic matter resistant to H_2O_2 oxidation) might be a valuable tool to gain information about landform ages (Favilli *et al.*, 2008). Generally, three processes are distinguished to form passive, or long residence time, soil organic matter fractions (e.g. Oades, 1995; Eusterhues *et al.*, 2003 and references therein): (i) chemical recalcitrance induced by structural properties, (ii) physical protection due to inclusion of organic matter into aggregates or micropores and (iii) protection through interaction with soil minerals and metal ions. The goal is to isolate organic material that formed at an initial stage of soil development and was bound since then in one of the afore mentioned ways, resulting in a very long turnover time (the recalcitrant and mineral-protected OM; Fallon and Smith, 2000). In addition to these mechanisms, decomposition of OM in mountain regions may also be inhibited by low soil temperatures in general (e.g. Mikan *et al.*, 2002), and especially pronounced under permafrost conditions

As this method is not based on dating of macro-remnants, the ages yielded are necessarily average ages that underestimate the real age of the soil (Wang *et al.*, 1996). With regard to us-

ing them as age indicators, in any case they must be interpreted as minimum ages giving a rough age estimation for the deposition of the underlying parent material (glacial, periglacial).

Chapter 4

Methods

4.1 Surface exposure dating (SED) using in-situ produced cosmogenic ^{10}Be

4.1.1 Principle and applications

The measured amount of certain cosmogenic nuclides allows for the determination of the time a rock surface has been exposed to cosmic rays. The amount of nuclide build-up over time is predictable (Gosse and Phillips, 2001), a precondition is to accurately calculating the site-specific (local) production rate. The most important nuclides for dating rocks are radioactive ^{10}Be, ^{26}Al, ^{36}Cl and stable ^{21}Ne and ^{3}He. This work uses the ^{10}Be nuclide; it is the one most appropriate for questions concerning glacial chronology.

Entering the earth's atmosphere, primary cosmic rays (mostly protons and α-particles) trigger cascades of secondary particles (especially neutrons) that interact with target elements in minerals in rock surfaces. Whereas primary particles are modulated by the sun's magnetic field (their flux is inversely proportional to solar activity) and the earth's dipole field, the flux of secondary particles is reduced with an increasing travel distance through the atmosphere. This means that nuclide production rates are higher at high latitudes and altitudes (Gosse and Phillips, 2001) and sea level high latitude production rates must be scaled to the site-specific position (Stone, 2000) (Fig 4.1). Surrounding topography and orientation as well as inclination of the sampled site are additional factors that influence the cosmic ray flux and hence the local production rate must be corrected for. Also coverage with snow or sediment reduces the local production rate very effectively and must be taken into account. This is very difficult, as accordant coverage thicknesses are not normally known.

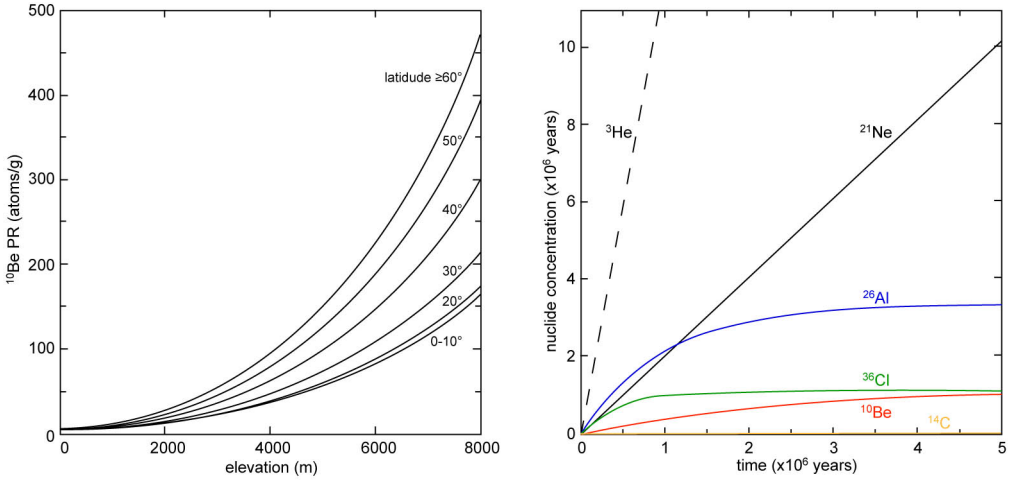

Fig. 4.1 Influence of altitude and latitude on the production rate (left),) and nuclide build-up with time for different stable (^{3}He and ^{21}Ne) and radioactive nuclides (right). Erosion is not taken into account in the right graph and would lead to an earlier approach of the saturation level (left graph from Ivy-Ochs and Kober, 2008, based on Stone, 2000; right graph from Ivy-Ochs and Kober, 2008).

Quartz is an ideal target mineral for isolating in-situ produced ^{10}Be. It is ubiquitous and is suitable for chemical treatment in order to avoid the influence of meteoric ^{10}Be. Due to its simple chemical structure and high erosional resistance, it fulfils the demand of a "closed system" (Lal, 1988). Three principal mechanisms by which isotopes are produced in terrestrial rocks can be distinguished (Lal and Peters, 1967; Lal, 1988): (1) high-energy spallation by nucleons, (2) neutron capture reactions and (3) muon-induced nuclear disintegrations. Spallation is by far the most important process for the production of ^{10}Be. Generally, an exponential decrease of the spallogenic ^{10}Be production with depth is assumed (Lal, 1991). However, several authors propose a depth profile that is "flat" (non-decreasing) for the first few centimetres below the surface, followed by an exponentially decreasing production rate in greater depths (e.g. Kubik and Reuther, 2007). In any case erosional processes at the surface have a substantial impact and lower the nuclide concentration, leading to an underestimation of the age of the landform. Modern studies make use of the fact that muon and neutron interactions show significantly different attenuation lengths to derive denudation rates (e.g. Braucher et al., 2009 and references therein).

In case of stable isotopes nuclide concentration increases linearly with time as described by the following simple equation (Nishiizumi *et al.*, 1993):

$$C_{(t)} = P_{(0)} \cdot t \qquad (4.1)$$

where $C_{(t)}$ (atoms g^{-1}) is the time dependent nuclide concentration, $P_{(0)}$ (atoms g^{-1} a^{-1}) is the site specific production rate at the surface and t (a) is the exposure age of the surface. With radionuclides the relationship becomes more complex:

$$C_{(t)} = \frac{P_{(0)}}{\lambda}\left(1 - e^{-\lambda t}\right) \qquad (4.2)$$

where λ (a^{-1}) is the decay constant. In both cases erosion is assumed to be zero, which is certainly not correct for the European Alps, even for crystalline rocks as addressed in this work. According to Cockburn and Summerfield (2004) erosion rates up to 10 mm ka^{-1} must be taken into account for crystalline rocks, especially in case spallation-dominated nuclides like ^{10}Be. Equation 4.2 expands to:

$$C_{(t)} = \frac{P_{(0)}}{\lambda + \frac{\rho\varepsilon}{\Lambda}}\left(1 - e^{-\left(\lambda + \frac{\rho\varepsilon}{\Lambda}\right)t}\right) \qquad (4.3)$$

where ρ (g cm^{-3}), ε (cm a^{-1}) is the erosion rate and Λ (g cm^{-2}) is the attenuation length. Principally, nuclides build up until accumulation equals radioactive decay. This saturation is reached after approx. 3-4 half-lives, meaning an upper age limit for ^{10}Be ($t_{1/2}$ = 1.5 Ma) of about 5-6 Ma with no erosion included (Fig. 4.1).

A basic assumption for the interpretation of calculated exposure ages is that $C_{(t)} = 0$ for t = 0, that is, the initial nuclide concentration is zero. The presence of inherited nuclides can be tested by comparing the exposure age of a stable nuclide with that for a radionuclide (Nishiizumi *et al*., 1993). In case of glacially polished bedrock for instance, a minor glacier re-advance removing only a few centimetres of material would lead to a lower age derived from the radionuclide than from the stable nuclide as a result of the decay during the interruption of cosmic ray exposition. Alternatively, a couple of radionuclides with differing $t_{1/2}$ can be used (e.g. Davis *et al*., 1999).

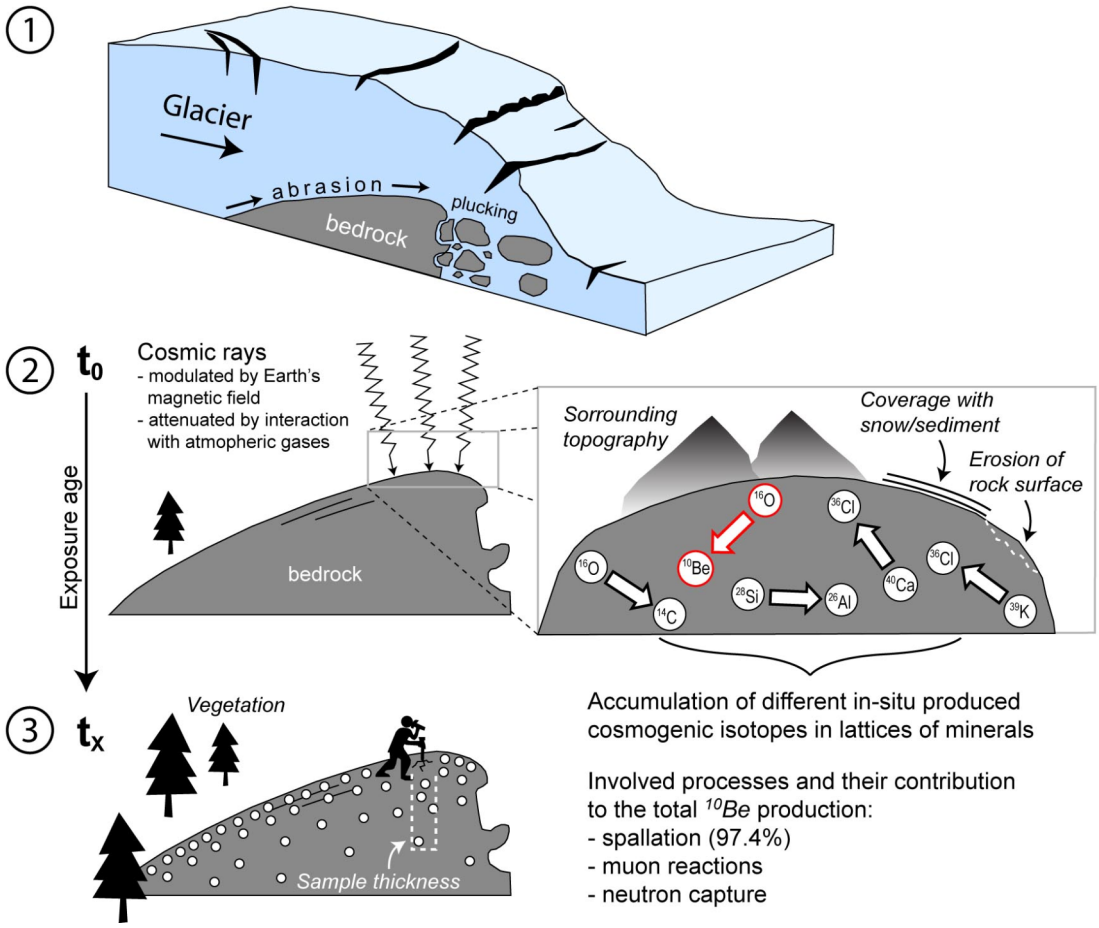

Fig. 4.2 Summarising sketch of the principle of SED using the example of a roche moutonnée. Cosmogenic nuclides are removed by glacial erosion (1). As soon as bedrock is exposed to cosmic rays (= t_0), nuclide build-up starts following different production paths, from which the most important ones are shown (2). After a certain time t_x a sample is removed and the accumulated nuclides since t_0 are measured (3). Factors influencing the local production rate are written in italics (modified from Reuther *et al*., 2006).

The AMS technique and the increasing number of detectable nuclides in different minerals opened the field of questions that can be addressed within Quaternary chronology and landscape evolution using SED. For comprehensive overviews of possible applications, reference is made to Gosse and Phillips (2001); Cockburn and Summerfield (2004); Ivy-Ochs and Kober (2008) and, with a special focus on glaciology and glacial geomorphology, to Fabel and Harbor (1999) and Reuther *et al*. (2006).

4.1.2 Field strategy and sample preparation

All samples were removed with hammer, chisel and partly with a drilling machine. For dating we used only the uppermost ≤ 5 cm of the rock surfaces. We followed strict sampling requirements and sampled only boulders with a height of ≥ 1.5 m on the top of moraine crests in order

to ensure the highest possible geomorphological stability (Gosse and Phillips, 2001; Ivy-Ochs and Schaller, 2010). Boulders that possibly have been covered by till and eroded out after moraine stabilization as well as boulders with evidence of spalling were avoided because it would lead to an underestimation of the effective exposure time (Reuther *et al.*, 2006; Ivy-Ochs *et al.*, 2007). Because of possible edge effects (Masarik and Wieler, 2003), marginal positions on sharply shaped boulders were not sampled. Roche moutonnées were sampled on or near the top. Here, lichen types and coverage were helpful indicators of snow influence and to identify areas that were split off in the past. All boulders sampled on the rock avalanche (Val Burdun) were at least 1.5 m high and flat-topped. In most cases, only one boulder per moraine large enough for surface exposure dating could be found. We are aware of the fact that ages obtained from different boulders on one and the same moraine show a certain variability and that there is a particular tendency to underestimate the true age (Putkonen and Swanson, 2003). From our point of view, however, in the case of a lack of several suitable boulders, it is better to rely just on one boulder with suitable size and position than to take into account a greater number of small and possibly unstable boulders. Furthermore, dating of additional associated landforms gives a morphostratigraphical framework and minimizes potential errors.

The samples were crushed, sieved and leached in order to obtain pure quartz following Kohl and Nishiizumi (1992) and Ivy-Ochs (1996). ^{9}Be solution was added to the dried quartz, which was then dissolved in 40% HF. Be was isolated using anion and cation exchange columns followed by selective pH precipitation techniques (Ivy-Ochs, 1996). The ^{10}Be/^{9}Be ratios were measured at the ETH Zurich Tandem Accelerator Mass Spectrometry (AMS) facility using ETH AMS standards S555 (^{10}Be/^{9}Be = 95.5 × 10^{-12} nominal) and S2007 (^{10}Be/^{9}Be = 30.8 × 10^{-12} nominal), both associated with a ^{10}Be half-life of 1.51 Ma (Kubik and Christl, 2009).

4.1.3 Age calculation

The surface exposure ages were calculated using a sea level and high latitude production rate of 5.1 ±0.3 ^{10}Be atoms/gram SiO_2/year with 2.2 % production due to muon capture. This production rate was scaled for latitude and altitude based on Stone (2000) and corrected for sample thickness assuming an exponential depth profile (Brown et al., 1992) with an effective radiation attenuation length of 155 g cm^{-2} (Gosse and Phillips, 2001), a rock density of 2.65 g cm^{-3} and a snow density of 0.3 g cm^{-3}. Erosion was assumed to be 3 mm ka^{-1} (Ivy-Ochs et al., 2004). Topographical (skyline) shielding was calculated based on Dunne et al. (1999) with a 25 m DEM (source: swisstopo) and a geographical information system (ArcGIS 9.2). The geomagnetic field

correction was omitted (Masarik et al., 2001; Pigati and Lifton 2004) because the effect of maximal 1-2 % is small in the Alps.

The snow cover was estimated according to the mean of the November - April snow heights measured between 1983 and 2002 at three nearby weather stations (data source: Swiss Federal Institute for Snow and Avalanche Research, MeteoSwiss). The values from these three stations, all roughly at the same altitude, are comparable. Thus, a mean snow height of 1.5 m over six months could be derived and seems to be a realistic value for 2500 m asl in this region. The theoretical snow height for each sample site was estimated using a mean snow height gradient of 0.08 m/100 m altitude difference (Auer, 2003). We also considered boulder shape, wind exposition and surrounding vegetation. These factors lead to a reduction of snow height compared to a flat area. In addition, satellite images taken in June from three different years (Spot images, 1993-1995), were compared in regard to the snow cover in the investigation area. Results from Bottas Glischas showed that at least for some years, a longer lasting snow cover needs to be considered. The derived recent snow cover is assumed to be representative for the whole Holocene. For the Val Burdun we took snow heights directly from the map sheet "Snow heights 1983-2002" of the "Atlas der Schweiz 2.0" (2004) as maximum values. At Aiguille du Midi no correction for snow was made because of the near-vertical surface slopes. Here, azimuth dependent angles were extracted from a topographical map to calculate skyline shielding.

Estimated errors are given on the 1σ level, including the measurement error and the effects of altitude/latitude scaling, topography and depth. Mean ages given are arithmetic means with errors calculated as described in Ivy-Ochs et al. (2009b).

4.2 Luminescence dating investigations

4.2.1 Principle and applications

Defects in crystal structures of minerals act as traps for electrons that were displaced to higher energy levels as a result of exposure to ionising radiation. Such materials may act as radiation dosimeters (Wintle, 2008) because the number of electrons is proportional to the amount of radiation absorbed. Released from the traps, the recombination in the crystal at luminescence centres results in the release of energy (light) (Fig. 4.3). Thus this luminescence signal is a measure of the radiation dose the mineral received.

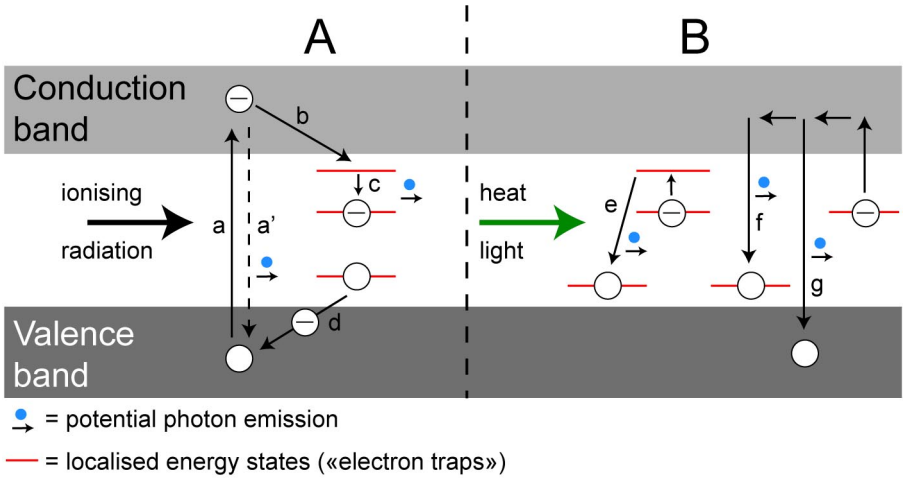

Fig. 4.3 Processes leading to a latent luminescence signal (A) and stimulation of luminescence by heat and light (B) (simplified):

a – Valence electrons are excited by ionising radiation and have sufficient energy to reach the conduction band, leaving a hole in the valence band.

a' – Most of the electrons recombine immediately with holes in the valence band.

b, c – Prompt transition of a few excited electrons into localised energy states ("electron traps").

d – Holes in the valence band may be filled by electrons from localised levels. As a result, holes from the valence band are transferred to localised levels.

e, f – Recombination with localised holes either via an unstable level (e) or via the conduction band (f).

g – Recombination with a hole in the valence band with energy loss emitted as light (luminescence).

(modified from Preusser *et al.*, 2008):

Luminescence dating techniques make use of this principle by provoking the recombination under laboratory conditions. The luminescence signal is used to determine the time that has elapsed since mineral grains were last exposed to daylight or heated to high temperatures. Depending on whether the luminescence signal is stimulated by heat or photons, a general distinction can be made between thermoluminescence and photoluminescence, the latter being of interest in this study. OSL was introduced by Huntley *et al.* (1985) using green laser-light for stimulation. Infrared stimulated luminescence (IRSL, introduced by Hütt *et al.*, 1988) is a particular kind of feldspar OSL that occurs during stimulation by light of about 850-900 nm wavelength (i.e. near IR). A summary of the different methods used in luminescence dating is given in Preusser *et. al* (2008).

The intensity of the luminescence signal is a measure of the absorbed energy that accumulated since the last reset (zeroing) caused by exposure to daylight. To yield sedimentation ages, this amount of absorbed energy – the *palaeodose (Gy)* – is related to the energy uptake over a year – the *dose rate (Gy* a^{-1}*)* (1 Gy = 1 J kg^{-1}):

Luminescence age (a) = Palaeodose (Gy) / Dose rate (Gy a^{-1}) (4.4)

For the calculation of the dose rate essentially three components must be considered (Preusser *et al*., 2008): (1) the cosmic radiation from space, which is influenced by factors such as geographical position, altitude, sediment overload; (2) the external radiation from neighbouring grains, primarily a result of the decay of ^{40}K, ^{232}Th and ^{238}U and (3) internal radiation from within the grain (mostly from ^{40}K). (1) and (2) are influenced by the physical properties of the sediment such as water content and density. The palaeodose is determined by comparing the natural signal with that induced by exposure to several known, artificial doses. Analyses in this study were carried out following the regenerative-dose protocol by Murray and Wintle (2000).

In the meantime, luminescence dating techniques are among the most important ones for Quaternary geochronologists with a broad application area (e.g. Stokes, 1999; Lian and Roberts, 2006; Bateman, 2008; Fuchs and Lewis, 2008). One of the biggest advantages is that it is possible to date the almost ubiquitously present quartz and feldspar directly, without being reliant on often lacking organic material.

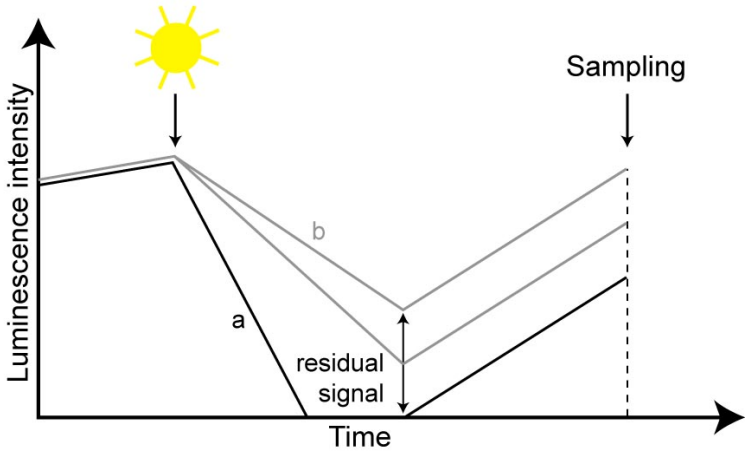

Fig. 4.4 Incomplete bleaching: The duration of exposure and the intensity of daylight is sufficient, all the grains will have no or at least strongly reduced amounts of charge left (a). In such a case, all the grains would give the same age when measured in laboratory. If the exposure to daylight is limited or varies from grain to grain (b), the charge of only a part of the grains will be reduced to zero and others retain different charge populations (residual). Case (b) is typical for fluvial and glaciofluvial environments (modified from Duller, 2008).

Thanks to technical refinements, it has become possible to detect the signal of single aliquots (Duller, 1995) or even single grains (overview in Duller, 2008), which to a certain extent reduces with the problem of incomplete and heterogeneous bleaching (Duller, 2008). Unlike for aeolian sediments, where the probability for a complete and homogeneous reset before deposi-

tion is high, in most other depositional environments (fluvial, glacial, periglacial) pre-existing (residual) charge must be expected to form part of the measured signal (Fig. 4.4).

This potentially leads to an overestimation of the palaeodose and, accordingly, of the calculated age. Possibilities for a statistical extraction of true burial palaeodoses are discussed in Bailey and Arnold (2006).

4.2.2 Field strategy, sample preparation and measurement setting

Field strategy

Rock glaciers were sampled at the talus apron at the front. To avoid the influence of superficially eroded and reworked material, we chose sampling spots in the upper third of the slope, clearly higher than the visible debris accumulation zones in the lower parts, but below the coarse blocks at the surface. The approx. 40° steep slopes showed a low stability, reducing the possible penetration depth to around 50 cm. Digging was carried out whenever possible underneath isolated boulders that protected the sandy matrix to a certain degree from collapsing immediately. We used an opaque cover to shield the sediment from daylight. Black closable plastic cylinders served as containers for transportation and storage of the sampled material.

For the determination of the specific activity of the surrounding sediment, samples for radioisotope analyses by gamma-spectrometry were taken at the same time.

Sample preparation

In laboratory the samples were treated under attenuated red light. The two outermost centimetres of the samples were removed on each side as these parts could have experienced light exposition under unfavourable circumstances. This material was used to determine the in situ water content of the sample. The separation of the quartz and the feldspar components was done as follows:

1.	Sieving	100–200 µm for single aliquots 200–300 µm for single grains
2.	Removing carbonates	10% HCl
3.	Removing organic material	30% H_2O_2
4.	Feldspar-flotation	0,2% HF; pH 2.4–2.7 with H_2SO_4 and H_2O dest., respectively; Dodecylamine; 5% HCl
5.	Density fractionation	Sodiumpolywolframate

		Quartz: 2.62–2.67 gcm^{-3}
		K-feldspar: <2.58 gcm^{-3}
		Na-Plagioclase : 2.58-2.62 gcm^{-3}
6.	Acid-treatment	Quartz: 40% HF; 37% HCl
		Feldspars: 10% HF; 10% HCl
7.	Sieving	90–160 μm for single aliquots
		200–250 for single grains

For single aliquot measurements this homogenised material was fixed on aluminium plates using silicon oil (diameter: 4 mm). For single grain measurements discs with 100 depressions arranged in a grid were used, each containing a grain of the size 200–250 μm.

Determination of the dose rate

To determine the specific activity of the sediment the radionuclides of the decay chain of ^{238}U, ^{232}Th and ^{40}K were determined by means of low level HPGe gammaspectrometry (Angewandte Physik Bergakademie Freiberg, IAF – Radioökologie GmbH Dresden, Germany).

The overall environmental dose rate (and luminescence age) was calculated with the ADELE program (Kulig, 2005). In order to asses the cosmic dose rate component, latitude, longitude, a mean altitude and an estimated thickness of the debris coverage at the sampling positions were taken into account The software-based calculation procedure follows Prescott and Hutton (1994). The efficiency of the exposition to radiation was corrected with density and water content of the sediment, mineral density, grain-size and etching parameters.

Optically stimulated luminescence measurements (OSL, quartz)

OSL single aliquot (90-160 μm, aliquot diameter 4 mm) measurements were carried out in the luminescence laboratory of the Sächsischen Akademie der Wissenschaften (SAW), Arbeitsstelle Geochronologie Quartär in Freiberg, Germany (Risø TL/OSL Reader DA 20). 20 aliquots of both the samples SAL1 and SAL2 were measured following the single-aliquot regenerative-dose (SAR) protocol (Murray and Wintle, 2000) for quartz, with four regeneration cycles after the natural signal, zero point, recycling point and sensitivity control. OSL emission was stimulated with blue LEDs at 125 C° and recorded after optical filtering (Hoya U 340). For each sample four additional dose recovery tests (Murray and Wintle, 2003) were applied to assess variability and reproducibility of the OSL-signals with the used measurement sequence and with known laboratory doses.

The samples SAL1, SUV1–4 and GiG1–2 were measured with the single grain technique (Lumineszenslabor des Geographischen Instituts der Universität Köln, Germany, Risø TL/OSL Reader DA 15). Luminescence emission was stimulated by a green laser (532 nm, ~50 Wcm^{-2}) and filtered with a Hoya U 340 filter. For each sample 2–4 discs were measured. For technical reasons, it was not possible to fill the discs (100 grains) completely. To estimate the degree of filling, the grains of some samples were counted under the microscope after the measurement. Determination of the equivalence dose was done after Murray and Wintle (2000). Dose recovery tests (Murray and Wintle, 2003) were carried out only for SAL1.

Infrared stimulated luminescence measurements (IRSL, feldspars)

Suitable pre-heating temperatures (220, 240, 260, 280 C°), filter (280, 410, 560 nm) and LED-power (10 or 90%) were evaluated with thermal transfer tests based on SAL1 (SAW, Freiberg). The optical filter fit to 3 typical IRSL emission wave-bands of feldspars with different properties (Krbetschek *et al*., 1997). After the measurement of the natural signal, four regeneration cycles, zero point, and recycling point followed, whereby for the first regeneration cycle a zero dose was applied. The temperature induced charge transfer could be detected as an OSL signal in relation to the estimated zero signal (three aliquots for each pre-heating level). This procedure was repeated for each luminescence emission (i.e. 280, 410, 560 nm).

IRSL single grain measurements were carried out at the University of Berne (Institute for Geology) for K-feldspars (12 ± 0.5 % potassium, samples SAL1, SUV2–4, GiG1–2). Additionaly, Na-plagioclase (2 ± 0.8 % potassium) was measured for SAL1 and SUV4 to test the lowered contribution of potassium to the internal dose. Again a measurement procedure after Murray and Wintle (2000) was used. A Risø TL/OSL DA 20 automated reader equipped with a special IR-single grain stimulation (IR laser, 150 mW, 830 nm) was used to perform luminescence emission at 50°C. According to the results from the thermal transfer tests, pre-heating temperature and optical detection filter were set at 280°C and 410 nm, respectively. Dose recovery tests were made for SAL1 (K-feldspar, plagioclase) and SUV2 (K-feldspar) (Murray and Wintle, 2003; Tab. 4.1).

Table 4.1 Overview of carried out analyses.

Sample	OSL-SA		OSL-SG		IRSL-SG(Kf)		IRSL-SG(plag)	
	N(aliquots)	DR	N(discs)	DR	N(discs)	DR	N(discs)	DR
SAL1	20	4	4	1	1	1	1	1
SUV1			2					

Sample	OSL-SA		OSL-SG		IRSL-SG(Kf)		IRSL-SG(plag)	
	N(aliquots)	DR	N(discs)	DR	N(discs)	DR	N(discs)	DR
SUV2	20	4	4		2	2		
SUV3			4		1			
SUV4			2		3		1	
GiG1			2		2			
GiG2			2		2			

SA = single aliquot; SG = single grain; Kf = K-feldspar: plag = plagioclase; N = number of measured aliquots and discs, respectively; DR = number of dose recovery tests.

4.2.3 Age calculation

The data gathered was analysed with the program ANALYST 3.24 (Duller, 2007). Determined equivalence doses were statistically evaluated in order to derive a palaeodose for the sedimentation age calculation. This includes essentially the calculation of the artithmetic mean, the median, the relative standard deviation and in some cases the "leading edge" procedure after Lepper and McKeever (2002). Sedimentation ages were calculated using ADELE (Kulig, 2005).

4.3 Measurement of Schmidt-hammer rebound values

4.3.1 Principle and applications

The Schmidt-hammer is a portable instrument originally developed to test concrete quality in a non-destructive way (Schmidt, 1950, 1951). A spring-loaded bolt impacting a surface yields a rebound- or R-value, which is proportional to the hardness (compressive strength) of a rock surface. Basu and Aydin (2004) discuss technical aspects of the Schmidt-hammer in detail. In this study, the N-type Schmidt-hammer (Proceq, Switzerland) was used (Fig. 4.5).

Applied in geomorphology, old rock surfaces exposed to weathering processes for a long time provide low R-values and vice versa. As the readings obtained are a function of not only the hardness of the surfaces but also their texture, only non-metamorphic (isotropic) rock types should be chosen for the application of the Schmidt-hammer (Williams and Robinson, 1983; McCarroll, 1987).

Fig. 4.5 The N-type Schmidt-hammer as used in this study. Note the pencil for scale.

Since the 1980s, the method has been successfully used for relative age dating of geomorphologic features such as moraines (e.g. Matthews and Shakesby, 1984; Winkler and Shakesby, 1995; Winkler, 2000, 2005), rock glaciers (e.g. Frauenfelder *et al.*, 2005; Kellerer-Pirklbauer *et al.*, 2008; Kellerer-Pirklbauer, 2008) or rock fall deposits (Nesje *et al.*, 1994; Deline and Kirkbride, 2009). Recent publications increasingly discuss the possibilities and limitations of calibrating R-values, for instance with results from ^{10}Be and ^{14}C-datings (e.g. Engel, 2007; Shakesby *et al.*, 2006) or photogrammetrical measurements (Frauenfelder *et al.*, 2005; Haeberli *et al.*, 2003).

4.3.2 Field strategy

On each mappable unit (e.g. moraine, rock glacier lobe) 50 randomly selected boulders/sites were measured, avoiding edges of boulders (Day and Goudie, 1977), spots that showed lichen growth as well as visual fissures or cracks. Only flat parts under dry conditions were considered (Williams and Robinson, 1983; Sumner and Nel, 2002). Normally just one measurement was carried out per boulder, however, in some cases with just a low number of suitable boulders, the biggest ones were measured at most three times.

4.3.3 Statistical evaluation

Reported is the arithmetic mean of 50 R-value records on each individual landform. Following the suggestions by Winkler (2000), we used a standard error based on the standard deviation in a 95% confidence interval to get statistically significant age differences:

$$x \pm 1.96 \times \sqrt{\left(\sigma / \sqrt{n}\right)} \qquad (4.5)$$

where x is the arithmetic mean, σ the standard deviation and n corresponds to the number of measurements.

4.4 Measurement of weathering rind thicknesses

4.4.1 Principle an applications

Weathering rinds are altered coloured zones constituting the outermost part of rocks, which originate from oxidation and dissolution. For a summary of commonly used definitions and an overview of involved processes see Oguchi (2001, 2004) and references therein. The time dependent rind growth towards the rock-centre is used as an indicator of relative ages of glacial and periglacial deposits. A great number of investigations have been carried out mainly on Holocene moraines and fluvial terraces with different lithologies in the USA and New Zealand (e.g. Chinn, 1981; Colman and Pierce, 1981; Whitehouse *et al*., 1986; McSaveney, 1992). Recent measurements on rock glaciers have been carried out for instance in Japan (Aoyama, 2005) or in the Swiss Alps (Laustela *et al*., 2003; Compeer, 2009; this study). An extensive overview of previous studies on weathering rinds since the 1960s is given in Oguchi (2001). Several relationships between rind thickness and time were derived: Cernohouz and Solc (1966) proposed a logarithmic function, Chinn (1981) a power function and investigation on a rock glacier in Switzerland yielded a logistic model to be the best representation of the measured weathering rinds (Laustela *et al*., 2003). Limitations and potential error sources such as erosion and the influence of porosity are discussed in Gordon and Dorn (2005) and Oguchi and Matsukura (1999).

4.4.2 Field strategy

At each site (top of moraines and rock glacier lobes) 50 rind-samples were chipped with a hammer from boulders with a minimum diameter of approx. 30-40 cm. The weathering rind was measured perpendicular to the surface with a 0.1 mm scale graduated magnifying glass. Edges and cracks leading to larger rind thicknesses and an overestimation of weathering stages were avoided. Also rock pieces that showed inside weathering traces indicating a pre-failure were omitted.

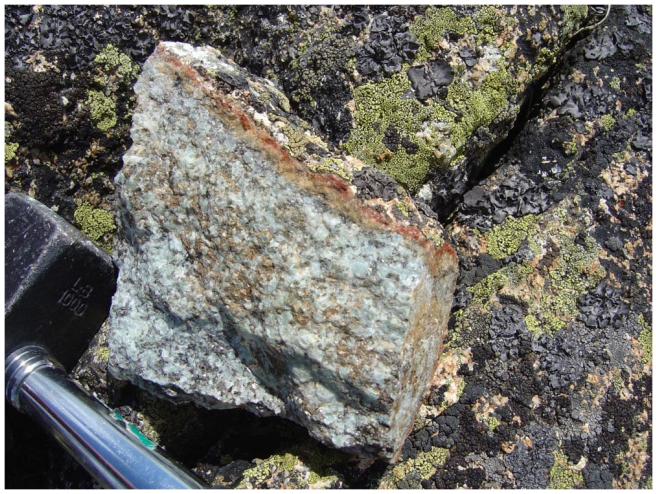

Fig. 4.6 A piece of Albula granite showing a well-pronounced weathering rind as it is was typically found in the Val Mulix. Below the reddish (iron-) oxidation layer, a thin black layer can be seen which originates from manganese.

4.4.3 Statistical evaluation

In literature the median, the modal value and the arithmetic mean of weathering rind thickness measurements are used to statistically separate landforms by their age. In this study both the mean and the median value are given as relative age indicators.

4.5 Pedological analyses

In the following, essentially field and laboratory procedures are described in a rather technical way. Principle concepts behind applied methods, together with soil formation in a more general sense, its connection to the investigated glacial and periglacial landforms and thus the role of soils as landscape formative elements is treated in Chapter 3.2.4.

4.5.1 Field strategy

Soil material was collected from excavated profile pits on undisturbed locations where no influence of creeping processes was visible. If possible, profiles were dug down to the C horizon. Per horizon 2-3 kg of soil material were removed for the analyses (Hitz *et al*., 2002). Colours were determined based on the Munsell colour system and the bulk density (fine earth and soil skeleton) measured using a specific soil core sampler.

4.5.2 Soil physical and chemical analyses

The oven-dried (60°C) samples were sieved to <2 mm and ball-milled for determination of C and N contents with a C/H/N-analyser (Elementar Vario EL, elementar Analysensysteme GmbH). Soil pH was measured in 0.01 M $CaCl_2$ using a soil solution ratio of 1:2.5. A combination of wet sieving for particles 2000-32 μm and X-ray sedimentometry (SediGraph 5100) for finer particles <32 μm was applied for analyzing the particle size distribution.

Measurement of the total element content of fine earth and skeleton was done by means of X-ray fluorescence (XRF) (Jenkins, 1999). Around 10 g of soil material were milled to < 50 μm in a tungsten carbide disc swing mill (Retsch® RS1, Germany). Four grams of soil powder was mixed with 0.9 g of Licowax® C Micro-Powder PM (Clariant, Switzerland), pressed into a 32 mm-pellet and analysed using an energy dispersive X-ray fluorescence spectrometer (SPECTRO X-LAB 2000, SPECTRO Analytical Instruments, Germany).

Fe, Al and Si concentrations were determined after treatment with sodium-dithionite (in the following labelled with "d", e.g. Fe_d) and NH_4-oxalate (buffered at pH 3, label "o"), respectively (McKeague et al., 1971). The extracts were centrifuged for 8 minutes at 4000 rpm and filtered (mesh size 0.45 μm, S&S, filtertype 030/20). Element concentrations were measured using atomic absorption spectroscopy (AAnalyst 700, Perkin Elmer). The amount of well crystalline Fe-oxide was calculated by the difference between its dithionite and oxalate extractable content (Fe_d – Fe_o). With respect to the Al/Si molar ratio and assuming that the sodium-pyrophosphate Al-fraction (Al_p) is negligible, the sum of imogolite and proto-imogolite allophane ("Imogolite-type material", ITM) was calculated as follows (Parfitt and Henmi, 1982; Parfitt *et al*., 1988):

$$\mathrm{ITM} = f \cdot \mathrm{Si_O}(\%) \tag{4.6}$$

with

$$f = 5 + 2.1 \cdot \left(\frac{Alo}{Sio} - 1 \right) \tag{4.7}$$

with Al_o and Si_o as the oxalate-extractable Al and Si (both in moles), respectively. Parfitt and Childs (1988) give a rough estimation of the concentration of ferrihydrite with $1.7 \cdot Fe_o$.

4.5.3 Separation of clay fraction and soil mineralogy

To separate the clay fraction (< 2mm), the fine earth samples (< 2 mm) were pre-treated at room temperature with diluted and Na-acetate buffered (pH 5) H_2O_2. At the end of the reaction, H_2O_2 was decomposed by heating the sample at 50 °C. The clay fraction was obtained by dispersion with Calgon and sedimentation in water. Specimens were then Mg-saturated, washed free of chloride and freeze-dried. Clay-aggregate samples, orientated on glass slides from a water suspension, were analysed using a θ-2θ Philips PW1820 diffractometer (40 kV, 30 mA, automatic theta compensating divergence slit, graphite monochromator) using Cu-Kα radiation. Slides were step-scanned from 2 to 15°2θ with steps of 0.02°2θ at 2 second intervals. The following treatments were performed: Mg-saturation, ethylene glycol solvation and K saturation, followed by heating for 2 hours at 335°C and 550°C (Fig. 4.7). When chlorite was present, the presence of kaolinite was checked with FT-IR (Brooker Optics, Tensor 27) analysis (OH-stretching region near 3695 cm^{-1}) on powder samples (3% milled soil material, 97% KBr) heated at 80°C for ≥ 2 h. Digitised X-ray data were routinely smoothed and corrected for Lorentz and polarisation factors (Moore and Reynolds, 1997). Diffraction patterns were smoothed by a Fourier transform function and fitted by the Origin™ PFM program using the Pearson VII algorithm. Background values were calculated by means of a non-linear function (polynomial 2^{nd} order function; Lanson, 1997). The *d*(060) region was studied on randomly oriented samples step-scanned from 58 to 64°2θ with steps of 0.02°2θ at 10 second intervals.

The semi-quantitative estimation of phyllosilicate concentration was performed by the combination of the areas of the ethylene glycol solvated, Mg-saturated, the K-saturated and heated (335 °C and 550 °C) samples. On the basis of these integrals, an estimate of clay minerals composition was performed. The sum of the areas between 2 and 15° 2θ, which were attributed to HIV (hydroxy interlayered vermiculites), smectite, vermiculite, mica, chlorite and kaolinite, were standardised to 100%. For the Mg-saturated and for the ethylene glycol solvation treatment, the area of the following peaks (d-spacings) were corrected by a weighting factor F: 1.6 nm with F = 0.453, 1.4 nm with F = 0.478, and 0.71 nm with F = 0.16 (Schwertmann and Niederbudde, 1993; Gjems, 1967; Laves and Jahn, 1972; Niederbudde and Kussmaul, 1978). For the determination of the kaolinite peak intensity, the possible contribution of chlorite to this signal was taken into account. Although the (semi-)quantification of clay minerals in soils is bedeviled by manifold problems (Kahle *et al*., 2002), the applied and standardised (sample preparation, treatments, measurement and calculation) procedure enabled the assessment of the variability of clay mineral assemblage amongst the sites.

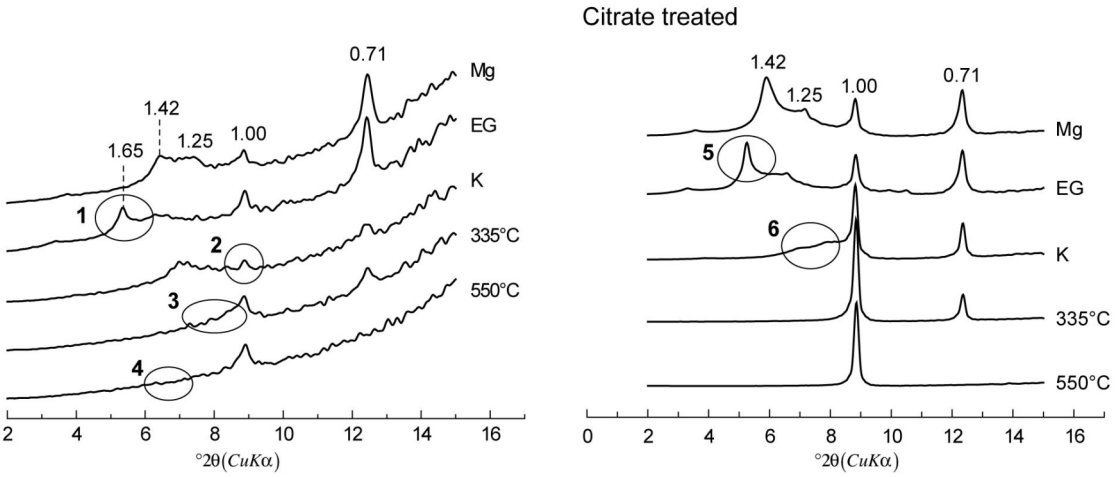

Fig. 4.7 Principle of the identification of clay minerals. Shown is the OE horizon from S4 (rock glacier middle part). Treatment with Mg, Ethylene glycol (EG), K and heating to 335°C and 550°C, respectively, leads to diagnostic peaks as a result of clay-type specific expansion and contraction behaviour. Important d-spacings are given in nm. Mg-saturation serves as an overview. The peak at 1.4 nm could be chlorite, vermiculite, smectite or vermiculite or smectite with hydroxy-interlayers. Peak 0.72 nm could be kaolinite or a *d*(002)-reflection of the 1.4 nm peak. The 1.0 nm peak represents mica.

1 – Shift of the 1.4 nm peak towards 1.65 nm indicates the presence of smectite.

2 – If vermiculite is present, K saturation would lead to an increase of the 1.0 nm peak.

3 – The collapse of HIV (hydroxy interlayered vermiculate) after heating to 335°C is shown by a relative increase of the 1.0 nm peak area with regard to the 1.4 nm peak.

4 – After heating to 550°C, the 1.4 nm peak has disappeared, indicating that no chlorite is present and that the 0.71 nm peak is due to kaolinite. If the 1.4 nm peak still persists, the presence of kaolinite must additionally be checked by FT-IR.

Citrate treated samples:

5 – The more pronounced peak at 1.65 nm after EG solvation evidences the presence of HIS (hydroxy interlayered smectite).

6 – For hydroxy-interlayered materials, the collapse of the interlayered 2:1 minerals after K saturation is greatly improved.

The quantitative mineralogical composition of the inorganic part of the fine earth (fraction < 2 mm) was obtained using Rietveld analysis (program AutoQuan, GE SEIFERT) of XRD patterns of randomly oriented specimens (Bruker AXS D8 Advance, Cu-Kα, 4-70° 2θ, 40kV, 40mA, 0.02°-steps, 4s/step, automatic theta compensating divergence and antiscattering slits, graphite monochromator).

4.5.4 Calculation of mass balance based on immobile titanium

Volumetric changes that occur during pedogenesis were determined by adopting the classical definition of strain, $\varepsilon_{i,w}$ (Brimhall and Dietrich, 1987; Chadwick *et al.*, 1990):

$$\varepsilon_{i,w} = \frac{\Delta z_w}{\Delta z} - 1 \qquad (4.8)$$

with Δz as the columnar height (m) of a representative elementary volume of protore (or unweathered parent material) p, and Δz_w is the weathered equivalent height (m) w. The calculation of the open-system mass transport function $\tau_{j,w}$ is defined by (Chadwick *et al*., 1990):

$$\tau_{j,w} = \left(\frac{\rho_w C_{j,w}}{\rho_p C_{j,p}} \left(\varepsilon_{i,w} + 1 \right) \right) - 1 \qquad (4.9)$$

where $C_{j,p}$ (kg/t) is the concentration of element j in protolith (e.g., unweathered parent material, bedrock), $C_{j,w}$ is the concentration of element j in the weathered product (kg/t), and with ρ_p and ρ_w represent the bulk density (t/m^3) of the protolith and the weathered soil, respectively. With n soil layers, the calculation of changes in mass of element j is given by (Egli and Fitze, 2000):

$$\bar{m}_{j,flux(z_w)} = \sum_{a=1}^{n} C_{j,p} \rho_p \left(\frac{1}{\varepsilon_{i,w} + 1} \right) \tau_{j,w} \Delta z_w \qquad (4.10)$$

where $\tau_{j,w}$ corresponds to the mass transport function $\varepsilon_{i,w}$ to the strain, and Δz to the weathered equivalent of the columnar height (m) of a representative elementary volume.

4.5.5 ^{14}C-dating of stable soil organic matter (SOM)

Amongst a number of methods tested to isolate stable organic matter (e.g. Bruun *et al*. 2008; Mikutta *et al*., 2005, 2006), the application of H_2O_2 (Plante *et al*., 2004) turned out to yield the SOM fraction with the highest ^{14}C-ages (Favilli *et al*., 2008).

The following procedure is slightly modified after Plante *et al*. (2004): 1 g of air-dried fine earth (fraction < 2 mm) was wetted during 10 min with distilled water, afterwards 90 ml of 10% H_2O_2 were added. Peroxide treatments were performed during 168 h (7 days) in parafilm covered 150 ml beakers at a minimum temperature of 50 °C. At the end samples were washed three times using deionised water and air-dried at 50°C during 24 h, followed by analyses for total C and N.

For ^{14}C-dating the samples were after heating catalytically reduced over cobalt powder at 550 °C to graphite. $^{14}C/^{12}C$ ratios and $\partial^{13}C$ were measured by means of AMS (see section 3.1.2.). The calendar ages were obtained using the OxCal 4.0.5 calibration program (Bronk Ramsey, 1995, 2001) based on the IntCal 04 calibration curve (Reimer *et al.*, 2004). The radiocarbon method has been widely used for decades and, therefore, here not described in detail. A comprehensive and up-to-date overview is provided, for instance, by Hajdas (2008).

4.5.6 Determination of the meteoric ^{10}Be concentration in a soil profile

The ^{10}Be abundance in a soil profile was estimated assuming that the overwhelming part of ^{10}Be is adsorbed in the fine earth fraction. The amount is consequently calculated according to

$$N = \sum_{a=1}^{n} \left(z_w \rho_w C_w f_w \right) \tag{4.11}$$

where N corresponds to the abundance of 10Be (inventory), zw to the thickness of the corresponding soil horizon, ρw being the bulk density of the soil horizon, Cw to the concentration (fine earth) in the corresponding soil horizon and fw to the relative fraction (% by weight) of fine earth in the soil horizon.

If the ^{10}Be inventory since the initiation of soil formation is known, then the time soils were exposed to meteoric ^{10}Be flux can be determined using the following equation (Maejima *et al.*, 2004):

$$\frac{dN}{dt} = q - \lambda N \text{, with N = 0 at t = 0} \tag{4.12}$$

$$t = -\frac{1}{\lambda} \ln\left(1 - \lambda \frac{N}{q}\right) \tag{4.13}$$

where t is the age of soil, λ is the decay constant of ^{10}Be (4.62×10^{-7}/y), N is the inventory of ^{10}Be in time t (atoms/cm^2) and q is the annual deposition rate of ^{10}Be (atoms/cm^2/y). The measured inventory N is the integral of concentration times soil density at the depth the profile was sampled (Pavic and Vidic, 1993; Maejima et al., 2004).

Errors in the quantification of the ^{10}Be abundance are due to analytical errors (AMS), density and soil skeleton measurements. An estimate of the error range was performed by

means of the maximum error. The range of error Δf can be estimated by the mean analytical error (^{10}Be) and the error Δy introduced due to soil analyses (density, soil skeleton).

$$\Delta f = \Delta x + \Delta y \qquad (4.14)$$

The ratio $\Delta f / f_{x,y}$ (with $f_{x,y}$ as the measured value) gives the relative error that equals the sum of the individual mean errors. The error for the density measurements and the soil skeleton determination was estimated to be 5% (for each parameter). In soil horizons having no soil skeleton the corresponding error was considered to be negligible. These assumptions are very conservative (Desaules and Dahinden, 2000). Accordingly, the estimated errors of the ^{10}Be inventory, and subsequently the derived surface age, vary from 8 to c. 21%.

This approach is referred to as the "open system ^{10}Be model" (Monaghan *et al.*, 1983; Pavich *et al.*, 1984). A comparison with the "closed-system model" (Lal, 1991), which uses changing ^{10}Be/^{9}Be ratios in authigenic phases of B- and C-horizons, can be found in Barg *et al.* (1997). This second approach was not applied here.

The choice of the average annual deposition rate q is a crucial point. In literature strongly varying values from different parts of the globe can be found (e.g. Monaghan *et al.*, 1985/86; Brown *et al.*, 1989: Maejima *et al.*, 2005). The values reported by Monaghan et al. (1985/86) seem reasonable for this study site and were adopted. Assuming a proportional relationship between deposition rate of ^{10}Be and amount of rainfall, values for q vary between 1.82×10^6 atoms cm^{-2} yr^{-1} (for 1500 mm yr^{-1} rainfall) and 1.21×10^6 atoms cm^{-2} yr^{-1} (for 1000 mm yr^{-1} rainfall, representing the mean global value). A simple extrapolation of modern values certainly yields just a rough approximation and differing values from the past are known (e.g. during the Maunder Minimum period: Heikkilä *et al.*, 2008). Thus, whichever values are taken, they are necessarily estimations, as deposition rates over time periods of thousands of years are not known.

Soil erosion rates

Knowing the real age of a landform and having the calculated ^{10}Be age derived from soils, soil erosion can be estimated by comparing the effective abundance of ^{10}Be measured in the soil with the theoretically necessary abundance for the correct age. To evaluate a possible erosion of the soils, we assume that the material is eroded from the surface at a constant rate E (Maejima et al., 2005). Equation (4.13) can be extended to:

$$t_{corr} = -\frac{1}{\lambda}\left(1 - \lambda\frac{N}{q - \rho E m}\right) \qquad (4.15)$$

where m is the measured concentration of ^{10}Be in the top eroding horizons (atoms/g), ρ is the bulk density (g/cm^3) of the top horizons and t_{corr} the "correct" age. Erosion rates are obtained from the difference $\Delta t = t_{corr} - t$ (Equations x and x) where the parameters Δt and t are known.

Measurement of meteoric ^{10}Be in soil samples

^{10}Be was extracted from soil samples using a modified method from Horiuchi et al. (1999). Four tenths of a milligram of $^{9}Be(NO_3)_2$ was added to 1-5 g of soil (< 2 mm fraction) and then heated for 3 h at 550 °C to remove organic matter. After cooling, it was put in a shaker and leached with 8 ml HCl (16%) overnight. The solid part was separated by centrifuge and leached again, the liquid was collected. After a second leaching, the soil residue was disposed of and the solutions obtained added together and heated at 80 °C until the volume reduced to ca. 1 ml. To remove the fine particles, 1 ml HNO_3 (65%) and 1 ml HCl (32%) was added to the sample, it was centrifuged and the fine particles removed. NaOH (16%) was added to the sample until it reached a pH value of 2, then 1 ml of conc. EDTA was added. The EDTA solution removes metals (Fe, Mn) in the form of EDTA complexes. NH_4OH was added until pH = 8 and the resulting gel containing $Be(OH)_2$, $Al(OH)_3$, and some $Fe(OH)_2$ and $Mn(OH)_2$ was precipitated. NaOH solution was added to the hydroxides until the pH value reached 14. The $Be(OH)_2$ and $Al(OH)_3$ redissolve and the solution containing Be and Al was separated by centrifuging. This procedure was repeated a second time to recover any remaining Be. Once again conc. HCl (32%) was added to the liquid (containing Be) to reach a pH = 2 and 1 ml of 10% EDTA was added to remove the last traces of Fe and Mn. The $Be(OH)_2$ and $Al(OH)_3$ were precipitated and subsequently centrifuged. If Fe was still present the gel was coloured yellow. HCl (32%) was added until the gel redissolved, it was then heated to reduce the volume to ca. 1 ml. Any Fe was removed with the anion exchange column, the cleaned solution was heated to near dryness. The Be and Al were separated with two different cation exchange columns. In the first stage the precipated gel was dissolved in HCl and passed through the cation exchange column where most of the Al stayed. After evaporation and precipitation, the $Be(OH)_2$ was dissolved in oxalic acid (stage two) and again passed through the second cation exchange column. This second procedure is based on the formation of Al complexes with oxalic acid, the Al also stays in the column. Pure $Be(OH)_2$ was precipitated with NH_4OH and subsequently dried at 70 °C. It was calcinated in an oven for 2 hours at 850 °C to obtain pure BeO. This BeO is later mixed with Cu powder and pressed into an accelerator target.

The $^{10}Be/^{9}Be$ ratios were measured at the ETH Zurich Tandem Accelerator Mass Spectrometry (AMS) facility (Synal et al., 1997) using ETH AMS standard S555 ($^{10}Be/^{9}Be$ = 95.5 10^{-12} nominal) with a ^{10}Be half-life of 1.51 Ma.

4.6 Laboratory reflectance spectroscopy

Rock surface spectra (Aiguille du Midi) were measured in the laboratory using an ASD FieldSpec Pro Fr spectro-radiometer, a Spectralon reference panel and a Thermo Oriel irradiance source. The hematite spectrum was taken from the Jet Propulsion Laboratory (JPL) Spectral Library (HEMATITE 0-1A). In order to identify absorption features for measurement, continuum removal was applied to the data. This is a means of normalising reflectance spectra to allow comparison of individual features from a common baseline. Continuum removal (Clark and Roush, 1984; Kruse *et al*., 1985; Green and Graig, 1985) was performed in ENVI 4.1 to facilitate the comparison of individual absorption features between different objects. In this method, a convex hull (the continuum) of a reflectance spectrum is divided by the spectrum itself and thus results in values ranging from 0 to 1. The convex hull is built utilising straight line segments that connect local reflectance maxima.

Chapter 5

Results

In the first part of this chapter, results focusing on landscape evolution in the greater area of Albulapass and Val Burdun are presented, followed by the investigations to date active rock glaciers with luminescence techniques. The comparison of surface exposure ages and spectral properties at Aiguille du Midi can be found in the last part of the chapter.

5.1 Val Mulix and Albula area

5.1.1 Surface exposure dating

All exposure ages are summarised in Tables 5.1 and 5.2. In Val Mulix there is only one boulder suitable for exposure dating on the Daun moraine fragment: boulder VM7 yielded an age of 14.7 ± 1.8 ka. We assign this age to the Daun stadial, which supports the geomorphological map of Maisch (1981). Although the sample was taken from a very big boulder > 1.5 m above the ground and near the moraine crest, (at least) a partial post-depositional exhumation and an intermittent influence of vegetation cannot be excluded. As a consequence, we interpret this as a minimum age. An overturning of the block can be ruled out due to its size. Compared to the other boulder samples in the area, we consider here a higher value for snow coverage (0.7 m) due to its relatively sheltered position and the presence of vegetation reducing the influence of wind and allowing snow cover to last longer.

We consider the age of VM1 (14.5 ± 1.2 ka) on the upper Egesen I lateral moraine as "too old." A possible scenario, besides pre-exposure, would be that deposition of this prominent boulder had already occurred towards the end of the Oldest Dryas without being affected by the following Egesen stadial re-advances during the Younger Dryas (there, the moraines were

accumulated laterally). In this case the age of VM1 would represent a minimum age of a Daun moraine that was then reoccupied during the Younger Dryas. A moraine formed as a result of multiple advances could also explain the pronounced moraine morphology (Fig. 2.5, D), which is not typical for isolated Daun moraines. These normally have a rather rounded shape and often show a solifluction overprint. Our weathering rind measurements support the hypothesis that this moraine could contain boulders deposited before the Younger Dryas. The marked difference between the values of the upper Egesen I (mean/median: 4.6 mm/4.0 mm) and the Egesen II moraine (mean/median: 3.1 mm/3.1 mm, see chapter 5.1.3) is high and can hardly be explained by the formation of two moraine sets within a few hundred years.

VM11 (10.5 ± 0.9 ka) gives an age for the Egesen II moraine that can be brought in line with ages obtained in other studies (Ivy-Ochs *et al*., 1996, 2009a; Federici *et al*., 2008; Hormes *et al*., 2008). The age of 15.2 ± 1.3 ka (VM6) on the same moraine is clearly too old for morphostratigraphical reasons. Pre-exposure must be assumed in this case. This picture does not change even when corrections for snow and erosion are left out.

Boulders VM2 (8.6 ± 0.6 ka) and VM5 (12.6 ± 1.0 ka) were sampled on the uppermost and the lowermost part of the relict rock glacier, respectively (Fig. 2.5, D, E). VM2 is a large flat-topped boulder, snow coverage was therefore estimated to be slightly higher than on VM5. As VM2 is relatively close to the debris source, it could give a rough idea about the ceasing of rock glacier activity. Nevertheless, considering the relatively dense lichen growth on the boulder, the highly developed vegetation coverage on the nearby debris cones and on the headwall itself, a deposition much later than the inactivation of the rock glacier seems to be rather unlikely. Assuming that VM5 (12.6 ± 1.0 ka) was not subject to pre-exposition, it could have been deposited initially on the moraine parallel uphill to the lower Egesen I moraine (see Fig. 2.5, D; 2.6), identifying it as formed during the main Egesen stage (a boulder from this moraine was sampled but was not datable). This would be in agreement with its position near the front of the rock glacier. The huge volume of the boulder (approx. 12 m^3) with its big base area makes a relatively stable position likely on the surface of the rock glacier also during the active phase. The age of boulder VM5 represents the time since deposition on the now destroyed moraine and also includes the travel time on the rock glacier and the time elapsed since cessation of activity. As the altitude was not always the same and the orientation of the boulder surface not fully constant, this age may be considered an approximate age of the moraine on which it was originally deposited.

Considering the travel distance at about 650 m, the age difference of 4000 years between VM2 and VM5 yields a mean annual deformation rate of the rock glacier of approximately 16 cm. Horizontal displacements in a dm-range are common for active rock glaciers as shown by aerial photogrammetry and direct deformation measurements (e.g. Kääb *et al*., 1997; Arenson *et al*., 2002). A precondition for this interpretation is that the boulder VM5 began to move shortly after its deposition on the moraine. The age of boulder VM4 (10.7 ± 0.9 ka) on the lower Egesen I moraine, which was also cut across by the rock glacier, shows that this cannot have been the case. The ice must have disappeared before the rock glacier started to move. According to an obviously shorter activity phase (about 2000-3000 years) a deformation rate about twice as high (around 30 cm/year) must be assumed, which is still reasonable. VM4 is slightly younger than one would expect for this position. Yet, taking the error range into account, a parallelisation for instance with the inner Egesen moraine (11.3 ± 0.6 ka) at the nearby Julierpass (Ivy-Ochs *et al*., 1996, 2006, 2009a) and with the Great Aletsch Glacier (10.6 to 11.9 ka, recalculated by Ivy-Ochs *et al*., 2008, based on data in Kelly *et al*., 2004b) is possible.

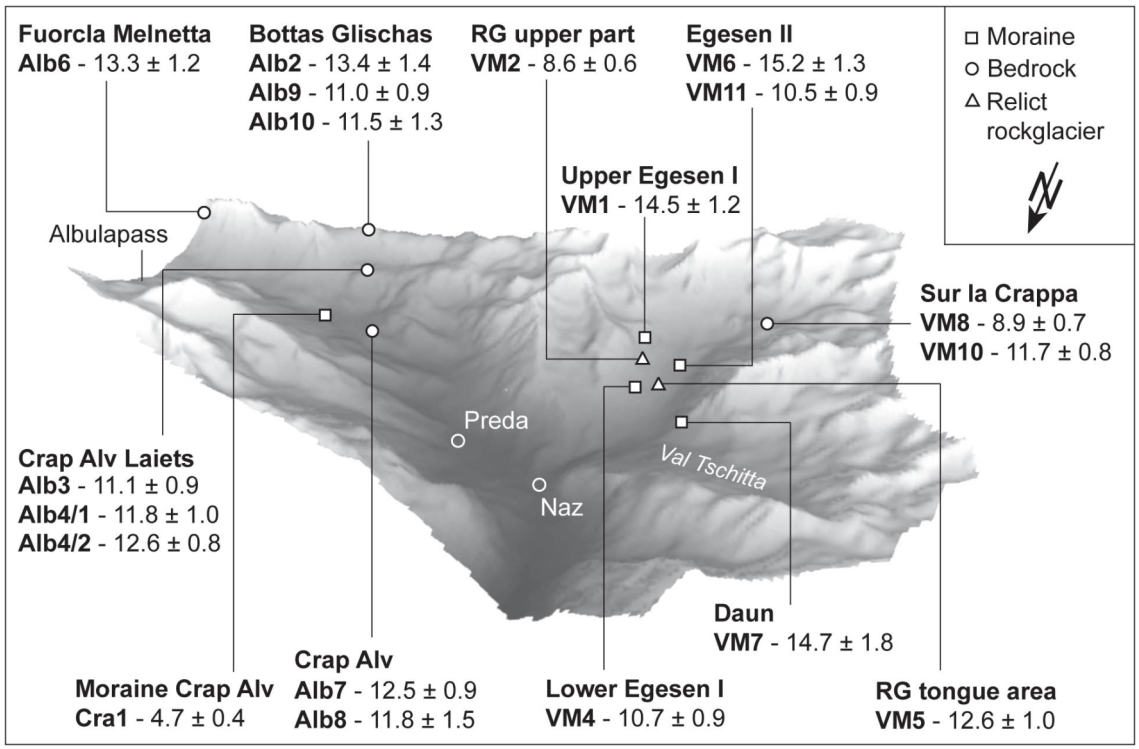

Fig. 5.1 Overview of exposure ages (in ka) measured in the Val Mulix and the Albula area.

VM10 (taken from the glacially polished bedrock at Sur la Crappa) yielded an exposure age of 11.7 ± 0.8 ka. It must be mentioned that the sample was taken – with respect to the main valley axis – at a slightly elevated and lateral position. Thus, this area may not have been affected by any potential minor re-advance that just reached the lower parts of the polished area.

The boulder VM8, which is closer to the theoretical central flow line of a past glacier (Fig. 2.5, F), gave 8.9 ± 0.7 ka, (Fig. 5.1). From these samples that were taken close to the moraines of 1850, we conclude that the main ice body in the Val Mulix has downwasted very fast to a near 1850 extension at the end of the Lateglacial period without any large-scale re-advances afterwards. This underlines the general concept of a Holocene glacier fluctuation pattern oscillating only in a very small range (see also Maisch, 1987; Maisch *et al*., 2000).

The transfluence pass Bottas Glischas, with an average altitude of almost 2600 m a.s.l., must have been covered with roughly 200 meters of ice during the LGM, as the clearly pronounced trimline around 2800 m a.s.l. indicates (especially the Crasta Mora to the east of Piz da las Blais, see Fig. 1). The overall morphology and the homogeneously and freshly striated landforms imply a basal sliding of (at least at times) a warm-based glacier that most probably eroded all the ^{10}Be accumulated prior to the late Würmian glaciation (Ivy-Ochs *et al*., 2007, 2009b). The ages found (Table 5.1a scenario C) at Bottas Glischas (ranging from 11.0 ± 0.9 ka (Alb9) to 13.4 ± 1.4 ka (Alb2) with a mean age of 12.0 ± 1.6 ka) and at Fuorcla Melnetta (13.3 ± 1.2 ka, Alb6) are consistent with this assumption. However, radiocarbon dates from peat bogs in and near the Engadine suggest that the inner Alpine ice-stream network had already collapsed by about 16 – 17 ka ago (e.g. Suter, 1981; Burga, 1987; Studer, 2005). With this in mind and assuming a simple surface lowering scenario during deglaciation, one would expect older ages at this elevation and position, taking the vertical proximity to the LGM ice surface into account. It seems likely that an ice-cap type glaciation remained at Bottas Glischas, also influencing the north slope towards Crap Alv Laiets. Here, Alb3, Alb4/1 and Alb4/2 yielded ^{10}Be ages of 11.1 ± 0.9 ka, 11.8 ± 1.0 ka and 12.6 ± 0.8 ka (Table 5.1b, scenario C), with a mean age for the deglaciation of this strongly eroded terrace of 11.8 ± 1.1 ka. Similar to situations dated at Nägelisgrätli in the Grimsel region in central Switzerland (Ivy-Ochs, 1996; Kelly *et al*., 2006; Ivy-Ochs *et al*., 2007), a possible explanation might be a local and dynamically rather inactive glaciation that remained after the retreat of the main ice body. Due to its north exposition, a possible snow-drift input (lee-effect from Bottas Glischas) and comparably good protection from solar radiation and wind erosion, perennial snow fields could have been of great importance.

The question arises, especially in the case of the uppermost level (Bottas Glischas, Fuorcla Melnetta), whether there was a long lasting ice mass until the beginning of the Bølling/Allerød-interstadial or alternatively a complete melting of the ice followed by a reglaciation during the Younger Dryas with a low erosional potential. This could have led just

to a temporary interruption of ^{10}Be-accumulation without considerable subglacial erosion of the bedrock. Both scenarios would result in similar exposure ages.

Alb7 and Alb8, taken on the roche moutonnée Crap Alv, give with 12.5 ± 0.9 ka and 11.8 ± 1.5 ka (mean age: 12.1 ± 1.3 ka) evidence that this polished bedrock site must have become ice-free at the beginning or latest within the Younger Dryas. In contrast, palynological investigations at a nearby-situated peat bog suggest a pre-Allerød age of ice recession (Burga in Maisch, 1981). Also the geomorphologic mapping is not fully conclusive in this respect. The locality can be interpreted as an area in between the Daun and Egesen glacial state with an ELA-depression value of 260 m derived from a nearby-located moraine (Maisch, 1981). At present, we do not have a plausible explanation for these contradictory findings. Unfortunately, sample Cra1 is not conducive to solving the problem because it yielded only 4.7 ± 0.4 ka - an age that can be ruled out with a high certainty from representing the real age of the moraine. Factors such as too-low correction values for erosion or snow, sediment or vegetation coverage may lead to calculated exposure ages that are younger than the real age of the landform. Yet, the fresh morphology of the bedrock surface gives no hint that a higher correction factor for erosion should be chosen. Due to the fact that the roche moutonnée is situated below the timberline, it seems that an influence of vegetation in the past should, at least, be considered as possible. Its effect on the local ^{10}Be production rate is generally estimated to be rather low, however, in the case of trees and leaves a reduction of less than 4% (Cerling and Craig, 1994; Plug *et al*., 2007). In order to reach ages that would assign the roche moutonnée Crap Alv to the Daun-stadial (> 14.5 ka), unrealistically high amounts of snow would be necessary. At this current stage, additional investigations are needed to clarify the situation.

Table 5.1a Cosmogenic nuclide concentrations and calculated exposure ages for the Albula region. Ages were calculated using an erosion rate of 3 mm per 1000 years. To emphasize the influnce of erosion and snow coverage, values without correction (A) are shown as well as ages with two different estimated snow heights, in each case only for snow (B, D) and additionally for erosion (C, E).

Location	**Bottas Glischas and Fuorcla Melnetta**			
Sample codes	**Alb 2**	**Alb 6**	**Alb 9**	**Alb 10**
Latitude (°N)	46.57	46.57	46.57	46.57
Longitude (°E)	9.81	9.83	9.81	9.81
Elevation (m a.s.l.)	2570	2680	2607	2585
Sample material	Granite	Granite	Granite	Granite
Sample thickness (cm)	3	5	5	4.5
Quartz (g)	58.59	42.34	65.32	56.95
^{10}Be (atoms g^{-1}*10^{4})	43.72	40.61	36.77	37.10
Surface dip angle (°)	18	28	0	30
Dip direction	120	90	0	138
Measurement error (%)	9.6	5.8	7.8	10.5
Local production rate (atoms g^{-1} yr^{-1})	37.79	40.55	38.70	38.15
Production rate (atoms g^{-1} yr^{-1}) *	36.67	34.21	37.09	35.89
Correction factor for shielding	0.995	0.880	0.999	0.977
(A) ^{10}Be age (yrs) (uncorrected) **	**11960 ± 1220**	**11900 ± 1110**	**9940 ± 840**	**10360 ± 1170**
Estimated snow cover (m for 6 months yr^{-1})	0.8	0.8	0.8	0.8
(B) ^{10}Be age (yrs) (Corrected for snow) **	**12910 ± 1310**	**12850 ± 1200**	**10730 ± 900**	**11190 ± 1260**
(C) ^{10}Be age (yrs) (Corrected for erosion and snow) **	**13350 ± 1360**	**13290 ± 1240**	**11030 ± 930**	**11520 ± 1300**
Estimated snow cover (m for 6 months yr^{-1})	1.2	1.2	1.0	1.0
(D) ^{10}Be age (yrs) (Corrected for snow) **	**13410 ± 1360**	**13100 ± 1220**	**10940 ± 920**	**11400 ± 1280**
(E) ^{10}Be age (yrs) (Corrected for erosion and snow) **	**13890 ± 1410**	**13560 ± 1260**	**112500 ± 950**	**11740 ± 1320**

*Production rate corrected for shielding (atoms g^{-1} yr^{-1})

** Estimated total error including measurement error and uncertainties in the altitude, latitude scaling, topography, and depth scaling

Table 5.1b Cosmogenic nuclide concentrations and calculated exposure ages for the Albula region. Ages were calculated using an erosion rate of 3 mm per 1000 years. To emphasize the influnce of erosion and snow coverage, values without correction (A) are shown as well as ages with two different estimated snow heights, in each case only for snow (B, D) and additionally for erosion (C, E).

Location	**Crap Alv Laiets**			**Roche moutonnée Crap Alv**		**Moraine Crap Alv**
Sample codes	**Alb 3**	**Alb 4/1**	**Alb 4/2**	**Alb 7**	**Alb 8**	**Cra1**
Latitude (°N)	46.57	46.57	46.57	46.58	46.58	46.58
Longitude (°E)	9.81	9.81	9.81	9.80	9.80	9.81
Elevation (m a.s.l.)	2325	2320	2320	2060	2070	2055
Sample material	Granite	Granite	Granite	Granite	Granite	Granite
Sample thickness (cm)	5	4.5	3.5	4.5	3.5	3
Quartz (g)	56.67	56.68	56.67	56.45	56.49	61.20
^{10}Be (atoms $g^{-1}*10^4$)	30.16	31.55	34.67	28.23	27.06	10.81
Surface dip angle (°)	12	30	10	10	20	25
Dip direction	45	270	155	50	85	8
Measurement error (%)	7.2	7.5	5.1	5.0	12.0	9.07
Local production rate (atoms g^{-1} yr^{-1})	32.18	32.07	32.07	26.87	27.06	26.78
Production rate (atoms g^{-1} yr^{-1}) *	30.25	29.91	30.67	25.28	25.61	25.07
Correction factor for shielding	0.980	0.968	0.985	0.977	0.975	0.960
(A) ^{10}Be age (yrs) (uncorrected) **	**9990 ± 830**	**10580 ± 960**	**11340 ± 730**	**11200 ± 760**	**10590 ± 1390**	**4320 ± 330**
Estimated snow cover (m for 6 months yr^{-1})	0.8	0.8	0.8	0.8	0.8	1
(B) ^{10}Be age (yrs) (Corrected for snow) **	**10790 ± 900**	**11420 ± 1030**	**12240 ± 790**	**12090 ± 820**	**11440 ± 1490**	**4660 ± 350**
(C) ^{10}Be age (yrs) (Corrected for erosion and snow) **	**11100 ± 920**	**11760 ± 1060**	**12640 ± 820**	**12480 ± 850**	**11780 ± 1530**	**4720 ± 360**
Estimated snow cover (m for 6 months yr^{-1})	1.2	1.2	1.2	1.0	1.0	
(D) ^{10}Be age (yrs) (Corrected for snow) **	**11210 ± 930**	**11870 ± 1070**	**12720 ± 820**	**12320 ± 840**	**11660 ± 1510**	**4750 ± 360**
(E) ^{10}Be age (yrs) (Corrected for erosion and snow) **	**11540 ± 960**	**12240 ± 1100**	**13150 ± 850**	**12720 ± 860**	**12020 ± 1560**	**4810 ± 370**

*Production rate corrected for shielding (atoms g^{-1} yr^{-1})

** Estimated total error including measurement error and uncertainties in the altitude, latitude scaling, topography, and depth scaling

Table 5.2a Cosmogenic nuclide concentrations and calculated exposure ages for the Val Mulix. Ages were calculated using an erosion rate of 3 mm per 1000 years. To emphasize the influnce of erosion and snow coverage, values without correction (A) are shown as well as ages with two different estimated snow heights, in each case only for snow (B, D) and additionally for erosion (C, E).

Location	**Upper Egesen I moraine**	**Rockglacier upper part**	**Lower Egesen I moraine**	**Rockglacier lower part**
Sample codes	**VM 1**	**VM 2**	**VM 4**	**VM 5**
Latitude (°N)	46.57	46.57	46.58	46.58
Longitude (°E)	9.76	9.76	9.76	9.75
Elevation (m a.s.l.)	2320	2310	2160	2080
Sample material	Granite	Granite	Granite	Granite
Sample thickness (cm)	4.5	4.5	5	5
Quartz (g)	56.82	58.45	58.52	58.53
^{10}Be (atoms $g^{-1}*10^4$)	40.29	23.82	26.54	29.36
Surface dip angle (°)	25	0	26	23
Dip direction	95	0	65	45
Measurement error (%)	4.4	4.9	5.0	4.9
Local production rate (atoms g^{-1} yr^{-1})	32.07	31.86	28.78	27.25
Corrected production rate (atoms $g^{-1}yr^{-1}$) *	29.24	29.34	26.03	24.59
Correction factor for shielding	0.947	0.957	0.943	0.941
(A) ^{10}Be age (yrs) (uncorrected) **	**13820 ± 1100**	**8130 ± 600**	**10220 ± 830**	**11970 ± 990**
Estimated snow cover (m for 6 months yr^{-1})	0.1	0.3	0.2	0.2
(B) ^{10}Be age (yrs) (Corrected for snow) **	**13960 ± 1120**	**8370 ± 620**	**10420 ± 840**	**12210 ± 1010**
(C) ^{10}Be age (yrs) (Corrected for erosion and snow) **	**14480 ± 1160**	**8550 ± 640**	**10700 ± 870**	**12600 ± 1040**
Estimated snow cover (m for 6 months yr^{-1})	0.3	0.5	0.4	0.4
(D) ^{10}Be age (yrs) (Corrected for snow) **	**14230 ± 1140**	**8530 ± 630**	**10620 ± 860**	**12440 ± 1030**
(E) ^{10}Be age (yrs) (Corrected for erosion and snow) **	**14770 ± 1180**	**8720 ± 650**	**10920 ± 880**	**12850 ± 1060**

*Production rate corrected for shielding (atoms g^{-1} yr^{-1})
** Estimated total error including measurement error and uncertainties in the altitude, latitude scaling, topography, and depth scaling

Table 5.2b Cosmogenic nuclide concentrations and calculated exposure ages for the Val Mulix. Ages were calculated using an erosion rate of 3 mm per 1000 years. To emphasize the influnce of erosion and snow coverage, values without correction (A) are shown as well as ages with two different estimated snow heights, in each case only for snow (B, D) and additionally for erosion (C, E).

Location	**Egesen II moraine**		**Daun moraine**	**Rockbarrier Sur la Crappa**	
Sample codes	**VM 6**	**VM 11**	**VM 7**	**VM 8**	**VM 10**
Latitude (°N)	46.57	46.57	46.58	46.57	46.57
Longitude (°E)	9.75	9.75	9.75	9.74	9.74
Elevation (m a.s.l.)	2145	2175	2120	2423	2460
Sample material	Granite	Granite	Granite	Granite	Granite
Sample thickness (cm)	3.5	5	4	4.5	5
Quartz (g)	55.46	55.77	58.76	61.9560	55.07
^{10}Be (atoms $g^{-1}*10^4$)	35.96	26.63	34.06	25.30	34.54
Surface dip angle (°)	41	25	30	0	9
Dip direction	135	75	140	0	70
Measurement error (%)	5.4	5.2	11.4	5.80	5.4
Local production rate (atoms g^{-1} yr^{-1})	28.49	29.08	28.01	34.33	35.18
Corrected production rate (atoms $g^{-1}yr^{-1}$) *	24.87	26.29	25.81	31.90	32.80
Correction factor for shielding	0.899	0.943	0.953	0.9527	0.972
(A) ^{10}Be age (yrs) (uncorrected) **	**14510 ± 1230**	**10150 ± 870**	**13230 ± 1620**	**8050 ± 660**	**10560 ± 750**
Estimated snow cover (m for 6 months yr^{-1})	0.1	0.1	0.7	0.8	0.8
(B) ^{10}Be age (yrs) (Corrected for snow) **	**14650 ± 1240**	**10250 ± 880**	**14150 ± 1730**	**8690 ± 710**	**11400 ± 810**
(C) ^{10}Be age (yrs) (Corrected for erosion and snow) **	**15220 ± 1290**	**10530 ± 900**	**14690 ± 1790**	**8880 ± 730**	**11740 ± 830**
Estimated snow cover (m for 6 months yr^{-1})	0.3	0.3	1.0	1.2	1.2
(D) ^{10}Be age (yrs) (Corrected for snow) **	**14930 ± 1270**	**10450 ± 890**	**14560 ± 1780**	**9030 ± 740**	**11840 ± 840**
(E) ^{10}Be age (yrs) (Corrected for erosion and snow) **	**15530 ± 1320**	**10740 ± 920**	**15130 ± 1850**	**9240 ± 760**	**12220 ± 870**

*Production rate corrected for shielding (atoms g^{-1} yr^{-1})

** Estimated total error including measurement error and uncertainties in the altitude, latitude scaling, topography, and depth scaling

5.1.2 Schmidt-hammer measurements

Measured Schmidt-hammer rebound values from both the Val Mulix and the Albula region are summarised in Table 5.3. Generally the mean values scatter in a very small range. Considering the standard error after Winkler (2000), the differences in the Val Mulix are in most cases statistically insignificant. The value of the terminal Egesen I moraine (Fig. 2.6; 5.3) is, however, an exception. The higher value (41.0 ± 2.1) indicates a younger age compared, for instance, to the polished bedrock site Sur la Crappa. From a morphostratigraphical point of view, this makes no sense and consequently has to be attributed to the method's inherent uncertainty. The value of the 1850 moraine (58.0 ± 1.9) clearly contrasts to those obtained from landforms that are assumed to be of Lateglacial age, yielding R-values between 35 and 40. Castelli (2000), Laustela (2003), Frauenfelder *et al.* (2005) and Compeer (2009) measured on a number of active rock glaciers with identical lithology in and around the same area values varying from approx. 40 – 45 near the tongue to 50 – 55 in the root zone. This fits nicely into the gap between the Lateglacial values and those attributed to the LIA, supporting the assumption that active rock glaciers can be attributed to the Holocene (Fig. 6).

Table 5.3 Measured Schmidt-hammer rebound values. Standard error is given after suggestion of Winkler (2000). Where not specially indicated, 50 measurements per landform were performed.

Localities Val Mulix	*1850 moraine*	*Sur la Crappa*	*Egesen II moraine*	*Upper Egesen I moraine*	*Egesen I terminal moraine*	*RG upper part*	*RG middle part*	*RG lower part*
Mean value	58.0 ± 1.9	37.8 ± 1.8	36.8 ± 2.1	35.6 ± 2.0	41.0 ± 2.1	37.5 ± 2.2	37.9 ± 2.2	37.9 ± 2.1

Localities Albula	*Crap Alv (n = 150)*	*Crap Alv Laiets (n = 150)*	*Bottas Glischas (n = 100)*
Mean value	39.5 ± 1.9	34.3 ± 1.9	33.3 ± 1.8

RG = Relict rock glacier

The results of the vertical sequence near the Albulapass are shown in the lower part of Table 5.3. Basically, the mean values vary in the same range as in the Val Mulix (upper part of Table 5.3). The roche moutonnée Crap Alv (39.5 ± 1.9) could be separated from the two other elevation levels (Crap Alv Laiets: 34.3 ± 1.9, Bottas Glischas: 33.3 ± 1.8) based on the significantly higher rebound values measured (that is, the values show no overlapping of the standard errors). This would mean that Crap Alv became ice-free later than the other two elevation levels. Taking the comparatively low resolution of the method into account, the interpretations have to be done with caution as yet.

5.1.3 Weathering rinds thicknesses

The histograms from the five measured sites in Val Mulix are given in Figure 5.2. Besides the absolute values, also the shape of the corresponding data histogram gives information about surface age distribution. Asymmetric histograms with more than one peak (bi- to trimodal) and a broader distribution (right skewed) are typical for old surfaces. To represent weathering rind thicknesses, in this study both the median and the mean value are shown.

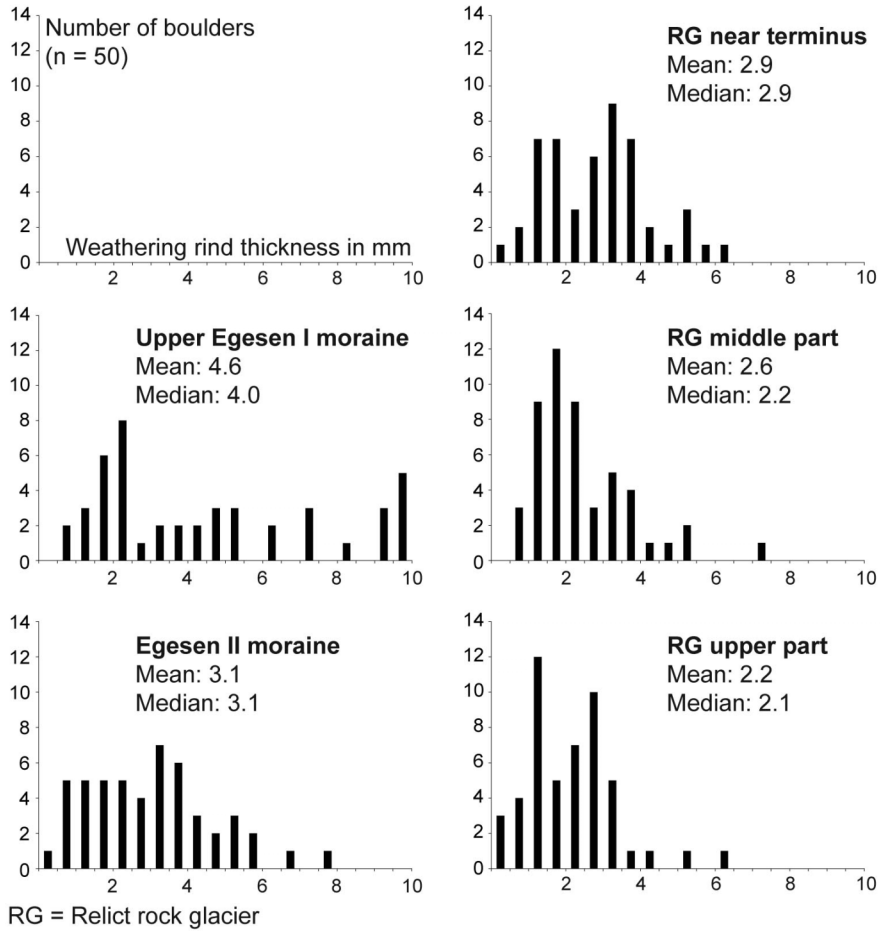

Fig. 5.2 Histogramms of measured weathering rind thicknesses from the Egesen I and Egesen II moraine as well as from different sites on the relict rock glacier. The age evolution on both the rock glacier and compared to the moraines is visible, represented by higher median/mean values and a shift to higher thickness values with increasing age of the landform.

The observed sequence of weathering rind growth is in line with the geomorphological settings in the Val Mulix and, therefore, seems to be an appropriate tool for reconstructing the relative process evolution. Histogram shape and statistical values clearly identify the upper Egesen I moraine (mean/median: 4.6 mm/4.0 mm) as the oldest landform investigated. The

values of the lower Egesen II moraine (mean/median: 3.1 mm/3.1 mm) and those from the tongue area of the relict rock glacier are close together, strengthening the hypothesis of a relatively parallel evolution of these landforms (Maisch, 1981). The middle and upper part of the relict rock glacier cannot be clearly distinguished (mean/median: 2.6 mm/2.2 mm and 2.2 mm/2.1 mm, respectively). However, a distinct age separation of the uppermost part from the tongue area (mean/median: 2.9 mm/2.9 mm) is evident. This general tendency does not change if the ten lowest or alternatively the five highest and the five lowest values are excluded, considering that young surfaces are always generated by split-off processes and also a certain chance exists that boulders with pre-existing weathering rinds are deposited. While the first case generally leads to "too young" ages, the second case suggests a "too old" age.

Our data agree with findings of Castelli (2000), Laustela *et al*. (2003) and Compeer (2009). They found mean maximum median values between 1.5 and 2 mm on lobes near the front of active rock glaciers in the same area. The relict rock glacier in this study can thus be clearly seen as another, older rock glacier generation than the present-day active ones.

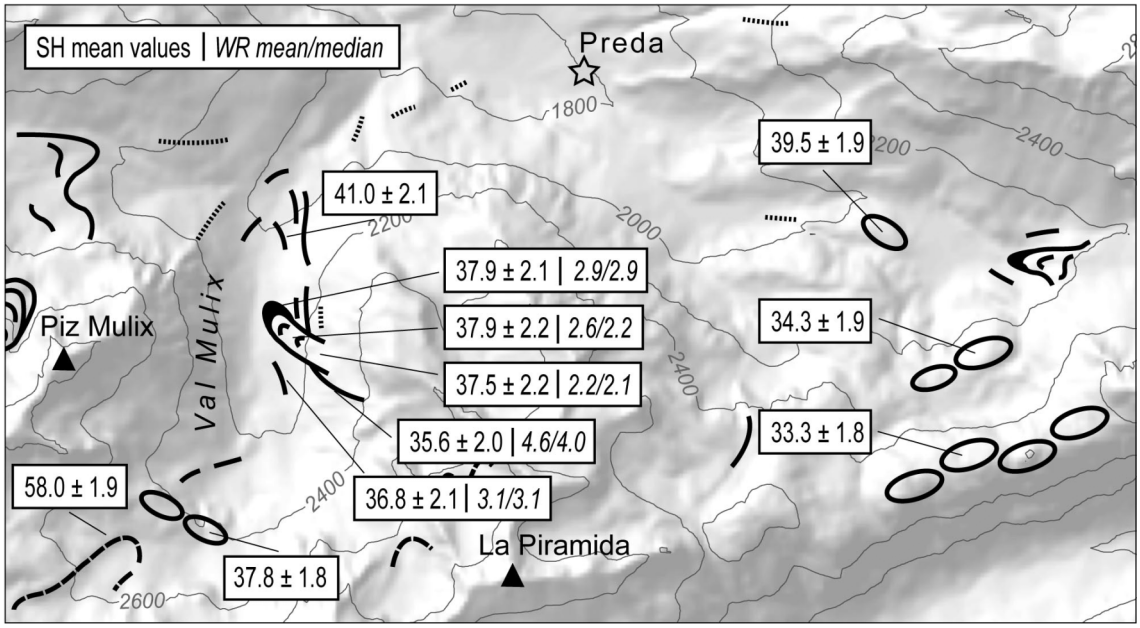

Fig. 5.3 Summarising overview of Schmidt-hammer (SH) and weathering rind (WR) measurements from the greater area of Albulapass (see also table 5.3 and Fig. 5.2). For detailed information on geomorphology see Fig. 2.6.

5.1.4 Soil chemical and mineralogical analyses

Profile photos of all sampled soils can be found in Appendix A. Table 5.4 gives some information about the sampling environment. All soils investigated have an identical parent material. S1 on the Daun moraine was the only profile surrounded by trees. The other sampling

sites were dominated by dwarf shrubs such as Ericaceae and Cladonia rangiferina. Similar to conifers, these contribute to an acidic substratum.

Table 5.4 General overview.

Site	Elevation (m a.s.l.)	Aspect (°N)	Slope (°)	Parent material	Vegetation	Land use	WRB (IUSS Working Group 2006)
S1	2100	35	11	Granite (Moraine material)	*Larix decidua Pinus cembra Ericaceae*	Natural forest, extensive pasturing possible	Umbric Podzol (Endoskeletic)
S2	2060	0	16	Granite (Rock glacier lobe)	*Ericaceae Cladonia rangiferina*	Natural alpine grassland, dwarf shrubs	Ortsteinic-Umbric Podzol (Episkeletic)
S3	2150	315	9	Granite (Moraine material)	*Ericaceae*	Natural alpine grassland, dwarf shrubs	Umbric Podzol (Endoskeletic)
S4	2130	300	8	Granite (Rock glacier lobe)	*Ericaceae Cladonia rangiferina*	Natural alpine grassland, dwarf shrubs	Umbric Podzol (Endoskeletic)
S5	2280	300	6	Granite (Rock glacier lobe)	*Ericaceae Cladonia rangiferina*	Natural alpine grassland, dwarf shrubs	Albic Podzol (Endoskeletic)

Physical and chemical properties

Except for S5, which was characterised by poorly developed horizons and weathering pockets, the soils showed an undisturbed evolution (according to their macromorphology as well as their chemical and physical properties) with no signs of erosion or burial. According to the visual impression in field, the soils on the moraines clearly showed a higher degree of development with more pronounced eluvial horizons (see pictures in appendix A). All soils in the study area have a loam in the topsoil and a loamy-sand texture in the subsoil (Table 5.5). The acidification of the developed soils is pronounced with pH-values in the topsoil generally between 3.0 and 4.0 (Table 5.6). The soils, especially the ones developed on the two moraines (S1 and S3), showed clear podzolisation features (Tables 5.5, 5.6, 5.7; Fig. 5.5) with a distinct eluviation and illuviation of Fe, Al and sometimes soil organic matter (SOM, especially in case of S5). Except for S2, very high amounts of C_{org} (> 200, partly > 300 g kg^{-1}) were measured in the topsoils.

Table 5.5 Some physical properties of the sampled soils in Val Mulix.

Site	Soil horizon	Depth (cm)	Munsell colour (moist)	Bulk density (g cm^{-3})	Skeleton[1)] (weight %)	Sand[2)] (g kg^{-1})	Silt (g kg^{-1})	Clay (g kg^{-1})
S1	O	0-13	5YR 1.7/1	0.37	3.1	502	386	112
	E	13-20	7.5YR 1.7/1	0.88	28.8	489	377	134
	Bhs	20-23	5YR 2/2	0.90	20.9	n.d.	n.d.	n.d.
	Bsm	23-50	5YR 3/4	1.75	60.9	823	154	23
	BC	50-70	10YR 5/4	1.68	53.2	n.d.	n.d.	n.d.
	C	>70	10YR 6/3	1.75	61.2	807	161	32
S2	OE	0-7	7.5YR 1.7/1	1.24	27.1	n.d.	n.d.	n.d.
	Bs	7-40	5YR 3/2	1.53	74.9	n.d.	n.d.	n.d.
	Bsm	40-60	7.5YR 4/4	n.d.	69.2	n.d.	n.d.	n.d.
	C	>60	10YR 4/4	1.93	78.9	n.d.	n.d.	n.d.
S3	O1	0-5	7.5YR 1.7/1	0.50	25.5	n.d.	n.d.	n.d.
	O2	5-10	10YR 2/2	0.49	17.0	494	369	137
	E	10-12	7.5YR 2/1	0.57	30.0	483	379	138
	Bhs	12-14	7.5YR 1.7/1	n.d.	27.1	n.d.	n.d.	n.d.
	Bs	14-26	5YR 3/4	0.81	50.1	793	181	26
	BC	26-60	10YR 4/6	1.36	67.9	814	154	32
S4	O	0-9	7.5YR 1.7/1	0.24	2.4	n.d.	n.d.	n.d.
	OE	9-18	7.5YR 1.7/1	0.40	5.8	n.d.	n.d.	n.d.
	Bs	18-30	5YR 2/3	1.32	56.6	n.d.	n.d.	n.d.
	BC	30-50	7.5YR 3/3	1.37	66.1	n.d.	n.d.	n.d.
	C	>50	10YR 4/4	1.51	75.3	n.d.	n.d.	n.d.
S5	O1	0-5	7.5YR 1.7/1	0.33	2.6	n.d.	n.d.	n.d.
	O2	5-10	7.5YR 1.7/1		12.4	n.d.	n.d.	n.d.
	E	10-15	7.5YR 4/2	0.70	36.5	n.d.	n.d.	n.d.
	Bhs	15-25	5YR 1.7/1	0.83	67.3	n.d.	n.d.	n.d.
	Bs	25-35	5YR 2/2	n.d.	64.3	n.d.	n.d.	n.d.
	BC	>35	10YR 3/4	1.54	72.5	n.d.	n.d.	n.d.

n.d.= not determined
[1)] Skeleton = Material > 2mm
[2)]Size fractions: Sand = 2000-63 μm; Silt = 63–2 μm; Clay = < 2 μm

All soils have a distinct amount of soil skeleton (material with a diameter > 2 mm), which usually increases with increasing soil depth and can be more than 70% by weight. These values are typical for moraines in Alpine areas.

Hardpan occurrence is pronounced in the Bsm horizon of S1, in case of S2 only small fragments in the cm-range were found. Bulk density of the Bsm horizon (1.75 g cm^{-3}) of S1 could be determined by measuring the volume of water that was replaced by dipping a piece of hardpan in a water-filled pail.

Detailed investigations using SED/EMS (Scanning Electron Microscope and Energy Dispersive Scanning; carried out by M. Egli) show a very porous nature of the Ortstein (Fig. 5.4). Coatings consist of minerals with Fe-, Al-oxyhydroxides, clays and organic matter. On the outer border of the Ortstein, Fe is accumulated. Formation of the Ortstein is due to intense eluviation of Fe, Al and subsequent formation of aggregates in the Bs horizon.

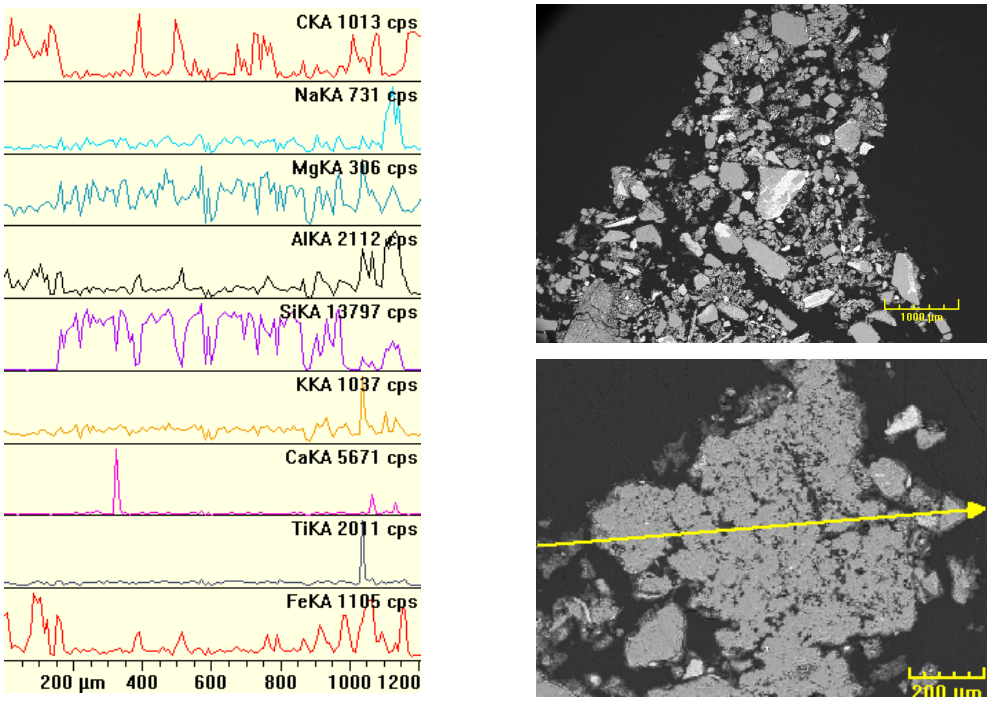

Fig. 5.4 SED/EMS measurements show the porous nature of Ortstein (upper right). Line scanning highlights C-, Al- and Fe- accumulations at the boarder of the ortstein (graphs CKA, AlKA and FeKa to the left; corresponding scanning path is given by the yellow arrow, lower right).

Oxalate and dithionite extractable amounts of Fe, Al and Si are presented in table 5.6 and Fig. 5.5, together with the ratio dithionite extractable/oxalate extractable in each case. Generally the concentration curves show a comparable shape with sometimes almost identical values (Egesen moraine, upper and middle part of the rock glacier). Also here, the podzolisation process is clearly represented by high amounts of Fe and Al in the Bs and Bhs horizons. Especially in the case of Al and Si the oxalate extractable part is higher than the one isolated with dithionite. Ratios of dithionite/oxalate extractable amounts are in most cases rather constant and low for Al and Fe, but show very high values for Si in the topsoil. A special case is the profile from the upper part of the relict rock glacier (S5), here strongly increased values for Fe were found in the topsoil.

A number of frequently used weathering indices are shown in Table 5.8. Elluvial horizons (here OE and E) and most pronounced illuvial horizons, mostly Bs or Bsm horizons, are highlighted with colours. Parameters referring to the total content of Ti are given for both skeleton (grain sizes > 2 mm) and fine earth. Differences "illuvial minus eluvial" provide a measure for the extend of translocation processes and thus for the degree of podzolisation. Based on geomorphology, a trend of weathering state in the form of S1 > S3 > S2 > S4 > S5 would be expected. However, a meaningful reconstruction of the expectable age trend cannot be achieved with the calculated indices. The overall picture that can be derived is rather chaotic and is characterised by a number of inversions, for instance for Al_d/Fe_d, which theoretically should increase with increasing age (Fitze, 1982; Bs(m) horizon S1: 1.06; S3: 1.36). Again striking are the values obtained from the profile S5: comparing E/OE horizons with Bs/Bsm horizons, the calculated difference in ferrihydrite content (as a measure for the podzolisation degree) is here about twice as high than in case of S1, although it is the youngest of the investigated soils.

Table 5.6 Chemical properties soils Val Mulix (fine earth).

Site	Soil horizon	Depth (cm)	pH ($CaCl_2$)	Org. C (g kg^{-1})	Total N (g kg^{-1})	C/N	Fe_t (g kg^{-1})	Si_o (g kg^{-1})	Al_o (g kg^{-1})	Fe_o (g kg^{-1})	Al_d (g kg^{-1})	Fe_d (g kg^{-1})	$Al_o + 0.5\ Fe_o$ (%)
S1	O	0-13	2.7	202.8	8.6	24	7.23	n.d.	n.d.	n.d.	n.d.	n.d.	n.d.
	E	13-20	3.2	45.9	1.5	30	13.94	0.06	2.92	2.36	3.31	5.32	0.41
	Bhs	20-23	3.5	50.5	2.0	26	34.54	0.24	7.03	10.30	8.48	17.91	1.22
	Bsm	23-50	4.4	28.3	0.9	33	34.01	7.54	20.05	6.29	15.93	15.07	2.32
	BC	50-70	4.4	3.9	0.2	16	24.86	1.36	3.25	1.20	2.54	2.84	0.38
	C	>70	4.6	2.3	0.3	9	20.82	0.92	2.04	0.79	1.66	1.69	0.24
S2	OE	0-7	3.4	151.2	5.8	26	11.74	0.11	3.87	3.97	4.02	4.67	0.59
	Bs	7-40	4.3	17.7	0.4	41	18.74	2.33	8.37	3.05	6.22	3.52	0.99
	Bsm	40-60	4.2	43.4	1.1	38	19.24	6.29	17.89	5.79	10.32	5.44	2.08
	C	> 60	4.6	4.2	0.2	17	17.21	1.07	3.36	1.20	2.84	1.51	0.40
S3	O1	0-5	3.4	305.1	16.2	19	11.03	n.d.	n.d.	n.d.	n.d.	n.d.	n.d.
	O2	5-10	3.4	189.9	5.0	38	19.55	n.d.	n.d.	n.d.	n.d.	n.d.	n.d.
	E	10-12	3.4	95.3	2.6	36	23.46	0.15	5.44	5.12	6.10	6.98	0.80
	Bhs	12-14	3.8	94.9	3.1	31	20.25	0.18	15.18	10.71	14.35	10.07	2.05
	Bs	14-26	4.2	44.8	1.2	36	29.45	2.54	18.68	11.31	14.90	10.96	2.43
	BC	26-60	4.7	3.5	0.2	21	25.34	1.70	4.70	2.05	2.65	2.55	0.57
S4	O	0-9	3.1	278.3	12.0	23	5.97	n.d.	n.d.	n.d.	n.d.	n.d.	n.d.
	OE	9-18	3.3	171.3	6.0	29	13.35	0.01	3.99	3.03	3.85	5.16	0.55
	Bs	18-30	4.1	75.9	2.6	30	28.00	1.11	19.81	10.50	19.78	10.75	2.51
	BC	30-50	4.4	33.0	1.4	24	24.69	2.10	11.48	3.58	10.60	3.92	1.33
	C	> 50	4.5	11.3	0.5	22	22.72	1.19	5.01	1.36	4.94	1.98	0.57
S5	O1	0-5	3.3	328.6	14.3	23	7.20	n.d.	n.d.	n.d.	n.d.	n.d.	n.d.
	O2	5-10	3.4	240.1	8.4	29	9.60	n.d.	n.d.	n.d.	n.d.	n.d.	n.d.
	E	10-15	3.9	23.7	0.5	48	3.53	0.00	0.85	0.44	0.95	1.12	0.11
	Bhs	15-25	4.1	88.2	3.4	26	28.73	0.51	11.89	10.03	12.82	12.12	1.69
	Bs	25-35	4.6	46.3	1.4	33	30.62	2.15	14.53	8.00	12.21	8.25	1.85
	BC	> 35	4.7	9.9	0.4	24	23.68	2.08	8.82	3.96	4.46	3.16	1.08

n.d.= not determined

Table 5.7 Concentrations of the main elements obtained by means of XRF. The values refer to the sum of earth and skeleton material.

Site	Soil horizon	Depth (cm)	OM* (g/kg)	CaO (g/kg)	MgO (g/kg)	K_2O (g/kg)	Na_2O (g/kg)	Al_2O_3 (g/kg)	Fe_2O_3 (g/kg)	SiO_2 (g/kg)	MnO (g/kg)	TiO_2 (g/kg)
S1	O	0-13	338.08	5.23	4.65	18.34	13.13	97.67	10.58	401.93	0.07	7.10
	E	13-20	56.22	9.33	7.58	27.23	20.32	147.22	21.77	594.84	0.20	7.70
	Bhs	20-23	68.75	13.92	10.95	23.79	21.69	149.20	47.87	552.81	0.39	7.13
	Bsm	23-50	19.01	22.57	13.36	21.60	27.84	158.45	43.25	622.90	0.68	5.30
	BC	50-70	3.14	19.65	11.32	29.36	27.75	149.77	31.60	680.39	0.56	4.34
	C	>70	1.51	15.33	9.14	29.32	29.73	145.26	25.34	701.68	0.55	3.77
S2	OE	0-7	189.56	8.22	4.67	28.03	20.92	124.13	16.49	562.41	0.15	4.68
	Bs	7-40	7.62	14.45	6.84	31.78	30.42	145.27	23.00	700.31	0.50	3.22
	Bsm	40-60	22.98	14.40	6.44	28.21	30.93	149.01	25.89	671.66	0.46	3.69
	C	>60	1.54	14.58	7.77	32.81	30.21	146.34	24.55	704.86	0.53	3.57
S3	O1	0-5	391.10	10.70	6.05	16.53	16.86	93.27	28.40	338.46	0.25	5.84
	O2	5-10	271.11	8.56	6.53	30.68	14.22	125.53	31.79	471.24	0.25	8.92
	E	10-12	114.70	19.06	8.63	32.44	17.10	157.43	41.58	508.00	0.46	10.84
	Bhs	12-14	118.86	10.76	5.52	28.90	18.96	155.07	30.81	488.83	0.23	6.17
	Bs	14-26	38.51	10.08	7.83	29.21	23.09	156.39	34.56	604.49	0.39	4.94
	BC	26-60	1.96	12.42	12.80	31.50	31.02	153.77	32.69	684.65	0.59	4.63
S4	O	0-9	467.35	5.38	3.00	12.82	12.49	64.38	8.82	273.46	0.01	4.75
	OE	9-18	277.52	8.79	5.18	22.69	15.33	121.63	19.70	446.10	0.09	7.71
	Bs	18-30	56.67	23.89	6.72	20.99	26.76	150.19	34.43	604.43	0.44	3.99
	BC	30-50	19.29	29.73	6.66	22.96	30.72	150.25	32.19	654.30	0.50	4.12
	C	>50	4.82	42.08	7.37	23.13	30.19	153.77	33.71	664.97	0.53	3.92
S5	O1	0-5	550.29	5.35	2.72	11.45	11.06	54.49	10.80	249.84	0.09	4.14
	O2	5-10	361.64	7.47	4.93	21.06	14.84	93.11	16.39	406.24	0.16	5.27
	E	10-15	25.93	7.28	5.68	36.26	20.28	119.85	9.42	744.00	0.18	3.51
	Bhs	15-25	49.63	12.35	7.01	33.43	24.87	140.06	29.15	640.74	0.45	4.15
	Bs	25-35	28.42	16.16	8.71	29.30	27.11	147.64	35.00	624.61	0.53	4.44
	BC	>35	4.69	15.77	9.51	31.74	26.44	144.07	29.91	680.00	0.56	3.96

*Organic matter = org C (fine earth and skeleton)*1.72

Daun moraine

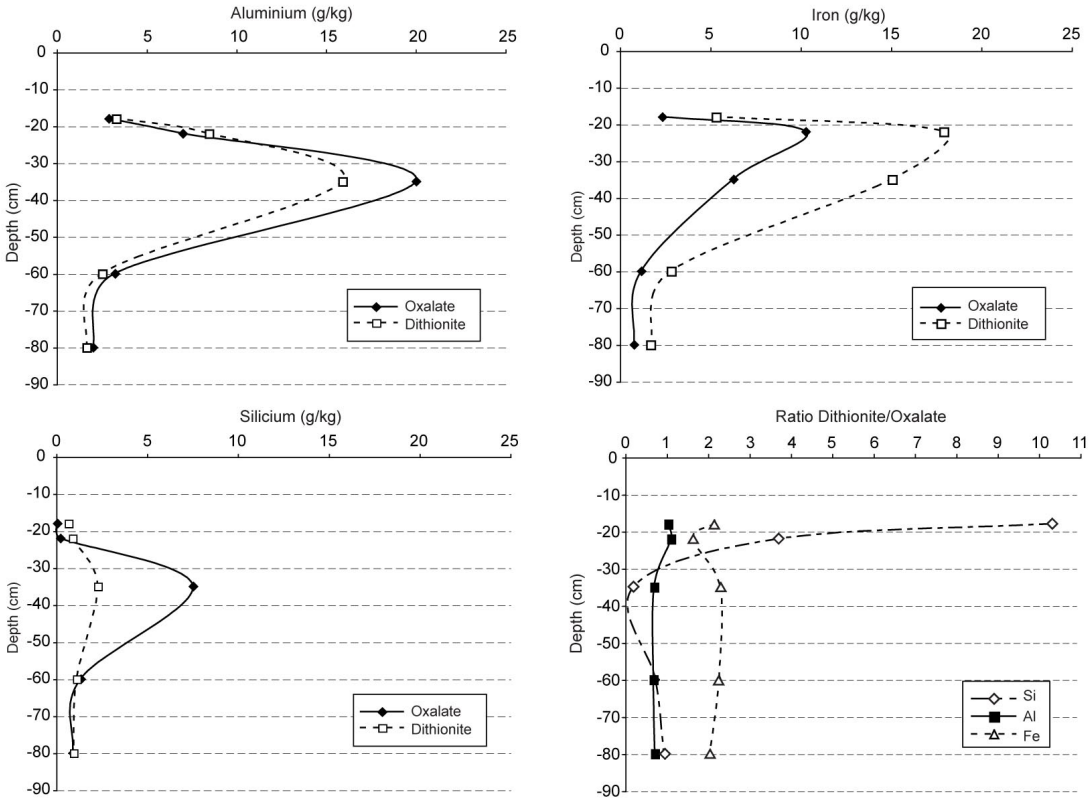

Egesen moraine

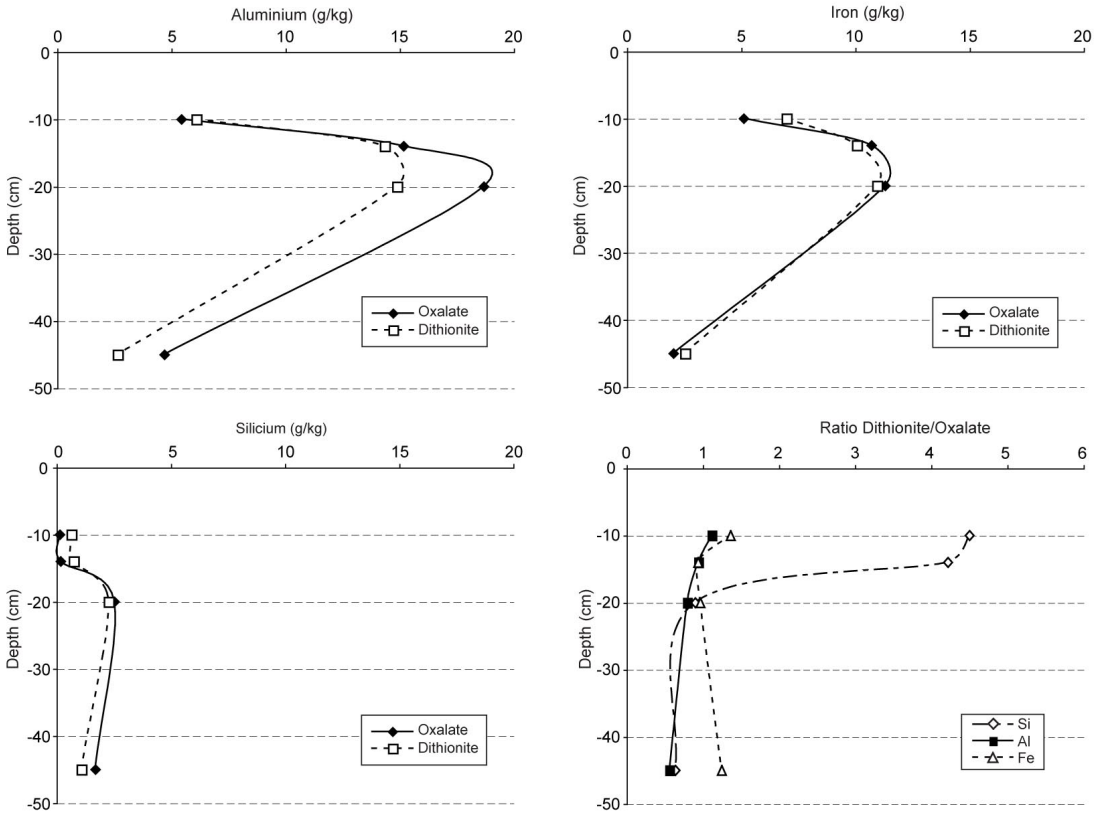

Rock glacier upper part

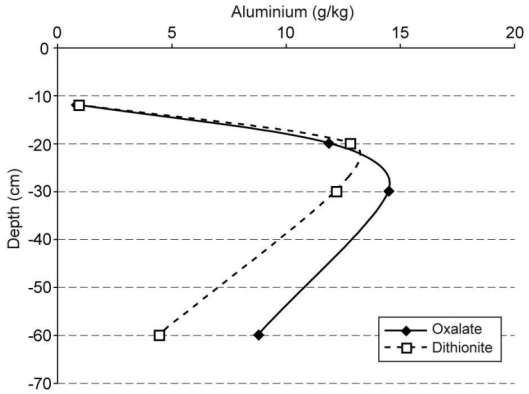

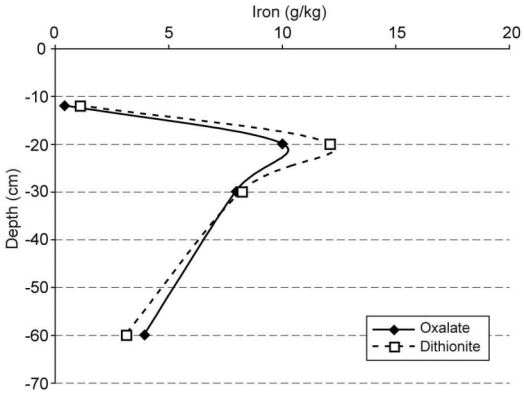

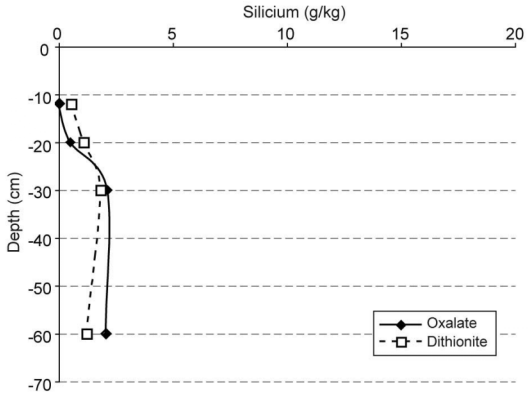

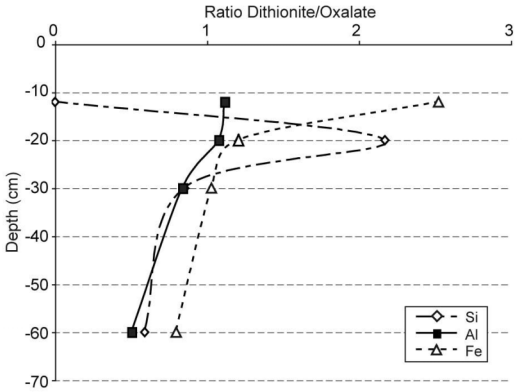

Rock glacier middle part

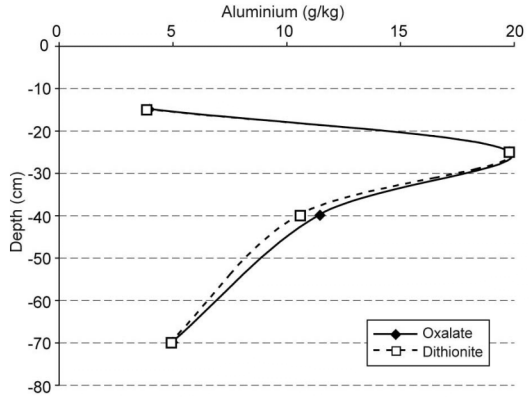

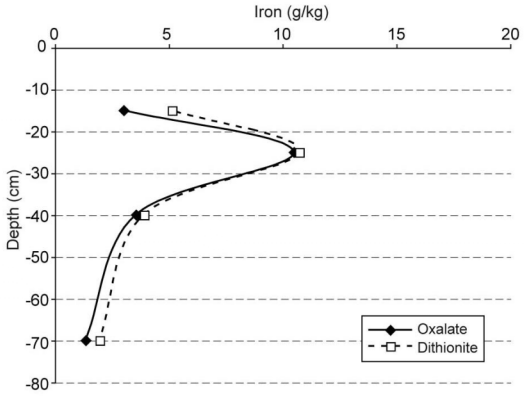

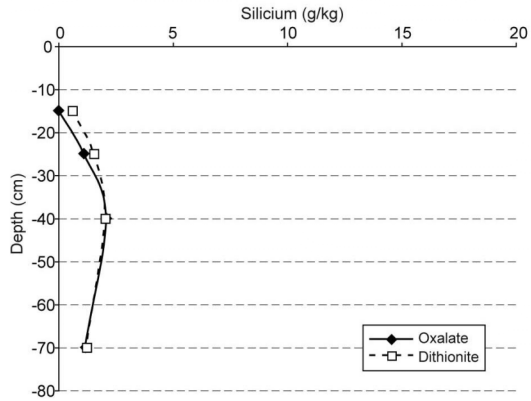

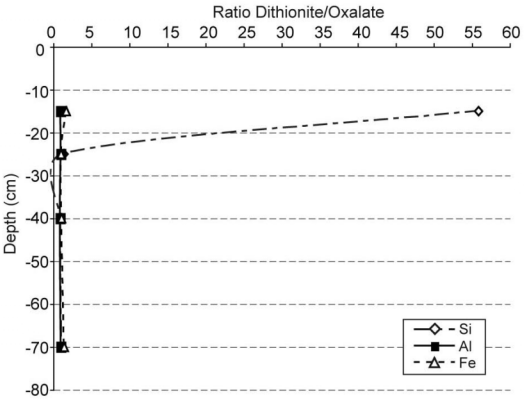

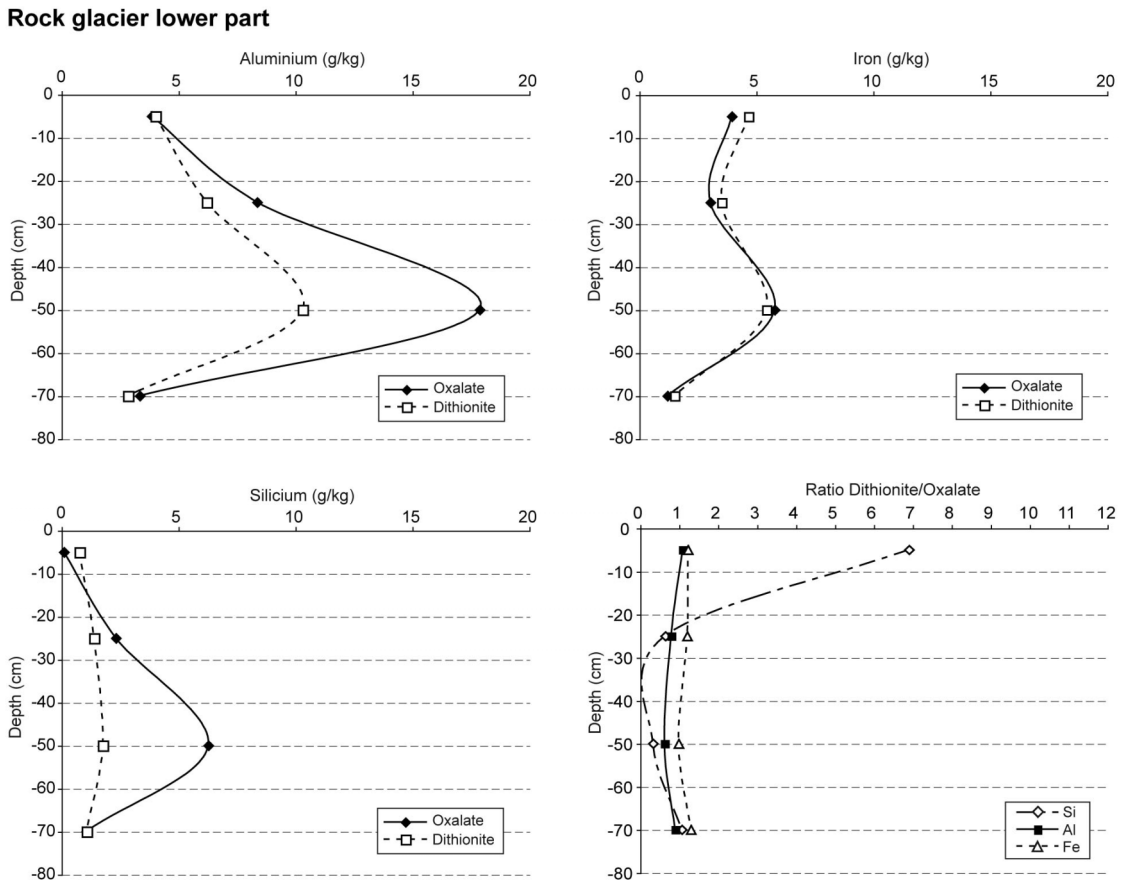

Fig. 5.5 Oxalate and dithionite extractable amount of Al, Fe and Si, in each case with the ratio dithionite extractable/oxalate extractable.

Table 5.8 Weathering indices from the soils of Val Mulix. Elluvial (E, OE) and most pronounced illuvial horizons (Bs, Bsm) are indicated in each case with yellow and orange, respectively.

Site	Soil horizon	Fe_d/Fe_{tot}	Fe_{tot}/Ti_{tot}		$Fe_{tot} - Fe_d$ (g/kg)	Al_d/Al_{tot}	Al_{tot}/Ti_{tot}		Al_d/Fe_d	$(Al_d/Al_{tot})/(Fe_d/Fe_{tot})$	Ferri-hydrite (g/kg)	ITM (%)
			f	s			f	s				
S1	O	-	1.74	1.93	-	-	12.04	23.16	-	-	-	-
	E	0.38	2.66	6.81	8.61	0.04	14.78	28.40	0.62	0.11	4.02	0.66
	Bhs	0.52	7.81	7.98	16.63	0.11	17.01	27.21	0.47	0.22	17.51	1.61
	Bsm	0.44	10.29	8.94	18.94	0.18	26.47	26.30	1.06	0.41	10.69	6.57
	BC	0.11	8.60	8.39	22.02	0.03	27.57	33.99	0.90	0.28	2.04	1.11
	C	0.08	8.08	7.65	19.12	0.02	29.08	38.34	0.98	0.27	1.34	0.71
S2	OE	0.40	3.80	5.78	7.07	0.07	19.67	43.29	0.86	0.17	6.74	0.88
	Bs	0.19	8.74	8.15	15.22	0.08	35.44	41.56	1.77	0.44	5.18	2.51
	Bsm	0.28	8.25	8.17	13.80	0.13	34.72	36.19	1.90	0.45	9.84	5.73
	C	0.09	8.39	7.94	15.70	0.04	36.59	36.12	1.89	0.43	2.05	1.04
S3	O1	-	3.95	8.49	-	-	12.50	16.72	-	-	-	-
	O2	-	3.59	7.30	-	-	11.71	16.38	-	-	-	-
	E	0.30	3.54	7.20	16.47	0.08	12.16	14.75	0.87	0.25	8.70	1.23
	Bhs	0.50	5.33	7.60	10.19	0.18	20.42	28.49	1.43	0.37	18.21	3.37
	Bs	0.37	8.54	7.59	18.49	0.18	24.08	33.99	1.36	0.48	19.23	4.82
	BC	0.10	8.61	8.05	22.79	0.03	26.90	30.71	1.04	0.33	3.48	1.52
S4	O	-	2.16	3.00	-	-	11.68	45.09	-	-	-	-
	OE	0.39	2.91	5.68	8.20	0.23	13.47	32.38	0.75	0.16	5.15	0.88
	Bs	0.38	10.95	9.23	17.26	0.38	30.14	36.14	1.84	0.67	17.85	4.65
	BC	0.16	9.42	8.93	20.77	0.14	29.82	33.62	2.70	0.85	6.08	3.12
	C	0.09	8.92	10.45	20.75	0.06	30.06	36.35	2.50	0.74	2.32	1.44
S5	O1	-	3.01	4.36	-	-	11.44	19.60	-	-	-	-
	O2	-	3.12	7.90	-	-	14.56	24.29	-	-	-	-
	E	0.32	1.76	5.46	2.41	0.13	30.69	29.13	0.84	0.05	0.75	-
	Bhs	0.42	8.10	8.31	16.61	0.35	19.81	39.38	1.06	0.43	17.05	2.75
	Bs	0.27	9.84	137.70	22.38	0.26	25.39	8.69	1.48	0.57	13.60	3.80
	BC	0.13	9.15	143.74	20.52	0.17	29.35	8.66	1.41	0.44	6.74	2.53

f = fine earth; s = skeleton; ITM = Imogolite type material

Mass balance calculations

Assuming an increasing element loss with increasing age (a more mature weathering state of the soil), the following order of elements lost can be expected: Daun moraine > Egesen moraine > rock glacier with increasing values from the front to the rooting zone. As shown in Fig. 5.6, this is actually the case, especially the element loss patterns of Si, Al, Na and K show a good representation of the expected trend based on morphostratigraphy. However, only the element K shows the expected trend for all sampled soil profiles.

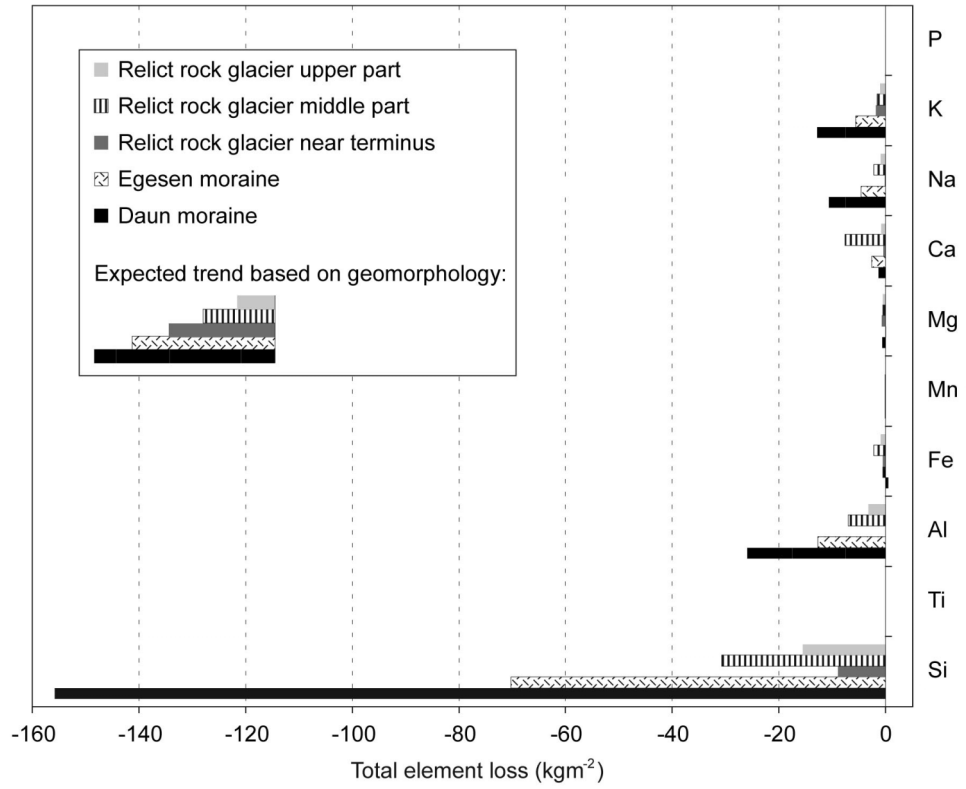

Fig. 5.6 Calculated mass balance based on immobile Ti. Assumption is that the older the soils are, the higher the element losses. Except for the profile near the rock glacier terminus, the calculated mass losses are in accordance with the expected trend based on morphostratigraphy, namely for Si, Al, Na and K.

A striking phenomenon is the chemical behaviour of the soil from the rock glacier front (dark grey bar in Fig. 5.6). Except for the element K, the calculated element loss values are very low to virtually inexistent and do not fit into the otherwise coherent trend. It should be mentioned that especially the frontal part of the rock glacier, subject to extensive mixing processes, experienced the most complex genesis. Source material at an initial stage likely was provided by an uphill deposited Egesen moraine, back-filled sediment and eventually also by material from a former Daun moraine (Maisch, 1981). An inhomogeneous and repeatedly

reworked composition, possibly accompanied by the incorporation of pre-weathered material, may adulterate the signal and lead to results that are difficult to interpret.

An additional disturbing factor is the high proportion of coarse blocks in the parent material. This was typical especially for the profiles on the rock glacier. Skeleton weight percentages of > 70 % are normal (see Table 5.5), whereby the biggest compounds are not even included. This hampers the formation of a well-pronounced pedogenic horizontation. Compared to the more homogenous composition of the two moraines, dislocation processes in the soils developed on the relict rock glacier follow more often preferential paths, for instance along the surfaces of boulders.

Soil mineralogy

All XRD and FT-IR patterns, as well as the results from the AUTOQUAN quantification, can be found in Appendices B and C, respectively. Mineralogical composition according to the semi-quantification of clays for E/OE horizons and selected C/BC horizons are summarised in Fig. 5.7. The latter are mainly characterised by chlorite and mica. For the C horizon of the Daun moraine profile, considerable amounts of mica/HIV (interstratification of mica and hydroxy-interlayered vermiculite) could be determined.

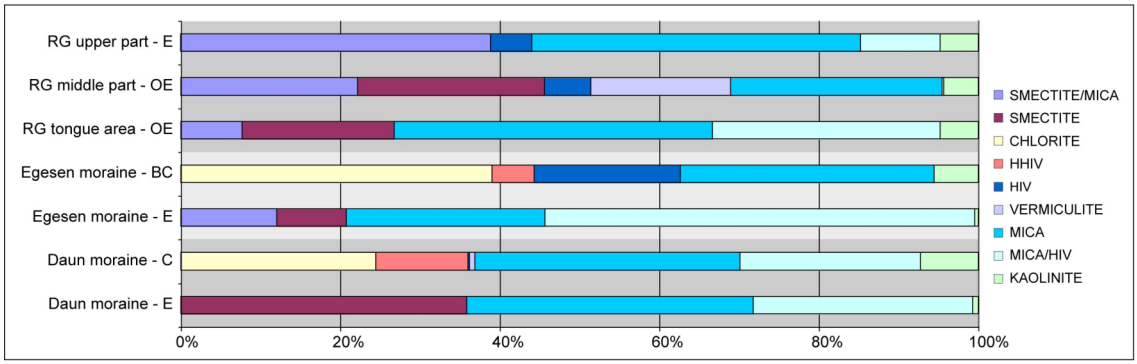

Fig. 5.7 Results of the semi-quantification of the clay fraction, in each case for the most weathered horizon (E/OE). As a reference, the C and BC horizons of the moraines are shown as well. Taking the amount of smectite as an age indicator, the Daun moraine shows clearly the highest degree of development. The middle and lower part of the rock glacier show surprisingly high amounts of smectite, the upper part no smectite at all. This is another indication that pre-weathered material might be present. C and BC horizons are characterised by high amounts of chlorite. (H)HIV = (highly)hydroxy-interlayered vermiculite.

The BC horizon of the Egesen moraine contains around 20% HIV, which is absent in the C horizon of the Daun moraine. The surprisingly high amounts of kaolinite in the C/BC horizons do not agree with only weak signals in FT-IR patterns (Fig. 5.8, Appendix B). This

might be the result of weak XRD signals for the 1.4 nm and 1.0 nm peaks, making an underestimation of the contribution of chlorite to the 0.7 nm peak likely.

Regarding the weathered horizons, the Daun moraine E horizon has by far the highest smectite content, followed by the middle and lower part of the rock glacier and the Egesen moraine. The upper part of the rock glacier contains no smectite; however, very high amounts of smectite/mica could be detected. Chlorite is not present anymore. Mica amounts are in a similar range for all horizons. Like in the C horizon, the E horizon of the Daun moraine shows high values of mica/HIV but no vermiculite and only very little kaolinite. The mica/HIV content is even more pronounced in the Egesen moraine E horizon. Also here, very low amounts of kaolinite were determined. Some vermiculite could only be found in the middle part of the rock glacier. Compared to the C/BC horizons, the significant loss of chlorite but comparable content of mica in the weathered horizons suggest that chlorite alteration is the main source for the formation of secondary clay, such as smectite.

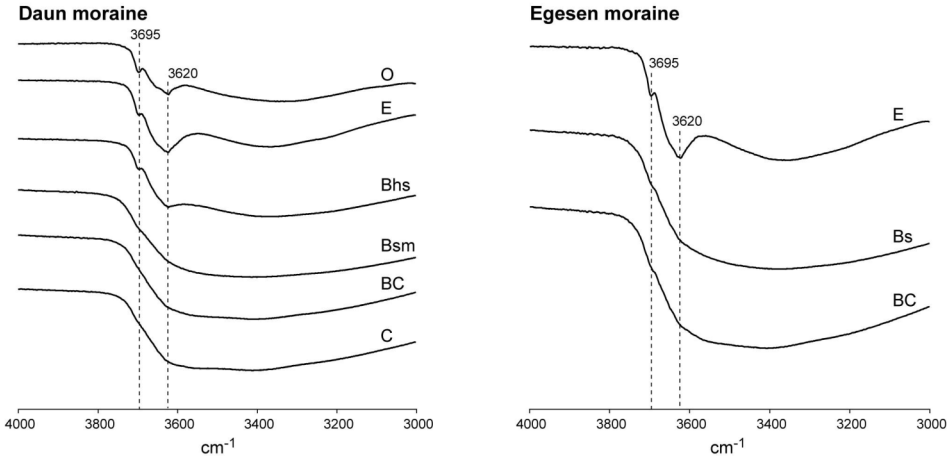

Fig. 5.8 FT-IR patterns from 3000 to 4000 cm^{-1} for the moraine profiles (for all patterns see appendix B). The peak around 3695 cm^{-1} is diagnostic for kaolinite. In most profiles it is distinct only for O and E horizons. For the lower horizons, only traces can be determined.

XRD measurements in the range between 58° and 64° 2-theta on powder samples provide information about the presence of di- and trioctahedral minerals, respectively. In all profiles, dioctahedral mineral gain in importance with an increasing degree of weathering (from C/BC to E/OE horizons). This goes along with a reduction of trioctahedral minerals, as indicated by a decrease of the peak near 60° 2-theta with regard to the peak near 62° 2-theta. In order to check the presence of hydroxy-interlayered smectite (HIS), samples that potentially contain HIS were treated with sodium citrate (see diffractogramms in Appendix B). An enlarged peak at 1.65 nm

after ethylene glycol saturation and a more pronounced collapse towards 1.0 nm after K-saturation compared to the non-treated samples are characteristic for the presence of HIS. Based on that, HIS could be identified in the E and OE horizon of the upper and middle part of the rock glacier, respectively.

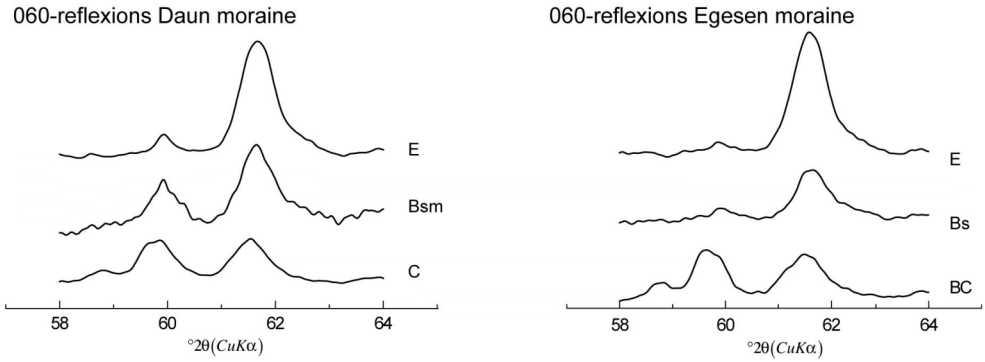

Fig. 5.9 060-reflexions from selected horizons of the moraine profiles. An increase of dioctahedral minerals with weathering (from the C/BC to the E horizon) is represented by the increasing relative importance of the peak near 62° 2-theta with respect to the peak near 60° 2-theta. A comparable behaviour was found for the profiles sampled on the relict rock glacier (Appendix B).

As described in Chapter 3, smectite constitutes an end product of mica alteration or alternative weathering paths starting for instance with chlorite. Therefore, the amount of smectite is positively correlated with the weathering state and – given that the formation factors other than time are comparable for the studied soils – thus the age of a soil. From this point of view, the soil developed on the Daun moraine can be identified as the oldest. A well-pronounced distinction against the Egesen moraine is obvious, which is in accordance with the X-ray diffractograms shown in Fig. 5.10. Within the relict rock glacier, a meaningful picture can be drawn with more weathered soils in the lower and middle part and a less developed profile in the upper part. The diffractogram of the lower part of the rock glacier gave only a weak signal. The peak positions and their relative importance, however, are the same as in the middle part. It is apparent that the mineralogical composition of the lower and middle part of the relict rock glacier reflects properties that speak for more developed soils than is the case for the Egesen moraine. This disagrees with the stratigraphic setting, speaking again for the presence of pre-weathered material with a disturbing influence in the soils developed on the relict rock glacier. This substantiates the impression that can be received also by other techniques applied here (mass balance calculation, chemical weathering indices, radiocarbon dating of stable SOM).

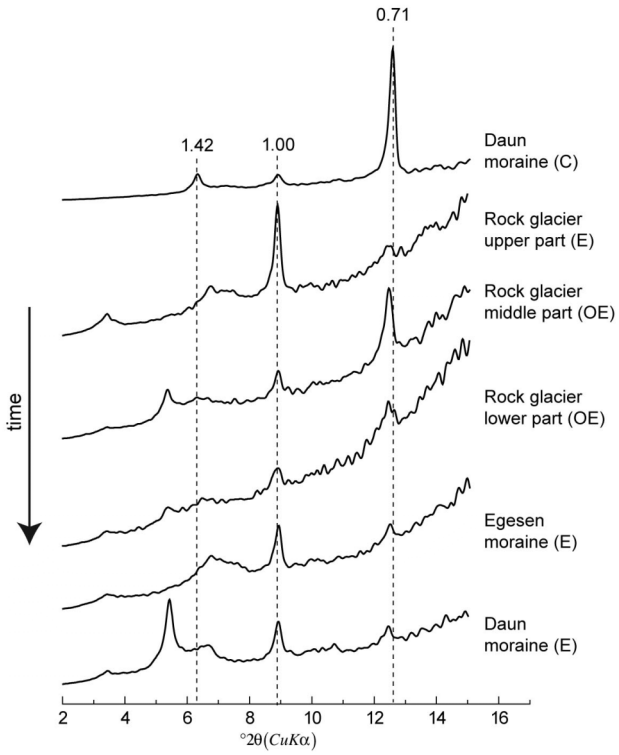

Fig. 5.10 XRD diffractograms (ethylene glycol saturated) from the most weathered horizon of each soil (E or OE horizons). The uppermost curve from the C horizon of S1 serves as a reference, representative for the parent material of all soils (for t = 0). The order of the XRD patterns is according to the age trend based on geomorphology. The Daun moraine can clearly be identified as older than the Egesen moraine. However, according to the patterns shown above, the rock glacier seems to be more developed than the Egesen moraine, meaning an age inversion. More proof that pre-weathered material might be present in the rock glacier.

Results of the AUTOQUAN analyses (tables are shown in Appendix C) give an additional impression of the mineralogical composition, separated into sand (2000-63 μm), silt (63-2 μm) and clay fraction (< 2 μm). However, a direct comparison to the values discussed above is not possible, as a different mineralogical spectrum – including components like quartz, epidote and feldspars – is analysed, and the percentages correspondingly refer to a different total. Furthermore, it is not possible to identify interstratified minerals using AUTOQUAN. A high value for smectite, for instance, can be made up of smectite itself and mica/smectite. The results generally show low values for kaolinite for the topsoils (except for the upper and middle part of the rock glacier with around 11% in each case) and not kaolinite at all for the lowermost horizons. This is another hint that kaolinite contents reported above for the C/BC horizons are too high.

Radiocarbon dating of stable SOM

Calibrated ages (1 sigma ranges) are listed together with the uncalibrated ages and C-losses due to H_2O_2 treatment in Table 5.9. In most cases the oldest ages are found in the upper soil, namely in O, OE or E horizons (S1, S2, S4 and S5). For S3 (from the lower Egesen I moraine), the oldest age was determined in the Bhs horizon. S5 is the only profile that shows re-increasing ages with depth.

Table 5.9 Radiocarbon ages measured from soil samples in Val Mulix.

Site	Horizon	Depth (cm)	C-loss (%) due to H_2O_2 treatment	UZ-No.	Uncal. ^{14}C ages (y BP) H_2O_2 treated	Cal. ages (1σ-range), y BP, H_2O_2 treated
S1	O	0-13	75.8	5486	2050 ± 50	2105-1948
	E(a)	13-20	34.6	5487	18750 ± 180	22466-22152
	E(b)	13-20	91.9	5564	4625 ± 60	5466-5297
	Bhs	20-23	93.8	5488	4025 ± 55	4569-4422
	Bsm	23-50	76.5	5489	3565 ± 55	3963-3730
	BC	50-70	n.d.	n.d.	n.d.	n.d.
	C	>70	n.d.	n.d.	n.d.	n.d.
S2	OE	0-7	57.9	5505	6795 ± 65	7680-7585
	Bs	7-40	88.2	5506	3785 ± 55	4247-4013
	Bsm	40-60	87.4	5507	3930 ± 60	4498-4256
	C	>60	n.d.	n.d.	n.d.	n.d.
S3	O1	0-5	59.2	5508	1770 ± 50	1776-1610
	O2	5-10	53.7	5509	4365 ± 60	5035-4855
	E	10-12	77.3	5510	5270 ± 65	6177-5943
	Bhs	12-14	84.8	5511	12440 ± 100	14704-14216
	Bs	14-26	87.1	5512	5600 ± 65	6437-6310
	BC	26-60	n.d.	n.d.	n.d.	n.d.
S4	O	0-9	38.4	5513	1210 ± 50	1228-1064
	OE	9-18	71.0	5528	5740 ± 65	6634-6470
	Bs	18-30	90.8	5529	1555 ± 50	1518-1400
	BC	30-50	n.d.	n.d.	n.d.	n.d.
	C	>50	n.d.	n.d.	n.d.	n.d.
S5	O1	0-5	43.1	5530	2965 ± 55	3244-3043
	O2	5-10	40.5	5531	2975 ± 55	3253-3071
	E	10-15	70.0	5565	8885 ± 80	10178-9892
	Bhs	15-25	95.5	5532	4040 ± 60	4781-4424
	Bs	25-35	89.9	5533	7955 ± 75	8979-8662
	BC	>35	n.d.	n.d.	n.d.	n.d.

n.d.= not determined

The E horizon from S1 was analysed twice, yielding first an age of more than 22,000 years (E(a)) and the second time only 5466-5297 years (E(b)). Taking generally accepted basics of glacial history into account, the first age makes no sense, as during this time the Alps for the

most part were covered with ice. The influence of limestone causing an overestimation of the age can be excluded. This is clearly shown by very low pH-values that do not exceed 3.2 in the uppermost two horizons (Table 5.6). S1 was taken on a moraine, which is an accumulative glacial landform. A conservation of pre-LGM soil material at the glacier base can consequently be ruled out. Furthermore, the big age difference within one and the same horizon poses questions about the reproducibility of the method. It must be mentioned that, in the case of the higher age, AMS-specific problems occurred (low current, small sample), making the lower age more reliable. Nevertheless, at least a certain susceptibility to input of external old material seems obvious and basically asks for a multiple age determination for each horizon in order to allow for statistical substantiation.

Focusing on the relict rock glacier (S2 near the tongue, S4 in the middle and S5 in the uppermost part), the ages generally vary within an acceptable range. However, contrary to expectations, S5 yielded higher ages than S2. Also, an age range of 10178-9892 years (E horizon of S5) in this position seems too old. A nearby sampled boulder (VM2) gave an age of 8.6 ± 0.6 ka. As suggested by weathering rind thicknesses and the age of VM1 (14.5 ± 1.2 ka), the glacial history and connected landscape evolution on the orographically right side of Val Mulix was not simple (see also Chapter 5.1.1). An incorporation of pre-weathered material is at least not impossible; this could explain the high ages in S2 and also in S3 (14704-14216 years), which should be younger than 10.7 ka with respect to VM4.

Meteoric ^{10}Be inventory in profile S1 (Daun moraine, Val Mulix)

Meteoric ^{10}Be infiltrates into soils and is adsorbed along the profile. Measured concentration are in the range of 1.5 to 7.0 × 10^{8} ^{10}Be atoms/g fine earth (Table 5.10).

Table 5.10 Meteoric ^{10}Be concentrations from the soil profile S1 on the Daun moraine, Val Mulix.

Soil horizon	Depth (cm)	Sample label	Material	^{10}Be/^{9}Be (1E-12)	Error (%)	Weight (g)	^{10}Be atoms/g (1E+8)
O	-7	ZB7350	Fine earth	30.761	3.3	5.009	2.0600
E	-17	ZB7351	Fine earth	16.508	3.0	3.501	1.6100
Bhs	-22	ZB7352	Fine earth	15.446	3.3	2.507	2.0420
Bsm	-35	ZB7353	Fine earth	42.957	5.2	2.028	7.1055
BC	-60	ZB7354	Fine earth	11.580	3.0	2.030	1.9326
C	-75	ZB7355	Fine earth	6.882	3.0	1.504	1.5654

A distinct increase of the ^{10}Be concentration in the Bsm horizon was detected, which indicates an active translocation of ^{10}Be within the soil profile. This translocation is due to

podzolisation processes where ^{10}Be migrates together with Fe, Al and/or SOM to greater soil depths. The ^{10}Be content corresponds well to oxalate extractable Al, suggesting bonding to metal oxides (Fig. 5.11). Furthermore, Kaolinite and dioctahedral vermiculite, seem to be a very efficient trap for ^{10}Be (Pavich *et al.*, 1985). In the investigated soil, smectite, vermiculite, chlorite, mica, kaolinite, HIV (hydroxy-interlayered vermiculites) and partly HIS (hydroxy-interlayered smectites) and interstratified minerals prevail in the clay fraction. Leaching of ^{10}Be from the soil column may lead to an underestimation of the age. A major loss of ^{10}Be with the acidic percolate, however, can be excluded due to the sharp decrease of ^{10}Be with soil depth, which is clearly shown in the given distribution of ^{10}Be in the soil profile.

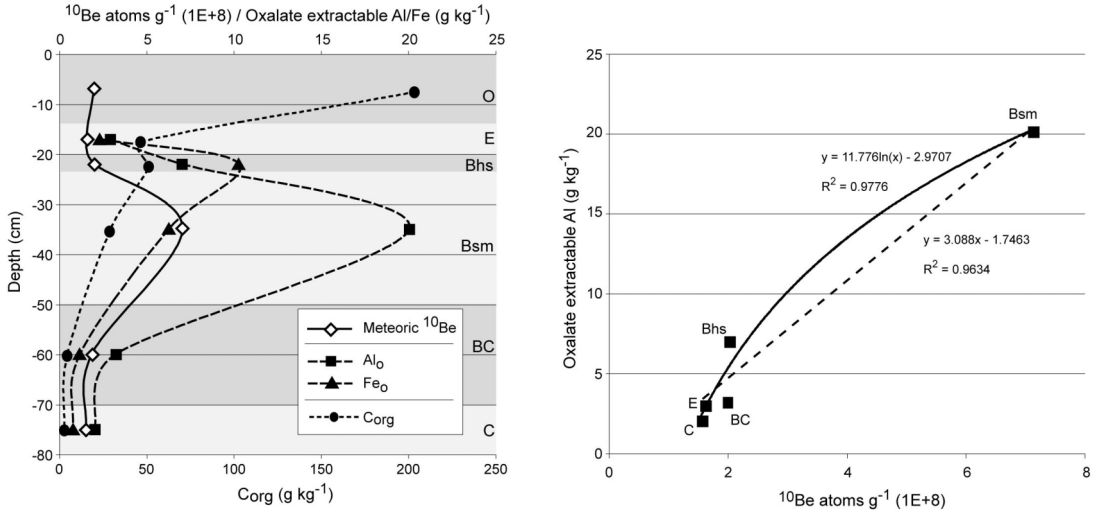

Fig. 5.11 Profile of measured meteoric ^{10}Be values, compared to oxalate extractable Al and Fe and C_{org} (left). Soil horizons are indicated by grey shadings. ^{10}Be content corresponds well to Al_O, suggesting bonding to metal oxides (right). This is supported by the high concentrations in the illuvial horizon (Bsm).

For age calculation, we used precipitation dependent ^{10}Be deposition fluxes, assuming a proportional increase of ^{10}Be deposition with increasing amounts of precipitation (Monaghan *et al.*, 1985/1986; see also Chapter 6). Based on HADES (2004), the area of the Daun moraine in Val Mulix receives 1200 to 1400 mm precipitation per year (mean annual corrected precipitation 1951-1980). Using these values in Formula 4.13, this gives a moraine age of 12.65 ka (1400 mm precipitation per year) to 14.84 ka (1200 mm precipitation per year). As described in Chapter 4.5.6, an estimated error of the ^{10}Be inventory and the subsequent derived surface age of 8 to c. 21% must be taken into account. Compared to the exposure age measured on the same moraine, boulder VM7 with 14.7 ± 1.7 ka, the moraine age derived from the meteoric ^{10}Be inventory is very similar, speaking for the potential of this approach.

With the age of VM7 as a reference (as the "expected age") and using equation x, an erosion rate of 4.3-6.2 mm/ky can be calculated. This value is low but reasonable. The calculated erosion rate is similar to the results of Granger *et al*. (2001), where catchment erosion rates at Adams Peak and Antelope Lake (north-eastern Sierra Nevada, CA, USA) were in the range between 15 and 60 mm/ky. Schaller *et al*. (2001) measured 20 – 100 mm/ky erosion rates for middle European river catchments. In these studies, an averaged erosion rate is obtained over a larger area. The Alpine soil investigated here, however, developed on a stable surface and at an almost flat position (see Table 5.4). Vegetation as well as the stony character of the site, render it much less susceptible to erosion. Boulders even shield the underlying soil from erosion (Granger *et al*., 2001). A high soil skeleton content as well as the vegetation cover prevent soils from erosion (Richter, 1998).

5.2 Val Burdun

5.2.1 Surface exposure dating

Boulders VB7 and VB12 give with 10.2 ± 0.9 ka and 10.5 ± 0.9 ka (mean age 10.3 ± 0.9), respectively, coherent ages for the stabilisation of the lower moraine (see Fig. 5.12 and Table 5.11b, Scenario C). Ages obtained from the higher level (10.4 ± 1.0 ka, VB5) and the lower level (9.8 ± 0.8 ka, VB6) of the upper moraines are not different within the stated errors. This suggests a deposition within a relatively short time span. Whereas VB7 and VB12 were taken on big boulders with a height of ≥ 1.5 m, the only available boulders in a good position on the upper moraines were comparably small and a complete coverage with snow during winter must be assumed. This makes a reasonable choice of snow heights for age correction even more difficult than it is anyway. In any case, we consider a higher snow value for these two boulders compared to big, isolated boulders meaningful and necessary. We therefore used 0.8 m snow for both VB5 and VB6 (Table 5.11b). VB12 is situated in a steep slope and sourrounded by light forest. We tried to account for the potential influence of snow moving downslope and – similar to VM7 on the Daun moraine in Val Mulix – for shadow and wind protection caused by trees. Accordingly, we chose also a somewhat higher value (0.7 m snow) than for VB7 on the same moraine (0.3 m snow).

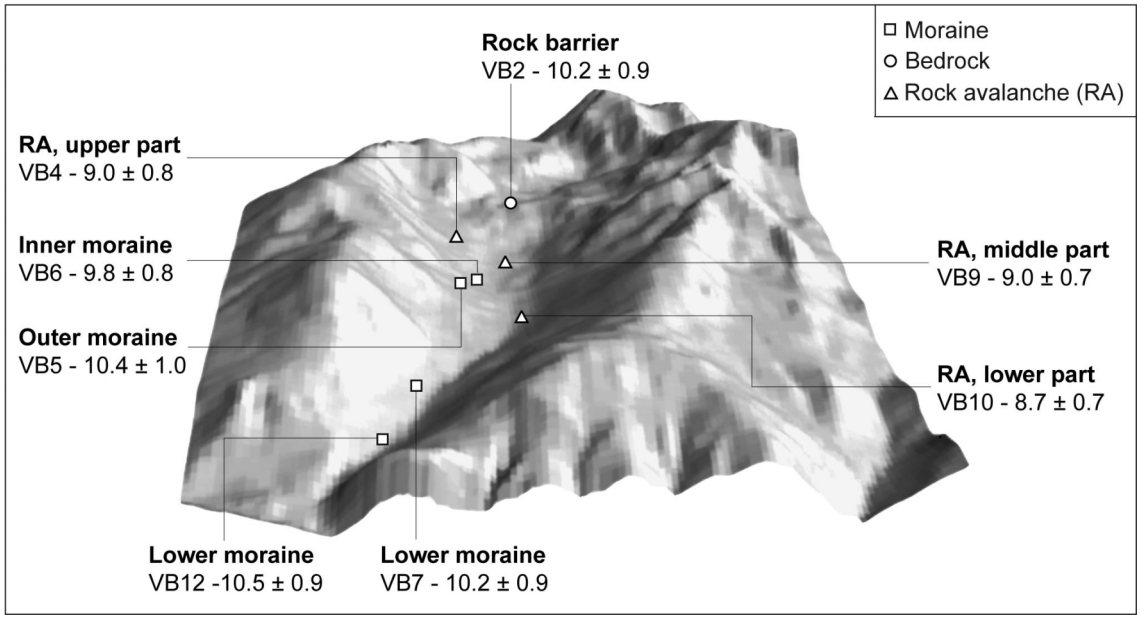

Fig. 5.12 Overview of calculated exposure ages (in ka) in Val Burdun. Ages are corrected for snow and erosion and correspond to Scenario C in Tables 5.11a and 5.11b.

VB4, VB9 and VB10 from the rock avalanche yielded 9.0 ± 0.8 ka, 9.0 ± 0.7 ka and 8.7 ± 0.7 ka, respectively (Fig. 5.12; Table 5.11a). Age distribution and a comparison with the moraine ages described above suggest a single event that took place by 8.9 ± 0.7 ka (mean age), most probably shortly after ice retreat. However, taking the small age differences and the partly overlapping errors of moraine ages and ages obtained from the rock avalanche into account, a deposition of the rock avalanche on a still present but inactive glacier cannot be completely ruled out. A glacial transport of the rock avalanche as proposed by Beer (2005) does not seem probable because glacier movement would have led to a decoupling of the deposit from the continuously supplied rock material in the upper part of the cirque, which is not the case. An additional indication for a single event is the morphology of the deposit. Looking downvalley, the flow path of the rock avalanche follows a right-hand bend. Here, on the orographically left side (corresponding to the undercut slope of a river), boulders were deposited up to higher elevation levels than this is the case in the lower flat part of the deposition area (see Fig. 2.8, E, below "VB1"). Furthermore, the rock avalanche shows a continuously decreasing thickness from the upper to the lower part. This does not go along with a repeated deposition of rock material on an active glacier but rather speaks for unique high-velocity event.

VB2 was taken from a polished bedrock barrier near the moraines deposited by the glacier during the Little Ice Age maximum extend around 1850. The spatio-morphological setting very much resembles of the situation in the Val Mulix (site "Sur la Crappa"). Also the

calculated age of VB2, 10.2 ± 0.9 ka (Fig. 5.12, Table 5.11a), is in the same range, providing further evidence for the fast ice retreat at the end of the last glacial cycle (at the end of the Younger Dryas). This is supported by the fact that the age of the exposure of the rock barrier is very close to the moraine ages.

Overall, the calculated ages reveal a meaningful picture of the evolution of characteristic landscape elements in Val Burdun. The stratigraphically older moraines downvalley from the 1850 moraines in this region are normally attributed to the Egesen stadial (Maisch, 1981; Suter, 1981), corresponding to a deposition during the Younger Dryas. From this point of view, the moraine ages calculated here, ranging from 9.8 to 10.5 ka, are rather young. Based on the morphostratigraphical situation, one could assume that the lower moraine can be parallelised with the Egesen I stage (approx. 12.5 ka) and the upper moraines with the Egesen II stage (approx. 11.5 ka). As the main unknown factor influencing exposure ages is the snow cover, a correction could be achieved by the addition of more snow, until ages in a corresponding age range result. However, this would ask for snow heights from 1.8 to 2.5 meters for 6 months (Table 5.11b, scenario G). Compared to values from the Atlas der Schweiz – which are supposed to represent maximum values as they refer to flat areas (Table 5.11b, Scenario E) – these snow values are extremely high and their choice without an independent age control does not seem appropriate.

Table 5.11a (A) = no snow (C) = with estimated snow coverage (E) = with AdS derived maximum values

Location	**Rock barrier**	**Rock avalanche**		
Sample codes	**VB 1**	**VB 4**	**VB 9**	**VB 10**
Latitude (°N)	46.53	46.53	46.53	46.54
Longitude (°E)	9.96	9.97	9.96	9.96
Elevation (m a.s.l.)	2670	2595	2442	2387
Sample material	Granite	Granite	Granite	Granite
Sample thickness (cm)	3	2	3.5	4
Quartz (g)	65.02	62.77	21.37	55.77
^{9}Be carrier	4.039E-04	3.927E-04	3.928E-04	4.035E-04
^{10}Be (atoms g-1*10^{4})	35.71	29.8	27.07	25.87
Surface dip (°)	9	4	0	21
Direction of dip	220	350	0	135
Measurement error (%)	7.4	7.1	5.2	5.6
Local production rate (atoms/g/yr)	40.27	38.38	34.75	33.51
Corrected production rate (atoms/g/yr) *	38.73	36.15	32.51	31.29
Correction factor for shielding	0.986	0.958	0.963	0.966
(A) ^{10}Be age (yrs) (uncorrected)**	**9240 ± 770**	**8260 ± 750**	**8350 ± 640**	**8280 ± 650**
Estimated snow cover (m for 6 month yr^{-1})	0.8	0.6	0.5	0.3
(B) ^{10}Be age (yrs) (Corrected for snow)**	**9980 ± 830**	**8750 ± 790**	**8750 ± 670**	**8530 ± 670**
(C) ^{10}Be age (yrs) (Corrected for erosion and snow) **	**10240 ± 850**	**8950 ± 810**	**8950 ± 690**	**8710 ± 690**
Estimated snow cover (m for 6 month yr-1)	1.3	1.2	1.2	1.2
(D) ^{10}Be age (yrs) (Corrected for snow)**	**10470 ± 870**	**9260 ± 840**	**9360 ± 720**	**9290 ± 730**
(E) ^{10}Be age (yrs) (Corrected for erosion and snow)**	**10750 ± 890**	**9490 ± 860**	**9590 ± 730**	**9520 ± 750**

* Production rate corrected for shielding (atoms g^{-1} yr^{-1})

** Estimated total error including measurement error and uncertainties in the altitude, latitude scaling, topography, and depth scaling.

Table 5.11b (A) = no snow (C) = with estimated snow coverage (E) = with AdS derived maximum values (G) = with snow heights necessary to reach ages corresponding to Egesen I (VB7 and VB12) and Egesen II (VB5 and VB6), respectively

Location	**Upper moraines**		**Lower moraine**	
Sample codes	**VB 5**	**VB 6**	**VB 7**	**VB 12**
Latitude (°N)	46.54	46.54	46.55	46.55
Longitude (°E)	9.97	9.97	9.97	9.97
Elevation (m a.s.l.)	2462	2454	2210	2125
Sample material	Granite	Granite	Granite	Granite
Sample thickness (cm)	2.5	5	7	5
Quartz (g)	60.02	61.96	50.12	61.65
^{9}Be carrier	4.051E-04	4.088E-04	4.090E-04	4.038E-04
^{10}Be (atoms g-1*10^{4})	30.06	28.96	25.02	24.22
Surface dip (°)	38	0	44	0
Direction of dip	215	0	332	0
Measurement error (%)	7.3	6.3	4.6	8.2
Local production rate (atoms/g/yr)	35.21	35.03	29.77	28.09
Corrected production rate (atoms/g/yr) *	32.20	32.74	26.04	25.36
Correction factor for shielding	0.934	0.975	0.912	0.941
(A) ^{10}Be age (yrs) (uncorrected)**	**9360 ± 860**	**8860 ± 690**	**9630 ± 870**	**9570 ± 830**
Estimated snow cover (m for 6 month yr^{-1})	0.8	0.8	0.3	0.7
(B) ^{10}Be age (yrs) (Corrected for snow)**	**10100 ± 930**	**9570 ± 750**	**9910 ± 890**	**10240 ± 910**
(C) ^{10}Be age (yrs) (Corrected for erosion and snow) **	**10370 ± 960**	**9810 ± 770**	**10170 ± 910**	**10510 ± 940**
Estimated snow cover (m for 6 month yr-1)	1.2	1.1	1.3	1
(D) ^{10}Be age (yrs) (Corrected for snow)**	**10500 ± 970**	**9850 ± 770**	**10910 ± 980**	**10530 ± 940**
(E) ^{10}Be age (yrs) (Corrected for erosion and snow)**	**10790 ± 1000**	**10100 ± 790**	**11220 ± 1010**	**10830 ± 970**
Estimated snow cover (m for 6 month yr-1)	1.8	2.4	2.4	2.5
(F) ^{10}Be age (yrs) (Corrected for snow)**	**11120 ± 1040**	**11150 ± 870**	**12120 ± 1090**	**12160 ± 1110**
(G) ^{10}Be age (yrs) (Corrected for erosion and snow)**	**11440 ± 1070**	**11480 ± 900**	**12510 ± 1120**	**12550 ± 1160**

* Production rate corrected for shielding (atoms g^{-1} yr^{-1})

** Estimated total error including measurement error and uncertainties in the altitude, latitude scaling, topography, and depth scaling.

5.2.2 Schmidt-hammer measurements

Compared to the Albula area and the Val Mulix, Schmidt-hammer rebound values are slightly higher with a typical mean value around 40 and varying in a very small range (Table 5.12). This might be due to the different geology in the two investigation areas. A reliable intercomparison of the two areas is, therefore, not possible. Based on the standard error suggested by Winkler (2000), the mean rebound values do not allow for distinguishing the different landforms in Val Burdun regarding their age. This confirms the finding from the greater area of Albulapass that processes within the Lateglacial are not resolvable with this method anymore.

Table 5.12 Measured Schmidt-hammer rebound values. Standard error is given after suggestion of Winkler (2000). Where not specially indicated, 50 measurements per landform were performed.

Localities	***Rock barrier***			***Rock avalanche upper part***		
	Orogr. right	*Orogr. left*	*Together (n = 100)*	*Upper part of boulders*	*Lower part of boulders*	*Together (n = 100)*
Mean value	41.1 ± 2.1	40.2 ± 2.1	40.7 ± 2.1	35.5 ± 1.9	44.2 ± 2.3	39.9 ± 1.9

Localities	***Rock avalanche middle part***	***Rock avalanche lower part***	***Lower moraine***	***Undefined deposit at approx. 2100 m***
Mean value	38.6 ± 2.0	39.1 ± 2.1	39.9 ± 2.0	39.1 ± 2.1

Noteworthy are the measurements carried out in the upper part of the rock avalanche. Here, the upper parts of the boulders with clear traces of weathering and lichen growth and the lower part of the boulders were measured separately. The lower, less weathered parts of the boulders gave a mean rebound value of 44.2 ± 2.3, which is significantly higher than the value measured for the upper part of the boulders (35.5 ± 1.9). The average of all 100 measurements in this part of the rock avalanche is 39.9 ± 1.9, comparable to the values from the other sites. The most probable explanation for this result might be the influence of snow and its effects on water availability and thermal insulation, both of which are key factors for chemical weathering processes.

5.2.3 Weathering rind thicknesses

Both histogram shape and mean/median values suggest an age trend with a lower age in the upper part of the rock avalanche and an increasing age of the deposit towards its lower parts. The upper and the middle part of the rock avalanche show comparable weathering rind thicknesses (2.4/2.2 mm and 2.6/2.5 mm, respectively); in the lower part a pronounced step to 3.7/3.3 mm is ascertainable. On the undefined deposit at c. 2100 m a.s.l., again slightly higher

values (4.2/3.9 mm) were measured. This is in agreement with its spatial position, identifying it as stratigraphically older. The weathering rind thickness trend on the rock avalanche, however, does not correspond to the measured exposure ages and the morphology of the deposit. Both point to a single event (see Chapter 5.2.1) and consequently one would expect similar thickness values on the whole length.

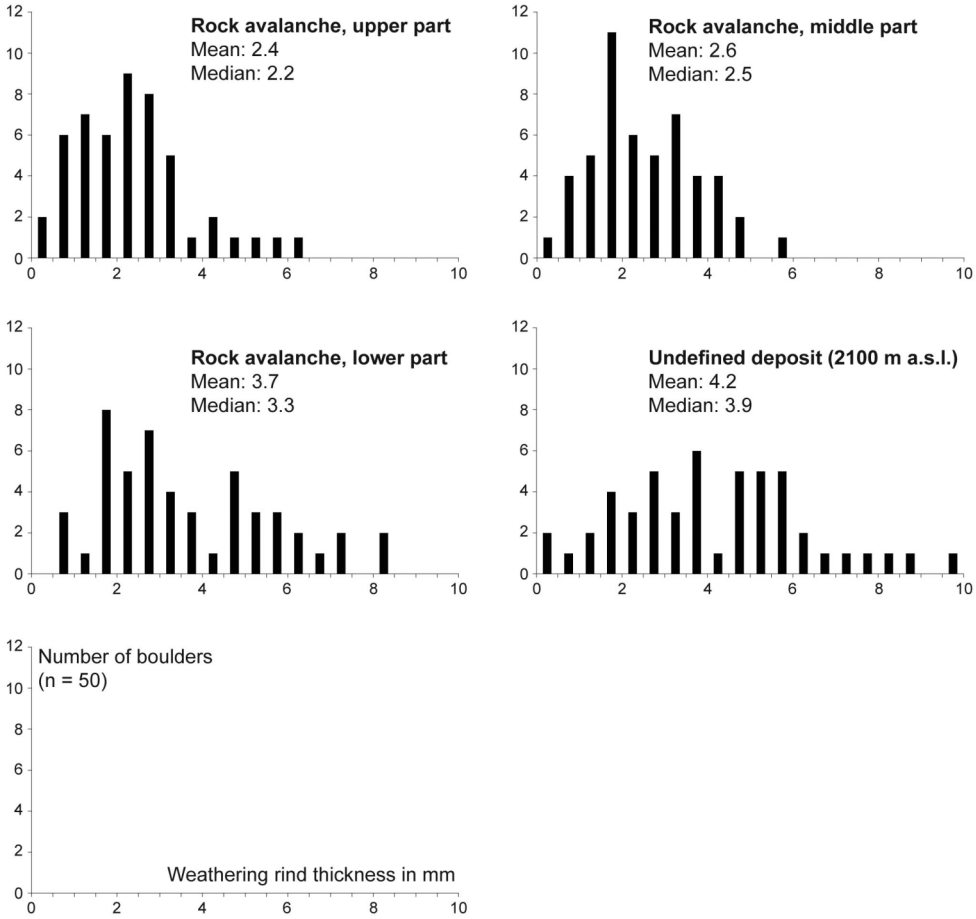

Fig. 5.13 Histogramms of weathering rinds measured in Val Burdun. Mean/median values suggest an age trend on the rock avalanche. This is not in accordance to surface exposure ages and geomorphology that speak for a single event.

Two main possible error sources are imaginable. First, it must be repeated that the lithological conditions are not perfect for the measurement of weathering rind thicknesses, as the rock material shows a slight metamorphic overprint. Second, as already mentioned in connection with measured Schmidt-hammer rebound values (Chapter 5.2.2), snow potentially plays an important role in the upper part of the rock avalanche. For technical reasons, weathering rinds often were measured on rather small boulders with diameters of < 1 m. Especially in the upper part of the rock avalanche, where the deposit shows a higher thickness,

these boulders were situated between large exemplars with heights and diameters of several meters. In these positions, great amounts of snow might be blown in already at the beginning of winter and snow cover likely will last until early summer in the following year. As indicated by lacking growth of lichen, a less structured surface of these smaller boulders (or lower parts of the big boulders) and a different surface colour, a clear effect of the stronger snow influence cannot be denied and most likely modifies the conditions for weathering rind growth. In the lower flat part of the rock avalanche, the fragments are more widely scattered and mostly deposited in only one layer. This may favour a more consistent build-up and melt-back of the snow cover and thus irregularities as found in the middle and upper part are reduced.

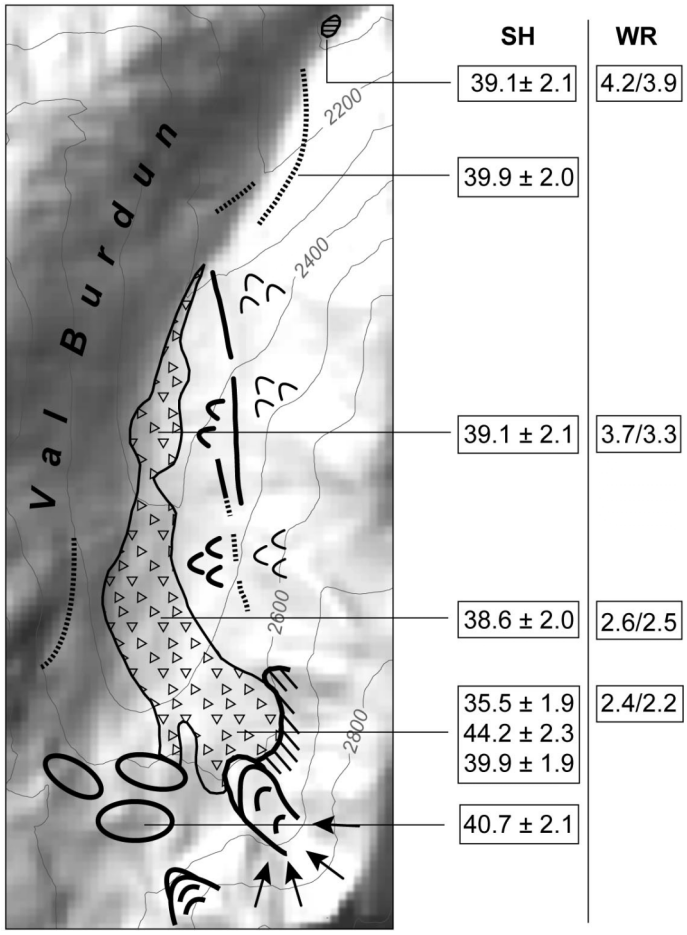

Fig. 5.14 Summarising overview of Schmidt-hammer rebound values (SH; mean values) and weathering rinds (WR; mean/median in each case) measured in Val Burdun (see also Table 5.12 and Fig. 5.13). The three SH-values from the upper part of the rock avalanche correspond to the upper and the lower part of the boulders, 39.9 ± 1.9 is the mean value. For detailed information on geomorphology see Fig. 2.7.

5.2.4 Soil chemical and mineralogical analyses

Pictures of the two sampled soil profiles can be found in Appendix A. Whereas S1 from the upper moraine is well above the tree line, S2is near but most probably not under direct influence of some larches. At both sites dwarf shrubs are dominant. Slope and aspect are comparable. S1 showed a well-pronounced and undisturbed development of soil horizons. For S2, soil evolution seems to be highly influenced by the more coarse-grained composition of the lower moraine. Here, no C or BC horizon could be reached.

Table 5.13 General characteristics of the soils sampled on the upper (S1) and the lower moraine (S2) in Val Burdun.

Site	Elevation (m a.s.l.)	Aspect (°N)	Slope (°)	Parent material	Vegetation	Land use	WRB (IUSS Working Group 2006)
S1	2350	10	17	Meta-Granite Moraine material	*Empetrum nigrum Vaccinium uliginosum*	Natural alpine grassland, dwarf shrubs	Umbric Podzol (Endoskeletic)
S2	2190	15	15	Meta-Granite Moraine material	*Empetrum nigrum, Juniperus communis, Rhododendron ferrugineum*	Natural alpine grassland, dwarf shrubs	Umbric Podzol (Episkeletic)

Physical and chemical properties

Both topsoil and subsoil of S1 are characterised by a sandy loam (Table 5.14). Skeleton weight percentages in the subsoils are near 70%. In the case of S2, many more large boulders were apparent, here especially must the skeleton values thus be understood as minimum values.

Compared to the soils of Val Mulix, pH values in the topsoils are slightly higher with 3.4 and 3.7, respectively. In the subsoils, the values increase to values near 4.5 (Table 5.15). Also C_{org} values are lower, not exceeding 150 g kg^{-1} in the topsoils (Table 5.15). C_{org} values are higher and pH values slightly lower for the uppermost horizon of S2 compared to S1. Whether this can be assigned to the age difference is questionable. Especially the pH values adjust comparably fast on acidic substrate and are not applicable as age proxies for soils with development times of several thousand years (see also Chapter 3.2.4). C/N ratios are very constant, varying for both soils between 20 and 24 and show no trend within the soil profiles.

Oxalate and dithionite extractable amounts of Al, Fe and Si nicely show the dislocation processes within the soil profile from the upper moraine (S1). This is particularly pronounced in

case of Al and Fe. As S2 was sampled down only to the Bs horizon, no decreasing values in the lower part can be observed. However, the values in the upper part give a meaningful picture with generally increasing contents from the OE to the Bhs and Bs horizon, namely for Fe and Al. For both soils dithionite extractable amounts are generally higher than the ones extracted by oxalate. Based on the curve patterns obtained, there is no evidence for buried soils or for extended mixing processes (Fig. 5.15).

Table 5.14 Some physical properties of the soils.

Site	Soil horizon	Depth (cm)	Munsell colour (moist)	Skeleton[1)] (weight %)	Sand[2)] (g kg^{-1})	Silt (g kg^{-1})	Clay (g kg^{-1})
S1	OE	0-15	7.5YR 3/1	26.4	689	267	44
	Bs1	15-30	5YR 2/2	50.6	n.d.	n.d.	n.d.
	Bs2	30-50	5YR 2/2	70.6	680	287	33
	BC	50-70	10YR 5/3	63.2	n.d.	n.d.	n.d.
	C	> 70	10YR 5/3	69.5	756	232	12
S2	OE	4-15	7.5YR 2/2	35.8	n.d.	n.d.	n.d.
	Bhs	15-37	7.5YR 2/1	69.4	n.d.	n.d.	n.d.
	Bs	> 37	5YR 2/2	70.8	n.d.	n.d.	n.d.

n.d.= not determined
[1)] Skeleton = Material > 2mm
[2)]Size fractions: Sand = 2000-63 μm; Silt = 63–2 μm; Clay = < 2 μm

Weathering indices calculated for the two soils are summarised in Table 5.17. Most of the values vary in a similar range. Like for the soils in Val Mulix, it is hardly possible to distinguish between the soils based on their weathering state and also here, value inversions can be observed. As an example, S1 shows higher values for Al_d/Fe_d for both Bs horizon compared to corresponding horizons of S2. As this ratio theoretically increases with increasing age, it should be lower for S1 than for S2. Also differences in ferrihydrite contents between OE and Bs horizons as an indicator of the podzolisation process suggest that S1 is slightly older than S2. Furthermore, both Al_{tot}/Ti_{tot} and Fe_{tot}/Ti_{tot} are lower for S1 with respect to the OE horizon. As Al and Fe are increasingly released with weathering, but Ti at the same time is rather immobile, this ratio should decrease with increasing age.

Table 5.15 Chemical properties of the soils (fine earth).

Site	Soil horizon	Depth (cm)	pH ($CaCl_2$)	Org. C (g kg^{-1})	Total N (g kg^{-1})	C/N	Fe_t (g kg^{-1})	Si_o (g kg^{-1})	Al_o (g kg^{-1})	Fe_o (g kg^{-1})	Al_d (g kg^{-1})	Fe_d (g kg^{-1})	$Al_o + 0.5\ Fe_o$ (%)
S1	OE	0-15	3.7	100.3	4.9	21	15.94	0.07	2.32	3.12	3.43	6.72	0.39
	Bs1	15-30	4.2	48.0	2.1	23	24.44	0.49	10.38	5.59	11.26	5.83	1.32
	Bs2	30-50	4.4	5.8	0.3	20	27.90	0.61	5.93	2.24	9.31	3.95	0.70
	BC	50-70	4.5	23.2	1.0	23	37.14	0.35	1.79	0.93	2.51	2.60	0.23
	C	> 70	4.7	3.3	0.2	20	33.83	0.30	1.09	0.61	1.90	2.23	0.14
S2	OE	4-15	3.4	146.1	6.1	24	17.53	0.03	2.20	3.01	2.47	6.03	0.37
	Bhs	15-37	3.9	53.6	2.7	20	25.00	0.09	4.20	4.22	5.61	10.23	0.63
	Bs	> 37	4.2	34.4	1.6	21	41.29	0.37	7.23	5.07	9.67	10.34	0.98

Table 5.16 Concentration of the main elements obtained by means of XRF. The values refer to the sum of earth and skeleton material.

Site	Soil horizon	Depth (cm)	OM* (g/kg)	CaO (g/kg)	MgO (g/kg)	K_2O (g/kg)	Na_2O (g/kg)	Al_2O_3 (g/kg)	Fe_2O_3 (g/kg)	SiO_2 (g/kg)	MnO (g/kg)	TiO_2 (g/kg)
S1	OE	0-15	126.9	3.3	7.1	33.5	17.9	126.7	23.8	537.5	0.2	6.7
	Bs1	15-30	40.8	6.7	9.6	29.5	21.0	143.0	36.5	479.6	0.4	5.3
	Bs2	30-50	2.9	8.6	14.3	32.8	20.7	147.4	41.7	566.3	0.6	6.7
	BC	50-70	14.7	10.4	20.4	37.7	23.0	148.7	55.5	615.1	1.0	8.6
	C	> 70	1.7	10.2	21.3	38.4	25.4	155.1	50.5	637.2	0.8	8.4
S2	OE	4-15	161.3	3.1	8.4	31.9	16.3	131.1	26.2	498.6	0.2	6.3
	Bhs	15-37	28.2	3.8	10.9	37.5	18.9	154.5	37.4	555.5	0.2	7.8
	Bs	> 37	17.3	9.4	16.4	32.5	19.0	157.1	61.7	496.8	0.7	10.3

*Organic matter = org. C (fine earth and skeleton)*1.72

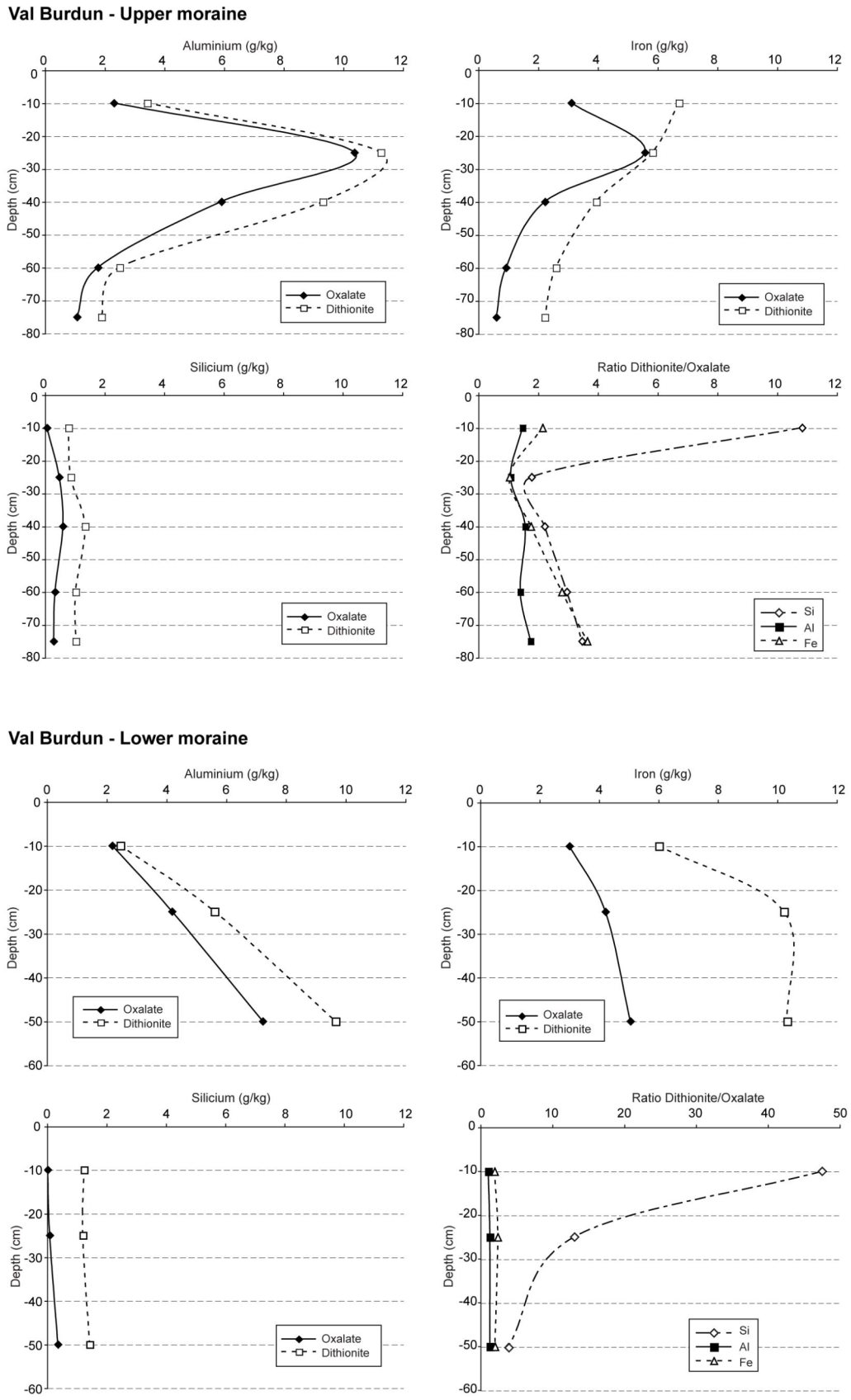

Fig. 5.15 Oxalate and dithionite extractable amount of Al, Fe and Si, in each case with the ratio dithionite extractable/oxalate extractable.

Table 5.17 Weathering indices from the soils of Val Burdun. Elluvial (OE) and most pronounced illuvial horizons (Bs) are indicated in each case with yellow and orange, respectively.

Site	Soil horizon	Fe_d/Fe_{tot}	Fe_{tot}/Ti_{tot}		Fe_{tot} - Fe_d (g/kg)	Al_d/Al_{tot}	Al_{tot}/Ti_{tot}		Al_d/Fe_d	$(Al_d/Al_{tot})/(Fe_d/Fe_{tot})$	Ferri-Hydrite (g/kg)	ITM (%)
			f	s			f	s				
S1	OE	0.42	4.13	6.70	9.22	0.05	16.62	21.71	0.51	0.13	5.30	0.53
	Bs1	0.24	8.00	8.38	18.60	0.16	23.71	23.69	1.93	0.65	9.49	2.41
	Bs2	0.14	7.29	7.22	23.95	0.12	19.49	18.78	2.36	0.88	3.81	1.47
	BC	0.07	7.52	7.56	34.54	0.03	15.25	16.08	0.96	0.48	1.58	0.49
	C	0.07	7.05	7.37	31.60	0.02	16.38	18.51	0.85	0.37	1.04	0.32
S2	OE	0.34	4.83	7.82	11.50	0.04	18.30	38.52	0.41	0.11	5.12	0.49
	Bhs	0.41	5.55	7.20	14.77	0.07	17.38	27.02	0.55	0.18	7.18	0.94
	Bs	0.25	6.97	7.73	30.95	0.12	13.44	21.04	0.94	0.49	8.62	1.69

f = fine earth; s = skeleton; ITM = Imogolite type material

Soil mineralogy

Mineralogical composition of the clay fraction as deduced by the semi-quantitative estimation (Chapter 4.5.3) shows a very similar picture for the weathered horizons of the two soils. Unlike the upper moraine, the lower moraine also contains small amounts of HIV and vermiculite. Whereas the C/BC horizons of the soils in Val Mulix were characterised by comparably high values of chlorite, this mineral is almost absent in the C horizon of the upper moraine. Instead, mica is by far the most important constituent, which is already obvious on a macroscopic scale.

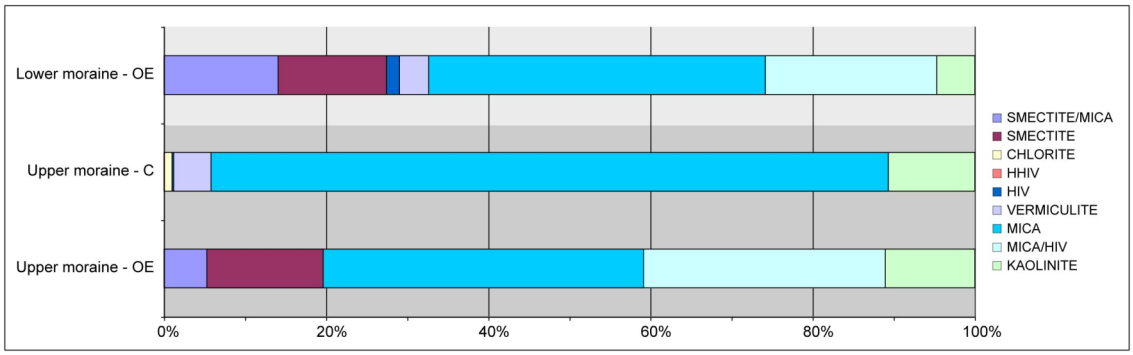

Fig. 5.16 Semi-quantification of the clay fractions in the OE horizons. Values for the C horizon of the upper moraine are also given. Smectite content in the lower moraine is slightly higher, which makes sense taking the geomorphic setting into account. Overall, the weathering state of the two soils based on the mineralogical composition is comparable. (H)HIV = (highly)hydroxy-interlayered vermiculite.

Smectite as well as smectite/mica present in these soils likely represent the result of mica alteration. Although the presence of kaolinite can be detected down to the C horizon (Fig. 5.17), the calculated amount is most likely too high, for the same reasons as described in Chapter 5.1.4.

Also in Val Burdun, 060-reflexions clearly show the increasing importance of dioctrahedral minerals (i.e., every third octahedral position is empty and the rest occupied by atoms with a valency of +3 such as Al) with an increasing degree of weathering (Appendix B). The peak representing trioctahedral minerals (near 60° 2-theta) is decreasing at the same time.

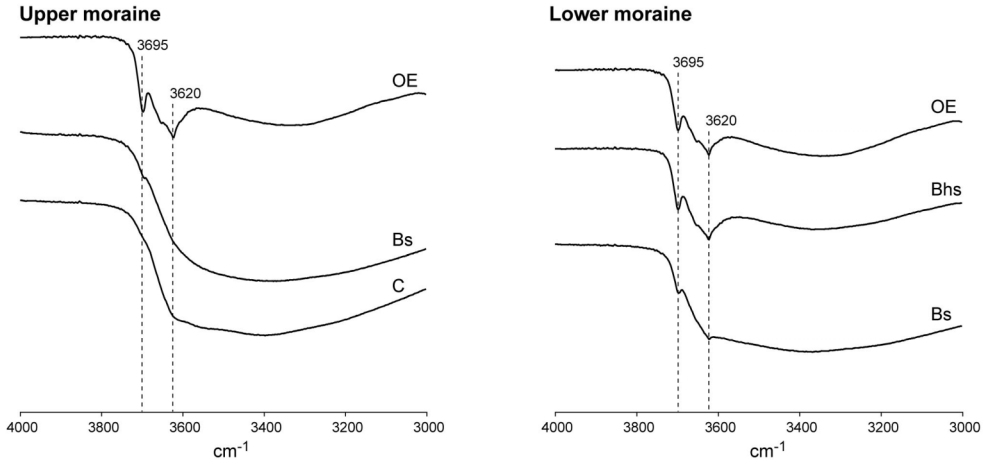

Fig. 5.17 FT-IR patterns for the range of 3000 to 4000 cm^{-1}. The kaolinite peak is well-pronounced in the top-soils and increasingly weak towards the lower horizons.

Using sodium citrate, HIS could be determined in the Bhs and the Bs horizon of the lower moraine. Especially in case of the Bhs horizon, the peak around 1.65 nm after treatment with ethylene glycol is more pronounced than for the non-treated sample and a more total collapse after K-saturation can be seen (Fig. 5.18).

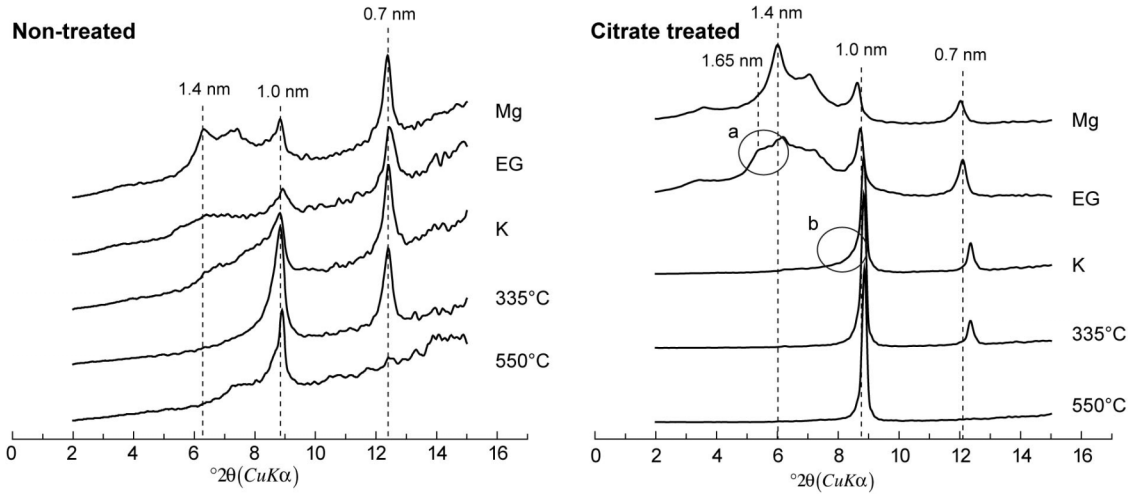

Fig. 5.18 Diffractograms of the Bhs horizon of the lower moraine. After treatment with sodium citrate (right), hydroxy interlayers of HIS are destroyed and HIS behaves like smectite, leading to a more pronounced peak at 1.65 nm after ethylene glycol treatment (a). Another indication is the total collapse after K-saturation to 1.0 nm (b).

Based on the mineralogical composition (Fig. 5.16) and the very similar diffractograms of the most weathered horizons (Fig. 5.19), no clear difference in the weathering state of the two soils can be observed. Taking the higher content of smectite/mica and a comparable amount of smectite into account, the lower moraine could be identified as slightly older. This makes

sense with respect to geomorphology and surface exposure ages that vary in a very small range of around 10.5 ka.

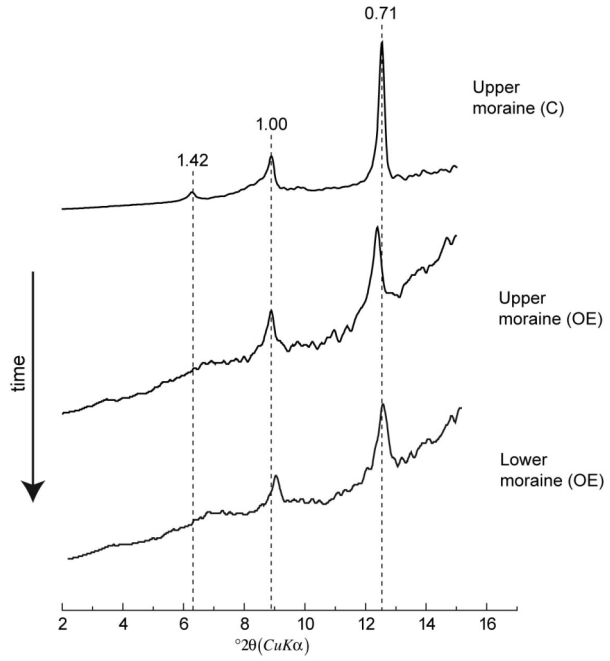

Fig. 5.19 XRD diffractograms (ethylene glycol saturated) from the most weathered horizon of each soil (E or OE horizons). The uppermost curve from the C horizon of S1 serves as a reference, representative of the parent material of both soils (for t = 0). The order of the XRD patterns is according to the age trend based on geomorphology.

Radiocarbon dating of stable SOM

As shown in Table 5.18, the calibrated radiocarbon ages measured in the profile of the upper moraine (S1) are much too young, ranging between approx. 3 ka (OE) and 5.5 ka (Bs2), with increasing age values with increasing depth. With regard to the exposure age obtained from a boulder on the same moraine (VM5, 10.4 ± 1.0 ka), dating of stable SOM in this case does not seem to be an appropriate tool to contribute to the development history of glacial deposits. A time lag of roughly 5 ka between moraine stabilisation and soil formation initiation does not seem reasonable. As morphology and chemical/physical properties of this soil give no indication for mixing processes, the most obvious explanation is that the chemical treatment was not efficient enough to remove all the organic carbon fractions that yield young radiocarbon ages.

The measured ages from profile S2 show pronounced differences. Whereas the OE horizon gives an age of just a few hundred years, in the Bhs horizon an age between 13 and 14 ka could be measured. With 7848 – 7696 years, the Bs horizon is again younger. This profile

showed no well-pronounced development of pedogenic horizons. Processes of rearrangement and the influence of soil material of the slope above (outside) the moraine cannot be ruled out. This might explain the age of the Bhs horizon, which seems too old when compared to the exposure ages measured on this moraine (VB7 and VB12 with, 10.2 ± 0.9 ka and 10.5 ± 0.9 ka, respectively).

Table 5.18 Radiocarbon ages obtained from H_2O_2 treated SOM.

Site	Horizon	Depth (cm)	C-loss (%) due to H_2O_2 treatment	UZ-No.	Uncal. ^{14}C ages (y BP) H_2O_2 treated	Cal. ages (1σ-range), y BP, H_2O_2 treated
S1	OE	0-15	85.9	5594	2875 ± 55	3078 - 2890
	Bs1	15-30	95.6	5595	4610 ± 60	5465 - 5087
	Bs2	30-50	74.7	5596	4790 ± 60	5595 - 5469
S2	OE	4-15	79.9	5597	470 ± 55	547 - 477
	Bhs	15-37	78.2	5598	11680 ± 95	13648 - 13422
	Bs	> 37	87.2	5599	6955 ± 70	7848 - 7696

5.3 Age determination of active rock glaciers using luminescence techniques

Sample preparation and all luminescence measurements were carried out by M. Fuchs (TU Dresden, Germany), under the supervision of M. Krbetschek (TU Freiberg, Germany) and in collaboration with several partners as mentioned in Chapter 4.2.2. In the following, a summarising overview of the main results and fundamental problems we faced are reported. An explanation of technical details is abandoned. Instead, emphasis is given on the discussion of how to interpret measured luminescence ages in regard to rock glacier characteristics and formation and how involved processes potentially influence travel paths of target mineral grains and hence the sedimentation ages.

5.3.1 Determination of the dose rate

The radionuclide analysis shows differing values for the three rock glaciers (Table 5.19). For SAL1 the specific activities of the ^{238}U-series and ^{232}Th-series are between 28 and 30 Bq/kg. Measurements from the rock glacier Suvretta show with 70-77 Bq/kg for ^{238}U, 45.5-46.5 Bq/kg for ^{232}Th and 750-775 Bq/kg for ^{40}K values that vary in a comparably small range. In case of GiG1 and GiG2 specific activities were c. 52 Bq/kg for ^{238}U, c. 36.5 for ^{232}Th and c. 705 Bq/kg for ^{40}K. Radioactive disequilibria in the ^{238}U-series are possible, as shown by depressed ^{210}Pb values in the samples GiG1 and GiG2.

Table 5.19 Determined dose rates.

Sample	Radionuclides			Cosmic dose rate	Water content	
	^{238}U (Bq/kg)	^{232}Th (Bq/kg)	^{40}K (Bq/kg)	(mGy/ka)	In situ (%)	Saturation (%)
SAL1	28.5 ± 0.7	29.17 ± 1.40	911.11 ± 3.72	144	4.6	15.7
SUV1	69.8 ± 1.4	45.58 ± 2.04	761.26 ± 2.92	190	2.5	9.0
SUV2	74.7 ± 1.6	45.56 ± 2.09	774.49 ± 3.20	190	4.5	15.9
SUV3	77 ± 6	45.5 ± 2	770 ± 50	171	4.4	16.6
SUV4	77 ± 5	46.5 ± 2	750 ± 50	171	4.6	44.4
GiG1	52 ± 4	36.5 ± 2	705 ± 40	250	3.4	18.0
GiG2	52 ± 4	36.5 ± 2	705 ± 40	250	3.3	18.4

SAL = Salteras; SUV = Suvretta; GiG = Gianda Grischa

For the cosmic dose rate, differing altitude above sea level and the damping effect of sediment overburden were taken into account. In both cases the chosen values have to be understood as rough means without consideration of possible variations. Thus, the cosmic dose rates of 171-250 mGy/ka are assumed to be representative for the whole incorporation time. More precise estimations would call for a detailed understanding of internal processes, which is hardly feasible. Effectivity of radioactive radiation was corrected with the water content at each site (values determined for each site in-situ and saturation values). Potential uncertainties as a result of the influence of ice and thawing processes near the front are mentioned in the discussion part (Chapter 6).

For the determination of the mineral-intern dose rate of K-feldspars, a potassium content of 12.5 ± 0.5% was assumed (Huntle and Baril, 1997), for plagioclase 2.0 ± 0.8% (personal communication M. Krbetschek, 2009).

5.3.2 Age calculation: overview and general statements

The following luminescence properties were taken into consideration: (a) intensity of the luminescence signal (counts per second), (b) the relation dose – luminescence (reproducibility, sensitivity) and (c) the bleaching quality (variability).

In general, the analysed material often showed problematic luminescence properties. Especially in case of quartz, the low signals sometimes hardly could be separated from the background noise. Most growth curves show a variable correlation of OSL-signal and applied laboratory dose, with high errors of the calculated data points and the connected curve fitting. High recycling ratios and test dose errors as well as the quality of zero points speak for inconsistent luminescence properties of the measured material. This is supported by a partly bad

reproducibility of OSL-signals with dose recovery tests, pointing again to a material-inherent, unsure relation between dose and luminescence. Although some good results could be achieved, mainly for single grain measurements recovery doses were underestimated (Fig. 5.20).

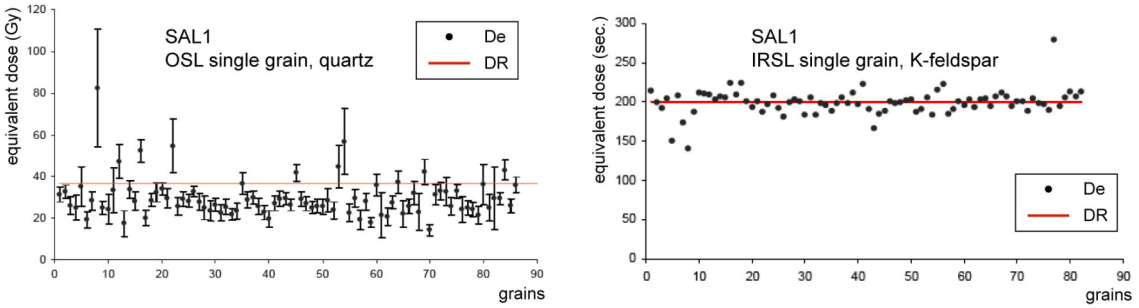

Fig. 5.20 Results from dose recovery tests for single grains of the rock glacier Salteras. The quartz grains (left) show a clear trend to underestimate the recovery dose (applied dose rate DR = 36.4 Gy). In the case of feldspar, a good reproducibility of the luminescence signals can be estimated, as indicated by the low dispersion around the dose rate of 200 s. De = equivalence dose.

In comparison, the overall luminescence characteristics of feldspars were better, above all of K-feldspars that showed a higher signal intensity than plagioclases. Also here, the growth curves suggest a variable correlation of signal and applied laboratory dose. However, initial IRSL-signals well above the background noise allowed for an improved curve fitting. Dose recovery tests for K-feldspars showed a comparable well reproducibility of the test doses. This is not the case for plagioclases, which showed a clear overestimation of the dose.

A central problem for the age calculation is the fact that in many cases only a low number of values per sample (single grains or aliquots, see also Tables 5.20, 5.21, 5.22) could be used to represent the distribution of equivalence doses. Like this, the identification of extreme values, value concentrations or even different value populations is difficult and only a rather random cutting of the whole dose spectrum is displayed.

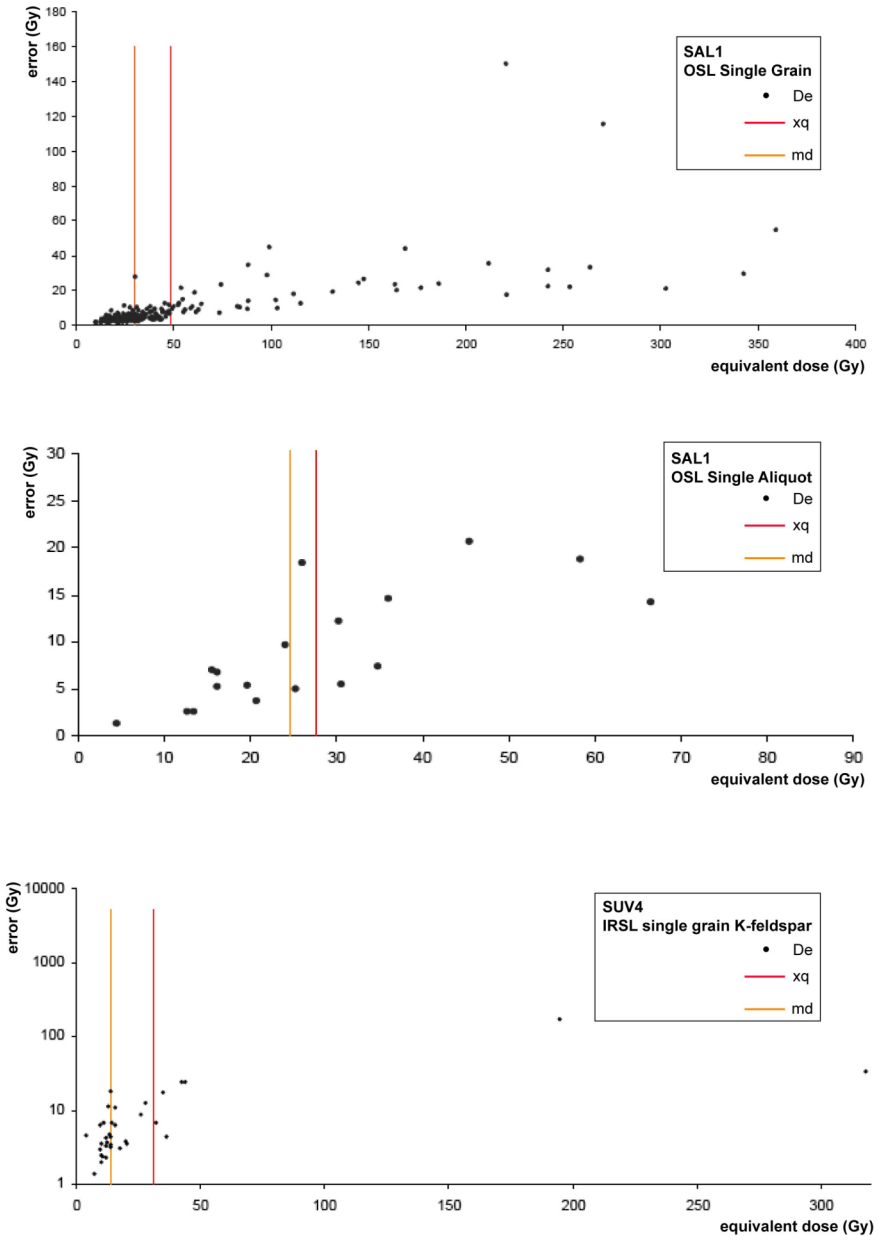

Fig. 5.21 Selection of palaeodose (De) distribution patterns for different samples, in each case with the arithmetic mean (xq) and the median (md). Values chosen for age calculation: *upper graph*: median (incomplete bleaching must be assumed, median represents the value concentration in the lower part much better); *middle graph*: arithmetic mean (median virtually identical); *lower graph*: arithmetic mean (comparable to median values of SUV2 and arithmetic mean of IRSL single grain measurement of SAL1). Note different scales!

Observations generally speak for a heterogeneous composition of the dose distribution, either caused by insufficient bleaching or as a result of factors connected to rock glacier dynamics, as discussed in Chapter 6.2.

The variability of equivalence doses, which is subject to several possible influence factors, and the low number of usable measurements makes drawing conclusions about the bleaching quality impossible and leads to high uncertainties in age calculation. For the same reason, the application of statistical approaches to deal with residual signals seems inappropriate. As a simple but transparent solution we used arithmetic means and median values for the calculation of sedimentation ages. Depending on the distribution pattern, it was decided which statistical value seems to be appropriate for each sample and kind of measurement (Fig. 5.21). If no pronounced bias occurred, we used the arithmetic mean. In case of skewed distributions of the equivalence doses clearly indicating the presence of insufficiently bleached or unbleached material – in most cases a positive stretching of the distribution – the median value was preferred. In cases of doubt, also similar values from samples with a better database and thus a higher reliability were included and contributed to the decision. The problematic characteristics of the material make the applicability of the "leading edge" approach (Lepper and McKeever, 2002) questionable. It is thus not further discussed here.

5.3.3 Calculated sedimentation ages

Tables 5.20, 5.21 and 5.22 summarise the calculated sedimentation ages for each rock glacier. Generally speaking they vary in an appropriate range of one-digit millennia. Five to eight ka are very similar ages to the ones derived with other approaches, for instance streamline interpolations using photogrammetric techniques (see Chapter 2.4). Basis for age calculation is highlighted with bold letters (median md or arithmetic mean xq). In each case a mean age for all calculated ages and for the ones with > 15 usable measurements, indicated by yellow cells, are given. For the rock glacier Suvretta, the age based on OSL single aliquot (49.9 ± 16.5 ka) is clearly an outlier and was therefore not included for the calculation of the mean age. Fifteen measurements are accepted as a minimum basis, which is necessary to roughly represent the true dose distribution and in this sense a "threshold of trust". The calculated ages in general become more and more meaningful with an increasing number of measurements available for the determination of the palaeodose. This is shown especially clearly in case of rock glacier Gianda Grischa, which yielded the material with the worst luminescence properties. The measurements of 40.6 ka (5 measurements) and 37.5 ka (only 2 measurements), respectively, certainly do not represent a meaningful age estimation for this rock glacier. In case of IRSL single grain measurements, 43 values were available and the corresponding age is 4.8 ka. This is in a range that is possible with respect to local glacial history. For age calculations with > 15 measurements in most cases the median was chosen.

Table 5.20 Calculated sedimentation ages for the rock glacier ***Salteras*** (Val Tschitta).

Sample	Method	N	xq ± se (Gy)	sd% (%)	md (Gy)	Age (ka)
SAL1	**OSL-SA**	18	**27.6 ± 3.7**	56.6	24.7	7.7 ± 1.3
SAL1	**OSL-SG**	234	48.4 ± 3.8	119.3	**29.5**	8.5 ± 1.4
SAL1	**IRSL-SG (kf)**	74	56.1 ± 11.4	175.3	**30.5**	6.9 ± 2.7
SAL1	**IRSL-SG (pl)**	9	40.6 ± 4.2	30.8	**38.4**	10.5 ± 1.6
Mean age						**8.4 ± 1.5**
Mean age yellow fields						**7.7 ± 0.8**

SA = Single aliquot; SG = Single grain; kf = K-feldspar; pl = Plagioclase; N = Number of included aliquots/grains; xq = Arithmetic mean; se = standard error; sd% = relative standard deviation; md = Median; bold = basis for age calculation; yellow background = ages based on > 15 measurements

Table 5.21 Calculated sedimentation ages for the rock glacier ***Suvretta*** (Piz Julier area).

Sample	Method	N	xq ± se (Gy)	sd% (%)	md (Gy)	Age (ka)
SUV1	**OSL-SG**	3	**206.3 ± 65.6**	55.1	204.2	49.9 ± 16.5
SUV2	**OSL-SA**	18	36.0 ± 8.7	102.7	**24.5**	5.8 ± 2.3
	OSL-SG	1	29.3 ± 2.5	-	29.3	7.0 ± 0.9
	IRSL-SG (kf)	60	90.0 ± 10.9	93.9	**39.4**	7.7 ± 2.6
SUV3	**OSL-SG**	58	43.9 ± 7.5	125.7	**17.7**	4.2 ± 2.0
	IRSL-SG (kf)	9	**11.4 ± 6.5**	170.5	3.6	2.2 ± 1.3
SUV4	**OSL-SG**	3	**11.7 ± 3.5**	51.6	8.7	3.1 ± 1.1
	IRSL-SG (kf)	35	**30.9 ± 9.9**	188.9	14.0	6.7 ± 2.4
	IRSL-SG (pl)	1	20.7 ± 4.4	-	20.7	5.4 ± 1.6
Mean age (without SUV1)						**5.3 ± 1.9**
Mean age yellow fields						**6.1 ± 1.5**

SA = Single aliquot; SG = Single grain; kf = K-feldspar; pl = Plagioclase; N = Number of included aliquots/grains; xq = Arithmetic mean; se = standard error; sd% = relative standard deviation; md = Median; bold = basis for age calculation; yellow background = ages based on > 15 measurements

Table 5.22 Calculated sedimentation ages of the rock glacier ***Gianda Grischa*** (Piz Julier area).

Sample	Method	N	xq ± se (Gy)	sd% (%)	md (Gy)	Age (ka)
GiG1	**OSL-SG**	5	**145.1 ± 29.8**	46.0	135.5	40.6 ± 9.6
	IRSL-SG (kf)	8	16.1 ± 3.6	62.8	**12.7**	2.8 ± 0.8
GiG2	**OSL-SG**	2	**133.8 ± 13.5**	14.2	133.8	37.5 ± 5.8
	IRSL-SG (kf)	43	113.5 ± 18.5	106.6	**21.8**	4.8 ± 5.2
Mean age (without GiG1 OSL-SG, GiG2 OSL-SG)						**3.8 ± 1.4**

SA = Single aliquot; SG = Single grain; kf = K-feldspar; pl = Plagioclase; N = Number of included aliquots/grains; xq = Arithmetic mean; se = standard error; sd% = relative standard deviation; md = Median; bold = basis for age calculation; yellow background = ages based on > 15 measurements

Because of the "caterpillar effect" described in Chapter 3.2.2, the oldest material of a rock glacier can be expected at the rock glacier base near the rooting zone. Accordingly, in an ideal situation with complete bleaching, a fast incorporation of the grain in the rock glacier body and no subsequent processes disturbing the build-up of the luminescence signal, the ages

determined should be interpreted as minimum ages. However, possible modifying processes are manifold and arguments speaking for an interpretation of calculated ages as minimum or maximum ages must be balanced against each other.

5.4 Exposure ages and surface colours at Aiguille du Midi

5.4.1 Elemental content

Results from XRF measurements show a very similar composition after conversion into oxide contents (Table 5.23). The high quartz content of the "Mont-Blanc granite" is represented by high amounts of SiO_2. Al_2O_3 and potassium oxide are further important constituents of the rock samples. The total values of over 90% mean that almost all possible compounds were measured. The comparable composition of the samples is an important indication that observed differences in colour are not due to inhomogeneities in lithology.

Table 5.23 Elemental composition of the samples based on XRF-measurements. Values are converted into oxide contents. LOI = Loss on ignition. The low standard deviation (SD) values indicate a comparable composition and demonstrate the homogeneity of the lithology.

	Samples Aiguille du Midi 1-5						
Element [%]	**AdM1**	**AdM2**	**AdM3**	**AdM4**	**AdM5**	**Mean**	**SD**
CaO	0.87	0.87	1.44	1.17	1.31	1.13	0.26
MgO	0.62	0.60	0.37	0.39	0.56	0.51	0.12
K_2O	5.09	5.22	4.91	5.28	5.37	5.17	0.18
Na_2O	3.12	2.84	2.74	2.80	2.78	2.86	0.15
Al_2O_3	13.62	13.58	13.67	13.82	12.89	13.52	0.36
Fe_2O_3	1.43	1.64	1.85	1.70	2.23	1.77	0.30
SiO_2	70.32	68.73	67.27	70.09	66.56	68.60	1.67
MnO	0.02	0.03	0.033	0.04	0.049	0.04	0.01
P_2O_5	0.06	0.07	0.072	0.07	0.091	0.07	0.01
TiO_2	0.26	0.30	0.310	0.31	0.334	0.30	0.03
ZrO_2	0.02	0.02	0.022	0.02	0.022	0.02	0.00
BaO	0.07	0.08	0.098	0.08	0.080	0.08	0.01
Rb_2O	0.03	0.03	0.031	0.03	0.034	0.03	0.00
WO_3	0.05	0.05	0.045	0.06	0.036	0.05	0.01
LOI	3.43	0.55	0.63	3.57	0.53	1.74	1.61
Total	99.02	94.61	93.49	99.43	92.89		

5.4.2 Surface exposure dating and comparison with measured spectra

The intensively red coloured sample "AdM1" shows the highest age (38.6 ± 1.2 ka), followed by "AdM5" (6.4 ± 0.3 ka), "AdM4" (5.6 ± 0.3 ka) and "AdM2" (1.5 ± 0.1 ka), where no colouring occurred. This is in agreement with the stated hypothesis and the sample description (Chapter 2.5). Generally, the ^{10}Be ages, especially "AdM1" with almost 40 ka, are remarkably

old and show big age differences. For the age calculation, erosion was neglected. Assuming a continuous small-scale loss of material from the rock surface, similar as with moraine boulders is the case, the ages given here should most probably be seen as minimum ages. Alternatively, if split-off of large-scale rock pieces (≥ tens of centimetres) is the dominating process, the presence of inherited isotopes must be taken into account and the calculated ages have to be interpreted as maximum ages.

Looking at the measured spectra (Fig. 5.22), a well pronounced correlation between surface exposure ages (Table 5.24) and the corresponding spectral signature in the range of approx. 380-580 nm is identifiable after continuum removal. As a reference, a piece of unweathered, fresh rock was also analysed ("AdMf").

Table 5.24 Calculated surface exposure ages. Colours correspond to the measured spectra shown in Fig. 5.22.

	Samples Aiguille du Midi 1-5				
	AdM1	**AdM2**	**AdM3**	**AdM4**	**AdM5**
Elevation (m a.s.l)	3800	3810	3750	3740	3740
Sample thickness (cm)	2.5	3.5	5.5	2.5	4.0
Surface dip (°)	85	85	49	79	79
Quartz (g)	58.13	57.03	58.26	56.77	56.68
^{10}Be (atoms g^{-1} *10^4)	157.63	6.03	24.28	24.84	28.28
Measurement error (%)	3	9.2	5	4.6	5.2
Local production rate not corrected (atoms g^{-1} yr^{-1})	75.59	76.00	73.57	73.17	73.17
Shielding factor	0.559	0.559	0.898	0.627	0.627
Corrected local production rate (atoms g^{-1} yr^{-1})*	41.24	41.11	62.85	44.77	44.34
^{10}Be date (yrs)**	**38,600 ± 1200**	**1,470 ± 140**	**3,870 ± 200**	**5,560 ± 260**	**6,390 ± 330**

* Corrected for shielding, sample thickness and surface dip
** Reported errors are only AMS errors.

According to the visual impression, the curve progression of "AdM2" is shaped very similarly to that of the unweathered sample. With increasing surface exposure ages and thus more pronounced weathering, a decrease in feature depth is ascertainable. A comparison with the continuum-removed spectrum of hematite permits the conclusion, that the spectra evolution with increasing age is, at least partly, influenced by hematite formation (Fig. 5.22). Thus, hematite content and its effects on rock surface colour can be interpreted as the main feature required in regard to the generation of spatial data fields of age distribution in rock walls.

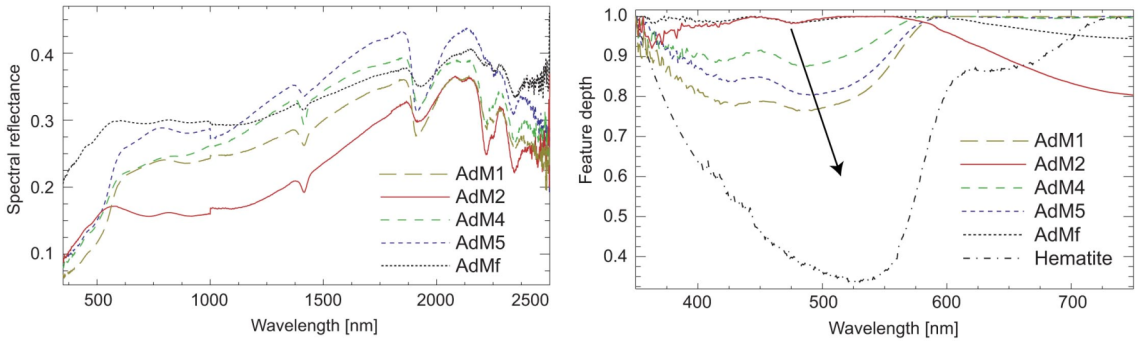

Fig. 5.22 Measured (left) and continuum removed (right) spectra. The arrow indicates the influence of Fe-oxide content with age.

Chapter 6

Discussion and conclusions

6.1 Landscape history in the greater area of Albulapass and Val Burdun

In this part of the study we try to reconstruct and validate the temporal framework of the Lateglacial and early Holocene landscape development in the greater area of Albulapass (Val Mulix and the Albula region) and in Val Burdun, both located in eastern Switzerland. The main aim is to enhance the database of absolute ages of climate-related glacial and periglacial landforms and to cross-check the results with different relative dating methods. Geomorphologic maps (Maisch, 1981; Beer, 2005) serve as a basis for the meaningful localisation of the sampling sites and provided guidance for the interpretation.

In the following, a discussion and summary of the main results from both investigation sites separated by method is given. Determined exposure ages were already set into a broader context and compared with other studies in Chapter 5. Further methodological statements are made about the combined approach used in this work.

6.1.1 Surface exposure dating

Comments on ages obtained

The suggested Daun age (Maisch, 1981) of the moraine formed by the confluence of the former Val Mulix and the Val Tschitta glacier, can be supported with a ^{10}Be exposure age of 14.7 ± 1.8 ka (sample VM7). This underlines the concept that this Lateglacial stadial must be positioned in the Oldest Dryas. However, for a further substantiation additional ages from Daun moraines are highly desirable to improve the temporal delimitation of the end of the Oldest Dryas and the onset of the Bølling/Allerød interstadial, respectively.

^{10}Be-ages in combination with the morphological situation show a main activity phase of the relict rock glacier in Val Mulix between the end of the Younger Dryas and the early Holocene. The derived estimation for the mean annual deformation rate of approx. 30 cm is in a comparable range to those reported in literature for active rock glaciers (Haeberli *et al*., 2006 and references therein). Despite the hypothetical character of the interpretation in the actual case (initial position of VM5 is unsure), the ages obtained prove the applicability of surface exposure dating on rock glaciers, given that the sampled boulders are large enough to ensure the highest possible stability.

We attach importance to the ages measured at the rock barrier near the LIA moraine (11.7 ± 0.8 ka and, at a lower position, 8.9 ± 0.7 ka) of the Val Mulix glacier and at an analogous situation in Val Burdun (10.2 ± 0.9 ka). These ages can be seen as direct evidence for the generally assumed (but rarely proved) rapid ice-retreat at the end of the Younger Dryas and for the subsequent Holocene glacier length variations, which have been reduced to a small spatial range framed by the 1850 extent.

In the Albula region, exposure ages from the transfluence Bottas Glischas (maximum/mean age: 13.4 ± 1.4 ka/12.0 ± 1.6 ka), from the Fuorcla Melnetta (13.3 ± 1.2 ka) and from Crap Alv Laiets (mean age: 11.8 ± 1.1 ka) do not support a simple LGM ice surface lowering model at higher altitudes. This would require older exposure ages, as shown by radiocarbon ages of nearby peat bogs, suggesting that the main Engadine valley would have been ice-free already by around 16 ka. The influence of a long-lasting local glaciation or even a reglaciation during the Younger Dryas and/or perennial snow must be assumed. This situation is highly reminiscent of the setting investigated in the Grimsel pass region (Ivy-Ochs, 1996; Kelly *et al*., 2006) and supports the scenario of a complex deglaciation history at high altitudes.

In Val Burdun, the three ages from the rock avalanche are very consistent, identifying this deposit as the result of a single event that happened around 8.9 ± 0.7 ka. The ages from the surrounding moraines are rather young and a straightforward assignment to a supra-regional Lateglacial scheme of stadials is not possible or would require unrealistically high amounts of snow for correcting the ^{10}Be ages. However, the moraine ages ranging from 9.8 ka to 10.5 ka make stratigraphicaly sense and make a scenario of a rock avalanche that happened shortly after ice-retreat look likely. This is not direct proof of the contribution of effects caused by paraglacial adjustments (see Chapter 3.2.3), but a time lag in the range of centuries is reasonable in this context and at least does not speak against such associated processes. An evaluation of

the possible influence of permafrost is hardly possible. Taking into consideration the overall climate during the early Holocene, which was characterised by increasingly warmer and wetter conditions, an additional influence of permafrost degradation cannot be ruled out. Modelling of modern permafrost distribution patterns (FOEN, 2005) shows on one hand that permafrost is still present in the starting zone of the rock avalanche and the area just below, also indicated by an active rock glacier occupying this niche (see also area description in Chapter 2). On the other hand, the setting in Val Burdun represents a typical crest-situation with a warm south side and a north side in the permafrost. Situations like this are vulnerable to failure events triggered in the permafrost-influenced rock slopes, as both observations in the last decades and modelling approaches show (e.g. Noetzli and Gruber, 2009)

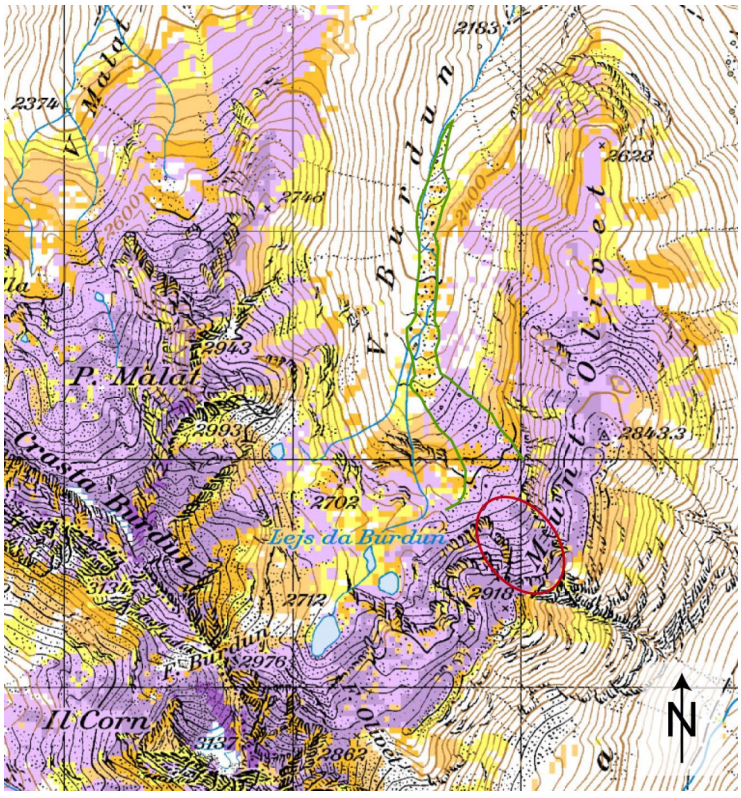

Fig. 6.1 Modelled potential permafrost distribution in Val Burdun (based on model "permaquant"; FOEN, 2005). Violet tones mean "continuous permafrost likely", yellow and orange tones "local permafrost possible". Scale is given by the 1 km mesh. Both the detachment zone (red circle) and the upper and middle part of the rock avalanche (outline in green) are within the zone of potentially continuous permafrost, which is primarily due to the NW orientation. The change to the area with local permafrost coincides with the transition to the lower, flatter part of the deposit. This setting might also have influence on chemical weathering activity, with reduced weathering rind formation rates as a consequence.

Methodical remarks

The choice of reasonable snow heights plays a crucial role in the calculation of ^{10}Be ages, especially in the Alps. As directly applicable snow height values from the past do not exist, they must be estimated, usually on very tentative evidence. A wide range of snow layer thicknesses is possible, especially in the case of bedrock sites, where snow accumulation is less restricted than on boulders. This leads to even more uncertainty. Figure 6.2 shows for Alb2 that a theoretical error of 0.6 m in the snow height estimation, which is not unlikely, would cause an age-shift of approx. 800 years. Taking the relatively short duration of Lateglacial oscillations into account, such errors are striking. If available, the integration of long-term snow-measurements (as done in this study) allows the derivation of more objectively explicable maximum values. However, local effects due to boulder shape etc. will largely keep their arbitrary character.

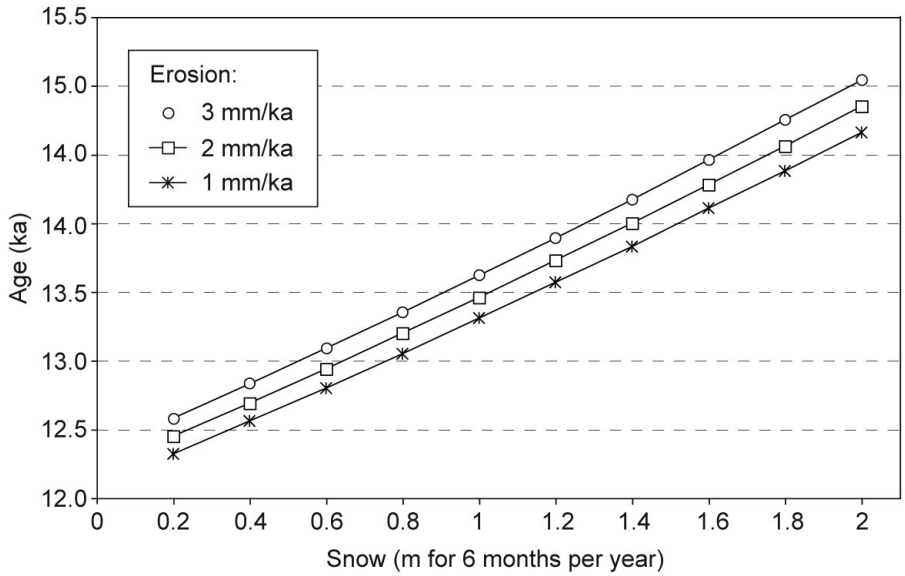

Fig. 6.2 ^{10}Be ages calculated for Alb2 with different amounts of snow and erosion rates (1, 2 and 3 mm/ka). The slope of the graphs shows the high influence of snow coverage on the measured age. An increase from 0.2 to 1.0 m snow for 6 months per year leads to ages older by roughly 1000 years. The erosion rate has a comparatively small effect on the age (about 300 years).

6.1.2 Schmidt-hammer rebound values and weathering rind thicknesses

In all regions, a detailed and appropriate resolution of geomorphic processes within the Lateglacial was not possible using Schmidt-hammer rebound values. This method, however, proved to be a helpful tool in distinguishing landforms in a larger timeframe also including the Holocene. Considering other studies conducted on nearby Holocene surfaces (active rock glaciers with the same lithology) and combining them with the findings of this work, the

following R-value ranges seem to be typical (Fig. 6.3): 30-40 for Lateglacial to early Holocene-aged surfaces, 40-50 for early Holocene to mid-Holocene-aged surfaces and 50-60 for increasingly younger and even modern surfaces (root zone of active rock glaciers, 1850 moraine). These value ranges are comparable with results of Shakesby *et al*. (2006) and Engel (2007). Engel (2007) reported that R-values from granitic surfaces lower than 29 can be assigned to pre-LGM landforms (Czech Republic). This would fit well with the time-dependent correlation of the R-values in the Albula region.

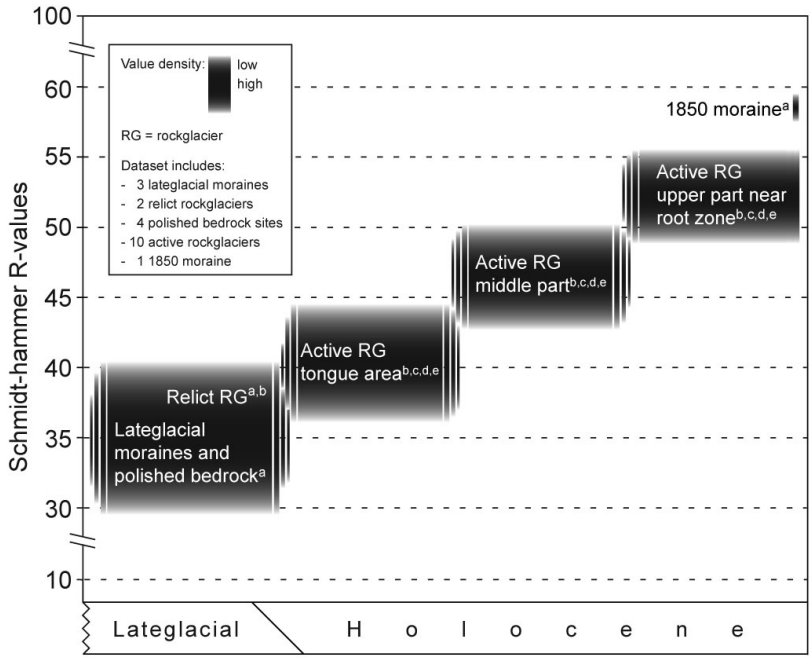

Fig. 6.3 Schematic presentation of Schmidt-hammer R-values from different landforms measured in the Albula region and in the adjacent Julier area (same lithology) with an approximate temporal assignment. Data is compiled from different authors: a = this study; b = Compeer (2009); c = Frauenfelder *et al*. (2005); d = Laustela (2003); e = Castelli (2000). A recent study carried out on granitic material (LIA and Lateglacial moraines) in tributary valleys south of the Engadin (Graf, 2010) is in accordance with the values proposed here.

Taking the exposure dating results and the geomorphological map of Val Mulix and the Albula area into consideration, weathering rind measurements generally yielded meaningful results along the proposed timeline. This method proved its ability to reconstruct Lateglacial process sequences. Furthermore, the values obtained – mean values 2.2 to 2.9 mm on the relict rock glacier; 3.1 and 4.6 mm for the Egesen II and the Egesen I moraine, respectively – represent a meaningful continuation of weathering rind thicknesses measured on nearby active rock glaciers with the same or at least a comparable lithology (Laustela, 2003; Compeer, 2009), varying from roughly 0.9 mm to 1.8 mm near the front (Fig. 6.4). It must be mentioned again that boulders near the front do not constitute the oldest rock material of any rock glacier and

accordingly not the whole Holocene is represented on the rock glacier surface. Furthermore, rock glacier activity not starting right after the transition from the Lateglacial to the Holocene is entirely possible. This might explain the gap between values measured on active rock glaciers and the ones measured on the relict rock glacier (Böhlert *et al.*, 2010b).

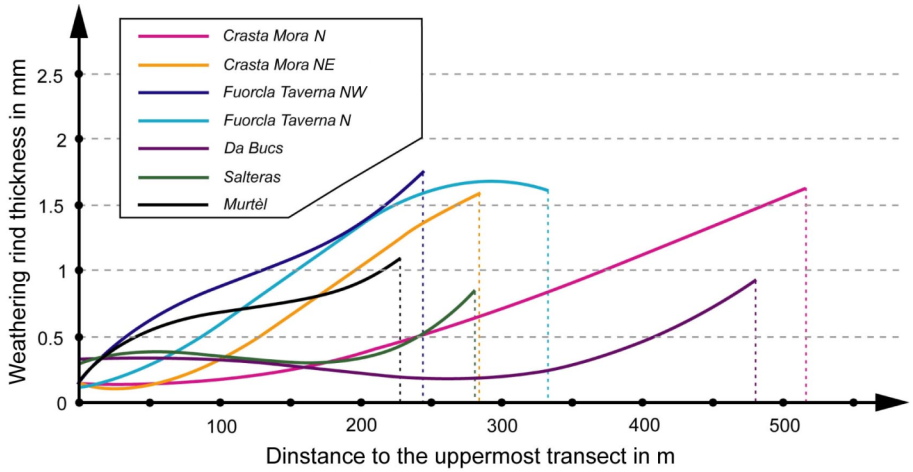

Fig. 6.4 Comparison of weathering rind mean values measured on different active rock glaciers (interpolated from measurements on several transects perpendicular to the flow direction on each rock glacier). Crasta Mora and Fuorcla Taverna are situated near Albula pass, Da Bucs and Salteras in Val Tschitta and Murtèl in the Corvatsch region, on the opposite side of the Upper Engadine main valley. Graphic slightly modified from Compeer (2009).

Compared to weathering rind thicknesses measured on the upper and middle part of the rock avalanche in Val Burdun (mean/median 2.4/2.2 mm and 2.6/2.5 mm, respectively), the lower part shows distinctly increased values (3.7/3.3 mm). The suggested age trend is not in accordance with measured exposure ages and the morphology of the deposit. Based on both, a single event with high velocities must be assumed. As mentioned in chapter 5, the geological setting might not have been ideal for rind measurements and, also indicated by Schmidt-hammer measurements carried out separately on the upper and lower parts of boulders, snow may play an important role. Fig. 6.1 shows that permafrost is likely in the area of the upper and middle part of the rock avalanche. In contrast, it is expected that in the lower flat part what permafrost appears is just sporadic. Unlike for measurements carried out on active rock glaciers (entirely permafrost) or in areas without any permafrost (like the sites in Val Mulix), the rock avalanche in Val Burdun summarises two different regimes within one landform. Permafrost – here understood as a function of a) altitude (determining air temperature) and b) slope and aspect (determining radiation) – the thickness and duration of snow coverage as well as the blocky character of the underground underlie reciprocal interactions. Possible net effects are generally lower ground temperatures, more snow and probably also lower water availability.

This might be especially true for the sampled smaller boulders in between, and shielded by, the bigger ones. Based on that, it is possible that the chemical weathering activity in the upper and middle part of the rock avalanche is suppressed. Weathering rinds that form within a certain time window are thus smaller compared to the lower part.

6.1.3 Soil chemical and mineralogical investigations

Relative weathering state parameters

As relative measures for soil age, a number of approaches describing soil development including weathering indices derived from soil chemistry, soil mineralogy with a main emphasis on the clay fraction and mass balance calculations were applied. Although a good representation of the geomorphologic setting could generally be achieved with mass balance calculations, the mineralogical composition and especially calculated weathering indices yielded an inconsistent picture. For Val Mulix, however, some main features that occurred with different methods can be repeatedly recognised. First, in most cases, the Daun moraine could clearly be identified as the oldest of the investigated landforms. A valuable separation of the Egesen moraine was thus possible. Secondly, several approaches underline the possibility of pre-weathered material, which influences the chemical and mineralogical characteristics of the soils developed on the relict rock glacier.

It is apparent that techniques including the soil profile as a whole (mass balance calculations, ^{10}Be inventory) in general gave more meaningful results than the ones referring to single horizons (weathering indices, mineralogy). This would speak for reallocation processes within the soil profiles, without changing the overall characteristics of the soils. As profiles of chemically extracted elements like Al, Fe and Si clearly show patterns of undisturbed soil evolution with no buried soils present, it can be assumed that these dislocations are of minor importance. Consequently, the incorporation of material that had already experienced a certain degree of weathering at the beginning of soil development is the most plausible explanation for the conditions found in the rock glacier profiles. The high amount of large size components may additionally have favoured the development of weathering pockets and a generally irregular distribution of the weathered material, making the evaluation of horizon specific parameters difficult.

This situation illustrates nicely that disturbing factors like redistribution processes and pre-weathering must be taken into account when using soils as relative age indicators (see also Caspari, 2007). Although established as a tool for estimating the relative ages of Quaternary

deposits (e.g. Birkeland, 1999; Zech *et al*., 2003), soil development data should thus be applied only in combination with other relative and/or numerical age data (Dahms, 2004).

Numerical approaches – ^{10}Be inventory and ^{14}C-dating of stable SOM

The inventory of ^{10}Be accumulated in soils – measured for the soil profile S1 on the Daun moraine in Val Mulix – proved to be a potentially powerful tool to derive ages of sedimentary accumulations like moraines. There is unfortunately no consensus to be obtained from the literature of the exact effect precipitation has on the ^{10}Be flux to an area. Besides ^{10}Be deposition fluxes derived from the amount of annual precipitation, also model-based approaches using constant fluxes exist (Willenbring and von Blanckenburg, 2009).

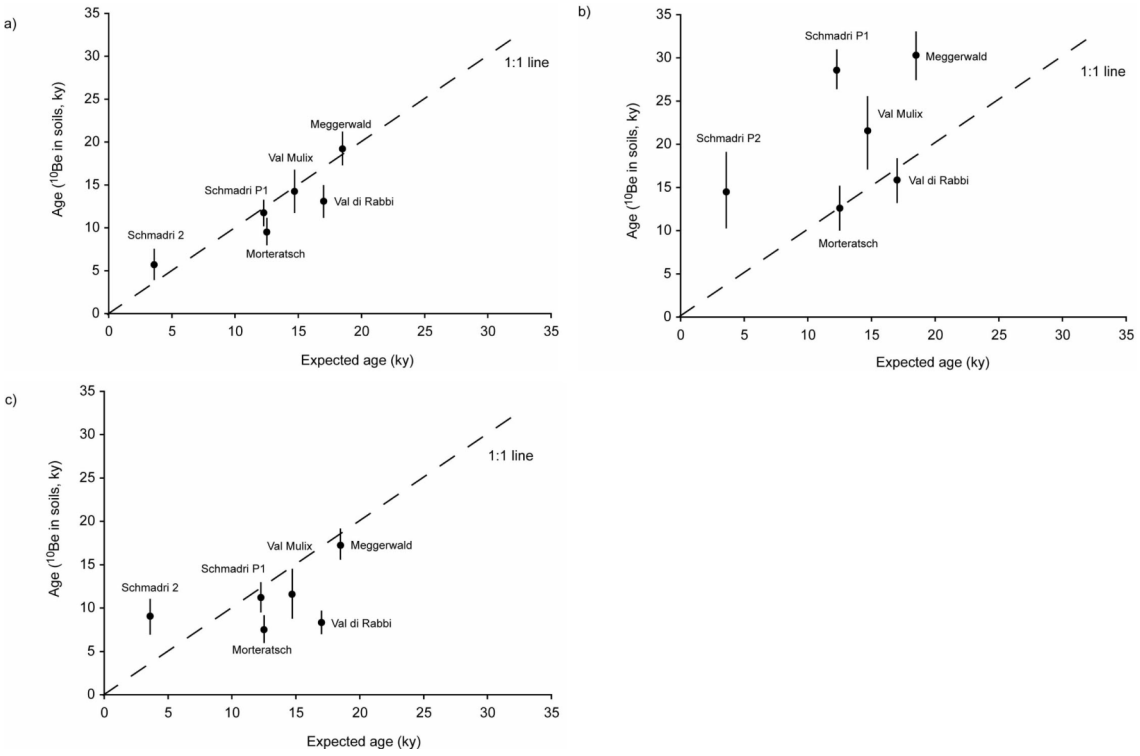

Fig. 6.5 Correlation between ^{10}Be ages derived from soil analyses and "expected" surface ages (reference surface age; derived either from surface exposure dating or from radiocarbon analyses); a) using ^{10}Be deposition rates as a function of the annual amount of precipitation, b) constant ^{10}Be deposition fluxes, c) constant ^{10}Be deposition fluxes like b) and assuming a background ^{10}Be level in the parent material. The best correlation can be achieved with the precipitation dependent approach (from Egli *et al*., 2010).

A comparison of a number of soils with a "known" age (from Switzerland and northern Italy, including the moraine profile discussed here), shows that with the precipitation-based deposition rate a better representation of the suggested age trend can be achieved (Egli *et al*., 2010; see Fig. 6.5). Based on that, we decided to use precipitation dependent ^{10}Be deposition

fluxes, assuming a proportional increase of ^{10}Be deposition with increasing amounts of precipitation (Monaghan *et al*., 1985/1986; scenario a) in Fig. 6.5).

The relation between the error of ^{10}Be deposition rates and the age error is non-linear (Egli *et al*., 2010). Thus, the calculated age is very sensitive to the choice of the annual amount of precipitation, which is especially true for underestimations of the ^{10}Be-deposition (Fig. 6.6). As an example, an overestimation of 40% of the precipitation dependent ^{10}Be-deposition causes an age-shift of approx. 30%. A comparable underestimation causes an age error of almost 70%, leading to landform ages that are too old. A reliable precipitation database is of central importance. However, measuring precipitation in mountain areas is a difficult task and long-term measurements for remote areas in many cases are not available at all. Because of that and also due to the laborious ^{10}Be-isolation procedure, this method either will likely keep a complementary function or will predominantly be applied in case of lacking organic matter and suitable rock material for radiocarbon dating and surface exposure dating, respectively.

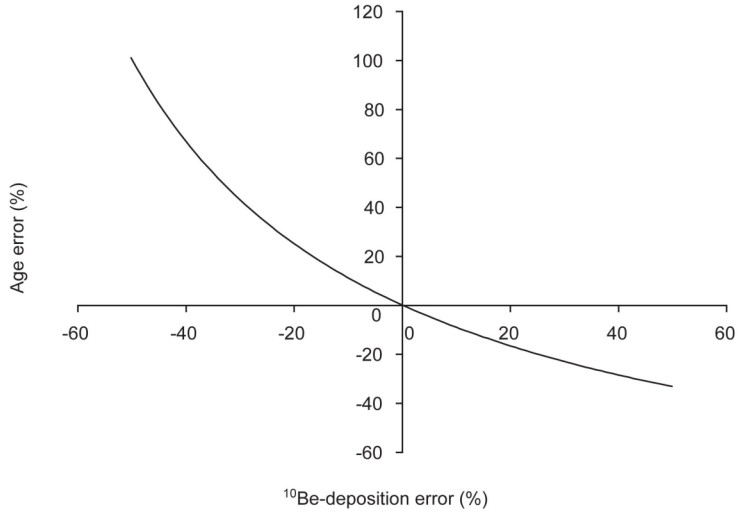

Fig. 6.6 Effect of errors of ^{10}Be-deposition rates estimation on the calculated surface age. Especially an underestimation of the ^{10}Be-deposition causes high age errors (from Egli *et al*., 2010).

The radiocarbon dating of resilient soil organic matter could not provide a decisive contribution to landscape evolution. Both ages that were too high or too low by several millennia with respect to an age assumed to be near a true age (based on geomorphologic mapping and ^{10}Be-dating) were detected. The first case speaks for the presence of pre-weathered material; the second suggests an inadequate removal of younger C-fractions. On one hand, this makes clear that only stable sites allowing for an undisturbed soil development without external input should be chosen. Because of landform-specific dynamics and the potential influence of

slope instabilities, respectively, this precondition might not have been completely fulfilled in case of the relict rock glacier and the lower moraine in Val Burdun. On the other hand, ages that are too young and also the rather questionable reproducibility in the case of the E horizon of S1 in Val Mulix call for an enhanced understanding of what the actually dated fraction consists of and whether the chemical procedure could be optimised. From a methodological point of view, the ages obtained will always be mean ages and never can be more than an asymptotic approximation of the theoretically highest possible value. A direct link to the geomorphic process behind the landform will thus not be derivable. Nevertheless, under suitable circumstances moraine minimum ages can be achieved and already at the current stage this can be done quite successfully, as shown in other studies (e.g. Favilli *et al*., 2009a, 2009b). Further efforts in this direction would certainly be worth considering.

6.1.4 Combining dating techniques

In this study it was shown that the combined application of a number of dating techniques can strengthen results that after an isolated interpretation of just one method may have been considered questionable (e.g. age of VM1 on the upper Egesen I moraine and accordant weathering rind values). Alternatively, with the help of different approaches valuable arguments that speak against findings of a certain dating method can be found (e.g. exposure age/geomorphology vs. weathering rinds of the rock avalanche). In this sense, the combined strategy facilitates the decision as to whether an age is reliable or not – a question that is always prevalent when dealing with dating issues.

Each dating technique requires different framework conditions to bring to bear its potential and every method has its own disturbing factors, to which it is susceptible. It is therefore necessary to consider an enlarged geomorphologic framework for the age interpretation, which is especially true for soil data providing a generalised representation of age relations (e.g. Dahms, 2004; Caspari, 2007). Taking processes possibly involved (in the past) into account can help to estimate the validity of the interpretation of the results, as done for instance for the luminescence ages (see below).

Dating landforms not only serves for the temporal assignment of the landform itself, but also provides the opportunity to derive minimum or maximum ages for related landforms (e.g. break through of relict rock glacier through Egesen moraine). For the rock glaciers south of Albula pass (active and relict ones), two main rock glacier activity phases could be derived: one starting soon after the ice retreat in the Younger Dryas with a main activity most likely in the

early Holocene and lasting approx. until the Holocene climate optimum and a second one lasting until today with an unsure onset between c. 6 and 10 cal ky BP (Böhlert *et al.*, 2010b). Radiocarbon ages, exposure ages (both from Crap Alv) together with soil analyses from the Crap Alv moraine (presumably Egesen-equivalent) and from a higher-altitude soil profile within the Egesen extension (Compeer, 2009) provided the necessary time marks.

6.2 Dating rock glaciers with luminescence techniques

6.2.1 General remarks

Calculated sedimentation ages fall into a sensible range of several thousand years, supporting the rock glacier age concept based on other dating techniques (Haeberli *et al.*, 2003). In order to interpret these ages, possible error sources must be taken into account. Besides weak signals as a result of material inherent characteristics – current data do not allow for a proper statistical evaluation – a number of processes and process combinations such as interactions with glaciers exist and are potentially involved in rock glacier formation. Transitions to glacial landforms and landform associations especially in the upper parts of the cirques near the rooting zone of the rock glaciers have to be regarded as very likely (Haeberli, 1975; Barsch, 1996). They create a whole spectrum of possible origins, deposition characteristics and travel paths of input material, all of them influencing the build-up of luminescence signals and thus the calculated age. Furthermore, there is not a full understanding of processes participating in the formation of rock glaciers and rock glacier dynamics. Material input through wind and within zones of extending flow (crevasses) as well as dislocation processes as a result of percolating melting water in the rock glacier body must at least be considered possible.

6.2.2 Possible sources of uncertainties and implications for age interpretation

Although not quantifiable, it is worth thinking about processes and mechanisms that may modulate luminescence ages. Here, a number of possible influences and questions that should be posed is given, separated by (A) deposition and incorporation, (B) transport and (C) exhumation and sampling (see Fig. 6.7). If a point named leads to minimum ages (i.e., the landform is potentially older than indicated by the calculated age) or maximum ages, respectively, this is mentioned in brackets.

A – Deposition and incorporation

- Has a time lag between deposition and incorporation to be considered (minimum ages)?

- Is it possible that material falling down from the headwall may have slid over perennial snowfields or avalanche residues in the rooting zone? This could result in an initial deposition in a more distal position (minimum ages) with regard to the headwall.
- Does the reduction to the grain size of a single mineral grain happen before or after incorporation? In the second case, only poorly bleached or even saturated material is expectable (maximum ages).
- Is the source material at least partly of a glacial origin (keeping in mind mixed forms and process combinations!)? If so, the residence time in the glacial deposit prior to rock glacier formation may be included in the luminescence signal (maximum ages).
- Was there a LIA-glaciation and what could be its effects? Possible influences are a certain erosive power creating new fine-grained material of LIA-glaciers (minimum ages), reduced coefficients of friction and coupled longer transport distances of rock material from the headwall (minimum ages, see above), or an interruption of debris input due to glacierisation of the headwall.
- The exposure to daylight was too short for a complete bleaching. As a consequence, poorly or non-bleached material was incorporated (maximum ages).

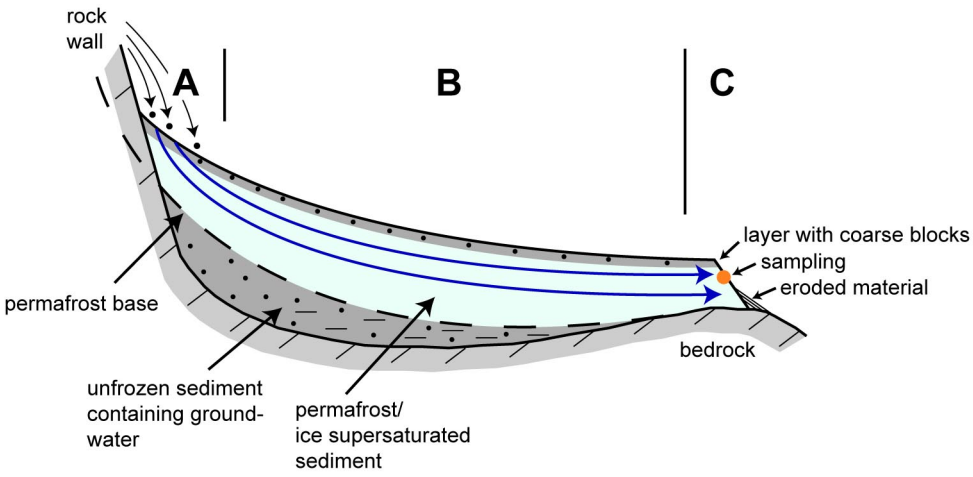

Fig. 6.7 Rock glacier model modified from Haeberli (1985). This example shows a tallus-derived rock glacier below a rock wall. The top layer with coarse block approximates the active layer. The blue arrows represent idealised trajectories of single grains subsequently removed at the front for luminescence dating. The measured age theoretically is the time the grain needed to travel this distance within the rock glacier body, protected from daylight. A – C label zones referring to the discussion of possible sources of uncertainties.

B – Transport

- How thick was the sediment cover during transport?
- Can this depth assumed to be +/- constant?

- How exactly would the trajectory of a single grain look like? Was it above or below the permafrost table? The differing water and/or ice content influences for the calculation of the dose rate, especially for the component resulting from cosmic ray flux.
- Are there pronounced extension/compression processes (crevasses?), and to which depth do they have an effect? Do they open the possibility for material input during the transport (minimum ages)?
- Permeability of permafrost body and probability of material input (minimum ages)?
- Horizontal displacement of mineral grains at the permafrost table due to meltwater influence (minimum ages)?
- Is an aeolian input of material possible (minimum ages)?
- Are there other possible mixing processes?

C – Exhumation and sampling

- Have thawing processes penetrating from the front and creating the possibility of mixing material due to melt water and possibly rain water input been taken into account?
- How can the risk of sampling eroded and reworked material be minimised? The following steps might help: 1. Samples should be taken above the clearly visible eroded material (debris cone). 2. Big boulders in the front have certainly not fallen down but rather melted out in situ. Digging below them provides a certain slope stabilisation and allows for deeper penetration depths.

As shown, there are several processes applicable to minimum as well as maximum ages. Due to the high probability of poorly or non-bleached material very "old" grains influencing the rock glacier age must be considered (probability of scenario "too old" is considered higher than "too young"). The choice of the median as a statistical value for determining the actual palaeodose therefore seems to be more appropriate than the arithmetic mean, which is highly sensitive to outliers causing an overestimation of the palaeodose. On the other hand, following an idealised rock glacier model, the oldest material must be expected at the base near the rooting zone of the rock glacier (see chapter 3.2.2), supporting the interpretation of the calculated ages as minimum ages.

Which elements of the factor combination described above prevail is not determinable on the database available. However, in glacial and periglacial environments, the measurement of single grains certainly makes sense. In case of a satisfying number of measured palaedoses, the

value distribution may give helpful hints about the presence of inhomogeniously bleached material. This makes for an appropriate choice for the statistical determination (here: mean value or median) of the value, which is used for the age calculation, easier and more reliable.

6.3 Exposure ages and spectral properties of rock surfaces at Aiguille du Midi (F)

We showed that analysing spectral properties of rock surfaces in steep walls with homogeneous lithology may be a tool for estimating the age distribution and related past rock fall activity in high alpine environments. The redder a rock surface, the longer this rock was exposed to weathering. In numerous cases, the correlation of rock fall initiation to changes in the permafrost conditions is rather weak and related forecast and mitigation possibilities are limited (Gude & Barsch 2005). Not only permafrost thawing but also other processes like general frost-thaw activities (physical weathering), seismic (neotectonic) activity or stress relief following deglaciation could induce rock falls.

Due to the topographic situation of the investigated sites, however, at least one process affecting the stability of rock walls can be excluded. A stress-relief following deglaciation of glacier ice did not occur because no glaciers covered the rock walls during (and after) the LGM. Rock fall is predominantly due to permafrost changes and frost-thaw activities. Although neotectonic activities have been rather low, their influence on rock falls cannot be fully excluded. The approach used will, therefore, not allow for the direct reconstruction of past permafrost conditions. It can give, however, indications about past and present-day rock fall activities. From this, the influence of permafrost on rock wall stability can at least partially be deduced. Inasmuch as global warming in general and local temperature and precipitation trends in particular are likely to influence the permafrost significantly, the stability of rock walls will also be affected.

Chapter 7

Synthesis and Outlook

Based on findings in this work, it can be suggested that the strategy of a combined application of relative and numerical dating techniques should be pursued. It provides the possibility of building up calibration curves for relative methods that have at least local validity. The relative methods in turn may strengthen/weaken numerical ages and can give useful indications in cases of doubt, especially when only a low number of numerical ages is available. This combined approach is an important instrument to improve the reliability of landform ages and associated palaeoclimatic information and process rates.

The results obtained also demonstrate the fundamental importance of a careful choice of appropriate sampling sites. Soil formation processes are especially likely to be disturbed by an unstable substratum or by the influence of pre-weathered material, which may be incorporated. For the interpretation of measured ages, it is essential that the main geomorphological framework of the investigation area is understood in advance. Geomorphic mapping with consideration of as many interconnected landforms as possible is, therefore, an important precondition for dating issues. A mutual control of obtained ages and to decide whether an age is accurate or not is only possible when (morpho-)stratigraphy and thus a relative temporal assignment is known or can be estimated on a reliable basis.

With a focus on landscape evolution in the Alps, it would be worth considering the following geomorphologic situations and important method refinements and combinations in future studies:

- Although often restricted by the absence of suitable boulders, one of the main points of interest is certainly an extended and substantiated age determination of stadials belonging to the Oldest Dryas and of those deposited after the Younger Dryas.

- Further ^{10}Be-ages from high elevation (bedrock) sites are indispensable for an improved discussion of the breakdown of the LGM ice masses. Also vertical transects ideally covering a time span from the Little Ice Age to the Most Extensive Glaciation (areas higher than today's visible trimline) would provide a relevant research topic. As shown in this study, the influence of snow and ice on a local scale is not to be neglected. Especially for the upper (older) bedrock sites, erosion will be of increasing importance.

- There is certainly need for an improved handling of uncertainties of ^{10}Be ages caused by snow coverage. Due to the highly individual geometries of sampled boulders and local topographical characteristics, the inter-annual and inter-seasonal patterns of snow accumulation and ablation vary in a broad range. Generalising assumptions about snow heights are thus not appropriate but in most cases the only possible approach. A continuous survey of the snow cover at some key sampling sites with automatic cameras during one or preferably several winter seasons could provide an initial basis for more reliable snow height estimations.

- Luminescence dating techniques seem to have the potential for yielding meaningful values for rock glacier ages. In order to minimise influencing factors possibly disturbing luminescence signals, future studies should focus on rock glaciers that show a simple geometry without pronounced zones of compressing/extending flow. Ideally, talus-derived rock glaciers that show no signs of glacial influence in the starting zone should be chosen. Furthermore, the inclusion of water/ice content should be considered in a more sophisticated way. Assuming a constant depth of the sampled material, a two-layer model with an upper layer of approx. 2 to 3 metres without ice (representing the active layer with coarse blocks) and a lower layer reaching down to the sampling depth with 70% ice as a suggestive mean value could be a simple but meaningful initial approach.

- Luminescence dating along a transect following the central flow line of a rock glacier would be highly interesting. The age distribution within the rock glacier body theoretically could provide information about deformation rates over time and would allow for the

derivation of connected climatic variations. Of course, technically demanding drillings would be necessary.

- A number of method combinations applied on rock glaciers – especially luminescence together with surface exposure dating – might yield insightful results. For instance, ^{10}Be ages from boulders deposited just in front of relict rock glaciers could provide information about the time of inactivation. Combined with luminescence ages that include the travel time and the time since inactivation, the time span during which the rock glacier was active could theoretically be calculated.

- As ^{10}Be and ^{14}C-measurments in soils are rather new approaches (especially in alpine environments), a number of methodological questions remain open. Those referring to chemical composition and stabilisation of H_2O_2-extracted organic matter pool as well as to sorption processes of ^{10}Be in soils and connected deposition rates are of particularly central importance and should be emphasised.

- Schmidt-hammer measurements carried out on spots with a known age like LIA moraines could provide reference values for local age-rebound value relationships and, applied in areas with different geology, rock type specific evolution patterns of r-values with time could be extracted.

- The relationships found at Aiguille du Midi look promising. However, they certainly represent only a first impression and further investigations in this field will be necessary to establish this approach as a commonly usable application. Doubtless of great importance is the enlargement of the survey sample size in order to be able to generate statistical correlations between surface exposure ages and spectral properties. These properties therefore have to be translated into quantifiable values. The long-term objective is to estimate surface ages of rock walls based on spatial data fields ascertained with remote sensing techniques. Potential follow-up studies will have to deal with the influence of variable slope aspects and altitudes as well as different lithologies. Steep places at high elevations should be preferred. Sampling locations that are situated too low are not suitable due to lichen growth disturbing the spectral signal. The same is true for flat spots where snow cover can develop more easily and remain for a longer time.

References

Aoyama, M. 2005. *Rock glacier in the northern Japanese Alps: palaeoenvironmental implications since the Late Glacial*. Journal of Quaternary Science 20(5): 471-484.

April, R., Newton, R., Truettner Coles, L. 1986. *Chemical weathering in two Adirondack watersheds: past and present-day rates*. Geological Society of America Bulletin 97: 1232-1238.

Arenson, L., Hoelzle, M., Springman, S. 2002. *Borehole Deformation and Internal Structure of Some Rock Glaciers in Switzerland*. Permafrost and Periglacial Processes 13: 117-135.

Atlas der Schweiz 2.0. 2004. Bundesamt für Landestopographie (ed.).

Auer, M. 2003. *Regionalisierung von Schneeparametern – Eine Methode zur Darstellung von Schneeparametern im Relief*. Publikation Gewässerkunde 304.

Augustinus, P.C. 1995a. Rock mass strength and the stability of some glacial valley slopes. Annals of Geomorphology 39: 55-68.

Augustinus, P.C. 1995b. *Glacial valley cross-profile development: the influence of in situ rock stress and rock mass strenth, with examples from the Southern Alps, New Zealand*. Geomorphology 14: 87-97.

Bailey, R.M., Arnold, L.J. 2006. *Statistical modelling of single grain quartz D-e distributions and an assessment of procedures for estimating burial dose*. Quaternary Science Reviews 25: 2475-2502.

Ballantyne, C.K. 2002. *Paraglacial geomorphology*. Quaternary Science Reviews 21: 1935-2017.

Ballantyne, C.K., Schnabel, C., Xu, S. 2009. *Exposure dating and reinterpretation of coarse debris accumulations ('rock glaciers') in the Cairngorm Mountains, Scotland*. Journal of Quaternary Science 24(1): 19-31.

Barg, E., Lal, D., Pavich, M.J., Caffee M.W., Southon, J.R. 1997. *Beryllium geochemistry in soils: evaluation of $^{10}Be/^{9}Be$ ratios in authigenic minerals as a basis for age models*. Chemical Geology 140: 237-258.

Barsch, D. 1996. *Rockglaciers: Indicators for the present and former geoecology in high mountain environments*. Springer, Berlin: 331 pp.

Basu, A., Aydin, A. 2004. *A method for normalization of Schmidt hammer rebound values*. International Journal of Rock Mechanics & Mining Sciences 41: 1211-1214.

Bateman, M.D. 2008. *Luminescence dating of periglacial sediments and structures*. Boreas 37: 574-588.

Bearth, P., Heierli, H., Roesli, F. 1987. Geologischer Atlas der Schweiz, Blatt 1237 Albulapass (Atlasblatt 81). Schweizerische Geologische Kommission/Landeshydrologie und -geologie (eds).

Beer, A. 2005. *GIS-basierte geomorphologische Kartierung in der Val Chamuera sowie morphochronologische Untersuchungen am Schwemm-/Murkegel der Val Champagna im Oberengadin (GR)*. Diploma thesis, University of Zurich, Switzerland. Unpublished.

Beniston, M., Diaz, H.F., Bradley, R.S. 1997. *Climatic Change at High Elevation Sites: An Overview*. Climatic Change 36: 233-251.

Beniston, M. 2005. *Mountain Climates and Climatic Change: An Overview of Processes Focusing on the European Alps*. Pure and Applied Geophysics 162: 1587-1606.

Benn, D.I., Evans, D.J.A. 1998. *Glaciers and glaciation*. Arnold, London: 734 pp.

Benn, D.I., Lehmkuhl, F. 2000. *Mass balance and equilibrium-line altitudes of glaciers in high-mountain environments*. Quaternary International 65-66: 15-29.

Birkeland, P.W. 1999. *Soils and geomorphology*. 3rd edition, Oxford University Press, New York: 430 pp.

Birkeland, P.W., Shroba, R.R., Burns, S.R., Price, A.B., Tonkin, P.J. 2003. *Integrating soils and geomorphology in mountains – an example from the Front Range of Colorado*. Geomorphology 55: 329-344.

Böhlert, R., Gruber, S., Egli, M., Maisch, M., Brandovà, D., Haeberli, W. 2008. *Comparison of exposure ages and spectral properties of rock surfaces in steep, high alpine rock walls of Aiguille du Midi, France*. In: Proceedings of the 9th International Conference on Permafrost, University of Alaska, Fairbanks: 143-148.

Böhlert, R., Egli, M., Maisch, M. 2008. Untersuchungen zur spätglazialen und frühholozänen Landschaftsentwicklung im Albulagebiet (Graubünden, Schweiz). In: Rothenbühler, C. (ed.), Klimaveränderungen auf der Spur, Samedan.

Böhlert, R., Egli, M., Maisch, M., Brandovà, D., Ivy-Ochs, S., Kubik, P.W., Haeberli, W. 2010a. *Application of a combination of dating techniques to reconstruct the Lateglacial and early Holocene landscape history of the Albula region (eastern Switzerland)*. Geomorphology, submitted.

Böhlert, R., Compeer, M., Egli, M., Brandovà, D., Maisch, M., Kubik, P.W., Haeberli, W. 2010b. *Dating of Lateglacial and Holocene rock glacier activity in a high Alpine region using a combined relative-numerical dating approach*. The Open Geography Journal, submitted.

Bolliger, T., Feijfar, O., Graf, H.R., Kälin, D.W. 1996. *Vorläufige Mitteilungen über Funde von pliozänen Kleinsäugern aus den Höheren Deckenschottern des Irchels (Kt. Zürich)*. Eclogae Geologicae Helvetiae 89: 1043-1048.

Bollinger, D., Hegg, C., Keusen, H.R., Latelin, O. 2000. Ursachenanalyse der Hanginstabilitäten 1999. Bulletin für angewandte Geologie 5/1: 5-38.

Boulton, G.S., Jones, A.S. 1979. *Stability of temperate ice caps and ice sheets resting on beds of deformable sediment*. Journal of Glaciology 24: 29-43.

Braucher, R., Del Castillo, P., Siame, L., Hidy, A.J., Bourlès, D.L. 2009. *Determination of both exposure time and denudation rate from an in situ-produced ^{10}Be depth profile: A mathematical proof of uniqueness. Model sensitivity and applications to natural cases*. Quaternary Geochronology 4: 56-67.

Brauer, A., Haug, G.H., Dulski, P., Sigman, D.M., Negendank, J.F.W. 2008. *An abrupt wind shift in western Europe at the onset of the Younger Dryas cold period*. Nature Geoscience 1: 520-523.

Brimhall, G.H., Dietrich, W.E. 1987. *Constitutive mass balance relations between chemical composition, volume, density, porosity, and strain in metasomatic hydrochemical sstems: results on weathering and pedogenesis*. Geochimica and Cosmochimica Acta 51: 567-587.

Bronk Ramsey, C. 1995. *Radiocarbon calibration and analysis of stratigraphy: The OxCal program*. Radiocarbon 37: 425-430.

Bronk Ramsey, C. 2001. *Development of the radiocarbon calibration program OxCal*. Radiocarbon 43: 355-363.

Brown, L., Stensland, G.J., Klein, J., Middleton, R. 1989. *Atmospheric deposition of ^{7}Be and ^{10}Be*. Geochimica et Cosmochimica Acta 53: 135-142.

Brown, E.T., Edmond, J.M., Raisbeck, G.M., Yiou, F., Desgarceaux, S. 1992. *Effective attenuation length of cosmic rays producing ^{10}Be and ^{26}Al in quartz: implications for surface exposure dating*. Geophysical Research Letters 9: 369-372.

Bruun, S., Thomsen, I.K., Christensen, B.T., Jensen, L.S. 2008. *In search of stable soil organic fractions: a comparison of methods applied to soils labelled with ^{14}C for 40 days or 40 years*. European Journal of Soil Science 59: 247-256.

Burga, C.A. 1987. *Gletscher und Vegetationsgeschichte der Südrätischen Alpen seit der Späteiszeit*. Denkschriften der Schweizerischen Naturforschenden Gesellschaft 101.

Bussy, F., Hernandez, J., von Raumer, J. 2000. *Bimodal magmatism as a consequence of the post-collisional readjustment of the thickened variscan continental lithosphere (Aiguilles Rouges/Mont-Blanc massifs, western Alps)*. Transactions of the Royal Society of Edinburgh: Earth Sciences 91(1-2): 221-223.

Caspari, T. 2007. *The soils of Buthan: parent materials, soil forming processes, and new insights into the palaeclimate of the Eastern Himalayas*. Kommission für Geomorphologie der Bayerischen Akademie der Wissenschaften (ed.); Relief, Boden, Klima (Band 22). Gebrüder Borntraeger, Berlin/Stuttgart: 128 pp.

Castelli, S. 2000. *Geomorphologische Kartierung im Gebiet Julierpass, Val Suvretta und Corvatsch (Oberengadin, GR), sowie Versuche zur Relativdatierung der morphologischen Formen mit der Schmidt-Hammer Methode*. Diploma thesis, University of Zurich, Switzerland. Unpublished.

Cerling, T.E., Craig, H. 1994. *Geomorphology and in-situ cosmogenic isotopes*. Annual Review of Earth an Planetary Sciences 22: 273-317.

Chadwick, O.A., Brimhall, G.H., Hendricks, D.M. 1990. *From a black to a grey box - A mass balance interpretation of pedogenesis*. Geomorphology 3: 369-390.

Chinn, T.J.H. 1981. *Use of rock weathering-rind thickness for Holocene absolute age-dating in New Zealand*. Arctic and Alpine Research 13: 33-45.

Clark, R.N., Roush, T. L. 1984. *Reflectance spectroscopy: Quantitative analysis techniques for remote sensing applications*. Journal of Geophysical Research 89(B7): 6329–6340.

Coaz, J.W.F. 1850. Blatt XX, Unterabthlg. 2, 1:50,000 (Original Messtischblatt). Archiv-Nr. L+T 468. Schweiz. Eidg. Stabsbureau, Bern.

Cockburn, H.A.P., Summerfield, M.A. 2004. *Gemorphological applications of cosmogenic isotope analysis*. Progress in Physical Geography 28: 1-42.

Colman, S.M., Pierce, K.L. 1981. *Weahtering rinds on andesitic and basaltic stones as a Quaternary age indicator, western United States*. US Geological Survey Professional Paper 1210.

Compeer, M. 2009. *Datierung von Blockgletschern und Bodenentwicklung auf spätglazialen Oberflächen. Geomorphologische und bodenkundliche Untersuchungen im Gebiet des Albulapasses*. Diploma thesis, University of Zurich, Switzerland. Unpublished.

Cornelius, H.P. 1929. Geologische Karte der Err-Julier-Gruppe, Spezialkarte Nr. 115.

Cornelius, H.P. 1935. Geologie der Err-Julier-Gruppe. Beiträge zur Geolog. Karte der Schweiz, 1. Teil (Das Baumaterial).

Cornelius, H.P. 1950. Geologie der Err-Julier-Gruppe. Beiträge zur Geologischen Karte der Schweiz, 2. Teil (Der Gebirgsbau).

Cossart, E., Braucher, R., Fort, M., Bourlès, D.L., Carcaillet, J. 2008. Slope instability in relation to glacial debuttressing in alpine areas (Upper Durance catchment, southeastern France): Evidence from field data and ^{10}Be cosmic ray exposure ages. Geomorphology 95: 3-26.

Cossart, E., Fort, M., Bourles, D., Carcaillet, J., Perrier, R., Siame, L., Braucher, R., 2010. Climatic significance of glacier retreat and rockglaciers re-assessed in the light of cosmogenic dating and weathering rind thickness in Clarée valley (Brianconnais, French Alps). Catena 80, 204-219.

Couterrand, S., Buoncristiani, J.F. 2006. *Paléogeographie du dernier macimum glaciere du Pleistocène de la Region du Mont Blanc, France*. Quartenaire 17(1): 35-43.

Crouvi, O., Ben-Dor, E., Beyth, M., Avigad, D., Amit, R. 2006. *Quantitative mapping of arid alluvial fan surfaces using field spectrometer and hyperspectral remote sensing*. Remote Sensing of Environment 104: 103-117.

Cruden, D.M., Hu, X.Q. 1993. *Exhaustion and steady-state models for predicting landslide hazards in the Canadian Rocky Mountains*. Geomorphology 8: 279-285.

Dahms, D.E. 2004. *Relative and numeric age data for pleistocene glacial deposits and diamictons in and near Sinks Canyon, Wind River Range, Wyoming, U.S.A.* Arctic, Antarctic, and Alpine Research 36(1): 59-77.

Dapples, F., Oswald, D., Raetzo, H., Lardelli, T., Zwahlen, P. 2003. *New records of Holocene landslide activity in the Western and Eastern Alps: Implication of climate and vegetation changes*. Eclogae Helvetiae Geologicae 96: 1-9.

Davis, P.T., Bierman, P.R., Marsella, K.A., Caffee, M.W., Southon, J.R. 1999. *Cosmogenic analysis of glacial terrains in the eastern Canadian Arctic: a test for inherited nuclides and the effectiveness of glacial erosion*. Annals of Glaciology 28: 181-188.

Day, M.J., Goudie, A.S. 1977. *Field assessment of rock hardness using the Schmidt hammer*. British Geomorphological Research Group, Technical Bulletin 18: 19-29.

Delaloye, R., Perruchoud, E., Avian, M., Kaufmann, V., Bodin, X., Hausmann, H., Ikeda, A., Kääb, A., Kellerer-Pirklbauer, A., Krainer, K., Lambiel, C., Mihajlovic, D., Staub, B., Roer, I. & Thibert, E. 2008. *Recent interannual variations of rockglaciers creep in the European Alps*. Proceedings of the Ninth International Conference on Permafrost, July 2008, Fairbanks, Alaska, 1: 343-348.

Deline, P. 2001. *Recent Brenva rock avalanches (Valley of Aosta): New chapter in an old story?* Suppl. Geogr. Fis. Dinam. Quat. 5: 55-63.

Deline, P. 2009. *Interactions between rock avalanches and glaciers in the Mont Blanc massif during the late Holocene*. Quaternary Science Reviews 28: 1070-1083.

Deline, P., Kirkbride, M.P. 2009. *Rock avalanches on a glacier and morainic complex in Haut Val Ferret (Mont Blanc massif, Italy)*. Geomorphology 103: 80-92.

Deline, P., Coviello, V., Cremonese, E., Gruber, S., Krautblatter, M., Jaillet, S., Malet, E., Morra Di Cella, U., Noetzli, J., Pogliotti, P., Rabatel, A., Ravanel, L., Sadier, B., Verleysdonk, S. 2009. *L'Aiguille du Midi (Massif du Mont Blanc) – Un site remarquable pour l'étude du permafrost des parois d'altitude*. In: Collection EDYTEM 8, Cahiers de Géographie, Neige et glace de montagne – Reconstitution, dynamique, pratiques: 135-146.

Desaules, A., Dahinden, R. 2000. *Nationales Bodenbeobachtungsnetz. Veränderungen von Schadstoffgehalten nach 5 und 10 Jahren*. Bundesamt für Umwelt, Wald und Landschaft (BUWAL), Schriftenreihe Umwelt Nr. 320, Bern.

Dixon, J.C., Thorn, C.E. 2005. *Chemical weathering and landscape development in mid-latitude alpine environments*. Geomorphology 67: 127-145.

Duller, G.A.T. 1995. *Luminescence dating using single aliquots: methods and applications*. Radiation measurements 24(3): 217-226.

Duller, G.A.T. 2007. Software ANALYST 3.24.

Duller, G.A.T. 2008. *Single-grain optical dating of Quaternary sediments: why aliquot size matters in luminescence dating*. Boreas 37: 589-612.

Dunne, J., Elmore, D., Muzikar, P. 1999. *Scaling factors fot the rates of production of cosmogenic shielding and attenuation at depth on sloped surfaces*. Geomorphology 27: 3-11.

Dorren, L.K.A. 2003. *A review of rockfall mechanics and modelling approaches*. Progress in Physical Geography 27,1: 69-87.

Eggenberger, U. 1995. *Mineral weathering in soils: experiments, field studies, and modeling*. PhD thesis, University of Berne, Switzerland.

Egli, M., Fitze, F. 2000. *Formulation of pedoligic mass balance based on immobile elements: a revision*. Soil Science 165(5):437-443.

Egli, M., Fitze, P., Mirabella, A. 2001. *Weathering and evolution of soils formed on granitic, glacial deposits: results from chronosequences of Swiss alpine environments*. Catena 45: 19-47.

Egli, M., Mirabella, A., Fitze, P. 2003. *Formation rates of smectites derived from two Holocene chronosequences in the Swiss Alps*. Geoderma 117: 81-98.

Egli, M., Mirabella A., Sartori, G., Giaccai, D., Zanelli R. 2007. *Effect of slope and aspect on transformation of clay minerals in alpine soils*. Clay Minerals 42: 375-401.

Egli, M., Brandovà, D., Böhlert, R., Favilli, F., Kubik, P.W. 2010. *^{10}Be inventories in Alpine soils and their possibilities for dating land surfaces*. Geomorphology, accepted.

Engel, Z. 2007. *Measurement and age assignement of intact rock strength in the Krkonose Mountains, Czech Republic*. Annals of Geomorphology 51(Suppl. 1): 69-80.

Erismann, T.H., Abele, G. 2001. *Dynamics of rockslides and rockfalls*. Springer.

Etienne, S. 2002. *The role of biological weathering in periglacial areas: a study of weathering rinds in south Iceland*. Geomorphology 47: 75-86.

Eusterhues, K., Rumpel, C., Kleber, M., Kögel-Knabner, I. 2003. *Stabilization of soil organic matter by interactions with minerals as revealed by mineral dissolution and oxidative degradation*. Organic Geochemistry 34: 1591-1600.

Fabel, D., Harbor, J. 1999. *The use of in-situ produced cosmogenic radionuclides in glaciology and glacial geomorphology*. Annals of Glaciology 28: 103-110.

Fabel, D., Stroeven, A.P., Harbor, J., Kleman, J., Elmore, D., Fink, D. 2002. *Landscape preservation under Fennoscandian ice sheets determined from in situ produced ^{10}Be and ^{26}Al*. Earth and Planetary Science Letters 201: 397-406.

Fallon, P.D., Smith, P. 2000. *Modelling refractory soil organic matter*. Biology and Fertility of Soils 30: 388-398.

Favilli, F., Egli, M., Cherubini, P., Sartori, G., Haeberli, W., Delbos, E. 2008. *Comparison of different methoes obtaining a resilient organic matter fraction in Alpine soils*. Geoderma 145: 355-369.

Favilli, F., Egli, M., Brandovà, D., Ivy-Ochs, S., Kubik, P.W., Maisch, M., Cherubini, P., Haeberli, W. 2009a. *Combination of numerical dating techniques using ^{10}Be in rock boulders and ^{14}C in resilient soil organic matter for reconstructing glacial and periglacial processes in a high alpine catchment during the late Pleistocene and early Holocene*. Radiocarbon 51(2): 537-552.

Favilli, F., Egli, M., Brandovà, D., Ivy-Ochs, S., Kubik, P.W., Cherubini, P., Mirabella, A., Sartori, G., Giaccai, D., Haeberli, W. *Combined use of relative and absolute dating techniques for detecting signals of Alpine landscape evolution during the late Pleistocene and early Holocene*. Geomorphology 112: 48-66.

Federici, P.R., Granger, D.E., Pappalardo, M., Ribolini, A., Spagnolo, M., Cyr, A.J. 2008. *Exposure age dating and Equilibrium Line Altitude reconstruction of an Egesen moraine in the Maritime Alps, Italy*. Boreas 37: 245-253.

Fiebig, M., Preusser, F. 2008. *Pleistocene glaciations of the northern Alpine Foreland*. Geographica Helvetica 3: 145-150.

Fischer, L., Kääb, A., Huggel, C. Noetzli, J. 2006. *Geology, glacier retreat and permafrost degradation as controlling factors of slope instabilities in a high-mountain rock wall: Monte Rosa east face*. Natural Hazards and Earth System Science 6: 761-772.

Fischer, L. 2009. *Slope Instabilities on Perennially Frozen and Glacierised Rock Walls: Multi-Scale Observations, Analyses and Modelling*. PhD Thesis, Department of Geography, University of Zurich, Zurich: 218 p.

Fitze, P. 1982. *Zur Relativdatierung von Moränen aus Sicht der Bodenentwicklung in den kristallinen Zentralalpen*. Catena 9: 265-306.

Florineth, D. 1998. *Surface geometry of the Last Glacial Maximum (LGM) in the southeastern Swiss Alps (Graubünden) ant its paleoclimatic significance*. Eiszeitalter und Gegenwart 48: 23-37.

Florineth, D., Schlüchter, S. 1998. *Reconstructing the Last Glacial Maximum (LGM) ice surface geometry and flowlines in the Central Swiss Alps*. Eclogae geologicae Helvetiae 91: 391-407.

Florineth, D., Schlüchter, S. 2000. *Alpine evidence for atmospheric circulation patterns in Europe during the Last Glacial Maximum*. Quaternary Research 54: 295-308.

FOEN (Federal Office for the Environment). 2005. Hinweiskarte der potentiellen Permafrostverbreitung in der Schweiz, Blatt Julierpass. Map of the potential permafrost distribution of Switzerland, map sheet Julierpass.

Frauenfelder, R., Kääb, A. 2000. *Towards a palaeclimatic model of rock glacier formation in the Swiss Alps*. Annals of Glaciology 31: 281-286.

Frauenfelder, R., Haeberli, W., Hoelzle, M., Maisch, M. 2001. *Using relict rockglaciers in GIS-based modelling to reconstruct Younger Dryas permafrost distribution patterns in the Err-Julier area, Swiss Alps*. Norsk Geologisk Tidsskrift 55: 195-202.

Frauenfelder, R., Laustela, M., Kaeaeb, A. 2005. *Relative age dating of Alpine rockglacier surfaces*. Annals of Geomorphology 49(2): 145-166.

Frauenfelder, R. 2005. *Regional-scale modelling of the occurrence and dynamics of rockglaciers and the distribution of paleopermafrost*. Haeberli, W., Maisch M. (eds.), Schriftenreihe Physische Geographie 45. Institute of Geography, University of Zurich.

Frauenfelder, R., Schneider, B., Kääb, A. 2008a. *Using dynamic modelling to simulate the distribution of rockglaciers*. Geomorphology 93: 130-143.

Frauenfelder, R., Hauck, C., Hilbich, C., Kneisel, C., Hoelzle, M. 2008b. *An integrative observation of kinematics and geophysical parameters of Gianda Grischa rock glacier, Upper Engadine, Swiss Alps*. In: Proceedings of the 9th International Conference on Permafrost, University of Alaska, Fairbanks: 463-468.

Fuchs, M., Lewis, A.O. 2008. *Luminescence dating of glacial and associated sediments: review, recommendations and future directions*. Boreas 37: 636-659.

Furbish, D. J., Andrews, J.T. 1984. *The use of hypsometry to indicate long-term stability and response of valley glaciers to changes in mass transfer*. Journal of Glaciology 30 (105): 199-221.

Gjems, O. 1967. *Studies on clay minerals and clay mineral formation in soil profiles in Scandinavia*. Norske Skogfersøksvesen 81: 301-415.

Glen, J.W. 1955. The creep of polycrystalline ice. Proceedings of the Royal Society of London 228(1175): 519-538.

Goodman, A.Y., Rodbell, D.T., Seltzer, G.O., Mark, B.G. 2001. *Subdivision of glacial deposits in southeaster Peru based on pedogenetic development and radiometric ages*. Quaternary Research 56: 31-50.

Golledge, N.R., Fabel, D., Everest, J.D., Freeman, S., Binnie, S. 2007. *First cosmogenic ^{10}Be age constraint on the timing of Younger Dryas glaciation and ice cap thickness, western Scottish Highlands*. Journal of Quaternary Science 22(8): 785-791.

Gordon, S.J., Dorn, R.I. 2005. *In situ weathering rind erosion*. Geomorphology 67: 97-113.

Gosse, J.C., Phillips, F.M. 2001. *Terrestrial in situ produced cosmogenic nuclides: Theory and application*. Quaternary Science Reviews 20: 1475-1560.

Gosse, J. 2005. *The contributions of cosmogenic nuclides to unraveling alpine paleo-glacier histories*. In: Huber, U., Bugmann, H., Reasoner, M. (eds.), Global Change in Mountain Regions: A state of Knowledge Overwiev. Springer, Switzerland: 39-50.

Graf, H.R. 1993. *Die Deckenschotter der zentralen Nordschweiz*. PhD thesis, ETH Zurich, Switzerland, No. 10205.

Graf, A.A., Strasky. S., Ivy-Ochs, S., Akçar, N., Kubik, P.W., Burkhard, M., Schlüchter, C. *First results of cosmogenic dated pre-Last Glaciation erratics from the Montoz area, Jura Mountains, Switzerland*. Quaternary International 164-165:43-52.

Graf, M. 2010. Altersbestimmung an neuzeitlichen Moränen mit Hilfe physisch-geographischer Datierungsmethoden im Berninagebiet (working title). Diploma thesis, University of Zurich, Switzerland. In preparation.

Granger, D.E., Clifford, S.R., Kirchner, J.W., Finkel, R.C. 2001. *Modulation of erosion on steep granitic slopes by boulder armouring, as revealed by cosmogenic ^{26}Al and ^{10}Be*. Earth and Planetary Science Letters 186: 269-281.

Granger, D.E. 2006. *A review of burial methods using ^{26}Al and ^{10}Be*. Geological Society of America Special Papers 415: 1-16.

Green, A.A., Craig, M.D. 1985. *Analysis of aircraft spectrometer data with logarithmic residuals*. In: Proceedings, AIS workshop, 8-10 April, 1985, JPL Publication 85-41, Jet Propulsion Laboratory, Pasadena, California: 111–119.

Grisch, A. 1907. Beiträge zur Kenntnis der pflanzengeographischen Verhältnisse der Bergünerstöcke In: Uhlworm, O., Schinz, H (eds), Beihefte zum Botanischen Centralblatt, Band XXII. Verlag C. Heinrich, Dresden, Germany: 255-316.

Gross, G., Kerschner, H., Patzelt, G. 1977. *Methodische Untersuchungen über die Schneegrenze in alpinen Gletschergebieten*. Zeitschrift für Gletscherkunde und Glazialgeologie 12: 223-251.

Gruber, S., Schläpfer, D., Hoelzle, M. 2003. *Imaging spectrometry in high-alpine topography: the derivation of accurate broadband albedo*. Proceedings of the the 3rd EARSeL Workshop on Imaging Spectroscopy, Oberpfaffenhofen, Germany, 13–16 May 2003: 10pp.

Gruber, S., Hoelzle, M., Haeberli, W. 2004a. *Permafrost thaw and destabilization of Alpine rock walls in the hot summer of 2003*. Geophysical Research Letters 31((L13504)). doi:10.1029/2004GL0250051.

Gruber, S., Hoelzle, M., Haeberli, W. 2004b. *Rock-wall temperatures in the Alps: Modelling their topographic distribution and regional differences*. Permafrost and periglacial processes 15: 299-307.

Gruber, S., Haeberli, W. 2007. *Permafrost in steep bedrock slopes and its temperature-related destabilization following climate change*. Journal of Geophysical Research 112: F02S18, doi:10.1029/2006JF000547.

Gruner, U. 2006. *Bergstürze und Klima in den Alpen – gibt es Zusammenhänge?* Bulletin für angewandte Geologie 11/2: 25-34.

Gude, M., Barsch, D. 2005. *Assessment of gemorphic hazards in connection with permafrost occurrence in the Zugspitze area (Bavarian Alps, Germany)*. Geomorphology 66: 85-93.

Haeberli, W. 1975. *Untersuchungen zur Verbreitung von Permafrost zwischen Flüelapass und Piz Grialetsch (Graubünden)*. Mitteilungen VAW Nr. 17, ETH Zürich, Zürich.

Haeberli, W. 1985. *Creep of mountain permafrost: internal structure and flow of alpine rock glaciers*. Mitteilungen der Versuchsanstalt für Wasserbau, Hydrologie und Glaziologie, ETH Zurich, No. 77.

Haeberli, W. 1982. *Klimarekonstruktionen mit Gletscher-Permafrost-Beziehungen*. Materialien zur Physiogeographie 4: 9-17.

Haeberli, W., Penz, U. 1985, *An attempt to reconstruct glaciological and climatological characteristics of 18 ka ice age in and around the Swiss Alps*. Zeitschrift für Gletscherkunde und Glazialgeologie 21: 351-361.

Haeberli, W. 1986. *Hydraulic effects at the glacier bed and related phenomena*. In: Mitteilungen VAW No. 90, ETH Zurich, Switzerland.

Haeberli, W., Hoelzle, M. 1995. *Application of inventory data for estimating characteristics of and regional climate-change effects on mountain glaciers: a pilot study with the European Alps*. Annals of Glaciology 21: 206-212.

Haeberli, W., Wegmann, M., Vonder Mühll, D. 1997. *Slope stability problems related to glacier shrinkage and permafrost degradation in the Alps*. Eclogae Geologicae Helvetiae 90: 407–414.

Haeberli, W., Hoelzle, M., Kääb, A., Keller, F., Vonder Mühll, D., Wagner, S. 1998. *Ten years after drilling through the permafrost of the active rock glacier Murtèl, Eastern Swiss Alps: answered questions and new perspectives*. Proceedings of the 7th International Conference of Permafrost, Yellowknife, Collection Nordicana 57: 403-410.

Haeberli, W., Kääb., A., Wagner, S., Vonder Mühll, D., Geissler, R., Haas, J.N., Glatzel-Mattheier, H., Wagenbach, D. 1999. Pollen analysis and ^{14}C age of moss reimains in a permafrost core recovered from the active rock glacier Murtèl-Corvatsch, Swiss Alps: geromorphological and glaciological implications. Journal of Glaciology 45(149): 1-8.

Haeberli, W., Brandovà, D., Burga, C., Egli, M., Frauenfelder, R., Kääb, A., Maisch, M. 2003. *Methods for absolute and relative age dating of rock-glacier surfaces in alpine permafrost*. In: Phillips, M., Springman, S., Arenson, L. (eds.), Proceedings of the 8th International Conference on Permafrost 2003, Zurich. Swets & Zeitlinger, Lisse: 343-348.

Haeberli, W., Hallet, B., Arenson, L., Elconin, R., Humlum, O., Kääb, A., Kaufmann, V., Ladanyi, B., Matsouka, N., Springman, S., Vonder Mühll, D. 2006. *Permafrost creep and rock glacier dynamics*. Permafrost and periglacial processes 17: 189-214.

Hajdas, I. 2008. *Radiocarbon dating and its applications in Quaternary studies*. Quaternary Science Journal 57(1/2): 2-24.

Hallet, B., Putkonen, J. 1994. *Surface Dating of Dyfnamic Landforms: Young Boulders on Aging Moraines*. Science 265: 937-940.

Harbor, J., Stroeven, A.P., Fabel, D., Clarhäll, A., Kleman, J., Li, Y., Elmore, D., Fink, D. 2006. *Cosmogenic nuclide evidence for minimal erosion across two subglacial sliding boundaries of the late glacial Fennoscandian ice sheet*. Geomorphology 75: 90-99.

Harden, J.W. 1982. *A quantitative index of soil development from field descriptions: examples from a chronosequence in central California*. Geoderma 28: 1-28.

Harris, C., Arenson, L.U., Christiansen, H.H., Etzelmüller, B., Frauenfelder, R., Gruber, S., Haeberli, W., Hauck, C., Hölzle, M., Humlum, O., Isaksen, K., Kääb, A., Kern-Lütschg, M.A., Lehning, M., Matsuoka, N., Murton, J.B., Nötzli, J., Phillips, M., Ross, N., Seppälä, M., Springman, S.M., Vonder Mühll, D. 2009. *Permafrost and climate in Europe: Monitoring and modelling thermal, geomorphological and geotechnical responses*. Earth Science Reviews 92: 117-171.

Häuselmann, Ph., Fiebig, M., Kubik, P.W., Adrian, H. 2007. *A first attempt to date the original "Deckenschotter" of Penck and Brückner with cosmogenic nuclides*. Quaternary International 164-165: 33-42.

Heierli, H. 1955. Geologische Untersuchungen in der Albulazone zwischen Crap Alv und Cinuoschel (Graubünden). Beiträge zur geologischen Karte der Schweiz, 101. Lieferung, Bern.

Heikkilä, U., Beer, J., Feichter, J. 2008. *Modeling cosmogenic radionuclides ^{10}Be and ^{7}Be during the Maunder Minimum using ECHAM5-HAM general circulation model*. Atmospheric Chemistry and Physics 8: 2797-2809.

Heuberger, H. 1966. *Gletschergeschichtliche Untersuchungen in den Zentralalpen zwischen Sellrain und Ötztal*. Wissenschaftliche Alpenvereinshefte 20. Universitätsverlag Wagner, Innsbruck.

Hippolyte, J.C., Bourlès, D., Braucher, R., Carcaillet, J., Léanni, L., Arnold, M., Aumaitre, G. 2009. *Cosmogenic ^{10}Be dating of a sackung ant its faulted rock glaciers, in the Alps of Savoy (France)*. Geomorphology 108: 312-320.

Hitz, C., Egli, M., Fitze, P. 2002. *Determination of the sampling volume for representative analysis of alpine soils*. Zeitschrift für Pflanzenernährung und Bodenkunde 165: 326-331.

Horiuchi, K., Minoura, K., Kobayashi, K., Nakamura, T., Hatori, S., Matsuzaki, H., Kawai, T., 1999. *Last-glacial to post-glacial ^{10}Be fluctuations in a sediment core from the Academician Ridge, Lake Baikal*. Geophysical Research Letters 26: 1047–1050.

Hormes, A., Ivy-Ochs, S., Kubik, P.W., Ferreli, L., Michetti, A.M. 2008. *^{10}Be exposure ages of a rock avalanche and a late glacial moraine in Alta Valtellina, Italian Alps*. Quaternary International 190: 136-145.

Huggett, R.J. 2003. *Fundamentals of Geomorphology*. Gerrard, J. (ed.), Routledge Fundamentals of Physical Geography Series, London and New York: 386 pp.

Huh, K.I., Csatho, B., van der Veen, C.J., Ahn, Y. 2006. *Reconstructing Holocene glacier changes in west Greenland from Multispectral ASTER imagery*. EOS, 87, Fall Meeting Supplement, Abstract C11A-1134.

Humlum, O. 1996. *Origin of rock glaciers: observations from Mellemfjord, Disko Island, central West Greenland*. Permafrost and Periglacial Processes 7: 361-380.

Humlum, O. 1997. *Active layer thermal regime at three rock glaciers in Greenland*. Permafrost and Periglacial Processes 8: 383-408.

Humlum, O. 1998. *The Climatic Significance of Rock Glaciers*. Permafrost and Periglacial Processes 9: 375-395.

Humphrey, N.F., Kamb, B., Fahnenstock, M., Engelhardt, H. 1993. *Characteristics of the bed of the lower Columbia Glacier, Alaska*. Journal of Geophysical Research 98: 837-846.

Hungr, O., Evans, S.G., Bovis, M.J., Hutchinson, J.N. 2001. A review of the classification of landslides of the flow type. Environmental & Engineering Geoscience 7(3): 221-238.

Huntley, D.J., Godfrey-Smith, D.I., Thewalt M.L.W. 1985. *Optical dating of sediments*. Nature 313: 105-107.

Huntley, D.J., Baril, M.R. 1997. The K content of the K-feldspars being measured in optical dating or in thermoluminescence dating. Ancient TL 15(1): 11 – 13.

Hütt, G., Jaek, I., Tchonka, J. 1988. *Optical dating – K-feldspars optical-response stimulations spectra*. Quaternary Science Reviews 7: 381-385.

Hydrologischer Atlas der Schweiz (HADES). 2004. Landeshydrologie, Bundesamt für Wasser und Geologie (ed.).

Ikeda, A., Matsuoka, N. 2006. *Pebbly versus bouldery rock glaciers: Morphology, structure and porcesses*. Geomophology 73: 279-296.

International Stratigraphic Chart. 2009. Published by the International Comission on Stratigraphy (ICS).

IPCC. 2007. *Climate Change 2007: The Physical Science Basis. Contribution of Working Group 1 to the Fourth Assessment Report of the Intergovernmental Panel on Climate Change*. Solomon, S., Qin, D., Manning, M., Chen, Z., Marquis, M.C., Averyt, K., Tignor, M., Miller, H.L. (eds.), Intergovernmental Panel on Climate Change, Cambridge and New York.

Ivy-Ochs, S. 1996. *The dating of rock surfaces using in situ produced ^{10}Be, ^{26}Al and ^{36}Cl, with examples from Antarctica and the Swiss Alps*. PhD thesis, ETH Zurich, Switzerland, No. 11763.

Ivy-Ochs, S., Schlüchter, C., Kubik, P.W., Synal, H.A., Beer, J., Kerschner, H. 1996. *The exposure ages of an Egesen moraine at Julier Pass, Switzerland, measured with the cosmogenic radionuclides ^{10}Be, ^{26}Al and ^{36}Cl*. Eclogae geologicae helvetiae 89(3): 1049-1063.

Ivy-Ochs, S., Heuberger, H., Kubik, P.W., Kerschner, H., Bonani, G., Frank, M., Schlüchter, C. 1998. *The age of the Köfels event: relative, ^{14}C, and cosmogenic isotope dating of an early Holocene landslide in the Central Alps (Tyrol, Austria)*. Zeitschrift für Gletscherkunde und Glazialgeologie 34(1): 57-68.

Ivy-Ochs, S., Schäfer, J., Kubik, P.W., Synal, H.A., Schlüchter, C. 2004. *The timing of deglaciation on the northern Alpine foreland (Switzerland)*. Eclogae Geologicae Helvetiae 97: 47-55.

Ivy-Ochs, S., Kerschner, H., Reuther, A., Maisch, M., Sailer, R., Schaefer, J., Kubik, P.W., Synal, H.A., Schlüchter, C. 2006a. *The timing of glacier advances in the northern European Alps based on surface exposure dating with cosmogenic ^{10}Be, ^{26}Al, ^{36}C and ^{21}Ne*. In: Siame, L.L., Bourlès, D.L., Brown, T.T. (eds.), In Situ-Produced Cosmogenic Nuclides and Quantification of Gelogical Processes. Geological Society of America Special Paper 415, Geological Society of America: 43-60.

Ivy-Ochs, S., Kerschner, H., Kubik, P.W., Schlüchter, C. 2006b. *Glacier response in the European Alps to Heinrich Event 1 cooling: the Gschnitz stadial*. Journal of Quaternary Science 21(2): 115-130.

Ivy-Ochs, S., Kerschner, H., Schlüchter, C. 2007. *Cosmogenic nuclides and the dating of Lateglacial and Early Holocene glacier variations: The Alpine perspective*. Quaternary international 164–165: 53-63. doi: 10.1016/j.geomorph.2007.10.024

Ivy-Ochs, S., Kerschner, H., Reuther, A., Preusser, F., Heine, K., Maisch, M., Kubik, P.W., Schlüchter, C. 2008. *Chronology of the last glacial cycle in the European Alps*. Journal of Quaternary Science 23(6-7): 559-573.

Ivy-Ochs, S., Kober, F. 2008. *Surface exposure dating with cosmogenic nuclides*. Quaternary Science Journal 57(1-2): 179-209.

Ivy-Ochs, S., Kerschner, H., Maisch, M., Christl, M., Kubik, P.W., Schlüchter, C. 2009a. *Latest Pleistocene and Holocene glacier variations in the European Alps*. Quaternary Science Reviews 28: 2137-2149. Doi:10.1016/j.quascirev.2009.03.009

Ivy-Ochs, S., Poschinger, A.V., Synal, H.A., Maisch, M. 2009b. *Surface exposure dating of the Flims landslide, Graubünden, Switzerland*. Geomorphology 103: 104-112.

Ivy-Ochs, S., Schaller, M., 2010. *Examining processes and rates of landscape change with cosmogenic radionuclides*. In: Froehlich, K. (ed.), Environmental Radionuclides: Tracers and Timers of Terrestrial Processes. Elsevier (in press).

Jäckli, H. 1957. *Gegenwartsgeologie des bündnerischen Rheingebietes. Ein Beitrag zur exogenen Dynamik alpiner Gebirgslandschaften*. Schweizerische Geotechnische Kommission (ed.), Geotechnische Serie, Lieferung 36. Kümmerly & Frey, Bern: 136 pp.

Jäckli, H. 1970. *Die Schweiz zur letzten Eiszeit*. Atlas der Schweiz, map 6, Wabern-Bern, Eidg. Landestopographie.

Jenkins, R. 1999. *X-ray Fluorescence Spectrometry*. 2nd edition, Wiley-VCH.

Jenny, H. 1941. Factors of Soil Formation. McGraw-Hill, New York.

Jenny, H. 1980. The Soil Resource. Springer, New York.

Johannesson, T., Raymond, C., Waddington, E. 1989. *Time-scale for adjustment of glaciers to changes in mass balance*. Journal of Glaciology 35(121): 355-369.

Kääb, A., Haeberli, W., Gudmundsson, G.H. 1997. *Analysing the creep of mountain permafrost using high precision aerial photogrammetry: 25 Years of monitoring Gruben rock glacier, Swiss Alps*. Permafrost and Periglacial Processes 8: 409-426.

Kääb, A., Frauenfelder, R. 2001. *Temporal variations of mountain permafrost creep*. In; Harris, C. (ed.), 1st European Permafrost Conference, Rome, Abstracts 56.

Kääb, A., Gudmundsson, G.H., Hoelzle M. 1998. *Surface deformation of creeping mountain permafrost. Photogrammetric investigations on rock glacier Murtèl, Swiss Alps*. Proceedings of the 7th International Permafrost Conference, Yellowknife, Canada. Collection Nordicana, Centre d'études nordiques, Université Laval: 531-537.

Kääb, A. 2005. *Remote sensing of mountain glaciers and permafrost creep*. Physische Geographie 48, University of Zurich, Switzerland.

Kääb, A., Huggel, C., Fischer, L., Guex, S., Paul, F., Roer, I., Salzmann, N., Schlaefli, S., Schmutz, K., Schneider, D., Strozzi, T., Weidmann, Y. 2005. *Remote sensing of glacier- and permafrost-related hazards in high mountain: an overview*. Natural Hazards and Earth System Sciences 23: 1-28.

Kääb, A., Frauenfelder, R., Roer, I. 2007. *On the response of rockglacier creep to surface temperature increase*. Global and Planetary Change 56: 172-187.

Kahle, M., Kleber, M., Jahn, R., 2002. *Review of XRD-based quantitative analyses of clay minerals in soils: the suitability of mineral intensity factors*. Geoderma 109: 191-205.

Keller, O., Krayss, E. 1993. *The Rhine-Linth Glacier in the upper Würm: A model of the last Alpine glaciation*. Quaternary International 18: 15-27.

Keller, O., Krayss, E. 2005. *Der Rhein-Linth-Gletscher im letzten Hochglazial*. Vierteljahresschrift der Naturforschenden Gesellschaft in Zürich 150(1-2): 19-32.

Kellerer-Pirklbauer, A., Wangensteen, B., Farbrot, H., Etzelmüller, B. 2008. *Relative surface age-dating of rock glacier systems near Hólar in Hjaltadalur, northern Iceland*. Journal of Quaternary Science 23(2): 137-151.

Kellerer-Pirklbauer, A. 2008. *The Schmidt-Hammer as a Relative Age Dating Tool for Rock Glacier Surfaces: Examples from Northern and Central Europe*. In: Proceedings of the 9th International Conference on Permafrost, University of Alaska, Fairbanks: 913-918.

Kelly, M.A., Buoncristiani, J.-F., Schlüchter, C. 2004a. *A reconstruction of the last glacial maximum (LGM) ice-surface geometry in the western Swiss Alps and contiguous Alpine regions in Italy and France*. Eclogae geol. Helv. 97: 57-75.

Kelly, M.A., Kubik, P.W., von Blanckenburg, F., Schlüchter, C. 2004b. *Surface exposure dating of the Great Aletsch Glacier Egesen moraine system, western Swiss Alps, using the cosmogenic nuclide ^{10}Be*. Journal of Quaternary Science 19: 431-441.

Kelly, M.A., Ivy-Ochs, S., Kubik, P.W., von Blanckenburg, F., Schlüchter, C. 2006. *Chronology of deglaciation based on ^{10}Be dates of glacial erosional features in the Grimsel Pass region, central Swiss Alps*. Boreas 35: 634-643.

Kerschner, H., Berktold, E. 1982. *Spätglaziale Gletscherstände und Schuttformen im Senderstal, nördliche Stubaieralpen, Tirol*. Zeitschrift für Gletscherkunde und Glaziologie 17: 125-134.

Kerschner, H. 1986. *Zum Sendersstadium im Spätglazial der nördlichen Stubaier Alpen, Tirol*. Zeitschrift für Geomorphologie Supplement 61: 65-76.

Kerschner, H., Ivy-Ochs, S., Schlüchter, C. 1999. *Paleoclimatic interpretation of the early late-glacial glacier in the Gschnitz valley, Central Alps, Austria*. Annals of Glaciology 28: 135-140.

Kerschner, H. 2002. *Gletscher-Klima-Beziehungen als klimageschichtliche Werkzeuge – ein Vergleich verschiedener Ansätze*. Grazer Schriften der Geographie und Raumforschung 38, Graz.

Kerschner, H., Hertl, A., Gross, G., Ivy-Ochs, S., Kubik, P.W. 2006. *Surface exposure dating of moraines in the Kromer valley (Silvretta mountains, Austria) – evidence for glacial response to the 8.2 ka event in the Eastern Alps*. The Holocene 16(1): 7-15.

Kerschner, H., Ivy-Ochs, S. 2008. *Palaeoclimate from glaciers: Examples from the Eastern Alps during the Alpine Lateglacial and early Holocene*. Global and Planetary Change 60: 58-71.

Khodakov, V.G. 1975. *Glaciers as water resource indicators of the glacial areas of the USSR*. International Association of Hydrological Sciences Publication 104: 22-29.

Klok, E.J., Oerlemans, J. 2002. *Model study of the spatial distribution of the energy and mass balance of Morteratschgletscher, Switzerland*. Journal of Glaciology 48(163): 505-518.

Kneisel, C., Hauck, C., Vonder Mühll, D. 2000. *Permafrost below the Timberline Confirmed and Characterized by Geoelectrical Resistivity Measurements, Bever Valley, Eastern Swiss Alps*. Permafrost and Periglacial Processes 11: 295-304.

Kneisel, C., Schwindt, D. 2008. *Geophysical mapping of isolated permafrost lenses at a sporadic permafrost site at low altitude in the Swiss Alps*. In: Proceedings of the 9th International Conference on Permafrost, University of Alaska, Fairbanks: 959-964.

Kohl, C.P., Nishiizumi, K. 1992. *Chemical isolation of quartz for measurement of in-situ produced cosmogenic nuclides*. Geochimica et Cosmochimica Acta 56: 3583-3587.

Kohler, T., Maselli, D. (eds.). 2009. *Mountains and Climate Change – From Understanding to Action*. Geographica Bernensia, Bern, Switzerland.

Konrad, S.K., Humphrey N.F., Steig, E.J., Clark D.H., Potter, N. Jr., Pfeffer, W.T. 1999. *Rock glacier dynamics and paleoclimatic implications*. Geology 27(12): 1131-1134.

Krbetschek, M.R., Götze, J., Dietrich, A. and Trautmann, T. 1997: *Spectral information from minerals relevant for luminescence dating*. In: Wintle, A.G. (ed.), A review on luminescence and electron spin resonance dating and allied research. Radiation Measurements 27: 695-748

Kruse, F.A., Raines, G.L., Watson, K. 1985. *Analytical techniques for extracting geologic information from multichannel airborne spectroradiometer and airborne imaging spectrometer data*. In: Proceedings, International Symposium on Remote Sensing of Environment, Thematic Conference on Remote Sensing for Exploration Geology, 4th, Environmental Research Institute of Michigan, Ann Arbor: 309–324.

Kubik, P.W., Ivy-Ochs, S. 2004. *A re-evaluation of the 0-10 ka ^{10}Be production rate for exposure dating obtained from the Köfels (Austria) landslide*. Nuclear Instruments and Methods in Physics Research B 223-224: 618-622.

Kubik, P.W., Reuther, A.U. 2007. *Attenuation of cosmogenic ^{10}Be production in the first 20 cm below a rock surface*. Nuclear Instruments and Methods in Physics Research B 259: 616-624.

Kubik, P.W., Christl, C., 2009. *^{10}Be and ^{26}Al measurements at the Zurich 6 MV Tandem AMS facility*. Nuclear Instruments and Methods B, doi: 10.1016/j.nimb.2009.10.054

Kuhn, M. 1981. *Climate and Glaciers*. International Association of Hydrological Sciences Publication 131: 3-20

Kulig. 2005. Erstellung einer Auswertesoftware zur Altersbestimmung mittels Lumineszenzverfahren. Faculty Mathematics Informatics TU Freiberg, Germany.

Lal, D., Peters, B. 1967. *Cosmic-ray produced radioactivity on the earth*. In: Handbook of Physics 46(2), Springer, Berlin: 551-612.

Lal, D. 1988. *In situ-produced cosmogenic isotopes in terrestrial rocks*. Annual Review of Earth and Planetary Sciences 16: 355-388.

Lal, D. 1991. *Cosmic ray labeling of erosion surfaces: in-situ nuclide production rates and erosion models*. Earth and Planetary Science Letters 104: 424-439.

Lal, D., Barg, E., Pavich, M. 1991. *Development of cosmogenic neclear methods for the study of soil erosion and formation rates*. Current Science 61: 636-639.

Lal, D., Chen, J. 2005. *Cosmic ray labeling of erosion surfaces II: Special cases of exposure histories of boulders, soils and beach terraces*. Earth and Planetary Science Letters 236: 797-813.

Lang, A., Moya, J., Corominas, J., Schrott, L., Dikau, R. 1999. *Classic and new dating methods for assessing the temporal occurrence of mass movements*. Geomorphology 30: 33-52.

Lanson, B. 1997. *Decomposition of experimental X-ray diffraction patterns (profile fitting): a convenient way to study clay minerals*. Clays and Clay Minerals, 45: 132-146.

Laustela, M. 2003. Messung und Analyse von Verwitterungsrinden zur relativen Altersdatierung ausgewählter Blockgletscher in den Bündner Alpen. Diploma thesis, University of Zurich, Switzerland. Unpublished.

Laustela, M., Egli, M., Frauenfelder, R., Kaeaeb, A., Maisch, M., Haeberli, W. 2003. *Weathering rinds measurements and relative age dating of rockglacier surfaces in crystalline regions of the Eastern Swiss Alps*. In: Phillips, M., Springman, S., Arenson, L. (eds.), Proceedings of the 8th International Concerence on Permafrost 2003, Zurich. Swets & Zeitlinger, Lisse: 627-632.

Laves, D., Jahn, G. 1972. *Zur quantitativen röntgenographischen Bodenton-Mineralanalyse*. Archiv für Acker- und Pflanzenbau und Bodenkunde 16: 735-739.

Lepper, K., McKeever, S.W.S. 2002. *An objective methodology for dose distribution analysis*. Radiation Protection Dosimetry 101(1-4): 349-352.

Li, Y., Fabel, D., Stroeven, A.P., Harbor, J. 2008. *Unraveling complex exposure-burial histories of bedrock surfaces under ice sheets by integrating cosmogenic nuclide concentrations with climate proxy records*. Geomorphology 99: 139-149.

Lian, O.B., Roberts, R.G. 2006. *Dating the Quaternary: progress in luminscence dating of sediments*. Quaternary Science Reviews 25: 2449-2468.

Lister, G.G. 1988. *A 15,000-year isotopic record from Lake Zürich of deglaciation and climatic change in Switzerland*. Quaternary Research 29: 129-141.

Lotter, A.F., Birks, H.J.B., Eicher, U., Hofmann, W., Schwander, J., Wick, L. 2000. *Younger Dryas and Allerød summer temperatures at Gerzensee (Switzerland) inferred from fossil pollen and cladoceran assemblages*. Palaeogeorgraphy, Palaeoclimatology, Palaeoecology 159: 349-361.

Lüthi, M., Funk, M. 1997. *Wie stabil ist der Hängegletscher am Eiger?* Spektrum der Wissenschaft 97(5): 21-24.

Lyell, C. 1830-1833. *Principles of Geology*. 3 volumes, John Murray, London.

Maejima, Y., Matsuzaki, H., Nakano, C. 2004. *^{10}Be concentrations of Red soils in Southwest Japan and its possibility of dating*. Nuclear Instruments and Methods in Physics Research B 223-224: 596-600.

Maejima, Y., Matsuzaki, H., Higashi, T. 2005. *Application of cosmogenic ^{10}Be to dating soils on the raised coral reef terraces of Kikai Island, southwest Japan*. Geoderma 126: 389-399.

Maisch, M. 1981. *Glazialmorphologische und gletschergeschichtliche Untersuchungen im Gebiet zwischen Landwasser- und Albulatal (Kt. Graubünden, Schweiz)*. Physische Geographie 3. Dissertation, Dept. of Geography, University of Zurich, Switzerland.

Maisch, M. 1987. *Zur Gletschergeschichte des alpinen Spätglazials: Analyse und Interpretation von Schneegrenzdaten*. Geographica Helvetica 2: 63-71.

Maisch, M. 1992. *Die Gletscher Graubündens. Rekonstruktion und Auswertung der Gletscher und deren Veränderungen seit dem Hochstand von 1850 im Gebiet der östlichen Schweizer Alpen (Bündnerland und angrenzende Regionen)*. Physische Geographie 33, Dept. of Geography, University of Zurich, Switzerland.

Maisch, M., Wipf, A., Denneler, B., Battaglia, J., Benz, C. 2000. *Die Gletscher der Schweizer Alpen. Gletscherhochstand 1850, Aktuelle Vergletscherung, Gletscherschwundszenarien*. Schlussbericht NFP31. 2. Auflage, VdF Hochschulverlag, Zürich: 373 pp.

Masarik, J., Frank, M., Schaefer, J.M., Wieler, R., 2001. *Correction of in-situ cosmogenic nuclide production rates for geomagnetic field intensity variations during the past 800,000 years*. Geochimica et Cosmochimica Acta 65, 2995-3003.

Masarik, L., Wieler, R. 2003. *Production rates of cosmogenic nuclides in boulders*. Earth an Planetary Science Letters 216: 201-208.

Matsuoka, N., Ikeda, A., Date, T. 2005. *Morphometric analysis of solifluction lobes and rock glaciers in the Swiss Alps*. Permafrost and Periglacial Processes 16: 99-113.

Matsuoka, N., Murton, J. 2008. *Frost weathering: Recent Advances and Future Directions*. Permafrost and Periglacial Processes 19: 195-210.

Matthews, J.A., Shakesby, R.A. 1984. *The status of the "Little Ice Age" in Southern Norway; relative age dating of Neoglacial moraines with Schmidt hammer and lichenometry*. Boreas 13(3): 333-346.

Matthews, J.A., Brunsden, D., Frenzel, B., Gläser, B., Weiss, B.B. 1997. *Rapid mass movements as a source of climatic evidence for the Holocene*. Publisher Paläoklimaforschung – Palaeoclimate Research 19: 444 pp.

Matthews, J.A., Shakesby, A. 2004. *A twentieth-century neoparaglacial rock topple on a glacier foreland, Ötztal Alps, Austria*. The Holocene 14(3): 454-458.

Mayr, F., Heuberger, H. 1968. *Type areas of late glacial and post-glacial deposits in Tyrol, Eastern Alps*. In: Richmond, G.M. (ed.): Glaciation of the Alps. INQUA International Congress, Boulder. Series in Earth Sciences 7: 143-165.

McCarroll, D. 1987. *The Schmidt hammer in geomorphology: five sources of instrument error*. British Geomorphology Research Group Technical Bulletin 36: 16-27.

McKeague, J.A., Brydon, J.E., Miles, N.M. 1971. *Differentiation of forms of extractable iron and aluminium in soils*. Soil Science Society of America Proceedings 35: 33-38.

McSaveney, M.J. 1992. *A manual for weathering-rind dating of grey sandstones of the Torlesse Supergroup, New Zealand*. Lower Hutt, Institute of Geological & Nuclear Science Limited.

Mercier, D. 2008. *Paraglacial geomorphology: Conceptual and methodological revival*. Géomorphologie: relief, precessus, environnement 4: 219-222.

MeteoSchweiz. 2010. http://www.meteoschweiz.admin.ch/web/de/klima/klima_schweiz.html. Access: 10.02.2010.

Mikan, C.J., Schimel, J.P., Doyle, A.P. 2002. *Temperature controls of microbial respiration in arctic tundra soils above and below freezing*. Soil Biology et Biochemistry 34: 1785-1795.

Mikutta, R., Kleber, M., Kaiser, K., Jahn, R. 2005. *Organic matter removal from soils using hydrogen peroxide, sodium hypochloride, and disodium peroxisulfate*. Soil Science Society of America Journal 69: 120-135.

Mikutta, R., Kleber, M., Torn, M.S., Jahn, R. 2006. *Stabilization of organic matter: association with minerals or chemical recalcitrance?* Biogeochemistry 77: 25-56.

Monaghan, M.C., Krishnaswami, S., Thomas, J.H. 1983. *^{10}Be concentrations and the long-term fate of particle-reactive nuclides in five soil profiles from California*. Earth and Planetary Science Letters 65: 51-60.

Monaghan, M.C., Krishnaswami, S., Turekian, K.K. 1985/1986. *The global average production of ^{10}Be*. Earth Planetary Science Letters 76: 279-287.

Moore, D.M., Reynolds, Jr. R.C. 1997. *X-ray diffraction and the identification and analysis of clay minerals*. 2nd edition, Oxford University Press, New York.

Munroe, J.S. 2008. *Alpine soils on Mount Mansfield, Vermont, USA: Pedology, history and intraregional comparison*. Soil Science Society of America Journal 72: 524-533.

Murray, A.S., Wintle, A.G. 2000. *Luminescence dating of quartz using an improved single-aliquot regenerative-dose protocol*. Radiation measurements 33: 57-73.

Murray, A.S., Wintle, A.G. 2003. *The single aliquot regenerative dose protocol: potential for improvements in reliability*. Radiation measurements 37: 377-381.

Nishiizumi, K., Winterer, E.L., Kohl, C.P., Lal, D., Arnold, J.R., Klein, J., Middleton, R. 1989. *Cosmic ray production rates of ^{10}Be and ^{26}Al in quartz from glacially polished rocks*. Journal of Geophysical Research 94(B12): 17907-17915.

Nishiizumi, K., Kohl, C.P., Arnold, J.R. 1993. *Role of in situ cosmogenic nuclides ^{10}Be and ^{26}Al in the study of diverse geomorphic processes*. Earth Surface Processes and Landforms 18: 407-425.

Nesje, A., Blikra, L.H., Anda, E. 1994. *Dating rockfall-avalanche deposits from degree of rock-surface weathering by Schmidt-hammer tests: a study from Norangsdalen, SunnmØre, Norway*. Norwegian Journal of Geology 74(2): 108-113.

Niederbudde, E.A., Kussmaul, H. 1978. *Tonmineraleigenschaften und –Umwandlungen in Parabraunerde-Profilpaaren unter Acker und Wald in Süddeutschland*. Geoderma 20: 239-255.

Noetzli, J., Hoelzle, M., Haeberli, W. 2003. *Mountain permafrost and recent Alpine rock-fall events: A GIS-based approach to determine critical factors*. In: Phillips, M., Springman, S., Arenson, L. (eds.), Proceedings of the 8th International Concerence on Permafrost 2003, Zurich. Swets & Zeitlinger, Lisse.

Noetzli, J., Gruber, S. 2009. Transient thermal effects in Alpine permafrost. The Cryosphere 3: 85-99.

Oades, J.M. 1995. *An overview of processes affecting the cycling of organic carbon in soils*. In: Role of Nonliving Organic Matter in Earth's Carbon Cycle, Zepp, R.G., Sonntag, C. (eds). John Wiley and Sons Ltd.; 293-303.

Oguchi, C.T., Matsukura, Y. 1999. *Effect of porosity on the increase in weathering-rind thicknesses of andesite gravel*. Engineering Geology 55: 77-89.

Oguchi, C.T. 2001. *Formation of weathering rinds on andesite*. Earth Surface Processes and Landforms 26: 847-858.

Oguchi, C.T., Noda, T., Matsouka, N. 2001. *Weathering rind characteristics of blocky deposits in a deglaciated cirque on Mt. Yakushi, the Northern Japanese Alps*. Annaual Report of the Institute of Geoscience, the University of Tsukuba 27: 17-23.

Oguchi, C.T. 2004. *A porosity-related diffusion model of weathering-rind development*. Catena 58: 65-75.

Ohlendorf, C. 1998. *High Alpine lake sediments as chronicles for regional glacier and climate history in the Upper Engadine, southeastern Switzerland*. Phd thesis, ETH Zurich, No. 12705.

Parfitt, R.L, Henmi, T. 1982. *Comparison of an oxalate-extraction method and an infrared spectroscopic method for determining allophane in soil clays*. Soil Science and Plant Nutrition 28. 183-190.

Parfitt, R.L, Childs, C.W. 1988. *Estimation of forms of Fe and Al – a review, and analysis of contrasting soils by dissolution and Mossbauer methods*. Australian Journal of Soil Research 26: 121-144.

Parfitt, R.L., Childs, C.W., Eden, D.N. 1988. *Ferrihydrite and allophane in four Andepts from Hawaii and implications for their classification*. Geoderma 41. 223-241

Paterson, W.S.B. 1994. *The physics of glaciers*. 3rd edition, Pergamon Press, Oxford: 480 pp.

Patzelt, G. 1975. *Unterinntal-Zillertal-Pinzgau-Kitzbühel, Spät- und postglaziale Landschaftsentwicklung*. Innsbrucker Geographische Studien 2: 309-329.

Pavich, J.M., Brown, L., Klein, J., Middleton, R. 1984. *^{10}Be accumulation in a soil chronosequence*. Earth and Planetary Science Letters 68: 198-204.

Pavich, M.J., Brown, L., Valette-Silver, J.N., Klein, J., Middleton, R. 1985. *^{10}Be analysis of a Quaternary weathering profile in the Virginia Piedmont*. Geology 13: 39-41.

Pavich, J.M., Vidic, N. 1993. *Application of paleomagnetic and ^{10}Be analyses to chronostratigraphy of Alpine glaciofluvial terraces, Sava River Valley, Slovenia*. In: Swart, P. (ed.), Climate Change in Continental Isotopic Records. Geophys. Monogr. 78: 263-275.

Penk, A., Brückner, E. 1901/1909. *Die Alpen im Eiszeitalter*. Tauchnitz, Leipzig.

Permafrost Subcommittee, National Research Council of Canada. 1988. *Glossary of Permafrost and Related Ground-ice Terms*. National Research Council of Canada Technical Memorandum 142: 156 pp.

Peters, T. 2005. Geologischer Atlas der Schweiz, Blatt 1257 St. Moritz (Atlasblatt 118). Bundesamt für Wasser und Geologie (ed.).

Pfiffner, O.A. 2009. *Geologie der Alpen*. Haupt Verlag, Bern/Stuttgart/Wien: 359 pp.

Pigati, J.S., Lifton, N.A. 2004. *Geomagnetic effects on time-integrated cosmogenicnuclide production with emphasis on in situ C-14 and Be-10*. Earth and Planetary Science Letters 226: 193–205.

Plante, A.F., Chenu, C., Balabane, M., Mariotti, A., Righi, D. 2004. *Peroxide oxidation of clay-associated organic matter in a cultivation chronosequence*. European Journal of Soil Science 55: 471-478.

Plug, L., Gosse, J., West, J., Bigley, R. 2007. *Attenuation of cosmic ray flux in temperate forest*. Journal of Geophysical Research 112, F02022, doi:10.1029/2006JF000668.

Prager, C., Zangerl, C., Patzelt, G., Brandner, R. 2008. *Age distribution of fossil landslides in the Tyrol (Austria) and its surrounding areas*. Natural Hazards and Earth System Sciences 8: 377-407.

Prescott, J.R., Hutton, J.T. 1994. *Cosmic ray contribution to dose rates for luminescence and ESR dating: large depths and long term variations*. Radiation measurements 23: 497-500.

Preusser, F., Geyh, M.A., Schlüchter, C. 2003: *Timing of Late Pleistocene climate change in lowland Switzerland*. Quaternary Science Reviews 22: 1435-1445.

Preusser, F., Degering, D., Fuchs, M., Hilgers, A., Kadereit, A., Klasen, N., Krbetschek, M., Richter, D., Spencer J.Q.G. 2008. *Luminescence dating: basics, methods and applications*. Quaternary Science Journal 57(1-2): 95-149.

Ravanel, L. 2006. *Contribution à l'étude des écroulements dans les parois à permafrost de la haute montagne alpine. L'éxemple du Petit Dru (massif du Mont-Blanc) depuis la fin du Petit Age Glaciere*. MSc thesis, Université de Savoie, France: 116 pp.

Ravanel, L., Deline, P. 2008. *The West Face of Les Drus (Mont-Blanc massif): slope instability in a high-Alpine steep rock wall since the end of the Little Ice Age*. Geomorphologie-Relief, Processus, Environnement 4 : 261-272.

Reimer, P.J., Baillie, M.G.L., Bard, E., Bayliss, A., Beck, J.W., Bertrand, C.J.H., Blackwell, P.G., Buck, C.E., Burr, G.S., Cutler, K.B., Damon, P.E., Edwards, R.L., Fairbanks, R.G., Friedrich, M., Guilderson, T.P., Hogg, A.G., Hughen, K.A., Kromer, B., McCormac, G., Manning, S., Bronk Ramsey, C., Reimer R.W., Remmele, S., Southon, J.R., Stuiver, M., Talamo, S., Taylor, F.W., van der Plicht, J., Weyhenmeyer, C.E. 2004. *IntCal04 terrestrial radiocarbon age calibration, 0-26 cal kyr BP*. Radiocarbon 46: 1029-1058.

Reitner, J. 2007. *Glacial dynamics at the beginning of Termination I in the Eastern Alps and their stratigraphic implications*. Quaternary International 164-165: 64-84.

Reuther, A.U., Ivy-Ochs, S., Heine, K. 2006. *Application of surface exposure dating in glacial geomorphology and the interpretation of moraine ages*. Annals of Geomorphology 142: 335-359.

Reuther, A.U., Urdea, P., Geiger, C., Ivy-Ochs, S., Niller, H.P., Kubik, P.W., Heine, K. 2007. *Late Pleistocene glacial chronology of the Pietrele Valley, Retezat Mountains, Southern Carpathians constrained by ^{10}Be exposure ages and pedological investigations*. Quaternary International 164-165: 151-169.

Richter, G. (ed.). 1998. *Bodenerosion. Analyse und Bilanz eines Umweltproblems*. Wissenschaftliche Buchgesellschaft, Darmstadt.

Righi, D., Huber, K., Keller, C. 1999. *Clay formation and podzol development from postglacial moraines in Switzerland*. Clay minerals 34: 319-332.

Roer, I., Kääb, A., Dikau, R. 2005. *Rockglacier acceleration in the Turtmann valley (Swiss Alps): Probable controls*. Norsk Geografisk Tidsskrift 59: 157-163.

Roer, I., Haeberli, W., Avian, M., Kaufmann, V., Delaloye, R., Lambiel, C., Kääb A. 2008. *Observations and considerations on collapsing active rockglaciers in the Alps*. Proceedings of the Ninth International Conference on Permafrost, July 2008, Fairbanks, Alaska, 2: 1505-1510.

Schaefer, J.M., Denton, G.H., Barrell, D.J.A., Ivy-Ochs, S., Kubik, P.W., Andersen, B.G., Phillips, F.M., Lowell, T.V., Schlüchter, C. 2006. *Near-Synchronous Interhemispheric Termination of the Last Glacial Maximum in Mid-Latitudes*. Science 312: 1510-1513.

Schaefer, J.M., Denton, G.H., Kaplan, M., Putnam, A., Finkel, R.C., Barrell, D.J.A., Andersen, B.G., Schwartz, R., McIntosh, A., Chinn, T., Schlüchter, C. 2009. *High-frequency Holocene glacier fluctuations in New Zealand differ from the northern signature*. Science 324: 622-625.

Schaller, M., von Blanckenburg, F., Hovius, N., Kubik, P.W. 2001. *Large-scale erosion rates from in situ-produced cosmogenic nuclides in European river sediments*. Earth and Planetary Science Letters 188: 441-458.

Schaller, M., Blum, J.D., Ehlers, T.A. 2009. *Combining cosmogenic nuclides and major elements from moraine soil profiles to improve weathering rate estimates*. Geomorphology 106: 198-205.

Schiermeier, Q. 2003. *Alpine thaw breaks ice over permafrost's role*. Nature 424: 712.

Schlüchter, C., Röthlisberger, C. 1995. *100,000 Jahre Gletschergeschichte*. In: Gletscher im ständingen Wandel. Vdf-Verlag ETH, Zürich: 47-63.

Schlüchter, C. 2004. *The Swiss glacial record – A schematic summary*. In: Ehlers J., Gibbard P.L. (eds.), Quaternary Glaciations - Extent and chronology, Part I: Europe. Elsevier, London: 413-418.

Schmid, S.M., Fügenschuh, B., Kissling, E., Schuster, R. 2004. *Tectonic map and overall architecture of the Alpine orogen*. Eclogae geologicae Helvetiae 97: 93-117.

Schmidt, E. 1950. *Der Beton-Prüfhammer – Ein Gerät zur Bestimmung der Qualität des Betons im Bauwerk*. Schweizerische Bauzeitung 68: 378-379.

Schmidt, E. 1951. *A Non-destructive concrete tester*. Concrete 59(8): 34-35.

Schulze, D.G. 2005. *Clay Minerals*. Encyclopedia of soils in environment, Elsevier.

Schwander, J., Eicher, J., Ammann, B. 2000. *Oxygen isotopes of lake marl at Gerzensee and Leysin (Switzerland), covering the Younger Dryas and two minor oscillations, and their correlation to the GRIP ice core*. Palaeogeorgraphy, Palaeoclimatology, Palaeoecology 159: 203-214.

Schwarb, M., Daly, C., Frei, C., Schär, C. 2000. *Mittlere jährliche Niederschlagshöhe im europäischen Alpenraum 1971-1990*. In: Hydrologischer Atlas der Schweiz, Blatt 2.6.

Schwertmann, U., Niederbudde, E. A., 1993. *Tonmineralbestimmung in Böden*. In: Tonminerale und Tone. Struktur, Eigenschaften, Anwendung und Einsatz in Industrie und Umwelt, Jasmund, K., Lagaly, G. (eds). Steinkopff Verlag, Darmstadt: 255-265.

Shakesby, R.A., Matthews, J.A., Owen, G. 2006. *The Schmidt hammer as a relative-age dating tool and its potential for calibrated-age dating in Holocene glaciated environments*. Quaternary Science Reviews 25: 2846-2867.

Shakesby, R.A., Matthews, J.A., Schnabel, C. 2008. *Cosmogenic ^{10}Be and ^{26}Al ages of Holocene moraines in southern Norway II: evidence for individualistic responses of high-altitude glaciers to milennial-scale climatic fluctuations*. The Holocene 18: 1165-1177.

Siegfried map (Topographischer Atlas der Schweiz), published 1870-1922, Eidgenössisches Topographisches Bureau (ed.).

Solomina, O., Haeberli, W., Kull, C., Wiles, G. 2008. *Historical and Holocene glacier-climate variations: General concepts and overview*. Global and Planetary Change 60: 1-9.

Spicher, A. 1980. *Tektonische Karte der Schweiz*. Schweizerische Geologische Kommission (ed.).

Stokes, S. 1999. *Luminescence dating applications in geomorphological research*. Geomorphology 29: 153-171.

Stone, J.O. 2000. *Air pressure and cosmogenic isotope production*. Journal of Geophysical Research 105/B10(23): 753-759.

Stroeven, A.P., Fabel, D., Hätterstrand, C., Harbor, J. 2002. *A relict landscape in the centre of Fennoscandian glaciation: cosmogenic radionuclide evidence of tors preserved through multiple glacial cycles*. Geomorphology 44: 145-154.

Studer, M. 2005. *Gletschergeschichtliche Untersuchungen und geomorphologische Kartierung im Raum Maloja-Val Forno*. Ein Beitrag zur regionalen Landschaftsgeschichte. Diploma thesis, University of Zurich, Switzerland. Unpublished.

Sumner, P., Nel, W. 2002. The effect of rock moisture on Schmidt Hammer rebound: tests on rock samples from Marion Island and South Africa. Earth Surface Processes and Landforms 27: 1137-1142.

Suter, J. 1981. *Gletschergeschichte des Oberengadins: Untersuchung on Gletscherschwankungen in der Err-Julier-Gruppe*. Physische Geographie 2, University of Zurich, Switzerland.

Swisstopo (Federal Office of Topography, Switzerland; ed.). 2009. *Die Schweiz während des letzteiszeitlichen Maximums (LGM)*. Map 1:50000 with the contribution of various authors.

United Nations Environment Programme (UNEP). 2009. *Climate change science compendium*. McMullen, C.P., Jabbour, J. (eds.).

van Husen, D. 1987. *Die Ostalpen und ihr Vorland in der letzten Eiszeit (Würm)*. Geologische Bundesanstalt Wien (ed.).

van Husen, D. 1997. *LGM and Late-Glacial Fluctuations in the Eastern Alps*. Quaternary International 38/39: 109-118.

van Husen, D. 2004. *Quaternary glaciations in Austria*. In: Ehlers J., Gibbard P.L. (eds.), Quaternary Glaciations - Extent and chronology, Part I: Europe. Elsevier, London: 1-13.

Vonder Mühll, D. 1993. *Geophysikalische Untersuchungen im Permafrost des Oberengadins*. PhD thesis, ETH Zurich, Switzerland, No. 10107.

von Raumer, J.F. & Bussy, F. 2004. *Mont Blanc and Aiguille Rouges – Geology of their polymetamorphic basement (external massifs, France-Switzerland)*. Mémoires de géologie (Lausanne) 42: 203 pp.

Wessels, M. 1998. *Natural environmental changes indicated by Late Glacial and Holocene sediments from Lake Constance, Germany*. Palaeogeography, Palaeoclimatography, Palaeoecology 140 : 421-432.

Wang, Y., Amundson, R. 1996. *Radiocarbon Dating of Soil Organic Matter*. Quaternary Research 45: 282-288.

Wanner, H., Beer, J., Bütikofer, J., Crowley, T.J., Cubasch, U., Flückiger, J., Goosse, H., Grosjean, M., Joos, F., Kaplan, J.O., Küttel, M., Müller, S.A., Prentice, I.C., Solomina, O., Stocker, T., Tarasov, P., Wagner, M., Widmann, M. 2008. *Mid- to Late Holocene climate change : an overview*. Quaternary Science Reviews 27 : 1791-1828.

WGMS, 2007. Glacier mass balance bulletin No. 9 (2004-2005). Haeberli, W., Hoelzle, M., Zemp, M. (Eds.).

Whitehouse, I.E., McSaveney, M.J., Knuepfer, P.L.K., Chinn, T.J.H. 1986. *Growth of weathering rinds on Torlesse sandstone, southern Alps, New Zealand*. In: Rates of Chemical Weathering of Rocks and Minerals, Colman S.M., Dethier D.P. (eds). Academic Press, Orlando; 419-435.

Willenbring, J.K., von Blanckenburg, F. 2009. *Meteoric cosmogenic Beryllium-10 adsorbed to river sediment and soil: Applications for Earth-surface dynamics*. Earth Science Reviews (accepted manuscript).

Williams, R.B.G., Robinson, D.A. 1983. *The effect of surface texture on the determination of the surface hardness of rock using the Schmidt hammer*. Earth Surface Processes and Landforms 8: 289-292.

Winkler, S., Shakesby, R.A. 1995. *Anwendung von Lichenometrie und Schmidt-Hammer zur relativen Altersdatierung prä-frührezenter Moränen am Beispiel der Vorfelder von Guslar-, Mitterkar-, Rofenkar- und Vernagtferner (Ötztaler Alpen/Österreich)*. Petermanns Geographische Mitteilungen 139: 283-304.

Winkler, S. 2000. *The little ice age maximum in the Southern Alps, New Zealand: preliminary results at Mueller Glacier*. The Holocene 10: 643-647.

Winkler, S. 2005. *The 'Schmidt hammer' as a relative-age dating technique: potential and limitations of its application on Holocene moraines in Mt Cook National Park, Southern Alps, New Zealand*. New Zealand Journal of Geology and Geophysics 48: 105-116.

Wintle, A.G. 2008. *Luminescence dating: where it has been where it is going*. Boreas 37: 471-482.

Zanelli, R., Egli, M., Mirabella, A., Giaccai, D., Abdelmoula, M. 2007. *Vegetation effects on pedogenetic forms of Fe, Al and Si and on clay minerals in soils in southern Switzerland and northern Italy*. Geoderma 141: 119-129.

Zech, W., Glaser, B., Abramowski, U., Dittmar, C., Kubik, P.W. 2003. *Reconstruction of the late quaternary glaciation of the Macha Khola valley (Gorkha Himal, Nepal) using relative and absolute (^{14}C, ^{10}Be, dendrochronology) dating techniques*. Quaternary Science Reviews 22: 2253-2265.

Zemp, M., Kääb, A., Hoelzle, M., Haeberli, W. 2005. *GIS-based modelling of glacial sediment balance*. Zeitschrift für Geomorphologie N.F. 138: 113-129.

Zemp, M. 2006. *Glaciers and climate change. Spatio-temporal analysis of glacier fluctuations in the European Alps after 1850*. Haeberli, W., Maisch M. (eds.), Schriftenreihe Physische Geographie 449. Institute of Geography, University of Zurich.

Zemp, M., Hoelzle, M., Haeberli, W. 2007. *Distributed modelling of the regional climatic equilibrium line altitude of glaciers in the European Alps*. Global and Planetary Change 56: 83-100.

Zreda, M.G., Phillips, F.M. 1995. *Insights into alpine moraine development from cosmogenic ^{36}Cl buildup dating*. Geomorphology 14: 149-165.

Zumbühl, H.J., Steiner, D., Nussbaumer, S.U. 2008. *19th century glacier representations and fluctuations in the central and western European Alps: An interdisciplinary approach*. Global and Planetary Change 60: 42-57.

Appendix

A – Pictures of sites (surface exposure dating and soils)

Val Mulix

Photo: M. Maisch, 2006

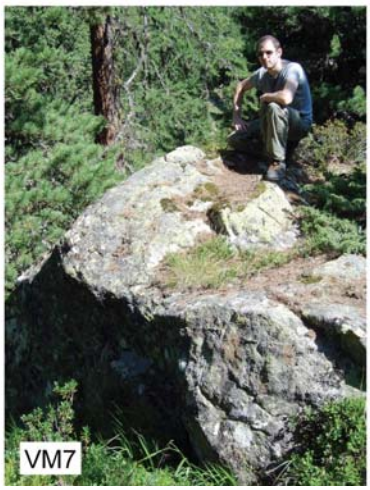


VM8


VM10

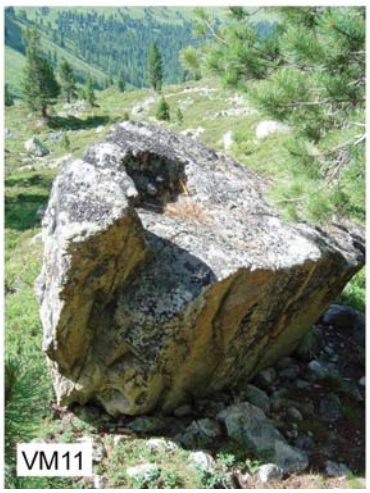
VM11

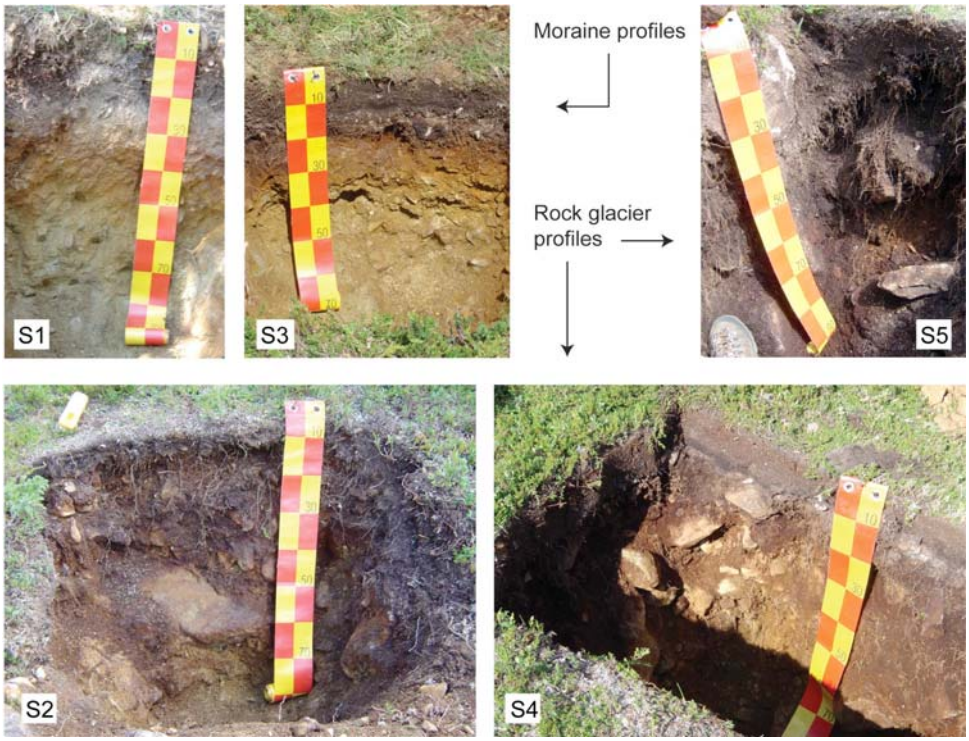
S1
S3
Moraine profiles
Rock glacier profiles
S5
S2
S4

Albula area


Alb2


Alb3


Alb4/1 and 4/2


Alb6

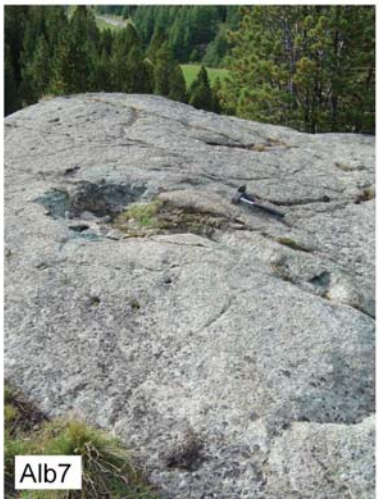
Alb7

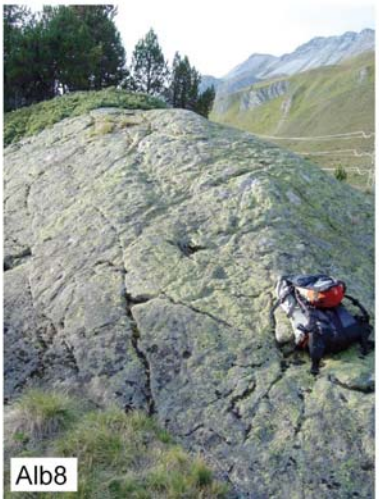
Alb8


Alb9


Alb10


Alb11


Cra1

Val Burdun

Photo: M. Maisch, 2007

Photo: M. Maisch, 2007

Photo: M. Maisch, 2007

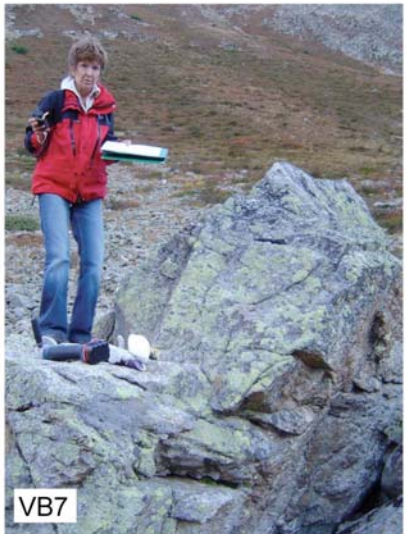

Photo: M. Maisch, 2007

B – X-ray and FT-IR patterns

Val Mulix – XRD (clay fraction)

In all XRD-patterns, the dashed lines represent the areas of 1.4, 1.0 and 0.7 nm, respectively.

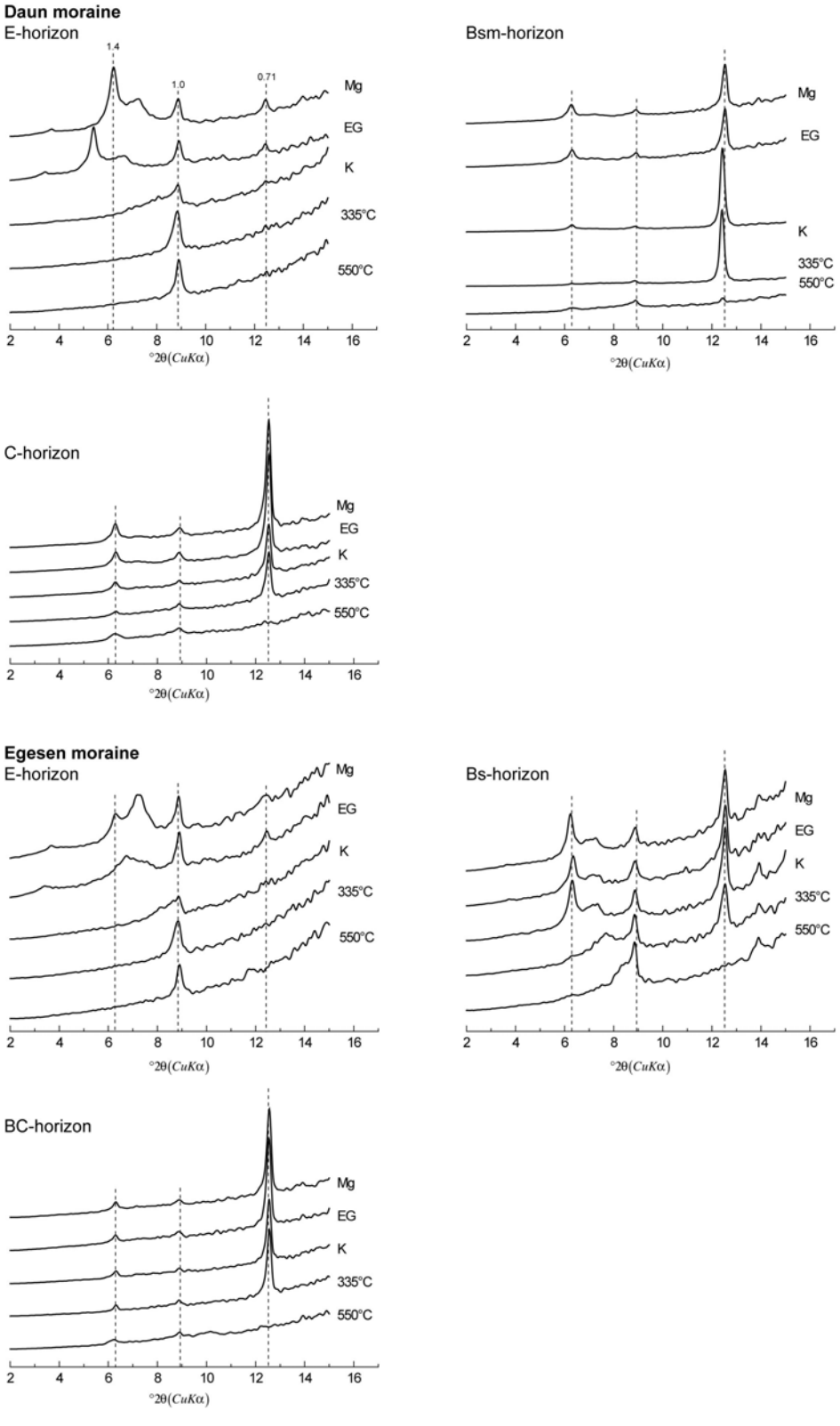

Rockglacier upper part

E-horizon

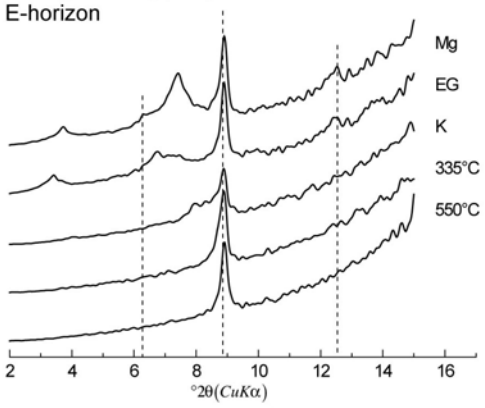

Bs-horizon

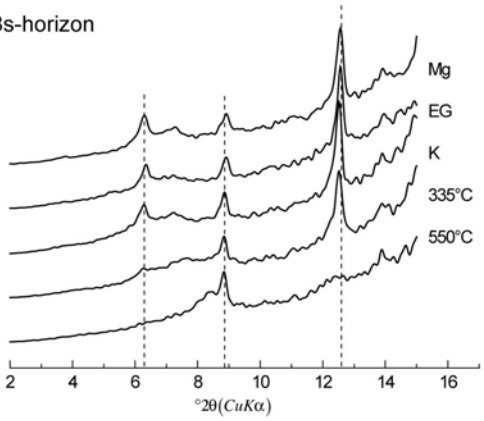

BC-horizon

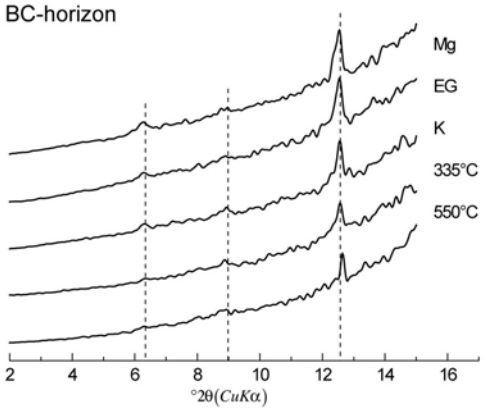

Rockglacier middle part

OE-horizon

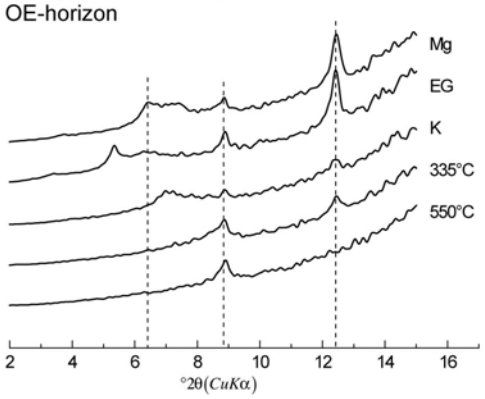

Bs-horizon

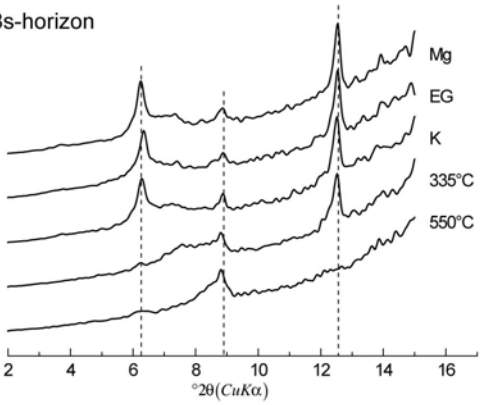

C-horizon

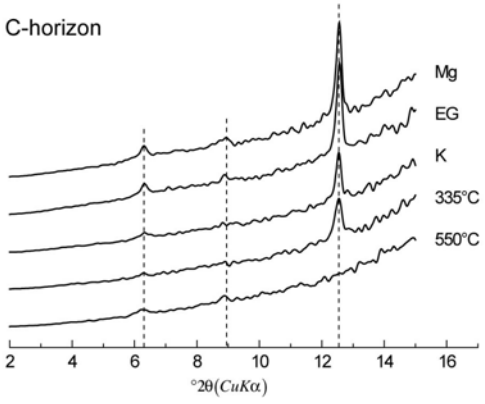

Rockglacier lower part

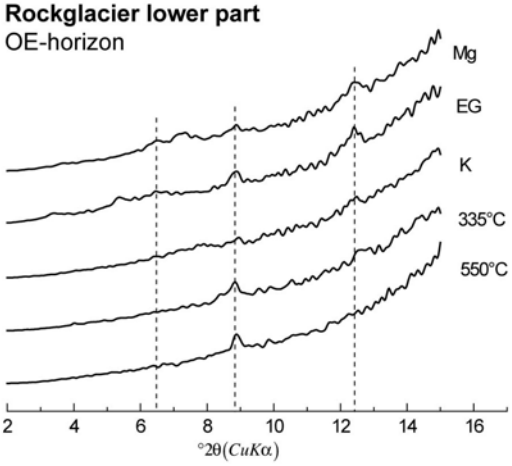

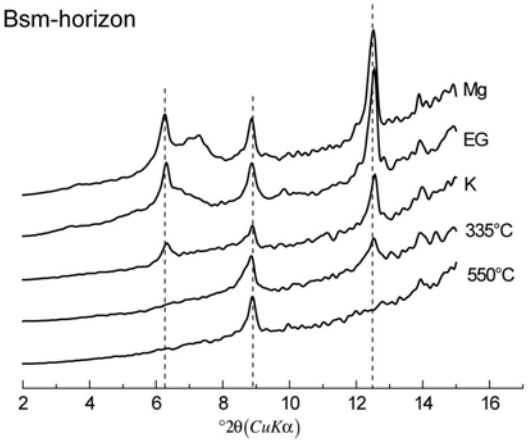

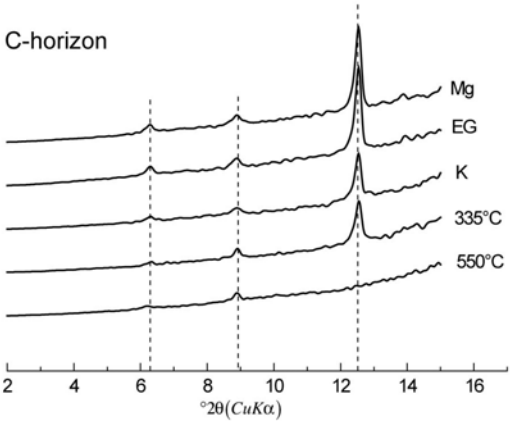

060-reflexions (Val Mulix)

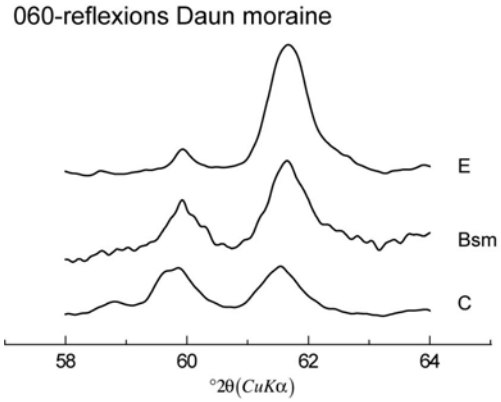

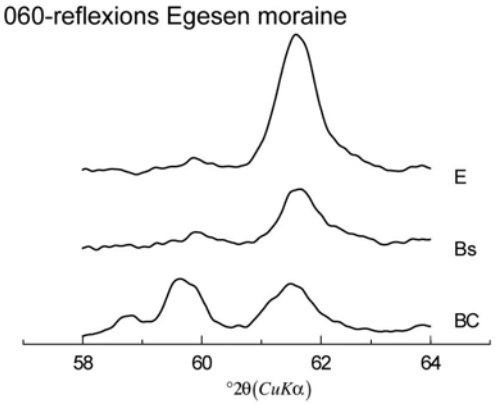

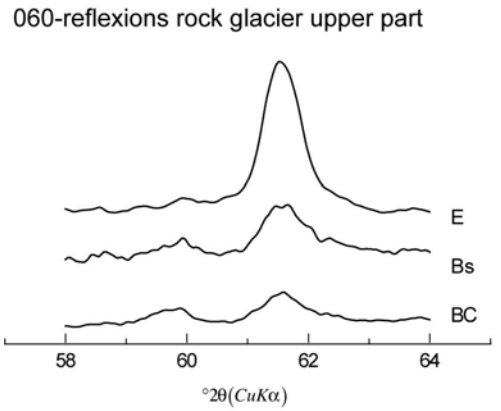

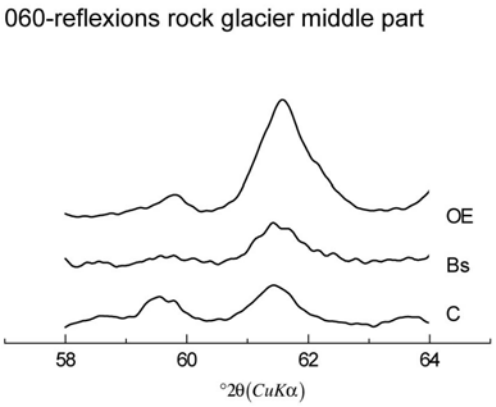

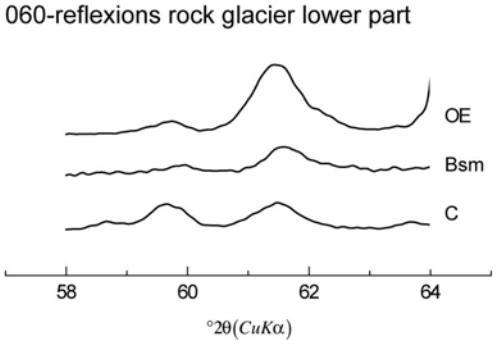

Citrate treated samples (Val Mulix)

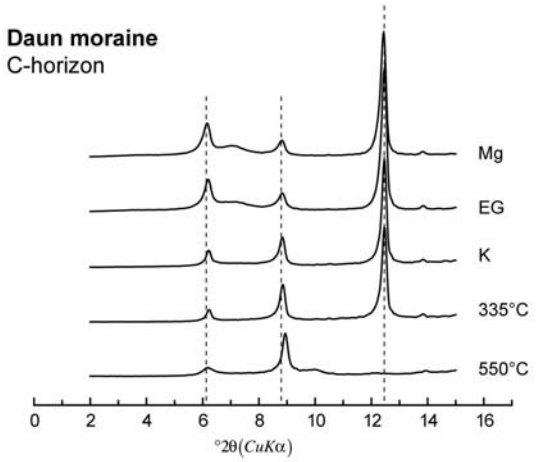

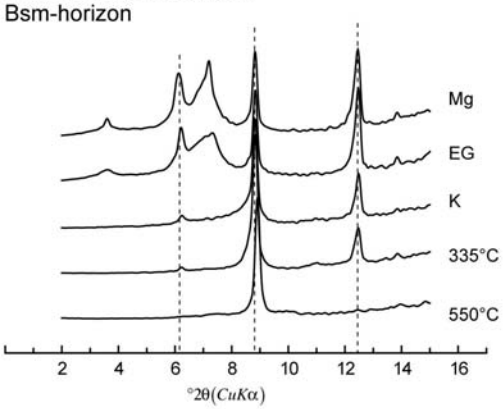

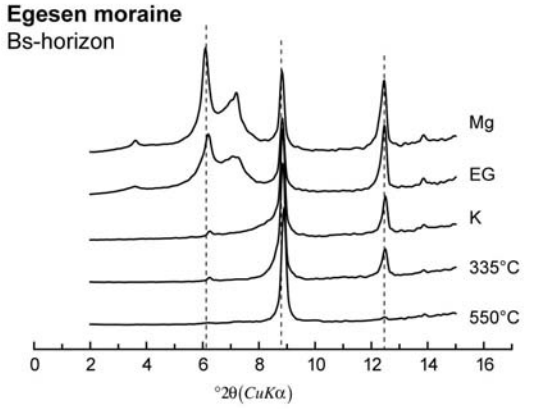

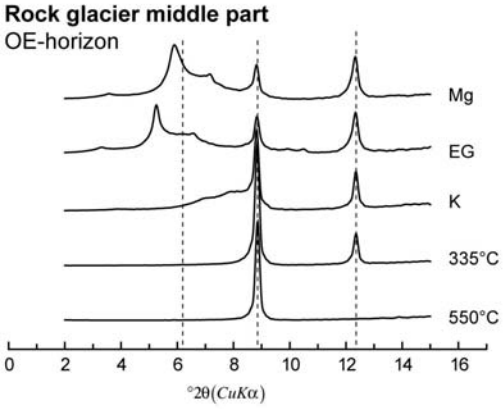

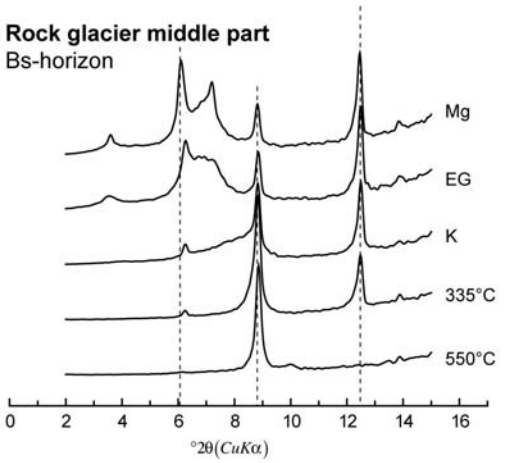

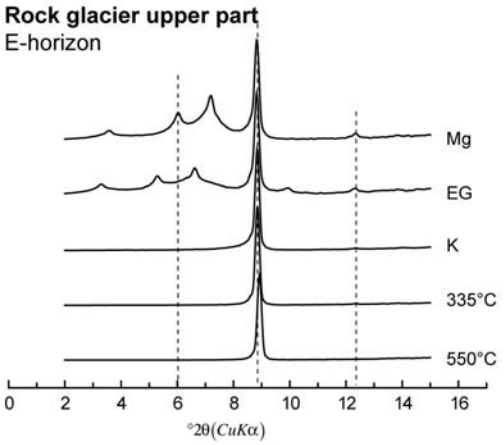

Val Mulix - FT-IR measurements (clay fraction)

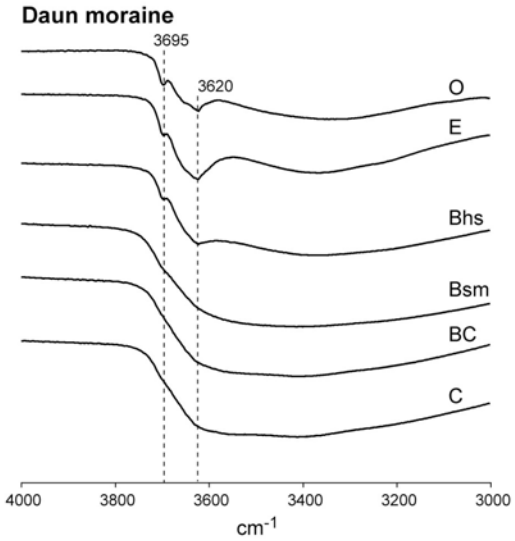

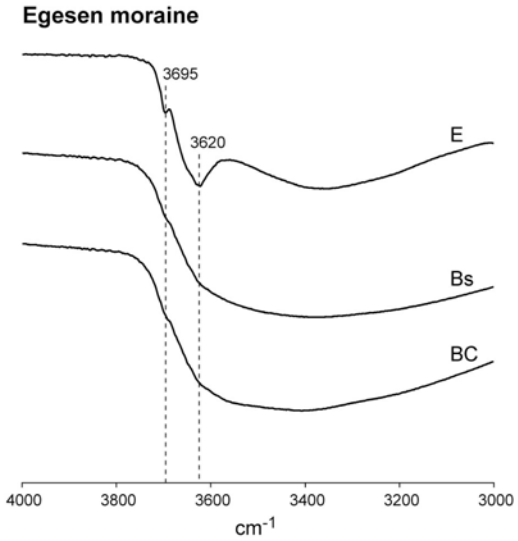

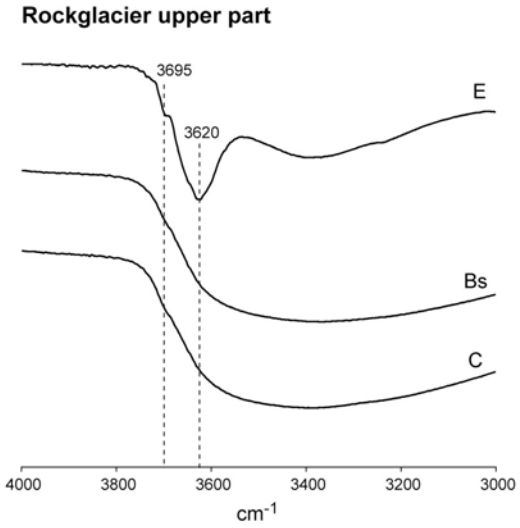

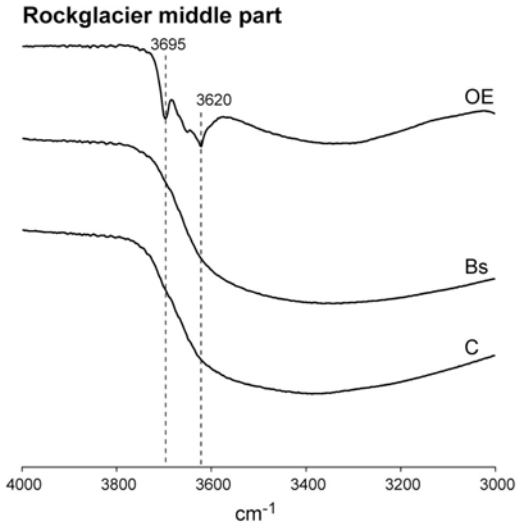

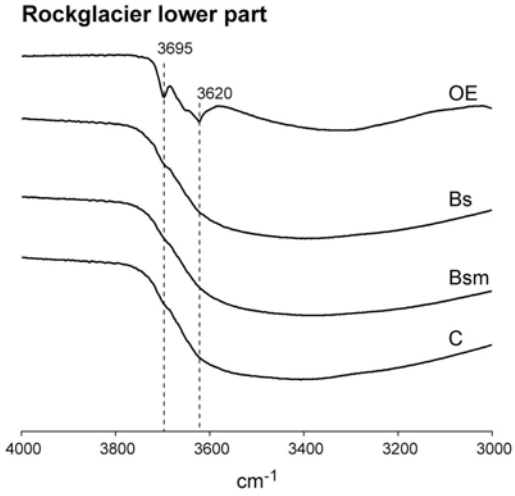

Val Burdun – XRD (clay fraction)

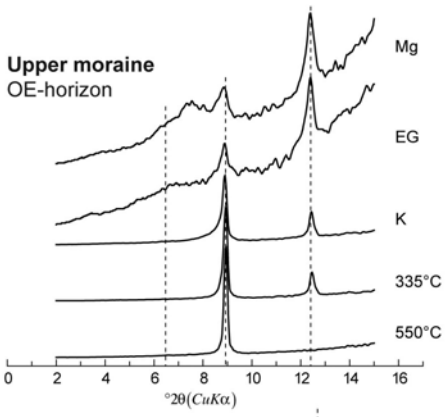

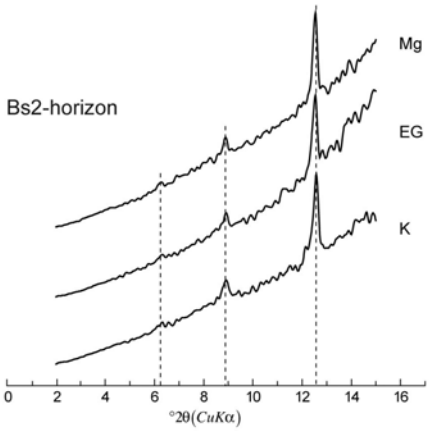

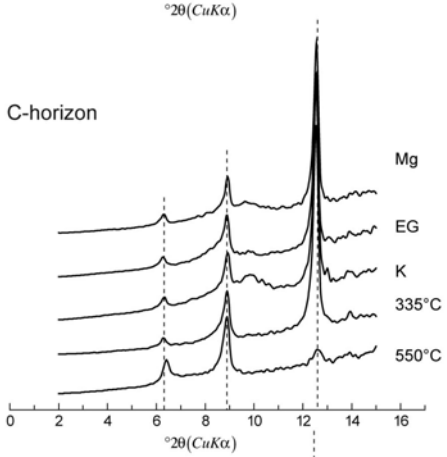

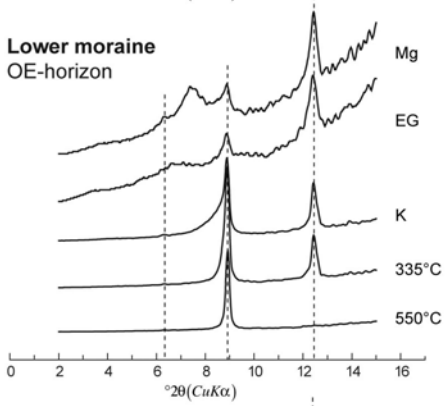

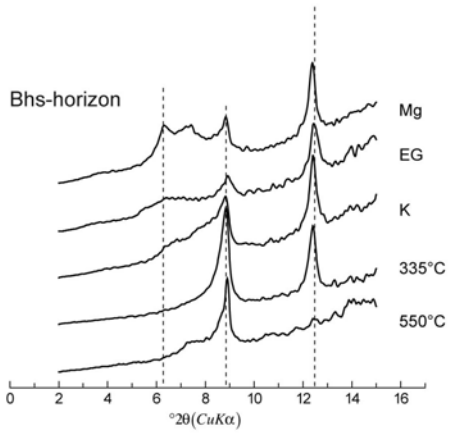

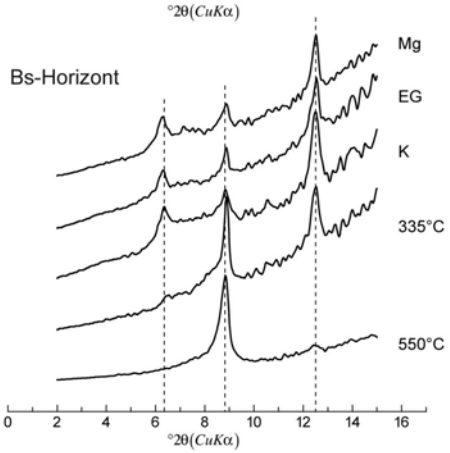

060-reflexions (Val Burdun)

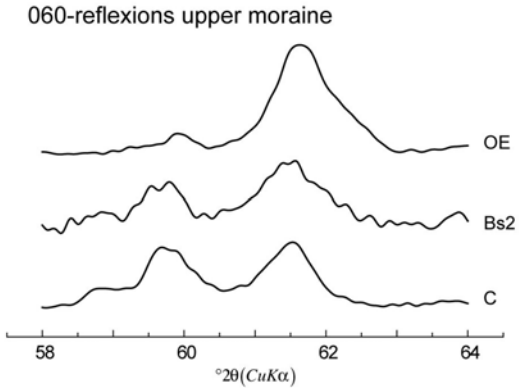

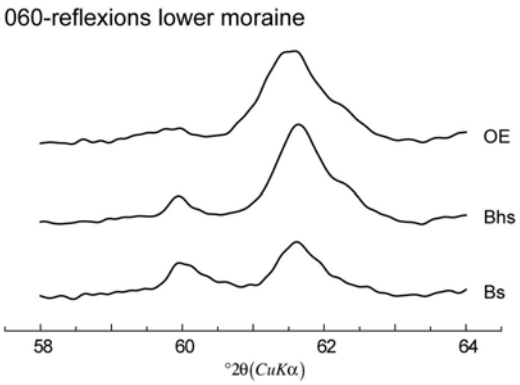

Citrate treated samples (Val Burdun)

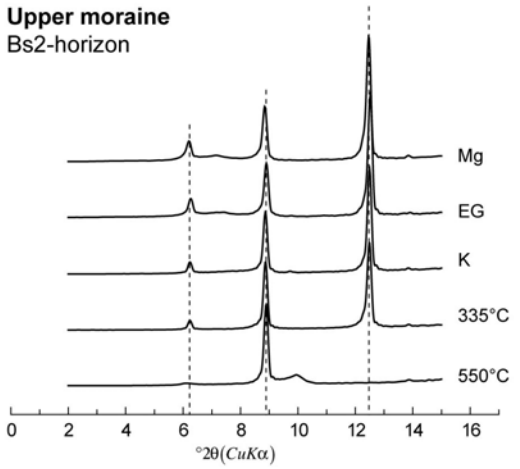

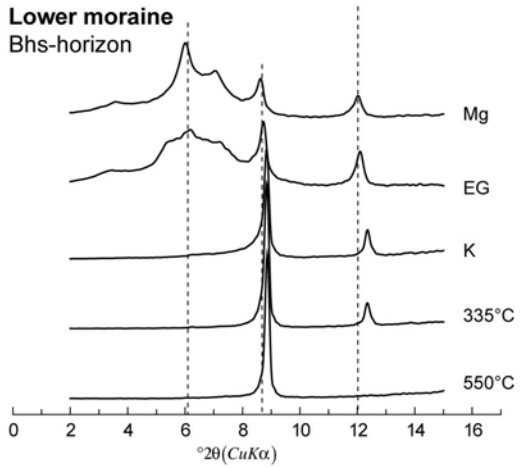

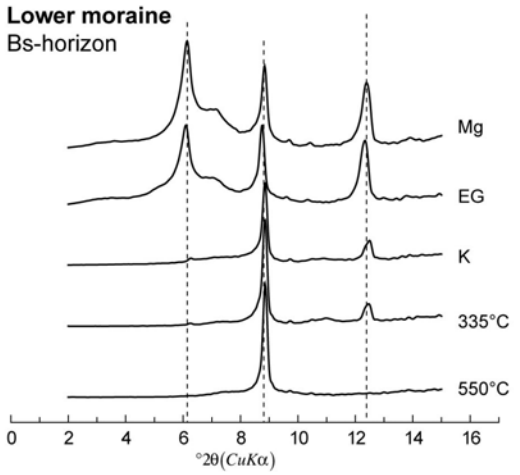

Val Burdun - FT-IR measurements (clay fraction)

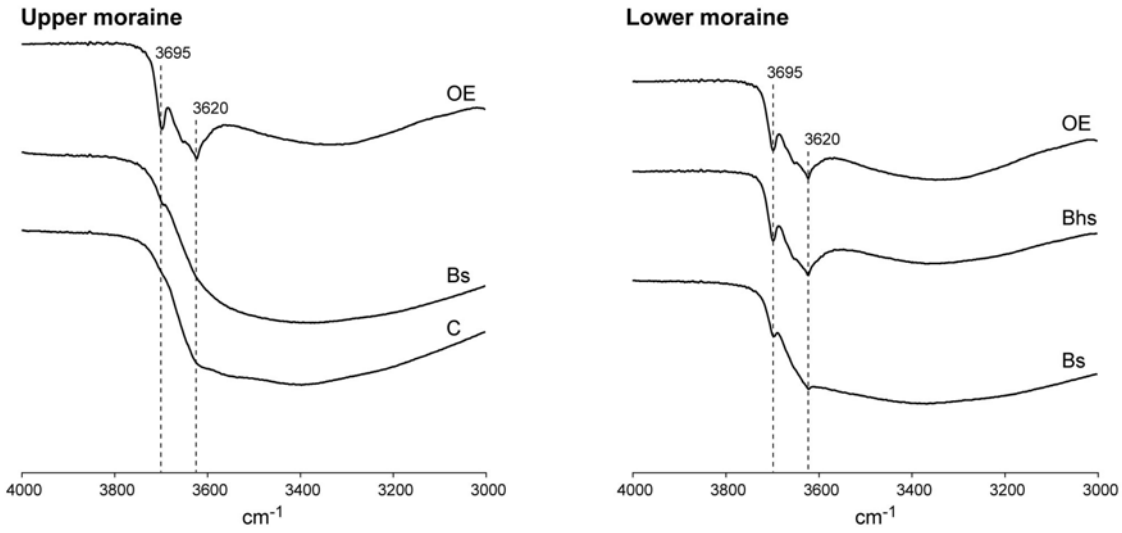

C – Mineral quantification (AUTOQUAN)

All values are given in %. Errors are on a 3 sigma level.

Daun moraine – E-horizon

	Sand			Silt			Clay		
Epidote	2.79	±	0.45	4.82	±	0.48	2.3	±	0.81
Microcline	6.8	±	0.57	6.71	±	0.69	4.48	±	1.08
Muscovite1M	4.27	±	0.72	12.3	±	1.08	24.42	±	1.98
Muscovite2M	5.62	±	0.57	12.66	±	0.87	24.95	±	2.01
PlagioclaseAlbite	22.74	±	0.75	23.02	±	0.99	6.53	±	1.2
Quartz	51.47	±	0.78	18.4	±	0.6	6.04	±	0.69
Smectite	6.31	±	1.05	20.98	±	1.5	29.7	±	3.3
Kaolinite				1.11	±	0.63	1.54	±	1.11

Daun moraine – Bhs-horizon

	Sand			Silt			Clay		
Chlorite	5.56	±	0.84	6.15	±	0.87	5.18	±	0.72
Epidote	5.51	±	0.42	6.46	±	0.48	2.64	±	0.75
Kaolinite	0.00	±	0.00	1.81	±	0.96	0.82	±	1.08
Microcline	7.72	±	0.57	6.5	±	0.66	1.68	±	0.99
Muscovite1M	4.91	±	0.87	7.64	±	1.02	16.74	±	1.68
Muscovite2M	6.26	±	0.66	9.01	±	0.78	16.81	±	1.62
PlagioclaseAlbite	29.55	±	0.84	27.34	±	1.05	11.96	±	1.11
Quartz	32.54	±	0.72	14.67	±	0.6	4.73	±	0.51
Smectite	7.95	±	1.32	20.41	±	2.04	39.4	±	3.00

Daun moraine – Bsm-horizon

	Sand			Silt			Clay		
Chlorite	8.51	±	0.96	14.43	±	1.32	8.10	±	1.29
Epidote	5.97	±	0.48	6.97	±	0.54	2.42	±	1.41
Kaolinite	0.27	±	0.84	2.18	±	1.02	3.77	±	2.43
Microcline	7.47	±	0.63	8.46	±	0.81	3.60	±	1.92
Muscovite1M	5.09	±	0.93	2.62	±	1.08	5.85	±	2.04
Muscovite2M	6.32	±	0.72	5.93	±	0.87	8.44	±	1.77
PlagioclaseAlbite	33.78	±	0.96	26.17	±	1.02	13.16	±	1.32
Quartz	25.34	±	0.66	18.51	±	0.72	7.16	±	0.93
Smectite	7.25	±	1.83	14.72	±	2.01	47.5	±	3.90

Daun moraine – BC-horizon	Sand			Silt			Clay		
Chlorite	7.76	±	0.81	14.54	±	1.11	20.33	±	1.74
Epidote	5.03	±	0.54	8.12	±	0.57	3.03	±	0.81
Kaolinite	0.00	±	0.00	0.33	±	0.78	0.00	±	0.00
Microcline	9.22	±	0.57	7.5	±	0.6	5.48	±	1.05
Muscovite1M	4.55	±	0.99	4.68	±	0.87	9.56	±	1.86
Muscovite2M	6.53	±	0.63	7.44	±	0.69	7.21	±	0.96
PlagioclaseAlbite	36.27	±	0.93	30.4	±	0.96	14.5	±	1.23
Quartz	26.5	±	0.63	20.68	±	0.63	8.10	±	0.84
Smectite	4.14	±	1.32	6.32	±	1.71	31.8	±	3.3

Daun moraine – C-horizon	Sand			Silt			Clay		
Chlorite	7.04	±	0.93	13.89	±	1.11	28.38	±	1.65
Epidote	3.02	±	0.42	5.44	±	0.60	2.78	±	0.81
Microcline	12.16	±	0.6	12.14	±	0.66	7.03	±	1.05
Muscovite1M	6.81	±	0.75	6.14	±	0.78	15.24	±	1.65
Muscovite2M	6.81	±	0.57	8.28	±	0.66	19.7	±	1.44
PlagioclaseAlbite	35.8	±	0.9	31.30	±	0.96	17.01	±	1.50
Quartz	28.36	±	0.66	22.83	±	0.66	9.86	±	1.11

Rock glacier lower part – OE-horizon	Sand			Silt			Clay		
Epidote	1.93	±	0.42	3.32	±	0.45	2.66	±	0.54
Kaolinite	0.65	±	0.51	2.12	±	0.78	12.69	±	1.11
Microcline	16.87	±	0.84	11.83	±	0.69	2.24	±	0.99
Muscovite1M	3.48	±	0.96	10.51	±	1.11	18.07	±	1.38
Muscovite2M	6.39	±	0.60	13.43	±	0.9	16.82	±	1.14
PlagioclaseAlbite	21.98	±	0.84	27.60	±	1.05	9.40	±	0.66
Quartz	41.63	±	0.81	15.76	±	0.63	5.05	±	0.45
Smectite	7.07	±	0.93	15.44	±	1.32	33.06	±	1.86

Rock glacier lower part – Bs-horizon	Sand			Silt			Clay		
Chlorite	5.13	±	0.78	12.57	±	1.23	14.81	±	1.92
Epidote	3.38	±	0.48	6.01	±	0.57	1.43	±	1.26
Microcline	14.81	±	0.90	14.57	±	0.93	11.72	±	1.65
Muscovite1M	3.48	±	0.78	3.58	±	0.69	22.88	±	2.43
Muscovite2M1	6.71	±	0.51	8.12	±	0.57	21.55	±	2.07
PlagioclaseAlbite	38.09	±	0.93	33.38	±	0.99	19.93	±	2.10
Quartz	28.39	±	0.60	21.77	±	0.66	7.67	±	1.05

Rock glacier lower part – Bsm-horizon									
	Sand			Silt			Clay		
Chlorite	4.87	±	0.84	18.4	±	2.37	5.63	±	1.95
Epidote	3.40	±	0.51	6.0	±	0.78	1.65	±	1.23
Microcline	15.01	±	0.87	13.64	±	0.78	8.82	±	2.58
Muscovite1M	3.52	±	0.60	5.28	±	0.96	29.3	±	3.6
Muscovite2M	6.84	±	0.51	7.18	±	0.75	27.2	±	3.3
PlagioclaseAlbite	37.38	±	0.93	29.18	±	1.20	22.44	±	2.28
Quartz	28.97	±	0.66	20.32	±	0.96	4.95	±	1.23

Rock glacier lower part – C-horizon									
	Sand			Silt			Clay		
Calcite	0.41	±	0.25	0.28	±	0.24	-	±	-
Chlorite	6.13	±	0.75	11.94	±	0.9	18.4	±	1.53
Epidote	3.64	±	0.48	6.33	±	0.57	3.5	±	0.84
Microcline	15.36	±	0.6	14.48	±	0.6	11.68	±	1.86
Muscovite1M	3.78	±	0.87	4.88	±	0.72	17.7	±	1.68
Muscovite2M	6.54	±	0.54	8.39	±	0.63	17.33	±	1.53
PlagioclaseAlbite	36.34	±	0.87	32.58	±	0.90	24.14	±	1.80
Quartz	27.80	±	0.60	21.1	±	0.57	7.26	±	1.05

Egesen moraine – E-horizon									
	Sand			Silt			Clay		
Chlorite	3.87	±	0.84	3.09	±	0.78		±	
Epidote	5.29	±	0.42	5.12	±	0.54	3.70	±	0.63
Kaolinite	0.24	±	0.75	1.07	±	0.81	0.65	±	0.66
Microcline	13.62	±	0.60	11.16	±	0.75	2.25	±	0.90
Muscovite	8.66	±	0.93	17.68	±	1.29	25.45	±	1.65
Muscovite	10.09	±	0.72	15.20	±	0.96	20.88	±	1.50
PlagioclaseAlbite	18.17	±	0.81	23.55	±	1.11	8.38	±	0.99
Quartz	27.88	±	0.69	6.43	±	0.63	3.37	±	0.45
Smectite	12.17	±	1.77	16.69	±	1.80	35.33	±	2.49

Egesen moraine – Bs-horizon									
	Sand			Silt			Clay		
Calcite	0.16	±	0.13	0.42	±	0.22	0.00	±	0.00
Chlorite	33.13	±	1.44	22.28	±	2.91	5.59	±	1.17
Epidote	1.15	±	0.30	4.79	±	0.57	0.00	±	0.00
Microcline	11.28	±	0.48	12.22	±	0.84	10.69	±	1.59
Muscovite1M	4.73	±	0.54	4.19	±	0.75	28.32	±	2.52
Muscovite2M	5.10	±	0.45	9.78	±	0.84	25.76	±	2.22
PlagioclaseAlbite	24.45	±	0.81	28.97	±	1.41	23.73	±	1.65
Quartz	20.00	±	0.45	17.35	±	1.02	5.91	±	0.81

Egesen moraine – BC-horizon									
	Sand			Silt			Clay		
Calcite	0.20	±	0.20	0.11	±	0.18	-	±	-
Chlorite	8.50	±	0.84	16.76	±	1.08	25.90	±	1.65
Epidote	2.52	±	0.36	3.20	±	0.45	2.11	±	0.99
Microcline	14.55	±	0.60	15.58	±	0.69	11.22	±	1.02
Muscovite1M	5.45	±	0.72	5.85	±	0.84	15.35	±	1.65
Muscovite2M	7.68	±	0.57	9.28	±	0.72	17.82	±	1.44
PlagioclaseAlbite	35.82	±	0.87	31.13	±	0.99	20.38	±	1.71
Quartz	25.28	±	0.63	18.10	±	0.63	7.23	±	0.63

Rock glacier middle part – OE-horizon									
	Sand			Silt			Clay		
Epidote	4.74	±	0.51	5.41	±	0.66	1.19	±	0.45
Kaolinite	2.64	±	0.63	4.58	±	1.11	11.79	±	1.11
Microcline	10.09	±	0.57	8.44	±	0.66	3.01	±	0.51
Muscovite1M	4.12	±	0.84	7.97	±	1.08	9.83	±	1.38
Muscovite2M	8.88	±	0.69	14.03	±	0.93	14.44	±	1.05
PlagioclaseAlbite	18.11	±	0.84	19.59	±	0.96	3.37	±	0.63
Quartz	34.94	±	0.72	18.31	±	0.69	6.17	±	0.51
Smectite	16.47	±	0.96	21.68	±	1.83	50.19	±	2.19

Rock glacier middle part – Bs-horizon									
	Sand			Silt			Clay		
Chlorite	7.05	±	0.93	34.89	±	2.97	8.56	±	2.19
Epidote	8.16	±	0.57	10.99	±	1.11	0.00	±	0.00
Microcline	12.37	±	0.60	7.63	±	0.90	8.82	±	2.67
Muscovite1M	4.32	±	0.72	6.15	±	1.08	26.20	±	4.20
Muscovite2M	6.98	±	0.60	7.25	±	0.93	27.70	±	3.30
PlagioclaseAlbite	35.51	±	0.90	20.30	±	1.44	23.85	±	2.85
Quartz	25.62	±	0.63	12.79	±	1.05	4.82	±	1.17

Rockglacier middle part – C-horizon									
	Sand			Silt			Clay		
Calcite	0.64	±	0.23	0.47	±	0.19		±	
Chlorite	7.10	±	0.84	15.14	±	1.08	18.73	±	1.41
Epidote	8.53	±	0.51	14.93	±	0.63	5.02	±	1.02
Microcline	10.62	±	0.57	10.41	±	0.63	13.03	±	1.35
Muscovite1M	3.46	±	0.87	2.96	±	0.60	15.09	±	1.92
Muscovite2M	6.56	±	0.57	9.10	±	0.69	23.98	±	1.71
PlagioclaseAlbite	37.51	±	0.87	29.78	±	0.99	17.44	±	1.74
Quartz	25.58	±	0.60	17.19	±	0.57	6.72	±	0.75

Rock glacier upper part – E-horizon									
	Sand			Silt			Clay		
Epidote	0.69	±	0.33	1.98	±	0.54	1.78	±	0.93
Microcline	18.17	±	0.72	19.39	±	0.84	0.26	±	0.45
Muscovite1M	5.85	±	0.69	13.37	±	0.99	6.10	±	0.96
Muscovite2M	7.53	±	0.54	18.53	±	0.93	30.90	±	1.86
PlagioclaseAlbite	12.91	±	0.69	26.01	±	0.99	32.79	±	1.71
Quartz	54.86	±	0.75	12.49	±	0.51	5.38	±	0.99
Smectite	-	±	-	8.24	±	1.41	1.75	±	0.45

Rock glacier upper part – Bs-horizon									
	Sand			Silt			Clay		
Chlorite	8.17	±	0.93	27.30	±	3.60	8.38	±	1.77
Epidote	3.88	±	0.57	3.74	±	0.84	0.95	±	1.23
Microcline	15.58	±	0.66	15.21	±	1.50	7.56	±	2.01
Muscovite1M	4.03	±	0.66	8.60	±	1.11	28.10	±	3.30
Muscovite2M	7.26	±	0.54	7.69	±	0.93	23.38	±	2.91
PlagioclaseAlbite	34.57	±	0.93	21.41	±	1.47	23.93	±	2.34
Quartz	26.50	±	0.66	16.07	±	1.23	7.74	±	1.26

Rock glacier upper part – BC-horizon									
	Sand			Silt			Clay		
Calcite	0.42	±	0.17	0.09	±	0.18	23.80	±	3.30
Chlorite	8.20	±	0.81	16.37	±	1.50	2.68	±	1.47
Epidote	3.78	±	0.54	4.61	±	0.48	9.44	±	2.46
Microcline	15.12	±	0.63	14.58	±	0.72	22.70	±	2.67
Muscovite1M	5.70	±	0.72	6.67	±	0.84	16.33	±	2.34
Muscovite2M	6.91	±	0.57	8.30	±	0.72	18.80	±	1.86
PlagioclaseAlbite	34.10	±	0.90	28.25	±	1.02	6.25	±	1.02
Quartz	25.76	±	0.63	21.15	±	0.75	23.80	±	3.30